The University Of Sheffield.

FLOOD-PEDESTRIAN SIMULATOR

AN AGENT-BASED MODELLING FRAMEWORK FOR URBAN EVACUATION PLANNING

THESIS

Submitted to the University of Sheffield in partial fulfilment of the requirements for the Degree of Doctor of Philosophy

by

Mohammad Shirvani

Department of Civil and Structural Engineering, the University of Sheffield

September 2021

Acknowledgments

Now that the challenging journey of my PhD research has come to an end, I wish to extend my sincere thanks to a number of people who played indispensable role in providing much needed academic and emotional support.

I am utterly grateful to my primary supervisor, Georges Kesserwani. I sincerely thank your invaluable advice and support in both academic and personal aspects throughout the research period. You selflessly coached me and instructed me in coding and hydraulic modelling and put all your effort to help me become a mature and independent researcher. You always had time for my meeting requests to provide direction, advice and solution to all kinds of issues ranging from methodological hurdles to publication dilemmas. I will always appreciate your feedback and inputs towards improving the clarity and cohesion in my writing. Your understanding of my personal circumstances and supports in providing financial aids have substantially paved the way towards the successful completion of this PhD. You are a good friend and supportive supervisor. I learnt a lot from you. Thank you so much Georges.

I would like to extend my gratitude to my second supervisor, Paul Richmond, from the Department of Computer Science. Thank you for your invaluable support and technical guidance. Talking to you always filled me with so much energy and passion. You always had positive words and views towards my work that encouraged me a lot. I very much appreciate that. I would like to thank Research Software Engineering group at the University of Sheffield, particularly, Mozhgan Kabiri Chimeh and Peter Heywood for providing vital technical support, especially at the beginning of the research.

I wish to thank all the colleagues in our office and research group whose assistance and feedback was monumental towards the success of this study. Thank you Janice Lynn Ayog, James Shaw, Xitong Sun, and Mohammad Kazem Sharifian. I am indebted to Gabriella Kakonyi, whose incredible advice, support and care played a vital role in my study and personal development. Bastian Saputra, thank you for your support, love and prayers. You all made the completion of my work much easier.

At last, I wish to extend my deepest gratitude to my parents back in Iran, Elham Nikzadeh and Aliakbar Shirvani. I could never come close to pursuing a PhD without your sacrifice, love and encouragement.

Declaration

This research has been performed between the months of February 2017 and August 2021, within the Department of Civil and Structural Engineering at the University of Sheffield, under the supervision of Dr Georges Kesserwani and co-supervision of Dr Paul Richmond from the Department of Computer Science.

I am aware of the University's Guidance on the Use of Unfair Means (www.sheffield.ac.uk/ssid/unfair-means). I undertake that all the contents and materials presented in this thesis are original and derived from my own work and have not been written for me neither in full nor partially by any other person. I also undertake that any quotation or paraphrase from any published or unpublished work has been acknowledged in this thesis.

Abstract

Agent-Based Modelling (ABM) is an increasingly used approach for characterisation of human behaviour in evacuation simulation modelling. ABM-based evacuation models used in flood emergency are developed mostly for vehicular scenarios at regional scale. Only a few models exist for simulating evacuations of on-foot pedestrians responding to floods in small and congested urban areas. These models do not include the heterogeneity and variability of individuals' behaviour influenced by their dynamic interactions with the floodwater properties. This limitation is due to the modelling restrictions pertaining to the computational complexity and the modelling flexibility for agent characterisation. This PhD research has aimed to develop a new ABM-based pedestrian evacuation model that overcomes these challenges through an ABM platform called Flexible Large-scale Agent Modelling Environment for the Graphics Processing Units (FLAME GPU). To achieve this aim, a hydrodynamic model has been integrated into a pedestrian model within the FLAME GPU framework. The dynamic interactions between the flood and pedestrians have been formulated based on a number of behavioural rules driving the mobility states and way-finding decisions of individuals in and around the floodwaters as well as the local changes in the floodwater properties as a result of pedestrians' crowding. These rules have been progressively improved and their added value has been explored systematically by diagnostically comparing the simulation results obtained from the base setup and the augmented version of the model applied to a synthetic test case. A real-world case study has been further used to specifically evaluate the added value of rules relating the individuals' way-finding mechanism to various levels of flood-risk perception. The findings from this research have shown that increasing the level of pedestrians' heterogeneity and the effect of pedestrians' crowding on the floodwater hydrodynamics yield to a considerably different prediction of flood risk and evacuation time. Besides, accounting for pedestrians' various levels of flood-risk perception has been found to be one determinant factor in the analysis of flood risk and evacuation time when there are multiple destinations. Finally, the sensitivity analysis on the simulation results have shown that the deviations in the simulation outcomes increases in line with the increase in the sophistication of human behavioural rules.

Table of Contents

List of Figures

Chapter 4

Appendix A

List of Tables

List of abbreviations

2D	Tow-dimensional
3D	Three-dimensional
ABM	Agent-based Modelling/Agent-based Models
BMI	Body Mass Index
CA	Cellular Automata
CFL	Courant–Friedrichs–Lewy
CPU	Central Processing Unit
CUDA	Compute Unified Device Architecture
DEFRA	Department for Environment Food & Rural Affairs
DEM	Digital Elevation Model
EA	Environment Agency
FDS	Fire Dynamics Simulator
FLAME GPU	Flexible Large Scale Agent Modelling Environment for the GPU
GIS	Geographic information system
GPU	Graphics Processing Unit
HR	Hazard Rating/Rate
IPCC	Intergovernmental Panel on Climate Change
LiDAR	It is an acronym of “Light Detection and Ranging” or “laser imaging, detection, and ranging”
LSM	Life Safety Model
MOE	Margin of Error
PC	Personal Computer
PDE	Partial Differential Equation
PDS	Parametric Design Studio
SFM	Social Force Modelling
UK	United Kingdom
US	United States

Publications

Most of the contents presented in this thesis have been published in:

- Shirvani, M., Kesserwani, G., and Richmond, P. (2021). Agent-based simulator of dynamic flood-people interactions. *Journal of Flood Risk Management*, **14**(2), e12695. DOI: https://doi.org/10.1111/jfr3.12695.

- Shirvani, M., Kesserwani, G., and Richmond, P. (2020). Agent-based modelling of pedestrian responses during flood emergency: mobility behavioural rules and implications for flood risk analysis. *Journal of Hydroinformatics*, **22**(5), 1078–1092. DOI: https://doi.org/10.2166/hydro.2020.031.

- Shirvani, M., and Kesserwani, G. (2021). Flood-pedestrian simulator for modelling human response dynamics during flood-induced evacuation: Hillsborough stadium case study. *Natural Hazards and Earth System Sciences*, **21**, 3175–3198. DOI: https://doi.org/10.5194/nhess-21-3175-2021.

Chapter 1

Introduction

1.1 Motivation

Urban flooding is one of the most widespread causes of interruption to people's lives. It frequently affects large populations in many parts of the world (Jonkman, 2005). Daily reports of major floods in Emergency Events Database (https://www.emdat.be/) and FloodList (https://www.floodlist.com) evidence that even the world's wealthiest and most technologically advanced countries are not immune to the disaster. Take for example the most recent severe floods that hit parts of China and the Western Europe. On 21 July 2021, more than a dozen cities and towns in the central Chinese province of Henan, home to approximately 12 million people, have experienced severe flooding after a heaviest rain in 1,000 years. The floods left at least 302 deaths and 50 people missing, as of 2 August (The Guardian, "China floods death toll …", 2 August 2021). Regions of Belgium, Netherlands, Luxembourg and Germany have also seen devastating floods after receiving up to two months of rainfall in only two days (14 and 15 of July 2021), according to the German national meteorological service (WMO, 2021). CNN reports that, as of 22 July, the death toll from these floods has increased to at least 205 and there seems to be more than 158 people that are unlikely to ever be found alive (Schmidt *et al.*, 2021). "While the inundation that devastated wide swathes of western and southern Germany occurred thousands of kilometres from the events in Henan, both cases highlighted the vulnerability of heavily populated areas to catastrophic flooding and other natural disasters." (Aravindan and Mackenzie, 2021). This statement is clearly indisputable and should be taken even more seriously when considering the frequency and intensity of the future floods.

Research has already shown that the likelihood of extreme flooding in urban areas is expected to dramatically grow worldwide as heavy rainfall events are projected to increase in future because of the ongoing climate change (Kovats and Osborn, 2016; Najibi and Devineni, 2018; World Bank, 2020; Blenkinsop *et al.*, 2021; Kahraman *et al.*, 2021). For instance, as reported by the UN Intergovernmental Panel on Climate Change (IPCC), the UK would experience a fivefold increase in the frequency of rainfalls with high intensities over the next few decades (IPCC, 2014; Kendon *et al.*, 2020), which may seriously affect more than 1.8 to 3.3 million people in the UK by urban floods by the 2050s (Kovats and Osborn, 2016). On the one hand, the extreme precipitation is projected to exceed the design capacity of the current local protection systems, e.g. dikes and levees, and infrastructures, e.g. piped drainage networks, which increases the flood risks from surface water run-offs in urban areas (Li *et al.*, 2016; Sayers *et al.*, 2020). On the other hand, there is already evidence that the flood risk could get worsened in the coming years due to the increase in urbanisation and population growth as a greater number of people are expected to settle in high-risk areas (Stevens *et al.*, 2014; Gu, 2019). To make the situation worse, NASA recently warns that the Moon wobble influencing its gravitational pull, which affects the Earth's tides, will exacerbate flooding effects in the next lunar cycle over the next decade, putting more lives in greater risks (NASA, "Study Projects a Surge ...", 7 July 2021). The future projection of deadly floods clearly underscores an especial focus on efficient preparation, adaptation and planning countermeasures to control and lessen the risks of flooding on people inhabiting urban areas.

Emergency evacuation is a common immediate countermeasure that typically follows an impending urban flooding (Simonovic and Ahmad, 2005; ESM *et al.*, 2010; Lim *et al.*, 2013). It could happen for a whole city or small populated areas in an emergency (Murray-Tuite and Wolshon, 2013). For instance, during the July 2021 floods in central China, more than 100,000 people were evacuated from the city of Zhengzhou, including 600 critically ill patients that had to be moved to a temporary shelter due to power outage (Woo and Qiu, 2021). In a more critical condition in Zhengzhou, amateur footages recorded hundreds of people waited to be evacuated as they were trapped inside metro carriages with floodwaters swirled around their chests (Davidson, 2021). During the July 2021 London floods, though not the whole city was forced to evacuate, people were moved out from smaller flooded zones for safety reasons. To mention a few existing on the news, 100 patients were transferred from London Hospital to another hospital after its basement was fully submerged

by the floodwaters (Stephens, 2021) and shoppers evacuated the Stratford Shopping Centre in East London as they were wading through water (Sky News, "Water flows through", 26 July 2021). The list goes on by including a number of urban evacuations that have happened in the US, Chile, and Canada due to extreme weather and flooding within the last few months (reports regularly get updated on https://floodlist.com/). Evacuation is an urgent action that must be carried out with little warning time in advance, which leaves emergency planners and decision makers only a tight time window for preparation and planning.

Preparation and planning of an evacuation process involves gathering information, materials and tools and using them to investigate the most effective strategy ahead of time for safely moving occupants out from a flooded zone (Lambert *et al.*, 2013). Choosing an approach in evacuation planning depends on the characteristics of the area and the nature of the event (Murray-Tuite and Wolshon, 2013). More specifically, for floods caused by dam-break or levee failures with raging deep floodwaters over a city or town, it is typical to consider planning for evacuation by motor vehicles through city networks; whereas, in the case of pluvial or fluvial floods in densely populated urban areas, where evacuation by motor vehicles is often impossible, decision makers are forced to consider planning for on-foot pedestrian evacuations (Coutinho-Rodrigues *et al.*, 2016). The latter usually constitutes more complications than vehicular evacuation planning due to the dynamics between pedestrians and flowing floodwaters, which may result in a set of complex interactions spanning across different dimensions and levels of uncertainty (Zheng *et al.*, 2019). Also, planning for pedestrian evacuation carries addressing multiple objectives simultaneously while accounting for flood-pedestrian interactions, such as finding escape routes, investigating accessibility of destinations, evaluating the magnitude of flood-risk to each individual pedestrian, evacuation time and so forth (Alonso Vicario *et al.*, 2020; Bernardini *et al.*, 2021). This complexity challenges the adaptation of analytical solutions to the problem (Chen *et al.*, 2021), which justifies the need for development of multi-objective decision-making tools that sufficiently integrate the flood-pedestrian interactions into the urban evacuation planning.

1.2 Research aim and objectives

The aim of this PhD research is *to develop a modelling framework for simulating pedestrian evacuation in flooded urban areas that is capable of capturing the two-way flood-pedestrian interactions considering the heterogeneity in a population's characteristics and behaviour at an individual level.* This modelling framework dynamically couples a hydrodynamic model with a pedestrian simulation model in a shared agent-based environment. In line with the aim of this research, the following general objectives have been formed:

Objective 1. *To integrate a well-established hydrodynamic model with a pedestrian simulation model within the FLAME GPU framework*

Objective 2. *To enhance the pedestrian characteristics and behaviours based on available survey data and empirical information*

Objective 3. *To investigate the coupled model capabilities over a real-world case study*

1.3 Research scope

Because of the scope of the project, the model is designed for, but not limited to, fluvial or pluvial flooding types that are the most relevant and recurrent cause of the major flooding events in urban areas. Due to the scale and scope of the research, this thesis does not account for peoples' daily routines, efficiency of warning alarms, and the traffic, which are mostly relevant in large-scale dam-break and flash-flood scenarios.

1.4 Scientific relevance

This research addresses the synergy between the human dimension and physical features of floods. Based on the facts, on the one hand, people behave differently under evacuation conditions and, thus, are exposed to different levels of flood risks. On the other hand, the microscopic interactions that occur between each flooded individual pedestrian and the floodwater under evacuation conditions define the overall response of the whole population. Therefore, modelling tools that support evacuation planning to provide a replication of reality need to explicitly incorporate the heterogeneity of evacuees and their realistic responses to

their surroundings and evolving floodwater at an individual level. Despite the recent advances in computing technology and the availability of the experimental data on human mobility and motion in floodwater, such models that explicitly address these features are not available in the literature. This research aims to fill that gap by incorporating available survey data and empirical formulae for characterisation of evacuees and their motion inside and around the floodwaters. Aerts (2020) states that "ignoring human adaptive influences in flood risk modelling is no longer an option", which also applies to the risk assessment part of the evacuation planning. With the traditional approach in the coupling of human and flood sub-systems, this would have never been addressed as capturing the effects of peoples physical presence on floodwater due to adaptive actions is either not possible or not efficient because of the computational complexity. This thesis also aims to fill that gap by developing and applying a new dynamic approach in the coupling, where the two-way interactions across and between the elements of the human and flood components could be captured in space and time. This capability would enable decision makers not only to plan for an efficient evacuation strategy but also to evaluate possible emergency interventions prior and during an event.

1.5 Scientific contribution

By achieving the research objectives, this thesis aims to make the following contributions to the field of pedestrian evacuation modelling for flood emergencies.

This PhD research is one step forward in linking the dynamic variations in floodwater properties with heterogeneous pedestrians' motion in response to flood-induced evacuation situations. The present modelling framework provides a game-like working environment with a high level of adaptability to different evacuation scenarios, which makes it easier for a planner/decision maker without any programming knowledge to work with it.

This research fulfils the main purpose of experimental research on studying submerged human-body stability limits and motion speed that aims to provide empirical formulae to bridge between human behaviour and computer simulations. The development of such models based on the existing experimental findings contributes towards future interdisciplinary research by identifying what has yet to be studied to better reinforce evacuation simulation models. In our case, we introduce the first attempt to capture the

influence of pedestrians' congestion on floodwater dynamics, which has never been thought of before in the context of experimental research, and, thus, calls for wider collaboration between researchers from different backgrounds to realistically quantify and formulate the hydrodynamic reaction to humans' physical presence. Also, this modelling framework provides foundations for future modelling attempts as the test cases designed in this thesis could be used as baseline for the evaluation of the future models.

1.6 Outline

Given the research motivation, aim and objectives and scope already presented in this chapter, the next six chapters are structured as follows:

Chapter 2 contains the review of previous literatures describing the techniques and approaches used in the pedestrian evacuation modelling. This chapter also overviews the advantages and limitations of the existing methods and highlights research gaps in the available flood-induced evacuation simulation models, including discussions on past studies that focused on small urban areas. Experimental studies on human stability and motion speed in floodwater that are conducted to support such pedestrian evacuation simulation modelling are also reviewed. Finally, the advantages of FLAME GPU over other available platforms with respect to the purpose of study are discussed, and an overview of FLAME GPU is also provided at the end of this chapter.

Chapter 3, which is dedicated to address **Objective 1**, presents a detailed description of the methodology behind the development of the flood-pedestrian simulator. It describes the formulation and features of the selected hydrodynamic model and the method used to implement it on FLAME GPU. This chapter includes the evaluation of the implementation of the hydrodynamic model on FLAME GPU. It describes the methodology for coupling the hydrodynamic model with a pedestrian model on FLAME GPU. The methodology for characterisation of pedestrians and their two-way interactions with floodwater are also provided in details in this chapter. Finally, the capabilities of the coupled flood-pedestrian model in capturing the two-way interactions between pedestrians and floodwater is evaluated for a synthetic test case.

Chapter 4, which is dedicated to address **Objective 2**, centred on the progressive augmentation in the modelling framework to improve characterisation of pedestrians and mobility behavioural rules in two subsequent phases. In the first phase, focus is given on characterising pedestrians with various body height and mass, and with a stability state and moving speed that relates to floodwater depth and velocity. To gain insight into the relative changes in the simulation outputs as new rules are gradually incorporated, qualitative analysis is performed as new rules are gradually incorporated. This is accompanied by further exploration on finding the relationship between the stability limits and moving speed of pedestrians on the risk-related metrics. In the second phase, improvements include enhancing the level of heterogeneity in the pedestrians' characteristics, i.e. by further incorporating age and gender, and a number of new behavioural rules to drive variable moving speeds of pedestrians both in dry and flooded zones. The new features are evaluated by reapplying the simulator for the same test case to analyse the relative changes in the simulation outputs, along with a sensitivity analysis to consider the uncertainty associated with the simulation of the behaviour of pedestrians in the simulation outputs.

Chapter 5, which is dedicated to address **Objective 3**, investigates further the capabilities of the model in simulating a real-world evacuation scenario. This chapter explores the relevance of simulation outcomes in finding the safest destinations and the spatial and temporal changes in the flood risks on pedestrians based on three levels of flood-risk perceptions, i.e. low, average and high. The relationship between the pedestrian's flood-risk perception and the uncertainties in their behaviour is also analysed.

Chapter 6 presents the discussions and conclusion of the thesis, including the highlights of the achievement of the research objectives. It discusses the significance of the major findings into the flood-induced evacuation simulation modelling area and lists the research's limitations. This chapter ends with some suggestions for future works and provides information on the availability of the model source code and outputs.

Chapter 7 closes the thesis with researcher's self-reflections on the research and some notes to help improvement of such modelling frameworks in future studies.

Chapter 2

Literature Review

2.1 Chapter overview

Sec. 2.2 reviews available ABM-based pedestrian evacuation models and discusses the benefits of ABM for the purpose of this research including the specific- and general-purpose agent-based pedestrian evacuation modelling tools. Sec. 2.3 overviews ABM-based pedestrian evacuation models for flood emergency and describes their advantages and limitations in relation to the purpose of this study. Sec. 2.4 reviews the recent experimental studies on human stability and motion speed in floodwaters that are conducted to support such pedestrian evacuation modelling. In Sec. 2.5, the incorporation of empirical information into ABM is discussed by reviewing available agent-based platforms capable of handling complex computations. Finally, Sec. 2.6 ends the chapter with an overview of the FLAME GPU by providing a summary on its history, and also describing its agent-agent communication mechanism and modelling procedure.

2.2 Overview of pedestrian evacuation modelling

With advances in computing technology, evacuation modelling have become a popular method to benefit safety design and emergency management. They commonly aim to describe pedestrian' motions and behaviours during the evacuation process under multiple what-if scenarios within a virtual environment created by computers (Şahin et al., 2019). These models have become a suitable substitute to the conventional methods, i.e. evacuation drills (Peacock et al., 2012) and animal experiments (Shiwakoti et al., 2011). The outputs of the models are useful to study the evacuation dynamics represented by multiple metrics, such as evacuees' density distribution, evacuation time and the number of possible casualties and injuries under different scenarios (Şahin et al., 2019). Analysis on the outputs of such simulations are useful for various applications, such as improving safety design of buildings (e.g. Cristiani and Peri (2019) and Helbing *et al.* (2005)), evacuation planning (e.g. Aleksandrov *et al.* (2019) and Yuan *et al.* (2018)), and so forth.

The earliest pedestrian evacuation simulation models could be dated back to 1970s (e.g. Okazaki, 1979). These models were developed based on mathematical methods provided by even earlier studies on human dynamics using empirical data (e.g. Henderson (1974) and Predtechenskii and Milinskii (1978). Basic concepts that are used in the modern evacuation simulations, are mainly introduced in 1990s (Ronchi, 2020). For instance, Thompson (1994) took the first steps in including human aspects, e.g. people characteristics, way-finding mechanisms and individual pedestrian's movement patterns, into the evacuation simulations. Since then, there has been a continuous shift from concerning homogenous pedestrians that exhibit uniform and simplistic behaviours to more advance ones that includes heterogeneous pedestrians that follow autonomous decision-making and diverse behavioural rules (Dong et al., 2020). Based on the adopted approach, pedestrian evacuation simulation models could be categorised into four main groups: (i) macroscopic-based models, (ii) Social Force Modelling (SFM)-based models, (iii) Cellular Automata (CA)-based models, and Agent Based Modelling (ABM)-based models. A brief review of studies in each group is provided in the following subsections, including the models' attributes, functions and purpose as well as the tools that were used to develop these models. At the end of each sub-section, the advantages and disadvantages of each approach is discussed with respect to their suitability for the purpose of the present study.

2.2.1 Macroscopic-based approach

Macroscopic approach refers to a term that considers pedestrians with uniform characteristics and decisions (Twarogowska et al., 2014). The models that use this approach are usually developed for large regional scales, where the population is large enough to be described by averaged quantities (Cristiani et al., 2014). In these models, the environment in which the pedestrians move is represented by a network of nodes, representing rooms, lobbies or intersections, connected with arcs that represent corridors, hallways, stairways or connections between the intersections (Hamacher and Tjandra, 2001). In these models, the pedestrians' movement is governed by a flow principle based on fluid dynamic equations (Helbing, 1998). The formulations that drive this technique has gone through a number of improvements over the past two decades. For instance, Hughes (2002) introduced the equations for simulating low-density and high-density crowds based on two-dimensional flow equations. In another study, Hughes (2003) also added a more intelligent components to the crowd decision-making based on their willingness to minimise travel time and avoid dens crowds. Colombo and Rosini (2005) also considered over-compression and failing accidents due to high crowd density into their simulations. This approach was also employed in hybrid models, i.e. coupled with force-based models, to study the interactions among pedestrians: for example, to study the disorder and blocking phenomena caused by emotional states of the crowd (e.g. Luh *et al.* (2012)), to investigate route choices based on potential values for selection (e.g. Guo *et al.* (2011)) and evacuees' different familiarity with the environment and their personal bias (e.g. Stubenschrott *et al.* (2017)).

EXITT (Levin, 1989) and EXIT89 (Fahy, 1991; Fahy et al., 1995) are the two widely used tools that employ macroscopic approach for pedestrian evacuation simulation. EXITT is the first commercial model that incorporates hazard data into the simulations by incorporating inputs from a fire simulator called HAZARD I (Bukowski et al., 1987). This tool also include different factors into the simulations, such as evacuee's age, gender, physical condition, crowd density and location of alarms and warnings times. EXIT89 is also another widely used tool that was developed by the academic to simulate pedestrian evacuations in highly dense areas from large premises.

This approach is known to be computationally efficient because of its simplicity in modelling individuals and environments thorough network of nodes and arcs (Hughes, 2003). However, with this approach, it is difficult to describe the geometry in detail and the

randomness in pedestrians' behaviour and their microscopic interactions among themselves and with the environment (Chen et al., 2021). These features are key parameters in the predictions of pedestrians' movement which influence the accuracy of the outputs, especially at urban scales with small features of the geometry and evacuees' diverse behaviour that needs to be models at the scale of each individual.

2.2.2 SFM-based approach

This approach considers individuals as particles subject to three main forces, i.e. goal force, repulsive force and attractive force, to drive the pedestrians' motion over a navigational map formed of magnetic fields (Helbing and Molnar, 1995). The navigation map encodes the features of the walkable area necessary for the individuals' way-finding decisions (Li *et al.* 2019; Jiang *et al.* 2020), e.g. the terrain obstacles and walls that need to be avoided as the individuals navigate and vector fields providing navigation to key destinations. Helbing *et al.* (2000) has improved this approach by further factoring in socio-psychological and physical forces into the mathematical equations describing the movement of pedestrians, including the microscopic interactions between pedestrians and their interactions with the environment features. This approach has been enhanced over the past decade through multiple studies for various purposes. For example, Zainuddin and Shuaib, (2010) further added decision-making capabilities to the pedestrians under evacuation condition, i.e. independence level on others and the ability to assess the crowdedness of an exit. They further improved the SFM formulations to incorporate a rush parameter which can reflect the panic influence on the moving speed of pedestrians to a certain level (Shuaib and Zainuddin, 2017). Han and Liu (2017) also incorporated a mechanism of communication between pedestrians to enable them decide on their movement direction according to the other's information. The SFM approach has also been improved for modelling pedestrian motion when there are multiple exits (e.g. Wang *et al.* (2016)) and conditions with higher and lower visibility of emergency signs (e.g. Yuan *et al.* (2018)). Some other studies also improved the modelling of interaction forces among the pedestrians: for example, to add the following behaviour of pedestrians in complex evacuation routes (Lin et al., 2016) and to factor in the relationships among the individuals for driving their group behaviour (Liu et al., 2019). There are also many other studies that improved the interactions between pedestrians and the environment for various purposes: for example, by incorporating a force between pedestrians

and multiple obstacles (Han et al., 2017) in complex small features (Zhang et al., 2012) and stairs movements (Li et al., 2021).

There are available pedestrian evacuation simulation tools that have been developed based on this approach. SimWalk Pro (Simwalk, 2020) and PTV Viswalk (PTV group, 2020) are commercially available tools that consider pedestrians as continues circles moving in a spatial domain. PedSim developed by Parametric Design Studio (PDS, 2021) is an open-source model that runs simplified pedestrian simulation in real time. This model also considers pedestrians as particles moving continuously in a spatial domain following the SFM formulations. Another tool using SFM is called FDS + Evac developed by VTT Technical Research Centre of Finland (Korhonen and Hostikka, 2009), which is developed to incorporate information of fire hazards into the simulations. This tool is accessible from another tool called Fire Dynamics Simulator (FDS) and is not separately accessible to the public.

This approach facilitates simulation of the interactions between pedestrians and the environment in small details, particularly it is suited for pedestrian motion simulation in small urban areas with complicated geometry features. However, this approach bears a limited capability in representation of heterogeneous individuals and it tends to oversimplify way-finding decision rules for the evacuees, particularly in scenarios with multiple exits (Chen et al., 2021). Nonetheless, when compared to other approaches, the SFM technique follows a more simplistic formulations to describe pedestrian movements and, thus, less computationally expensive. This, in turn, makes SFM suited to be combined with other modelling techniques, i.e. with CA and ABM, to enrich the characterisation of pedestrians and their behavioural rules for more complex evacuation scenarios.

2.2.3 CA-based approach

The CA approach is a grid-based technique in discrete space, time and states, where each cell, representing evacuees, updates its state in time and space according to its current state and the state of adjacent cells via a number of evolution rules. These rules govern the pedestrians' interactions and describe a number of transition probabilities to drive their movement towards a new location. CA-based models could also encompass static and dynamic fields around each cell towards any destinations, which could simulate the higher likelihood of pedestrians choosing the shortest route as it is expected under emergency

conditions (Haghani et al., 2019). CA enables the modeller to incorporate large variety of pedestrians' behaviour under evacuation condition, such as herding (e.g. Marconi and Chopard (2002)), exit bias (e.g. Li *et al.* (2008)), jamming (e.g. Burstedde et al., (2001)) and panic (e.g. Kirchner and Schadschneider (2002)). Early CA-based models also improved the simulation of the interactions that exist between the individuals and the environment. For example, Helbing *et al.* (2003) incorporated the spatial dependency of evacuees to study how it influences the evacuation time and dynamic congestions. Studies, such as Isobe *et al.* (2004), Nagai *et al.* (2004) and Cao *et al.* (2015) also investigated how the number and location of exits influence the evacuation time in rooms with poor visibility. Li *et al.* (2008) also studied the impact of evacuee's familiarity with exits and environment layout on their evacuation decisions. Yang *et al.* (2009) studied the effect of building information, e.g. alarms and signs, on the evacuation efficiency. Ma *et al.* (2012) simulated the evacuation in tall buildings by also taking into account the lifts and refugee areas. In a more small scale modelling, Fang *et al.* (2016b) studied the evacuation of aircraft passengers by factoring in their hesitation time and the location of their seats. Other studies also aimed to improve simulation of the interactions between the pedestrians by accounting for various parameters, such as crowd density (e.g. Guo *et al.* (2013)), pressure between pedestrians and their physical ability (e.g. Was (2005)), poor vision and psychological tension (e.g. Li *et al.* (2019)), and fatigue factor (e.g. Ding *et al.* (2017a)). The CA-based models are also combined with SFM to simulate wider range of interactions. For example, Chen *et al.* (2020), Guo and Huang (2008), Song *et al.* (2006) and Yang *et al.* (2005) integrated SFM into CA-based modelling frameworks to incorporate larger number of interactions, such as repulsion, friction and attraction, to study how these interactions influence the evacuation process. In a flood-related study, Zheng *et al.* (2019) developed a CA-based model to simulate pedestrian evacuation from a flooded underground station, where pedestrians were featured with an ability to go to higher places with lower risks and hold support objects.

STEPS (Mott Macdonald, 2020), EXODUS (Fire Safety Engineering Group (FSEG), 2021) and PedGo (TraffGo HT, 2013) are the three widely used CA-based pedestrian evacuation simulation tools that are accessible for the public use. STEPS simulate pedestrian evacuation from various facilities. It also provides an enhanced three-dimensional (3D) visualisation of pedestrians in different environment layout. EXODUS is another powerful tool that aims from a 3D visualisation. It comprises a number of sub models for both evacuation simulation and pedestrian analysis. This tool allows the modeller to incorporate

fire hazard data into the simulations to account for people-fire interactions into the evacuation processes. PedGo is also another CA-based tool that provides a large number of graphical plots for evacuation analysis and planning by simulating evacuation processes under different scenarios.

Similar to SFM, this approach have limited capability in representation of heterogeneous evacuees. Besides, CA-based models depends on conceptualisation of a fundamental framework, i.e. discretisation, homogeneity and implicit behavioural rules, which limits their applicability for more complicated scenarios, especially evacuation modelling in urban areas. Although this shortcoming could be overcome by setting up various update rules, it is incapable of capturing evacuees' non-adaptive behaviour, e.g. physical immobility due to losing stability. Furthermore, from modelling point of view, at most, one evacuee could be assigned to a cell, which makes it difficult to simulate highly dense crowds. Because of these limitations, the attraction of developers has been shifted from CA approach towards using the ABM technique, which is explained in more details in the next subsection.

2.2.4 ABM-based approach

ABM is a bottom-up technique that enables simulation of dynamic actions and interactions of heterogeneous and autonomous decision-making entities, called 'agents', within a dynamic network or system at an individual level (Bonabeau, 2002). These interactions could constitute both the feedback between individual agents and their reactions to external elements which may lead to changes in agent's behaviour and their spatial and temporal state (Heckbert *et al.*, 2010; Van Dam et al., 2012; Wilensky and Rand, 2015). Agents can be set to different attributes and characteristics and they can represent different entities, varying from institutional, e.g. policies, to more physical ones, e.g. infrastructures. Over the past few decades, ABM has become the mainstream technique for pedestrian evacuation simulations because of its capability to simulate the complex behaviour of humans in emergency situations and capture the emergent phenomena (i.e. crowd herding, flocking and queuing), as a result of microscopic interactions among evacuees (An, 2012; Railsback and Grimm, 2019).

ABM-based pedestrian evacuation models have been continuously improving during the past two decades. To mention a few studies focused on improving agents characterisation

and interactions, Joo *et al.* (2013) and Lee *et al.* (2010) focused on improving the agent's perception aspect and decision-making abilities. Hassanpour and Rassafi (2021) and Busogi *et al.* (2017) enabled agents to make decisions based on dynamic environments. Yuksel (2018) incorporated an ad-hoc technique to train agents to enable them change and adjust their behaviours autonomously. Niu *et al.* (2018) incorporated a membrane computing technique with ABM to make agents autonomous based on dynamically updated knowledge throughout the simulations. Sharma *et al.* (2018) and Zhou *et al.* (2016) also combined the fuzzy logic with ABM to account for the uncertainty in human behaviour, i.e. moving speed, under panic and stress. In addition, models where developed and configured for simulating evacuations in various spaces, e.g. concert venues (Wagner and Agrawal, 2014), airplanes (Liu et al., 2014), classrooms (Delcea et al., 2020), and buildings (Chu and Law, 2019). More importantly, employing ABM has proved to be an effective approach to factor in hazard features into the evacuation simulations. Previous studies has examined the influence of various hazards on the interactions between evacuees and the environment and how it influence the simulation outcome. For example, Shi *et al.* (2009) examined the influence of high temperatures and concentrations of smoke on the physiological harm under fire situations. Li *et al.* (2020) explored how high temperatures and concentrations of smoke in a fire-induced evacuation situation may influence evacuee's movement patterns and navigation decision making. Other studies also investigated the effect of smoke diffusion (e.g. Nguyen *et al.* (2013)) and flame spread (e.g. Tan *et al.* (2015)) on the behaviour of evacuees in fire conditions. Furthermore, researchers have considered social behaviour of people in ABM for simulation of evacuation processes. For instance, Pan *et al.* (2006) investigated the influence of social factors, e.g. social identity, on the emergent behaviour of the population, i.e. competitive, herding and queuing behaviours. Their model was later on extended by Chu *et al.* (2013) by further considering the individuals experience, social group and crowd interactions through a set of predefined behavioural rules. Based on empirical information, Von Sivers *et al.* (2016) also proposed an algorithm for modelling helping behaviour during evacuation. Also, considering that evacuees may follow the others in unfamiliar environments, as for example pointed out by Albi *et al.* (2016), the tendency of pedestrians to follow the others has been accounted for by considering peer-seeking behaviour (e.g. Chen and Wang. (2021)), leader-follower behaviour (e.g. Fang et al., 2016a), and active-passive agent characterisation based on different knowledge of spatial layout under evacuation (e.g. Richardson *et al.* (2019)). Even employing ABM enabled the

modellers to incorporate non-physical aspects, such as emotional adaptation of evacuees to the other's state under evacuation conditions (Zhou et al., 2020; Zou and Chen, 2020).

ABM is known to be the most computationally intensive approach as numerous calculations needs to be done to simulate various interactions at different temporal and spatial levels (Chen et al., 2021). Also, the direct validation of agent-based models is a grand challenge due to the complexity of modelling non-observable scenarios combined with the uncertainties associated with the emergent behaviours and the scarcity of validation datasets of such type (An et al., 2020; Zhuo and Han, 2020; Aerts 2020). Nonetheless, employing ABM for pedestrian evacuation processes carries a number of advantages (Zhuo and Han, 2020; Chen et al., 2021). First, ABM technique does not rely on a fixed conceptual framework to characterise the simulation environment and evacuees, which in turn provides the flexibility to use different methods for building the evacuation simulation, e.g. by specifying continuous agents (i.e. evacuees) and discrete agents (i.e. geometry features). Second, it provides the flexibility to characterise heterogeneous agents, specifically incorporate a population's various characteristics which makes the evacuation simulation seem close to reality. Third, ABM enables modelling agents as autonomous decision-making entities and, thus, suitable to capture emergent behaviour of heterogeneous pedestrians during an evacuation process, such as queuing, flocking and herding behaviour, which is an important component to simulate the collective behaviour of a crowd. Fourth, agents representing pedestrians can be set to react to institutional strategies (e.g. advance emergency warnings), dynamic environments (e.g. hazard propagation) and evacuation decision (e.g. informed of available emergency exits). Last but not least, considering the diversity of the evacuation scenarios, ABM can be easily combined with other methods to adjust agents' behaviours and decision-making rules. Therefore, compared to other approaches, ABM makes the evacuation simulations seem closer to reality and it is a more flexible approach, particularly to enrich characterisation of agents and their behavioural rules to increase the level of accuracy in pedestrian evacuation simulations.

There are a number of commercially and scholarly available tools that simulate pedestrian evacuations based on ABM approach. A few popular examples of such tools are outlined in Table 2.1. These tools only rely on user-specified set of values that define agents' attributes. Simulex (Thompson et al., 1997) is one of the first commercially available tools that represent human body with a three-circle model moving through discrete spaces illustrated via AutoCAD DXF maps with an aim to find optimal evacuation routes in

buildings and estimating the travel distance of evacuees. Pedestrian Dynamics (Incontrol Enterprise Dynamics, 2020), MassMotion (Oasys, 2020) and Pathfinder (Thunderhead Engineering Consultants, 2021) are the other widely used tools that enable pedestrian simulation with high level of details and continuous spatial environments for both indoor and outdoor spaces. These tools provide a number of exclusive capabilities to suite specific purposes. For instance, MassMotion provide access to its source code for customising and modifying pedestrians' behaviour and constructing dynamic linkage to external software packages. Pathfinder allows modellers to account for social relationships, e.g. connect family and friend, into the simulation. AvatarSim (Sharma, 2009) and SAFEgress (Chu et al., 2013) are also other tools developed by academics. AvatarSim is created in Java with a graphical user interface and can be displayed on a web browser. This tool focuses on adding human behavioural parameters, i.e. stress, anger, and panic, to the evacuation simulation in indoor spaces. SAFEgress also focuses on the inclusion of a social parameter, i.e. group intimacy, into the evacuation modelling with an aim to study how it influences evacuation patterns and performances in terms of exit choices. These tools are specifically focused on enhancing the evacuees' motion and their interrelationship interactions, group and social behaviour as well as a detailed representation of the virtual environment to produce realistic simulations of evacuation processes. Among these tools, Pathfinder is the only tool that is capable of incorporating fire origin/propagation data. Studies on analysing the direct influence of a particular hazard on evacuation processes have shifted towards using general-purposes ABM platforms that are outlined in the next paragraph.

Table 2.1: Available ABM-based tools for pedestrian evacuation simulation.

ABM-based tool	Owner/ Developer	Accessibility	Application	Hazard input
Simulex	Thompson *et al.* (1997)	Commercial	Indoor spaces: to find optimal evacuation routes in buildings.	No
Pedestrian Dynamics	InControl	Commercial	Indoor/outdoor spaces: for crowd management in complex infrastructures.	No
MassMotion	Oasys	Commercial	Indoor/outdoor spaces: for general purpose, e.g. building design.	No
Pathfinder	Thunderhead Engineering Consultants, Inc.	Commercial	Indoor/outdoor spaces: for general purpose, evacuations from stadiums, hospitals, skyscrapers, aircraft, etc.	Fire data only
AvatarSim	Sharma (2009)	Academic	Indoor spaces: to study human behaviour parameters, e.g. stress, anger and panic, on the evacuation process.	No
SAFEgress	Chu *et al.* (2013)	Academic	Indoor spaces: to study the effect of human and social behaviours on the evacuation process.	No

Netlogo (Wagner and Agrawal, 2014), MASON (Trivedi and Rao, 2018), GAMA (Ta et al., 2017), Anylogic (Busogi et al., 2017) and FLAME (Kiran et al., 2010) are the available multi-agent simulation toolkits that have the capability to build pedestrian evacuation models. Unlike the ABM-based pedestrian evacuation tools, these platforms require users to define the agents' attributes and their characteristics within the ABM framework. These descriptions may include designing the spatial environment, incorporating the hazard information or setting up dynamic linkage with external models, and configuring the interactions that exist between and across the three main components: pedestrians, the spatial environment and the hazard propagation. Compared to the ABM-based pedestrian evacuation tools, configuring general-purpose ABM tools provide the modelling flexibility required to incorporate more features and interactions across the hazard and evacuees' behaviour. Therefore, this capability made the technique the most suitable option to develop flood-induced evacuation simulation models to study human-flood interactions at different spatial scales.

2.3 ABM-based models for flood emergency

There are a number of evacuation modelling frameworks that are built upon the ABM paradigm for representation of space-time distribution of a flooded population. As one of the very first instances, Dawson *et al.* (2011) employed NetLogo to couple a flood inundation model with a vehicular evacuation simulation. They used GIS data to describe the geographical features and a number of behavioural rules for human interactions together with flood-incident management measures, e.g. evacuation strategy, warning time, and flood event conditions, e.g. storm surge, time of the day. A decade later, Barnes *et al.* (2021) developed an agent-based evacuation model at a macro scale using NetLogo to analyse how incorporation of population characteristics, i.e. age, gender and walking speed, would influence the overall evacuation time from a city. Alonso Vicario *et al.* (2020) used GAMA to include the flooding extent information into ABM with an aim to study the effects of human behaviour, starting time of the event and advance warning on the simulation outcomes under different evacuation conditions. These simulation models highlight the direct relationship between the evacuation time predictions and the estimation of flood-risk on people. They concluded that any misleading prediction of evacuation time may result in unrealistic estimation of flood risks on people and vice versa. This includes the delays associated with the stability issues, causing people to get stuck in floodwaters for some time and/or temporarily change their destination to avoid direct contact with floodwaters. Also, these works underpin the importance of coupling people's behaviour, characteristics and attributed with flood hazard information, i.e. depth, velocity and extent, into the evacuation modelling (Aerts *et al.*, 2018). But, these macroscopic ABM-based models, e.g. Dawson *et al.* (2011), are developed for vehicular emergency evacuation, which means they are not designed for simulating pedestrians' evacuation processes in and around small hubs (< 0.5 km × 0.5 km in size), i.e. shopping centres or sports venues. For microscale evacuation modelling, where pedestrians need to be individually modelled, only a few ABM-based evacuation models are currently available that can be coupled with hydrodynamic information. These models are outlined in Table 2.2 along with their advantages and limitations with respect to their applicability for simulating pedestrian evacuation in urban areas, which are discussed in details in the next paragraph.

Table 2.2: Available ABM-based pedestrian evacuation models for urban flood emergency.

Model name	Developer	Application/purpose	Hydrodynamic input	Advantages	Limitations
Life Safety Model (LSM)	BC Hydro and HR Wallingford	To estimate the number of casualties and injuries during severe floods due to dam breaks to support flood risk management.	outputs from various commercially available 2D hydrodynamic models (e.g. Telemac-2D, TuFlow, MIKE 21)	•Incorporates traffic distribution and traffic jams •Incorporates certain capacities of buildings in withstanding the floodwater •People could be modelled as individuals and in groups •Could incorporate flood warnings to people •Incorporates the locations of shelters and refuge areas	•Does not consider heterogeneity in pedestrians characteristics •Hydrodynamic information is imported manually and requires synchronisation in space and time •Instability state of pedestrians is determined based on hydrodynamic information, i.e. by pairing floodwater depth and velocity. •Does not incorporate variable moving speeds of pedestrians
HEC-LifeSIM	US Army Corps of Engineers	To estimate the number of casualties and injuries during severe floods due to dam break to support flood risk management.	outputs from HEC-RAS	•Includes traffic distribution •Incorporates a wide range of structure attributes •Incorporates a wide range of emergency warning attributes at different zones •Incorporates data uncertainty •Provides a graphical user interface	•Does not consider heterogeneity in pedestrians characteristics •Hydrodynamic information is imported manually and requires synchronisation in space and time •Does not consider the instability state of pedestrians •Does not incorporate variable moving speeds of pedestrians
FlooPEDS	Bernardini *et al.* (2017a)	To study evacuees' motion and path choices in urban flooding to support the design of urban solutions, i.e. architectural components like handrails, raised flooring systems in hazardous areas.	Built-in hydrodynamic model	•Incorporates a modified SFM to drive realistic evacuation behaviour of people in response to urban layout and floodwater •Incorporates variable moving speeds based on hydrodynamic information •Enables temporal and spatial risk analysis at an individual level	•Does not consider heterogeneity in pedestrians characteristics •Only a limited number of pedestrians could be modelled •Simulation time is limited to alleviate computational cost •Stability limits and moving speeds of pedestrians are simplistic and are only dependant on hydrodynamic information

The ABM-based pedestrian evacuation models for urban flood studies listed in Table 2.2 are mainly developed within their own ABM framework, meaning that they do not use any of the general-purpose ABM-tools summarised in Sec. 2.24. One of these models is called Life Safety Model (www.lifesafetymodel.net) developed by BC Hydro and HR Wallingford, which allows to analyse evacuation patterns of pedestrians along streetscapes and crossings (Lumbroso and Di Mauro, 2008; Lumbroso and Davison, 2018). LSM is capable of incorporating the interactions between vehicles, via a traffic model, and includes a pedestrian flow model accounting for people movement as they relay warnings to each other (Lumbroso *et al.,* 2011; Lumbroso *et al.,* 2015). More specifically, this model enables estimation of evacuation time and the number of injuries and casualties based on local information of floodwater on each person (Lumbroso and Di Mauro, 2008). In the LSM model, the instability and drowning state of people are used as a metric to quantify the flood risk on people and to control their mobility in floodwater (Lumbroso and Davison, 2018). The stability threshold for people is defined by combination of floodwater depth d (m) and depth-averaged velocity magnitude v (m/s) for a person of average height and weight according to experimental data (0.6 $m^2/s \leq d \times v \leq 1.7$ m^2/s). Also, LSM is limited to considering uniform height and weight for all the people alongside a constant walking speed in floodwater. Another model is HEC-LifeSIM developed by the US Army Corps of Engineers. HEC-LifeSIM is capable of simulating individuals' responses to an emergency warning with the floodwater propagation as they interact with the features of an urban layout, e.g. roads and buildings, with an aim to estimate fatalities under flood-induced evacuation conditions (Aboelata and Bowles, 2008). These ABM-based evacuation simulation tools were developed to inform emergency plans for severe flood types, such as in the immediate aftermath of a dam-break or a tsunami wave (e.g. Lumbroso *et al.*, 2021). The focus of these tools is mainly on estimating the loss of life, pinpointing bottlenecks and high-risk areas, and assessing how flood warnings of an impending flash flood could reduce the number of casualties and injuries. For this type of risk analysis, individuals' microscopic decisions and actions are considered insignificant in influencing the overall simulation outcomes due to the scale and speed of floodwater flow. However, for the most common flood types in urban areas, e.g. surface water due to extreme rainfall, less attention has been given to model the microscopic responses, down to the scale of the moving individuals, in and around flooded urban hubs (Ramsbottom *et al.* 2006). In this context, Bernardini *et al.* (2021) imported outputs of a flood model into MassMotion, to analyse flood risk differences in microscale

and macroscale modelling with and without including pedestrians' microscopic evacuation behaviour. They concluded that incorporating pedestrians' microscopic evacuation behaviour in microscale modelling could significantly influence the spatial and temporal changes in flood risk to people, i.e. up to 15 % in absolute terms, when compared to macroscale modelling. Their findings also suggest the need to further incorporate non-homogeneous characteristics of people in a more flexible microscale modelling framework, which may result in additional differences to the analysis of flood risk to people.

One first effort in designing an ABM-based evacuation model capable of capturing microscopic responses of pedestrians at a small urban scale was taken by Bernardini *et al.* (2017a). They developed FlooPEDS by incorporating the standard SFM for pedestrian dynamics (Helbing and Molnar, 1995), which was adapted to further model individuals' moving speed and stability states in floodwater. The coupling with the hydrodynamic model was used to receive information on the changes in the floodwater conditions within the urban environment. With the coupling technique, the stability state of pedestrians were evaluated based on the experimental data and recommendations in Ishigaki *et al.* (2009), Chanson *et al.* (2014) and Matsuo *et al.* (2011), though individuals' way-finding decisions were solely influenced by behavioural rules of the SFM. Similar to LSM, this model uses the stability state of evacuees in floodwater as a metric to quantify the flood risk to people. The mobility of people in FlooPEDS is also controlled by their stability state, i.e. defined based on whether they are exposed to extreme floodwaters with $d \times v \geq 1.2$ m^2/s or not. This model benefits from an experimental-based modified SFM to also include more realistic variable motion speeds of pedestrians in floodwater and path choices. However, FlooPEDS adopts a serial approach, by running one of the SFM and hydrodynamic model at a time, and a number of simplifications to alleviate runtime and dynamic memory costs, i.e. using uniform floodwater conditions on coarse subdomains, limiting the number of pedestrians up to 300 with uniform characteristics and the simulation time to less than 600 s (Bernardini *et al.*, 2017a). Due to the serial execution of hydrodynamic model and the evacuation model, meaning one model runs after another, only the one-way influence of floodwater on pedestrians is considered. This means that, with this approach in coupling, the influence of pedestrians' physical presence and adaptive actions cannot be captured. Furthermore, the heterogeneity of pedestrians' characteristics is generally neglected; and thus, realistic features of a population, such as age, gender and body height and mass distribution, are not accounted for in the simulations.

To support pedestrian evacuation modelling, a number of laboratory-based experimental studies has been undertaken to define the human stability limits and motion speed under different flow regimes. These studies commonly aimed to provide empirical data that could be integrated into pedestrian evacuation models for characterisation of individuals' behaviour. In the next section, some of these studies are reviewed.

2.4 Empirical data for pedestrian evacuation modelling

Many studies have considered critical pairs of water depth and velocity as the only main evidence of instability of humans in floodwater (e.g. Cox *et al.* (2010)). But, through a number of studies, it was found that the instability conditions are considerably influenced by non-hydraulic parameters (Martinez-Gomariz et al., 2016), specifically human body height and mass (Russo et al., 2013). In this context, Russo *et al.* (2013) conducted experiments on real human subjects to identify stability limits of humans. They proposed a formula to estimate flood hazard criteria based on both the characteristics of human subjects, i.e. body mass and height, and hydrodynamic properties, i.e. flow velocity and depth. However, their formula is limited to fast-flowing streetscape flood conditions with flow velocity (v = 1.88 m/s) and low depths (d = 0.15 - 0.2 m maximum). Xia *et al.* (2014a) and Xia et al. (2014b) proposed experimentally derived formulae for estimation of incipient velocities at the threshold of toppling and sliding states of partially submerged humans. In the derivation of the proposed formulae, they considered water flow depth and human body characteristics, i.e. mass and height, under different ground slopes. Arrighi *et al.* (2017) also proposed a new dimensionless instability criterion for submerged people to facilitate risk assessment of people in floodwaters. This criterion was demonstrated through curves pairing hydrodynamic properties with human features to discern stability conditions among different individuals.

To study moving speeds of partially submerged individuals, Ishigaki et al. (2009) used laboratory flumes to relate human walking speed to an estimated specific force based on water depth and velocity. This research was conducted with a specific application for planning evacuations in an underground flooding condition, mainly to more accurately estimate evacuation time. Almost a decade later, Postacchini *et al.* (2018) conducted a set of experiments to estimate the speed of people in relation to the specific force following the work of Ishigaki *et al.* (2009). They provided an empirical formula for estimating people's

walking speed in floodwater. Later on, Lee et al. (2019) quantified the walking and running speed of assisted and unassisted elderly people in swimming pools with water depths of 10, 20, 30, 40 and 50 cm. Their study identifies a significant difference in the evacuation speed of the elderly relative to that of younger ones moving in the same depth of water. More recently, Bernardini *et al.* (2020) have improved the formulae of Postacchini et al. (2018) to further account for people's gender, age and body characteristics. Bernardini and Qualiarimi (2020) also proposed a 'maximum excitement condition' factor relevant to the increased moving speeds of pedestrians under evacuation condition. Dias et al (2021) also conducted experiments to investigate walking speed of individuals for three different water levels (d = 0.08 m, 0.43 m, and 0.90 m). They concluded that the average walking speed would drop around 22 % and 41 % for d = 0.43 m, and d = 0.90 m, respectively. Their finding seems to be useful to estimate evacuation times and evacuation planning purposes considering motion patterns. However, they did not study the effects of pedestrians' characteristics, i.e. gender, age, height and weight, and water flow properties, i.e. depth and velocity, on the human walking behaviour.

2.5 Integration of empirical information into ABM

Incorporation of empirical information into ABM as behavioural rules is an ideal alternative to characterise pedestrians' motion under evacuation (Bernardini et al., 2017b). However, increasing the complexity of behavioural rules leads to a significant increase in the computational requirement and, thus, it is not feasible through the available general-purpose ABM frameworks mentioned in Sec. 2.2.4. Parallel computing resources, in particular Graphics Processing Units (GPUs), offer a feasible solution to the computational demand when simulating such complexity. The reason is that the architecture of GPUs are different from the Central Processing Units (CPUs) as they offer hundreds of arithmetic processing units to handle intensive computations on Personal Computers (PCs). There are a few ABM frameworks that are developed to build and execute models on GPUs to handle such computationally complex systems.

One of these frameworks is called MCMAS developed by Laville *et al.* (2013). This framework is a generic toolkit that is designed to facilitate implementation of ABM on GPUs by providing a set of C++ functions and commonly used data structures to build various

models. Another tool is called TurtleKit, developed by Michel (2013), which is a java library for running multi-agent based simulations on GPUs. Similar to MCMAS, TurtleKit also provides a number of predefined data and code structures, which in turn facilitates the programming process. However, these frameworks are operational based on a set of predefined algorithms and data structures which limits the implementation of a full range of possible agent behaviour in their modules; thus, they are incapable of incorporating empirical information as behavioural rules for pedestrian characterisation. In addition to that, they are developed based on a hybrid CPU-GPU modelling approach, which highly decreases the computing parallelism as the data needs to be frequently transferred between CPU and the GPU. One ABM framework that resolves these issues is called FLAME GPU, which carries two main advantages in comparison with MCMAS and TurtleKit that stand out its suitability for the purpose of this research. Firstly, it comprises a set of modifiable scripts for specification of agents' characteristics and behavioural rules at different sophistication level. Secondly, it aims from a built-in communication mechanism between the agents that is suitable to specify a wide range of interactions across and between multiple agents at different temporal and spatial scales.

2.6 FLAME GPU

FLAME GPU is an extension to the generic FLAME framework (see Sec. 2.2.4) developed by the scholars at the University of Sheffield (Richmond et al., 2009; Richmond et al., 2010; Chimeh and Richmond, 2018). Developed since 2008, FLAME GPU enabled modellers to run agent-based simulations in various areas of science, such as biology (Konur et al., 2015; Tamrakar et al., 2017), medicine (Seekhao et al., 2018), criminology (Romano et al., 2009), social science (Kurdi et al., 2015), psychology (Beklaryan et al., 2021), entomology (Johnson and Hoe, 2013), economy (Kaczyński, 2020) and traffic management (Heywood et al., 2015). One key design feature of FLAME GPU that facilitates ABM for the modellers is that it does not require specialised knowledge of GPU programming on parallel computing platforms, i.e. CUDA (or Compute Unified Device Architecture).

FLAME GPU involves a standard procedure to create and run a CUDA simulation program by processing three inputs, as shown in Fig. 2.1. The *XMLModelFile.xml* is where a user defines formal agent specifications, including their descriptive information, type,

numbers, properties, *etc.* An agent can be specified in space as either *discrete* or *continuous* (FLAME GPU Technical Report and User Guide, 2022). *Discrete agents* have fixed coordinates and must be pre-allocated in the memory of the GPU as 2D grid of size of a power of two number (e.g. 64 × 64, 128 × 128, 256 × 256, 512 × 512, *etc.*). *Continuous agents* change their coordinates and their population; they can be of any population size (within the limitations of available GPU memory). The *input.xml* file contains the initial conditions of the variables of state of all the defined agents. In a *single C script*, the behaviour rules to update all agents are implemented, and includes *Transition functions* to achieve dynamic passing of the information stored in the agents as they get simultaneously updated (FLAME GPU Technical Report and User Guide, 2022). The agents' communication mechanism is explained in details in the next sub-section as it is necessary for understanding the dynamic coupling approach used in the present research.

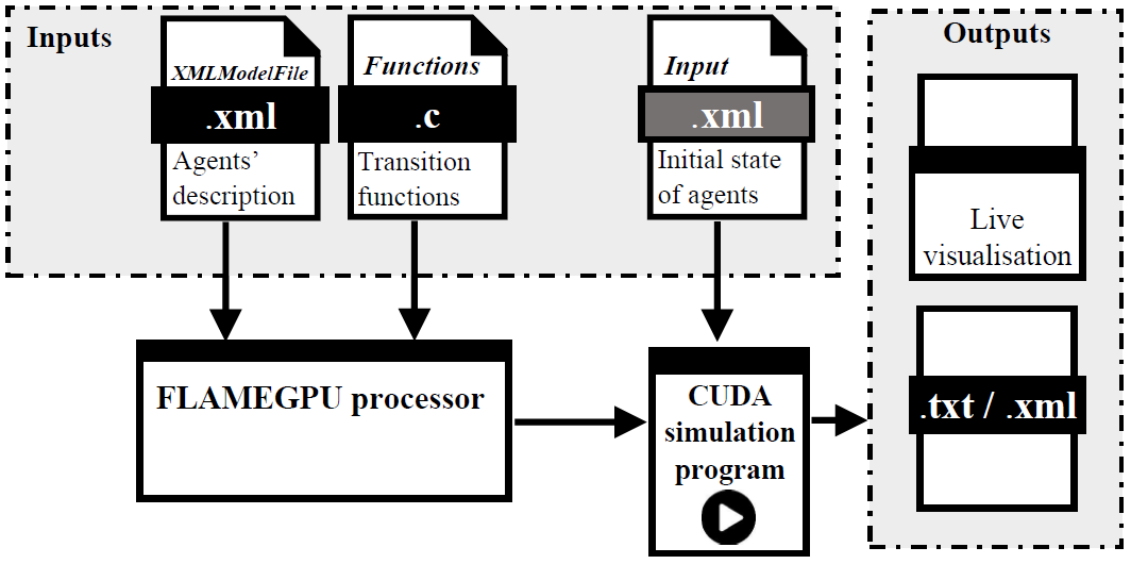

Figure 2.1: The process for generating and running an agent-based simulation program on FLAME GPU (http://www.flamegpu.com/home).

2.6.1 Agent-agent communication mechanism

The communication between multiple agents on FLAME GPU is made possible through sharing a dynamic memory between all the agents where a number of messages could be concurrently accessed. In this section, this dynamically shared memory storage on the GPU is called *message pool*. The communication between agents and the message pool is made possible through two sets of transition functions called *output* and *update message functions*, which are specific to FLAME GPU environment. The process of an agent's communication with the message pool is illustrated in Fig. 2.2, where an agent is illustrated by a vertical layer and output and update message functions are illustrated by a grey and green horizontal layers. To update the state of an agent, an output message function duplicates the agent's information and pass it as a single message to the message pool. Subsequently, an update message function loads the information from the message pool to the agent, where it could be processed in the evaluation of the next state of the agent. The state of each agent is described by the information that it holds in their memory via a set of variables. These variables are case dependant and should be specified by the users. This process is repeated in the next iteration of the simulation. For multiple agents, the same principal applies, where the same message function could be employed by the similar agents to ensure that all of them receive the same set of variables from the others in the environment. FLAME GPU enables the modeller to specify an unlimited number of message functions to load and process different series of variables required to characterise the dynamic interactions between the agents.

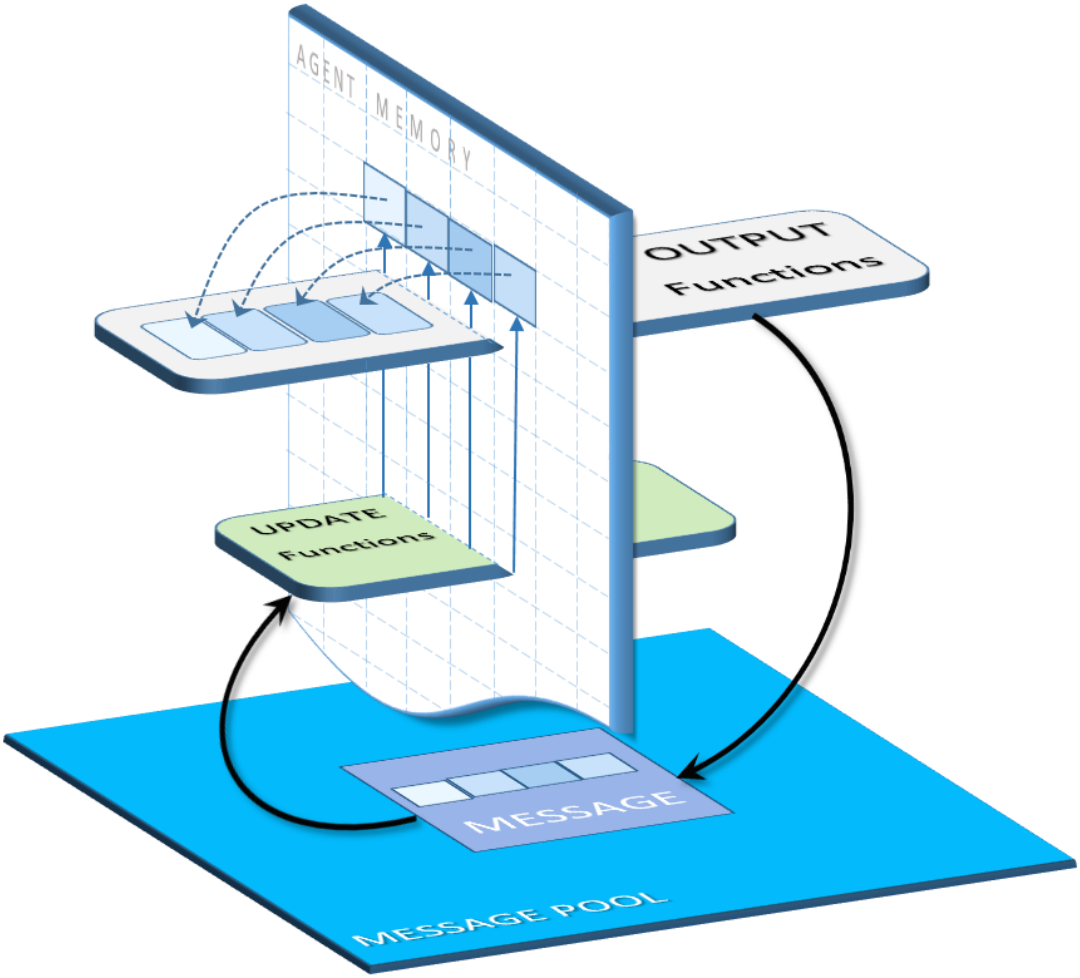

Figure 2.2: Communication mechanism of agents: vertical layer represents an agent memory that stores multiple variables. The variables stored by each agent is represented by squares with different shades of blue colour. These variables are duplicated on a single message that will be passed to another agent via the message pool, which is done through an output message function (illustrated by horizontal grey rectangle). Subsequently, any agent is able to obtain the message from the message pool, and process the data to update their own state in the next time-step. This is done via update functions (illustrated by horizontal green rectangle), which enable agents to receive specific set of variables from the message pool.

2.6.2 Modelling on FLAME GPU

Building a model on FLAME GPU relies on specification of: (i) 'XMLModelFile.xml' template, which includes the model specification and agent properties; and (ii) 'functions.c' behavioural script, which includes all the mathematical formulations to drive agents' behaviours.

- **XMLModelFile.xml**

XMLModelFile.xml aims X-Machine Mark-up Language (XMML) schemas and can be specified by a name and four main elements on FLAME GPU as described below (Fig. 2.3).

- 'Environment' element: includes all the global variables and constants that exist in the shared modelling environment. These variables and constants could be defined by a type and name. The functions.c script is also introduced to the modelling environment within this element by its name.
- 'Xagent' element: contains all the agents' descriptions, including all the variables held in the memory of the agents, message functions to help their state transition through time, their initial and update state, their type (i.e. whether they are discrete or continuous in space), and their population size specified through a buffer size. In the memory of each agent, variables are defined by a name and type, i.e. integer, float, double and boolean data types. Message functions could also be specified by a name, current and next state to derive their execution sequence in time, and whether the message function is an output function or an update function type. For each message function, the user can specify the message name and type that needs to be passed between the agents.
- 'Messages' element: includes the messages specified by a name, size and the variables that need to be passed between the agents (using the message functions specified for in the xagent element). Similar to specification of the variables for the agents, each variable in the message functions could also be specified by a type and name.
- 'Layers' element: is where the modeller could organise the execution sequence of agent message functions, either within one similar layer (for concurrent execution) or subsequent layers for serial execution with respect to their execution sequence.

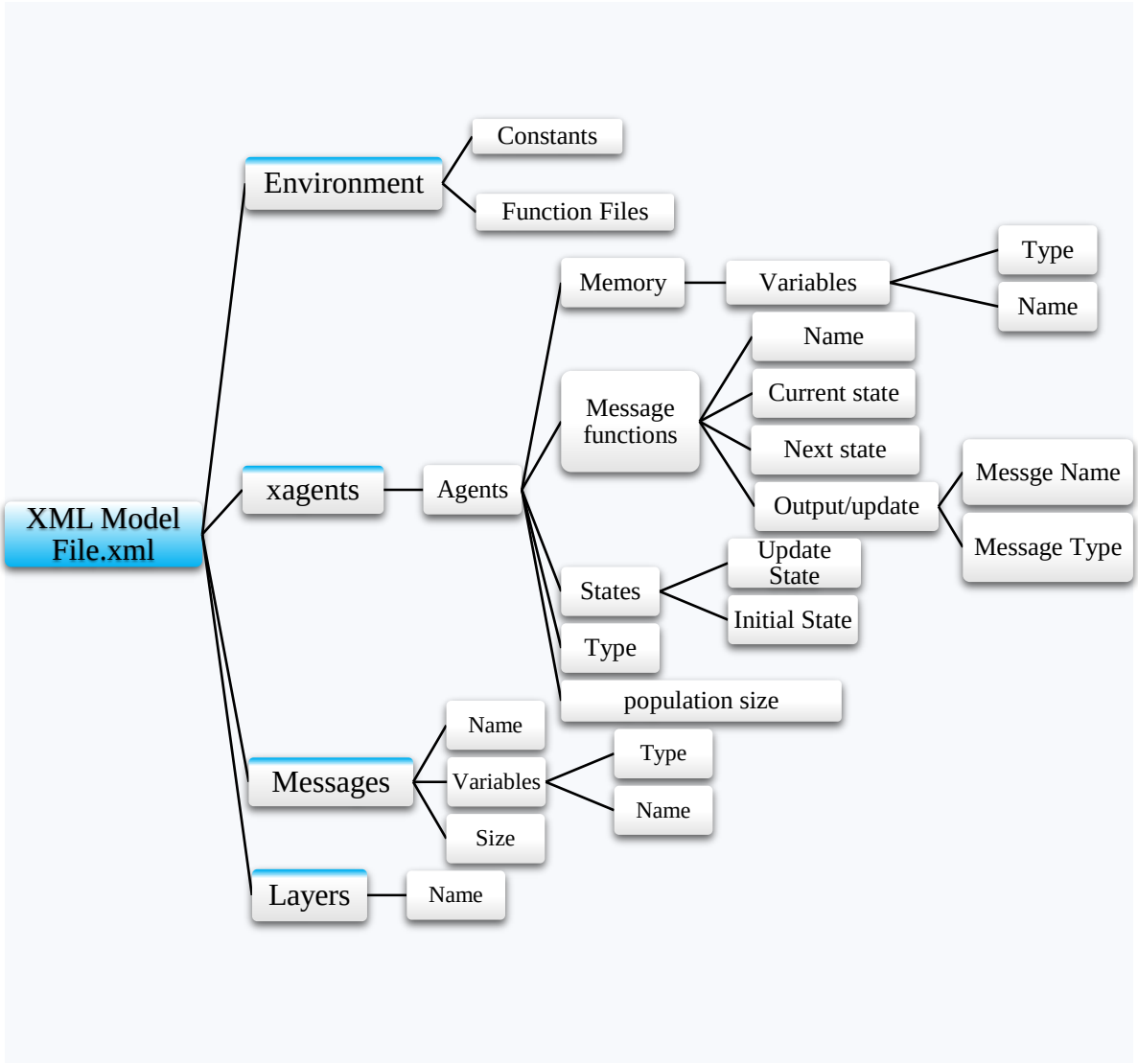

Figure 2.3: Hierarchical structure of 'XMLModelFile.xml' template

- **Functions.s**

Functions.c is a C script shared between all the agents. It contains a number of agent functions including the message functions to update each agent's state. Agent functions refer to a number of logical and mathematical operations which are directly coded in functions.c, usually within the update functions. At each iteration of the simulation, all the functions specified in functions.c script are executed in a sequential form on GPU, but concurrently for all the agents in the environment. Figure 2.4 is an illustration of how the state of agents updates during one iteration of the simulation using the output and update functions including multiple agent functions. As explained in Sec. 2.6.1, agents have access to their neighbouring agents' variables as they receive messages from the message pool through the update

functions. Through the agents' functions, the variables already stored in the memory of the agents are then evaluated as the state of the agent get updated through time. This process is then repeated over the next iteration and is applied to all the agents in the environment.

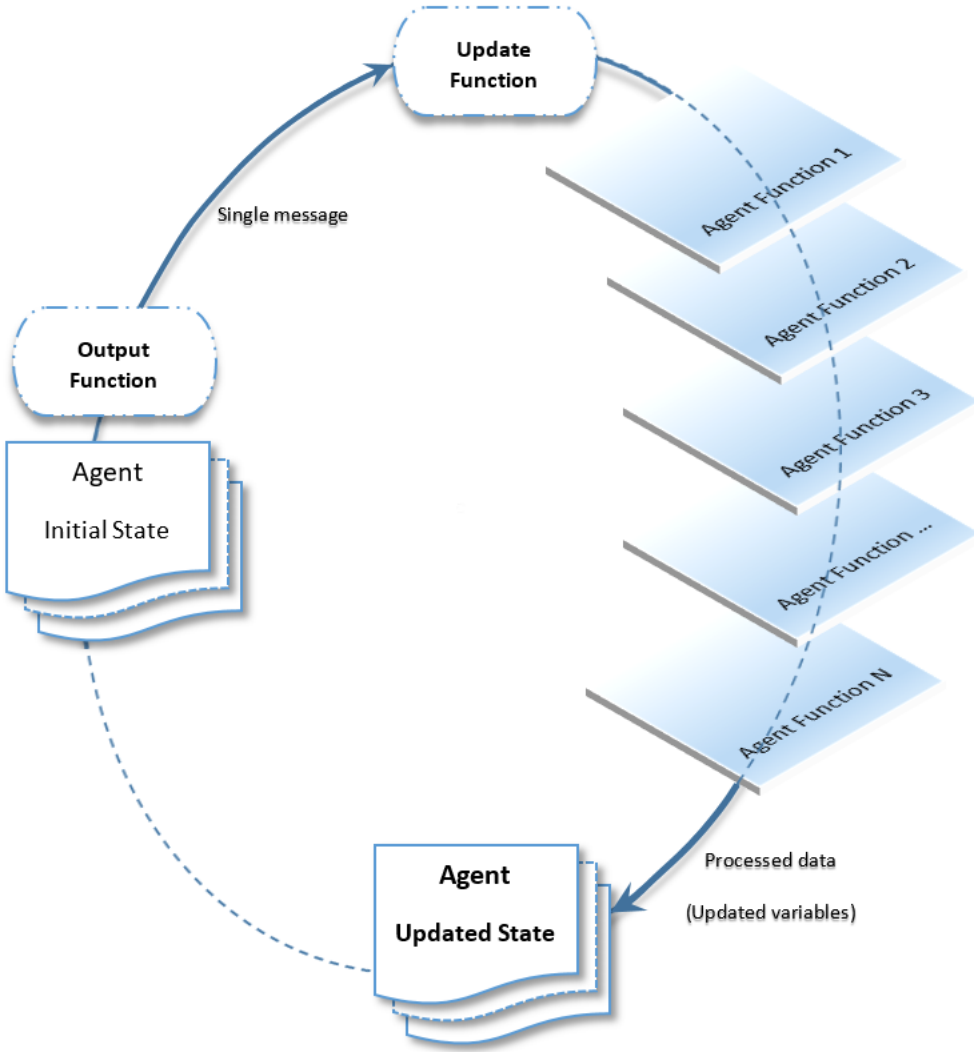

Figure 2.4: Illustration of how an agent update its state in each iteration of simulation on FLAME GPU via functions.c and the messages passed between the agents. The process starts by agents sending their initial state, through a set of variables, to the others via a single message. Then, the update message function loads the other's data from the message pool and subsequently use a number of logical/mathematical functions (agent functions) to update their states directly on GPU. This process is performed for all the agents at the same time and repeats in each simulation iteration.

Chapter 3

Coupling a hydrodynamic model with a pedestrian model on FLAME GPU

3.1 Chapter overview

This chapter, which aims to address Objective 1, elucidates the methodology used to couple the hydrodynamic model with a pedestrian model on FLAME GPU, as well as a preliminary evaluation of its capabilities in capturing the two-way interactions between pedestrians and floodwater. Sec. 3.2 describes the formulation and properties of the selected hydrodynamic model. Sec. 3.3 describes the method used to implement the hydrodynamic model on FLAME GPU, along with an evaluation process for its implementation through academic test cases. Sec. 3.4 describes the coupling approach by firstly providing an overview of the pedestrian model and then explaining the implemented behavioural rules. Sec. 3.5 presents a preliminary evaluation of the coupled model's capabilities through a synthetic test case. Finally, the key findings and conclusions are summarised in Sec. 3.6.

3.2 Overview of the selected hydrodynamic model

The selected hydrodynamic model is formulated based on the mathematical description of water flows using the solution of Shallow Water Equations (SWE) on a numerical grid, which are often employed as a basis for flood simulations (Teng et al., 2017). SWE is described by a system of hyperbolic Partial Differential Equations (PDEs) in the form of physical conservation laws for mass and momentum. These PDEs are characterised by variables of states that are related to physical fluxes (Toro, 2001). In the vectorial form these variables and physical fluxes can be expressed as:

$$\frac{\partial \mathbf{U}}{\partial t} + \frac{\partial \mathbf{F}(\mathbf{U})}{\partial x} + \frac{\partial \mathbf{G}(\mathbf{U})}{\partial y} = \mathbf{S}(\mathbf{U}) \tag{3.1}$$

in which (x, y, t) are the space-time coordinates, **U** is a vector including the flow variables, **F**(**U**) and **G**(**U**) are the flux vectors in x- and y-axis directions, and **S**(**U**) is the source term vector that contains bed and friction slopes in x- and y-axis directions. **U,** **F**(**U**) and **G**(**U**) are expressed as:

$$\mathbf{U} = \begin{pmatrix} h \\ q_x \\ q_y \end{pmatrix},\ \mathbf{F}(\mathbf{U}) = \begin{pmatrix} q_x \\ \frac{{q_x}^2}{h} + \frac{1}{2}gh^2 \\ \frac{q_x\, q_y}{h} \end{pmatrix},\quad \mathbf{G}(\mathbf{U}) = \begin{pmatrix} q_y \\ \frac{q_x\, q_y}{h} \\ \frac{{q_y}^2}{h} + \frac{1}{2}gh^2 \end{pmatrix} \tag{3.2}$$

$$\text{and } \mathbf{S}(\mathbf{U}) = \begin{pmatrix} 0 \\ gh(S_0^x - S_f^x) \\ gh(S_0^y - S_f^y) \end{pmatrix}$$

Where h (m) is the depth of water, q_x (m^2/s) and q_y (m^2/s) are the unit-width flow rate in x- and y-axis directions, g is the gravitational constant (≈ 9.81 m/s^2), S_0^x and S_0^y are topography terms in x- and y-axis directions, and S_f^x and S_f^y are friction terms in x- and y-axis directions:

$$S_0^x = -\frac{\partial z}{\partial x} \quad , \quad S_0^y = -\frac{\partial z}{\partial y} \tag{3.3}$$

$$S_f^x = \frac{{n_m}^2 u\sqrt{u^2+v^2}}{h^{4/3}} \quad , \ S_f^y = \frac{{n_m}^2 v\sqrt{u^2+v^2}}{h^{4/3}}$$

Where, z is the bed level, n_m is a friction factor based on the Manning's roughness coefficient, and $u = q_x/h$ and $v = q_y/h$ are water velocities in x- and y-axis directions respectively.

The selected hydrodynamic model solves SWEs via a shock-capturing Finite Volume (FV) scheme in its first-order formulation to keep the computational stencil limited to the information stored in the immediate neighbours sharing its four interface (Wang *et al.*, 2011). The shock-capturing method refers to a technique that is often used in fluids dynamics to simulate discontinuous flow transitions including shocks within the numerical solution. These discontinuities are connected by solving the so-called Riemann problem to present a continuous 2D representation of water surface (Kesserwani et al., 2008). FV method assumes that **U** is distributed as a piecewise-constant over a grid composed of a number of computational cells spanning the domain with inter-elemental discontinuities across interfaces.

To approximate SWE, the FV scheme discretises the computational domain in space and time. A uniform two-dimensional domain $[x_{min}, x_{max}]\times[y_{min},y_{max}]$ is divided into N_x and N_y number of computational cells in x- and y-axis directions respectively for the spatial discretisation. Figure 3.1 represents a 2D a calculation stencil showing a nominated cell $I_{i,j}$ and its adjacent neighbours. The interfaces of the computational cells are denoted by $x_{i-1/2} = x_{min}+(i-1)\Delta x$ and $y_{j-1/2} = y_{min}+(j-1)\Delta y$ for $i = 1, \ldots, N_x+1$ and $j = 1, \ldots, N_y+1$, where $\Delta x = (x_{max} - x_{min})/N_x$ *and* $\Delta y = (y_{max} - y_{min})/N_y$ are the length of the cells in x- and y-axis directions. Also, midpoint values are defined as $x_i = 0.5(x_{i-1/2} + x_{i+1/2})$ and $y_j = 0.5(y_{j-1/2} + y_{j+1/2})$. These values are specified at the centre of the computational cells. In this section each computational cell is denoted by $I_{i,j} = [x_{i-1/2}, x_{i+1/2}] \times [y_{i-1/2}, y_{i+1/2}]$ and $\mathbf{U}^n_{i,j}$ is a piecewise-constant approximation of **U** over a cell $I_{i,j}$ at time $t^n=n\Delta t$, where Δt is time step and n is a positive integer. Considering the temporal and spatial discretisation of Eq. (3.1) by FV method, $\mathbf{U}^n_{i,j}$ could be evaluated in the next time step (at t^{n+1}) via the following formula:

$$\mathbf{U}^{n+1}_{i,j} = \mathbf{U}^n_{i,j} - \frac{\Delta t}{\Delta x}\left(\tilde{\mathbf{F}}^n_{i+1/2,j} - \tilde{\mathbf{F}}^n_{i-1/2,j}\right) - \frac{\Delta t}{\Delta y}\left(\tilde{\mathbf{G}}^n_{i,j+1/2} - \tilde{\mathbf{G}}^n_{i,j-1/2}\right) - \Delta t(\mathbf{S}_{i,j}) \qquad (3.4)$$

in which, $\tilde{\mathbf{F}}^n_{i+1/2,j}$, $\tilde{\mathbf{F}}^n_{i-1/2,j}$, $\tilde{\mathbf{G}}^n_{i,j+1/2}$, and $\tilde{\mathbf{G}}^n_{i,j-1/2}$ are spatial flux approximations based on two arguments numerical flux functions ($\tilde{\mathbf{F}}$ and $\tilde{\mathbf{G}}$) for solving Riemann problem to connect the

discontinuities. For example, $\tilde{\mathbf{F}}^{n}_{i+1/2,j}$ is calculated by $\tilde{\mathbf{F}}(\mathbf{U}_L, \mathbf{U}_R)$ with $\mathbf{U}_L = \mathbf{U}_{i,j}$ and $\mathbf{U}_R = \mathbf{U}_{i+1,j}$ at the interface between $I_{i,j}$ and $I_{i+1,j}$. As can be seen in Fig 3.1, this is also applied to $\tilde{\mathbf{F}}^{n}_{i-1/2,j}$, $\tilde{\mathbf{G}}^{n}_{i,j+1/2}$, and $\tilde{\mathbf{G}}^{n}_{i,j-1/2}$. For evaluating the numerical flux functions, the hydrodynamic model employs Harten-Lax-van Leer (HLLC) formulations (Wang *et al.*, 2011).

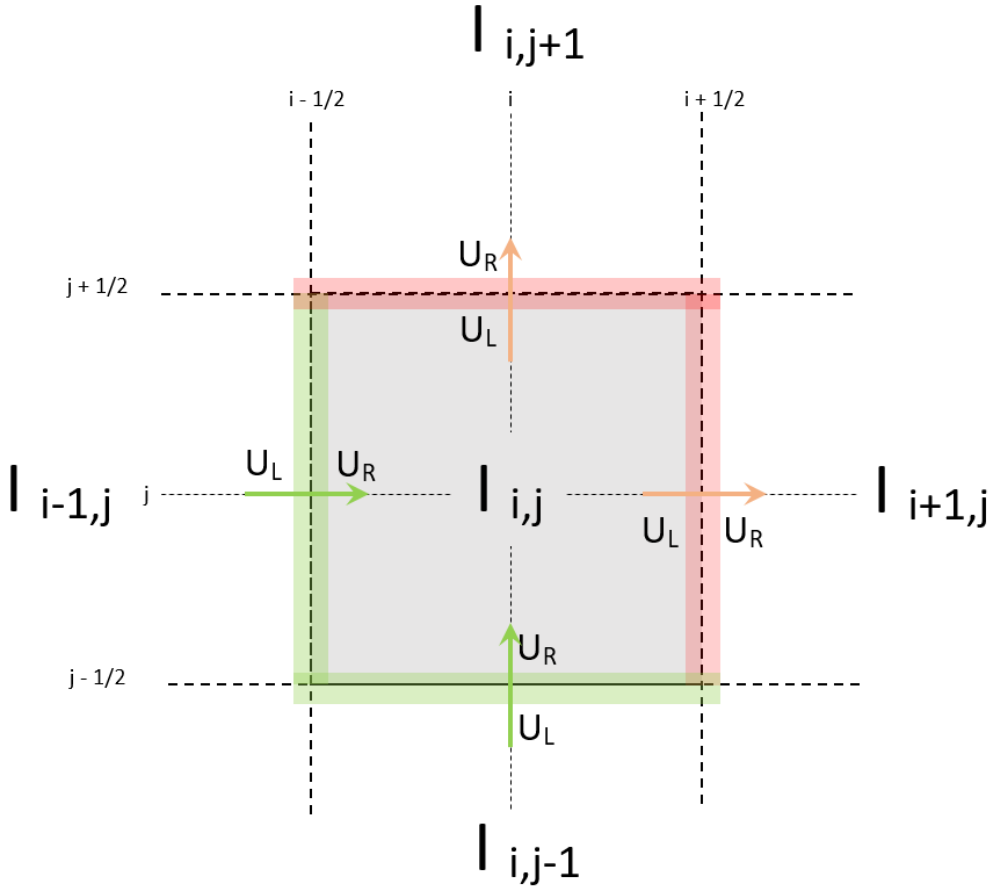

Figure 3.1: 2D calculation stencil showing adjacent neighbours to the cell $I_{i,j}$.

The hydrodynamic model on a CPU solves Eq. (3.4) for each of the computational cell in a sequential order handled by a for-loop. For a serial solution, the sequential order of this for-loop is usually controlled by two integer variables as indicators to the position of each computational cell on a 2D grid: i.e. i starting at 1 to N_x and j starting at 1 to N_y, both in increments of 1. This for loop ensures that the block of codes solving Eq. (3.4) is executed explicitly for all computational cells one after another over a sequence of $N_x \times N_y$ iterations.

This means that once $\mathbf{U}_{i,j}^{n+1}$ is calculated for $I_{i,j}$, the solution is carried to the next computational cell, e.g. $I_{i+1,j}$ to approximate $\mathbf{U}_{i+1,j}^{n+1}$ in the next time step.

3.3 Implementation of the hydrodynamic model on FLAME GPU

On FLAME GPU, each computational grid is represented by a grid of discrete flood agents. The formulation of the hydrodynamic model, including Eq. (3.4), is coded within the functions.c script, which is executed simultaneously over all the $N_x \times N_y$ flood agents in the domain (see Sec. 2.6.2). This means that the sequential update of computational cells, or the flood agents, as it is usually handled by for-loops on CPUs explained in Sec 3.2, is not functional on FLAME GPU. To resolve this issue, the information regarding the coordinates of the flood agents is used instead to locate each agent's immediate neighbours. The coordinates of each flood agent in *x*- and *y*-axis directions are hereafter denoted by *x* and *y* that are integers representing the position of each flood agent in the computational grid of $N_x \times N_y$ in size. As solving Eq. (3.4) for the grid of flood agents requires accessibility of the flood information for Riemann solution from neighbouring agents (see Sec. 3.2), the agent-agent communication mechanism of FLAME GPU (previously explained in Sec. 2.6.1) is used. This method is explained in details in the following subsection.

3.3.1 Obtaining information from neighbouring agents

To enable each flood agents to identify their neighbours, all flood agents are set to share the *x* and *y* variables to other agents via an output message function (previously explained in Sec. 2.6.1). An example is presented in Fig. 3.2 which illustrates a local agent, located at $x = 3$ and $y = 3$, and its neighbouring agent on the north, east, south and west interfaces. The local flood agent, which represents any flood agent on the grid (denoted by *Agent*), passes its coordinate to its adjacent flood agents and also receives its' neighbours coordinates via a *Message*. The arrow (→) in Fig. 3.2 represents a pointer to the memory of *Agent* and *Message*. Through this process, each flood agent is then enabled to identify the exact location of its adjacent counterpart by comparing its own coordinate to the ones received from the neighbours via the neighbours' messages. For instance, considering the example illustrated in Fig 3.2, while *Agent* stores $x = 3$ and $y = 3$, the surrounding neighbours are storing different coordinate data relative to their location at each side, e.g. eastern neighbour has $x = 4$ and $y = 3$. These differences between the coordinate data stored by the *Agent* and those received

from the neighbouring agents are used within a number of conditional statements to form an algorithm for solving Eq. (3.4) via functions.c script file that is executed for all the flood agents at the same time (see in Fig. 3.3).

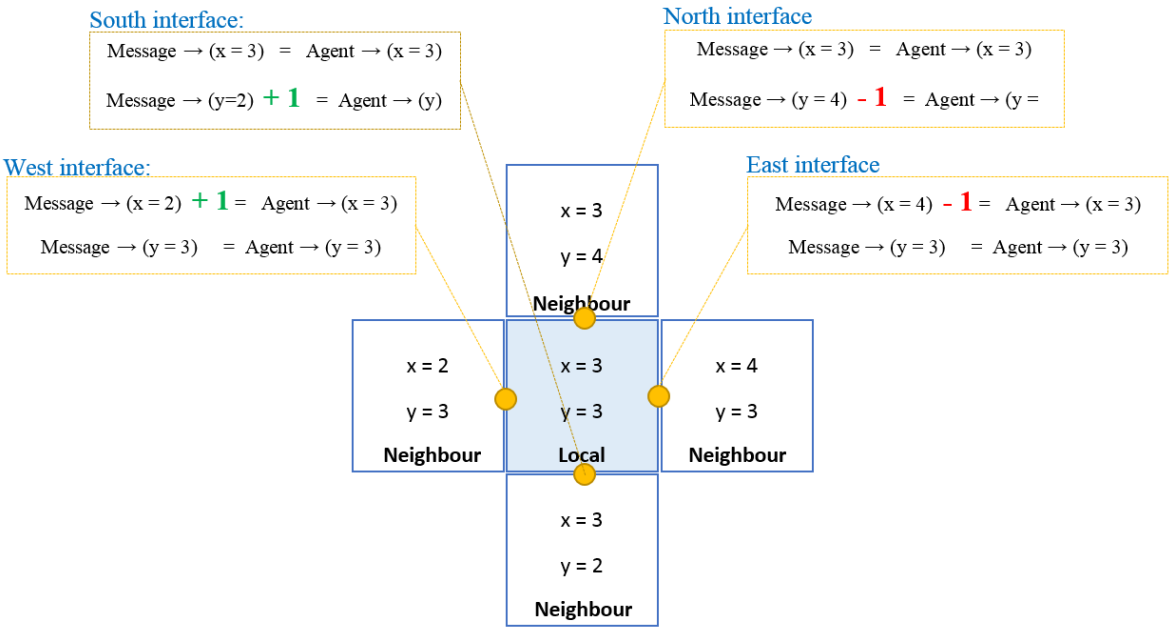

Figure 3.2: An example of a local agent, located at x = 3 and y = 3, and its neighbouring agent on the north, east, south and west interfaces.

3.3.2 Updating the state of flood agents

Figure 3.3 illustrates the algorithm that is formulated in the functions.c source code to simultaneously update the state of flood flow variables stored in the flood agents' memory via Eq. (3.4). This algorithm enables each flood agent to obtain $\mathbf{U}_L$ and $\mathbf{U}_R$ from its neighbours to approximate the numerical fluxes ($\tilde{\mathbf{F}}$ and $\tilde{\mathbf{G}}$) at its interfaces. Each flood agent autonomously make a self-evaluation of the coordinate data, i.e. x and y, received from its neighbours via a logical argument formulated by if-then conditional statements. This enables flood agents to locate the exact location of its neighbours, particularly to evaluate whether the information is received from the north, east, south or west. Based on the location of the neighbouring agents, each flood agent then decides whether to use the data on the right ($\mathbf{U}_R$) or left side ($\mathbf{U}_L$) of its interfaces. After acquiring the required $\mathbf{U}_L$ and $\mathbf{U}_R$ from the neighbouring agents, each flood agent is then set to evaluate the numerical fluxes at its

interfaces ($\tilde{\mathbf{F}}_{East}$, $\tilde{\mathbf{F}}_{West}$, $\tilde{\mathbf{G}}_{North}$, and $\tilde{\mathbf{G}}_{South}$). Once these fluxes are concurrently evaluated by all the flood agents, they use Eq. (3.4) to evaluate **U** in the next iteration of the simulation ($\mathbf{U}^{update}$).

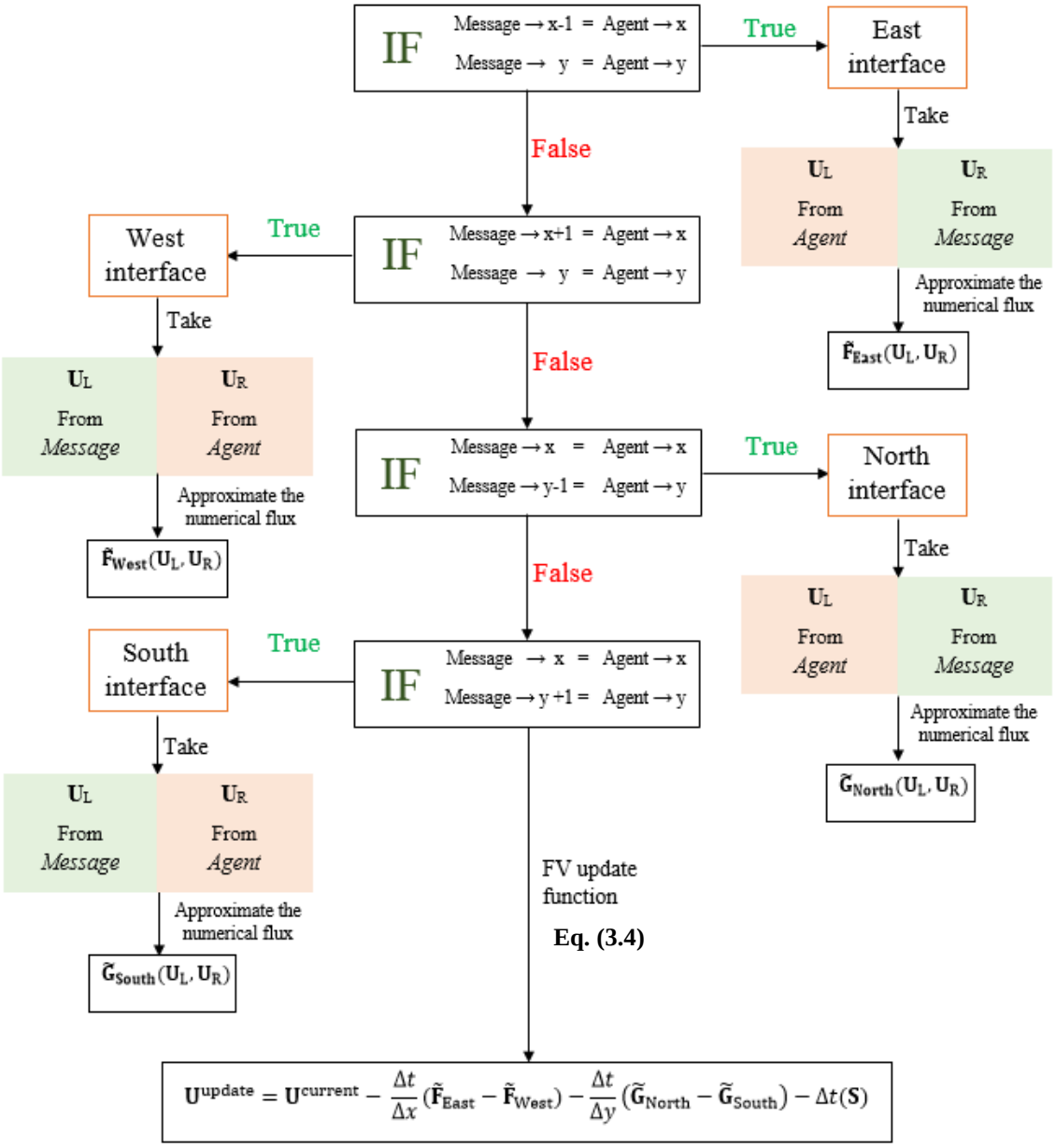

Figure 3.3: The algorithm coded in functions.c to enable each flood agent use appropriate neighbouring flow variables for approximation of the fluxes at its interfaces and update its state via the solution of Eq. (3.4). The numerical fluxes at east, west, north and south interfaces are denoted by $\tilde{\mathbf{F}}_{\mathrm{East}}$, $\tilde{\mathbf{F}}_{\mathrm{West}}$, $\tilde{\mathbf{G}}_{\mathrm{North}}$, and $\tilde{\mathbf{G}}_{\mathrm{South}}$ and the current state of the flow variables is denoted by $\mathbf{U}^{\mathrm{current}}$ and in the subsequent time-step this is denoted by $\mathbf{U}^{\mathrm{update}}$.

3.3.3 Updating the state of flood agents located at the boundaries

As the flood agents located at the boundaries of the computational grid are not able to obtain the required information from at least one of their sides, they use their own information to calculate the fluxes at the interfaces. This is done by temporarily reconstructing the missing $\mathbf{U}_L$ and/or $\mathbf{U}_R$ at any of the north, east, south and west boundaries denoted by $\mathbf{U}_{NORTH}$, $\mathbf{U}_{EAST}$, $\mathbf{U}_{SOUTH}$ and $\mathbf{U}_{WEST}$ (see the example in Fig 3.4). Figure 3.4 illustrates an example of how a flood agent located at the east boundary uses the local face variables within the numerical flux approximation function ($\tilde{\mathbf{F}}$) to produce the reflective and transmissive behaviour of water flow at a wall or open boundary, respectively. The local face variables are initially assigned with the agent's state variable **U** and they are also necessary to avoid memory access conflict due to the parallel computations on FLAME GPU.

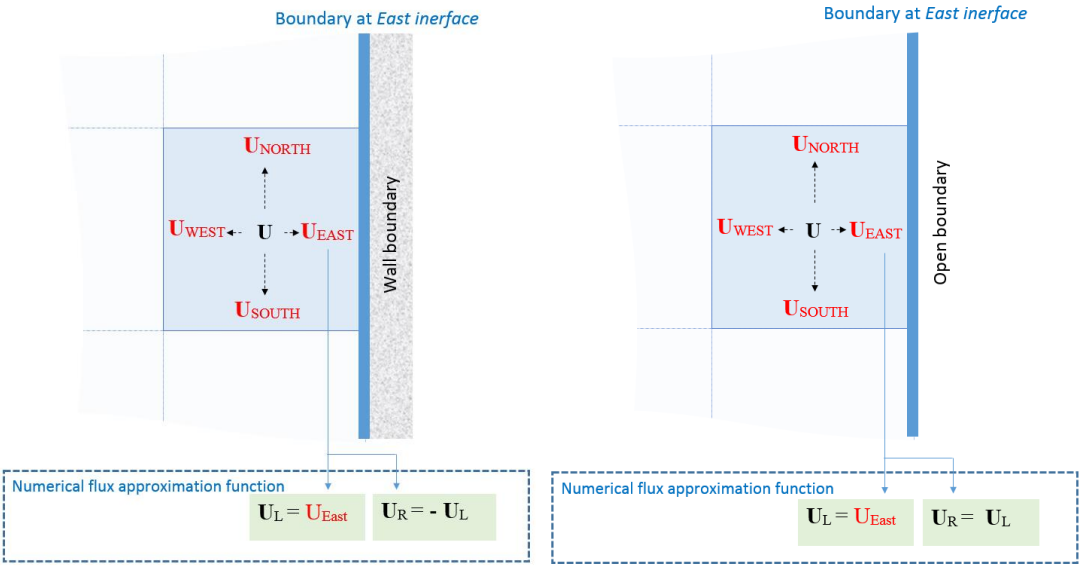

(a) (b)

Figure 3.4: Illustration of a how the missing $\mathbf{U}_R$ is reconstructed via a $\mathbf{U}_{EAST}$ local face variable at the east interface of a flood agent that is located at the east boundary of the computational grid to produce: (a) wall (or reflective) and (b) open (or transmissive) boundary conditions.

More details and guides regarding the description and modification of functions.c and XMLModelFile.xml for implementation of the hydrodynamic model on FLAME GPU are provided in Appendix B.

3.3.4 Evaluation of the hydrodynamic model implementation

The hydrodynamic model's numerical scheme (Wang et al., 2011) has already been validated for a wide range of applications, varying from academic tests (e.g. in Kesserwani and Sharifian (2020)) to real-world applications (e.g. in Xia *et al.* (2019)), and also it has been used in industry-standard flood models, such as TUFLOW-FV (BMT-WBM, 2018) and Infoworks ICM (Lhomme et al., 2010). The purpose here is to evaluate the robustness of this well-established formulation when implemented in a non-sequential manner on FLAME GPU against the outputs obtained from the standard sequential implementation the CPU. To validate the non-sequential implementation, two symmetrical dam-break flow tests are selected for which alternative predictions are available.

The first test, Test 1, considered symmetric 2D water propagation over a flat, frictionless, and initially wet area, and the second test, Test 2, involved a wave propagation over a rough, initially dry area including three mounds. The simulations on FLAME GPU were conducted on a Dell OptiPlex 990 Desktop PC with an Intel Core i7-2600 CPU, 8 GB installed RAM and an Nvidia Quadro K600 graphics card that has 192 CUDA Parallel-Processing Cores and 1 GB GPU Memory. The spatial domain for both the test cases is characterised by a grid of 128 × 128 flood agents.

- **Test 1: Radial dam-break flow**

This test is often used to verify the implementation of newly developed shock-capturing flood models (Toro, 2001; Wang *et al.*, 2011). The wave propagation happens after instantaneous removal of an imaginary cylinder-shaped dam located in the centre of a 40 m × 40 m square area, causing a circular wave moving outwards from the centre. The thin 2.5 m radius circular wall of this dam retained an initial column of water 2.5 m deep. The rest of the area outside the dam is covered with 0.5 m of still water. A reference solution was produced by solving the SWE along the radial direction $r = \sqrt{x^2 + y^2}$ (Toro, 2001) by a second-order accurate scheme over a fine mesh made of 1001 × 1001 rectangular elements (Wang *et al.*, 2011). Figure 3.5 compares the outputs produced by the non-sequential hydrodynamic model on FLAME GPU to those produced by the sequential counterpart on MATLAB and the reference solution, in terms of water depth (h) and unit-width discharge ($q = hu$) cross sections along the radial direction at times t = 1.4 s and t = 4.7 s (following Toro 2001 and Wang *et al.*, 2011). The predicted water depth and discharge preserve the radial symmetry at

both output times t = 1.4 s and t = 4.7 s, and the outputs of the non-sequential hydrodynamic model were identical to those the sequential counterpart, both agreeing well with the reference solution. The discrepancies relative to the reference solution are expected as the latter was computed on a mesh resolution that is 8 times finer and using a higher-order accurate solver.

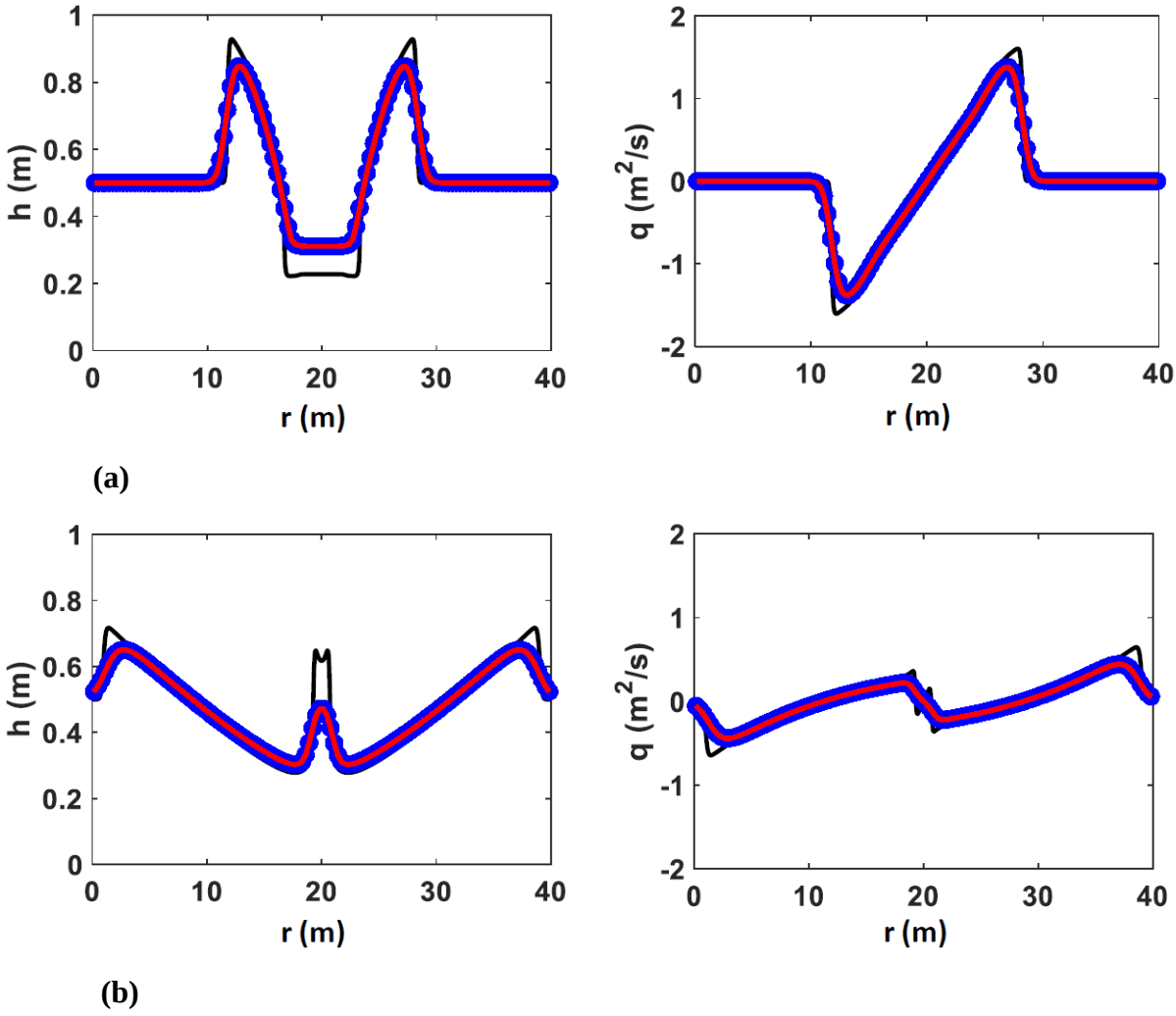

Figure 3.5: Profiles of water depth and unit-width discharge simulated by the non-sequential hydrodynamic model on FLAME GPU (red line) against those simulated by the sequential model counterpart on MATLAB (blue circle-marked line) and the reference solution (solid black line).

- **Test 2: Dam-break flow over terrain with wetting-and-drying**

The hydrodynamic model on FLAME GPU was then applied to reproduce dam-break flows over a rough terrain with uneven ground elevation. This test was used to evaluate the robustness of its formulation implementation relevant to handling wetting-and-drying and step-terrain slopes. It assumes a dam-break wave propagating over a 75 m × 30 m closed area with an initially dry floodplain including three mounds. The imaginary dam was located along x = 16 m blocking an initial body of water with a height of 1.875 m. The roughness is represented by Manning coefficient n_M = 0.018 s $m^{-1/3}$. Figure 3.6 (left) shows the simulated water surface elevation produced at the same output times as the results in Huang *et al.* (2013) shown in Fig. 3.6 (right). As shown in Fig. 3.6, the outputs delivered by the non-sequential hydrodynamic model on FLAME GPU were similar to those of Huang *et al.* (2013), both demonstrating the capability to capture wave reflections, wetting-and-drying fronts, and to conserve mass as the dam-break flood ultimately settles decelerated by friction effects. Note that the reason for the discrepancies is that Huang *et al.* (2013) used triangular mesh structure for the hydrodynamic solver; whereas, the hydrodynamic model on FLAME GPU uses quadrilateral grid structure.

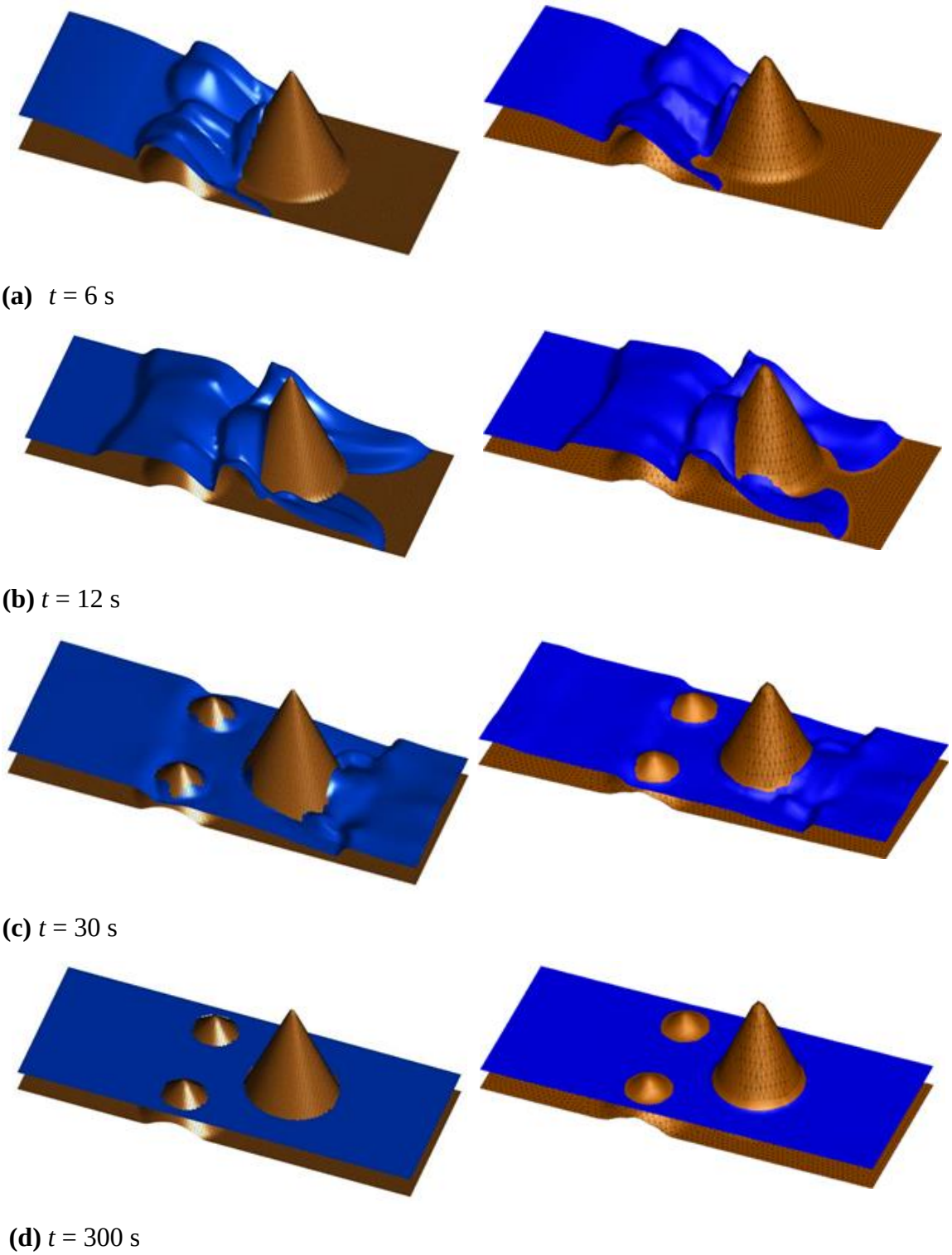

(a) t = 6 s

(b) t = 12 s

(c) t = 30 s

(d) t = 300 s

Figure 3.6: Dam-break flow over terrain with wetting-and-drying. Free-surface elevation maps simulated by the non-sequential hydrodynamic model on FLAMEGPU (left) compared to the simulated results reported in Huang *et al.* 2013 (right).

3.4 Dynamic coupling with a pedestrian evacuation model

To couple the hydrodynamic model with a pedestrian model, the properties of the hydrodynamic model were integrated into a pedestrian model that has already been implemented on FLAME GPU (Karmakharm *et al.,* 2010). The coupling process involves merging the flood agents' descriptions within the pedestrian model's XMLModelFile.xml and the flood formulations, i.e. SWE solution including Eq. (3.4), into the pedestrian model's functions.c behavioural script.

3.4.1 Pedestrian model specification

The selected pedestrian simulation model is built upon a SFM formulation to govern the movement of pedestrian agents and their interactions with each other and with the environment features (Helbing and Molnar, 1995; Helbing et al., 2000). Pedestrian agents are described as continuous space agents as they can change position (represented as a continuous value) in space and over time. The SFM formulation is embedded within the functions.c executable for all the pedestrian agents updating their states in space and time. Aiming from SFM capability, the space between pedestrian agents is controlled by each one's perceptive steering forces (Karmakharm *et al.,* 2010), which ensures that the pedestrian has a physical radius given its continuous location position. In the meantime, the pedestrian agents receive information from the navigation agents that influence their way-finding decisions from the navigation map (Jiang *et al.* 2020). The navigation agents are defined to be of discrete type with fixed coordinates on a grid that forms a navigational field. Each singular navigation agent stores information that a pedestrian requires to carry on with their movement at the discrete location. In particular, this information conveys the direction to key destinations and their location on the map (e.g. the entrances, exits, and walkable pathways), and obstacles that pedestrian agents must avoid (e.g. walls and terrain blocks). For this study, a grid resolution of 128 × 128 navigation agents is defined to provide pedestrian agents with the information on the location and direction of the entrances/exits and the terrain features in the study area.

3.4.2 Communications between flood agents and pedestrian agents

The information stored in the pedestrian agents' memory and the flood agents' memory is passed between them through the FLAME GPU's agent-agent communication mechanism previously explained in Sec. 2.6.1. To do that, the navigation agents are used as the shared communication interface that are set to receive the information of a pedestrian agent at their location and send back an update to the flood agent and vice versa. For this purpose, the grid of navigation agents are defined in coincident to the grid of flood agents. Through this communication mechanism, a set of two-way interactions between the pedestrian agents and the flood agents have been formulated.

The information that is shared from each flood agent to the coincident navigation agent includes its position x (m) and y (m), terrain properties in terms of height z (m) and Manning's roughness parameter n_M (s $m^{-1/3}$), and the states of the floodwater variables in terms of water depth h (m) and velocity components $u = q_x/h$ (m/s) and $v = q_y/h$ (m/s). Which in turn, the navigation agent converts the information received from the flood agent into a flood Hazard Rate (HR) quantity, which is retrieved by any pedestrian agent walking in its spatial area. The HR quantity in pluvial or fluvial flooding with low probability of debris could be estimated as $HR = (V + 0.5) \times h$ where V stands for the velocity magnitude estimated as $V = \sqrt{u^2 + v^2}$ (Ramsbottom *et al.*, 2004, Kvočka *et al.*, 2016). Depending on the categorisation of the HR by the UK Environment Agency (EA), pedestrian agents are set to autonomously flag themselves with one of the four flood risk states: 'low' ($0.0 < HR < 0.75$), 'medium' ($0.75 < HR < 1.5$), 'high' ($1.5 < HR < 2.5$) and 'highest' ($2.5 < HR < 20$).

Pedestrian agents are also assigned a role and accordingly pass certain information to the navigation agent where they are located at a certain time. This is to incorporates any local change in the terrain properties caused by pedestrians' presence or actions, namely: due to local and temporal grouping of *evacuees* in certain zones leading to increasingly higher surface roughness; or, due to sandbagging by *responders* leading to a local change in the height of the terrain. The navigation agent processes the information on such changes, received by the pedestrian agents, and passes them back to the hydrodynamic model to dynamically updates the surface roughness's Manning's parameter (n_M) or the ground elevation (z) in the hydrodynamic model. Then, it passes the updated terrain parameters back to the flood agent at its equivalent position. Next subsection describers the behavioural rules governing the interactions between the flood and pedestrian agents.

3.4.3 Implementation of the primary behavioural rules

This section explains the behavioural rules incorporated within the pedestrian model's functions.c script to process the information dynamically exchanged between the flood, navigation and pedestrian agents. Two different sets of pedestrian behavioural rules are implemented depending on the *role* assigned to the pedestrian agents, i.e. either to be *evacuees* or *responders*. *Evacuee agents* are pedestrian agents evacuating *during a flood* without a prior warning. When there is no floodwater, the walking speed of the pedestrian agents is set to 1.4 m/s to represent the average human walking speed (Wirtz and Ries, 1992; Mohler *et al.,* 2007). Nonetheless, the existing behavioural rules already governed by the SFM allow the pedestrian agents to locally increase or decrease their walking speed (e.g. when they need to abruptly change direction to avoid collisions with each other or with existing obstacles located in the study area). Once a non-zero water depth is received by any navigation agent on the navigation map (i.e. from the flood agent at its same location), the pedestrian agents will no longer be entering the study area, and those remaining, i.e. the evacuee agents, will be leaving to an emergency exit destination (specified by the user on the navigation map). Evacuee agents in flooded zones receive the flood HR quantity from the navigation agents where they are located. A *flood risk state* is then assigned to each of these evacuee agents based on the four HR ranges used by the UK Environment Agency (2006) for identifying the level of flood risk to people. These ranges define the *low*, *medium*, *high* or *highest* flood risk state of HR (see Table 3.1). Evacuee agents are also assigned a *walking speed state* that is assumed to be constant per *flood risk state*, such that:

- When an evacuee agent is in a low flood risk state, it is able to accelerate its escape via a brisk walk that is on average 1.8 m/s (Mohler *et al.* 2007);
- When an evacuee agent is in a medium to high HR flood risk state, it needs to decelerate walking speed to 0.9 m/s and 0.45 m/s, respectively. These walking speeds are within the average range of human walking speeds in floodwater (Lee *et al.* 2019); and

When an evacuee agent is at the highest flood risk state, it cannot walk in floodwater due to instability issues and thus has a waking speed of 0 m/s.

Table 3.1: States of evacuee pedestrian agents in floodwater selected based on the ranges for HR tabulated in the flood hazard matrix of the UK Environment Agency (2006).

Hazard Rating (HR) ranges		**Flood risk state**	**Walking speed state**
From	To		
0	0.75	Low - safe to walk	1.8 m/s - brisk walk
0.75	1.5	Medium - mildly disrupted	0.9 m/s - slow walk
1.5	2.5	High - disrupted	0.45 m/s - slower walk
2.5	20	Highest - trapped	0.00 m/s - no walk

Meanwhile, the evacuee agents that are present on the flooded navigation agents are counted: their number, N_p, is used to locally update the Manning's roughness coefficient n_M in the hydrodynamic model as $n_M = n_M + N_p\, n_M$ (see Fig. 3.7-left). The updated coefficient n_M is then passed back to the flood agent at the navigation agent's location to represent the effects of the presence of individuals and groups of people on floodwater hydrodynamics. For this study, the initial n_M parameter is set to be equal to 0.01 s $m^{-1/3}$, representative of clear cement (Chow, 1959), and no more than 20 evacuee agents are allowed to simultaneously occupy the area of a navigation agent, which means that any local amendment in n_M cannot exceed 0.2 s $m^{-1/3}$.

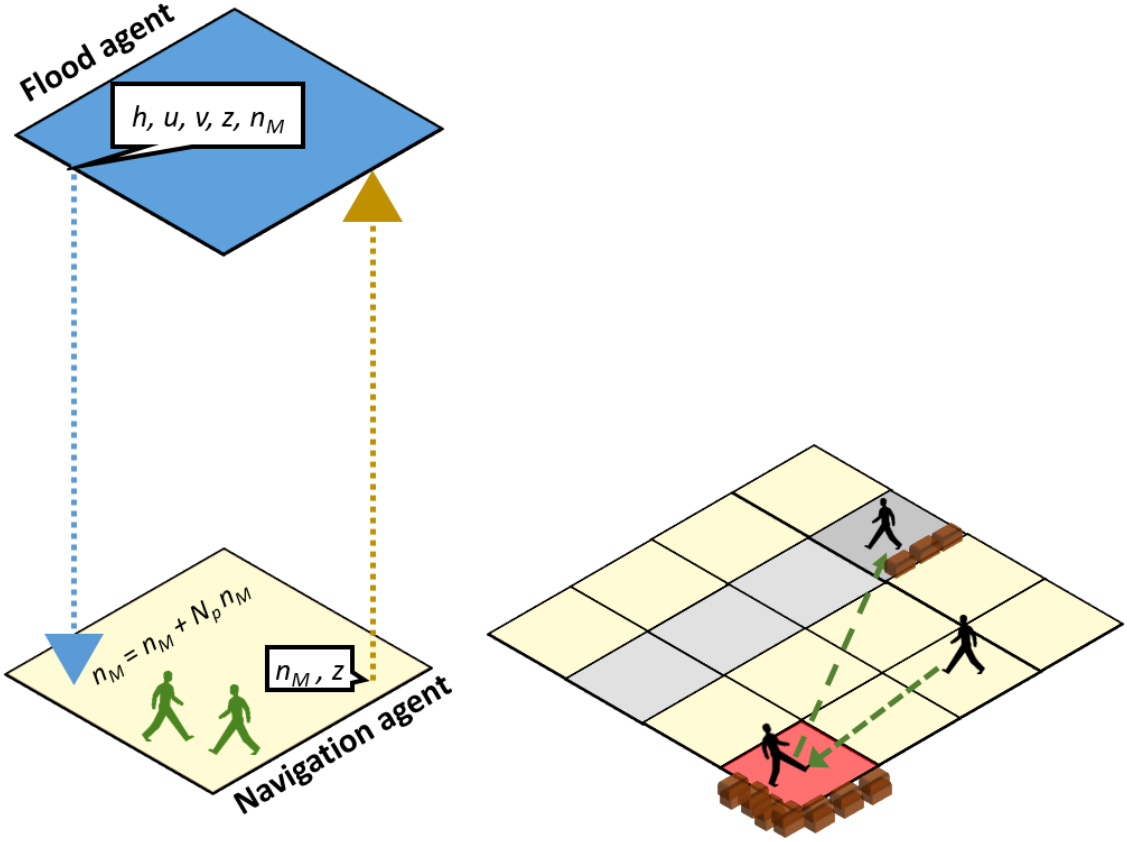

Figure 3.7: Dynamic passing of stored information between a flood agent and pedestrian agents (evacuees) facilitated via the navigation agent that is aligned to the flood agent (left). Procedure for pedestrian agents (responders) deploying a sandbag barrier (right): red navigation agent represents a 'sandbag storage' destination and grey navigation agents represent the deployment destination.

Responder pedestrian agents form a group of the existing pedestrian agents, who are emergency first responders, taking a series of actions to construct a flood barrier within a specified *time window* due to an advanced flood warning. A standard sandbagging procedure is implemented to form the temporary barrier, which is an appropriate choice to support this study. To govern the movement and actions of responder agents, destinations of the sandbag storage and of the location of flood barrier are initially specified on the navigation map (Fig. 3.7-right). Responder agents get information to walk to the location of the sandbag storage. Once they reach it, they are set to wait for 30 seconds representative of a picking up duration (specified), and then pick up the information on the dimension of a sandbag from the navigation agents spanning the sandbag storage location (Fig. 3.7-right). Responder agents are then redirected to carry up this information to the navigation agents spanning the

temporary flood barrier, which are set to receive it after a wait of 30 seconds representative of a safe drop out duration. The 30-second wait for picking up and dropping time is assumed here; but, as it is case dependent, the users may select other values depending on the case study. Responder agents are set to go and share their information with one (specified) first navigation agent representative of the starting location for the deployment. As the dimension of a sandbag is smaller than the area of a navigation agent, the first navigation agent is set to accumulate the received information until it has enough to cover one horizontal layer of sandbags all-over its area. Then, the first navigation increments the ground elevation parameter, z, by one unit of sandbag thickness. The process then moves to the adjacent navigation agent spanning the flood barrier's location, and so on until the single layer of sandbags reach either a wall or an obstacle existing in the study area. Responder agents then repeat the overall process N_L times, until all the navigation agents spanning the flood barrier's location are filled up with N_L (specified) layers of sandbags. After N_L rounds, the height of the ground elevation parameter at the navigation agents spanning the flood barrier's location has become $z \times N_L$. This new height for the ground evaluation is then passed to the flood agents at their aligned location (Fig. 3.7-left), i.e. to incorporate the changes from the presence of sandbags in the hydrodynamic model.

3.5 Preliminary evaluation of the coupled flood-pedestrian model on FLAME GPU

A synthetic case study was specifically designed to evaluate the coupled flood-pedestrian model in capturing the dynamic interactions between pedestrians and floodwater flows. The case study involves a shopping centre filled with people exposed to flooding. It distinguishes two independent scenarios, one with the *pedestrians* as *evacuees*, and another involving them as *responders*. Scenario 1 assumes that there is no early warning nor an early evacuation plan, and focuses on the behaviour of pedestrians as evacuees during the propagation of the floodwater while moving to an emergency exit (Fig. 3.8a). Scenario 2 focuses on mitigation options on the number of the responders and thickness of a flood barrier needed for a safe and effective deployment upstream of the emergency exit (Fig. 3.8b). Scenario 2 also requires a specified lead time, taken to be 12 hours. This time was selected assuming severe flood warnings were issued for the areas surrounding the shopping centre, though the

shopping centre had remained open (e.g. as with the case of Meadowhall shopping centre during November 2019 floods, which opened despite an early warning of half-a-day (www.bbc.co.uk/news/uk-50341846).

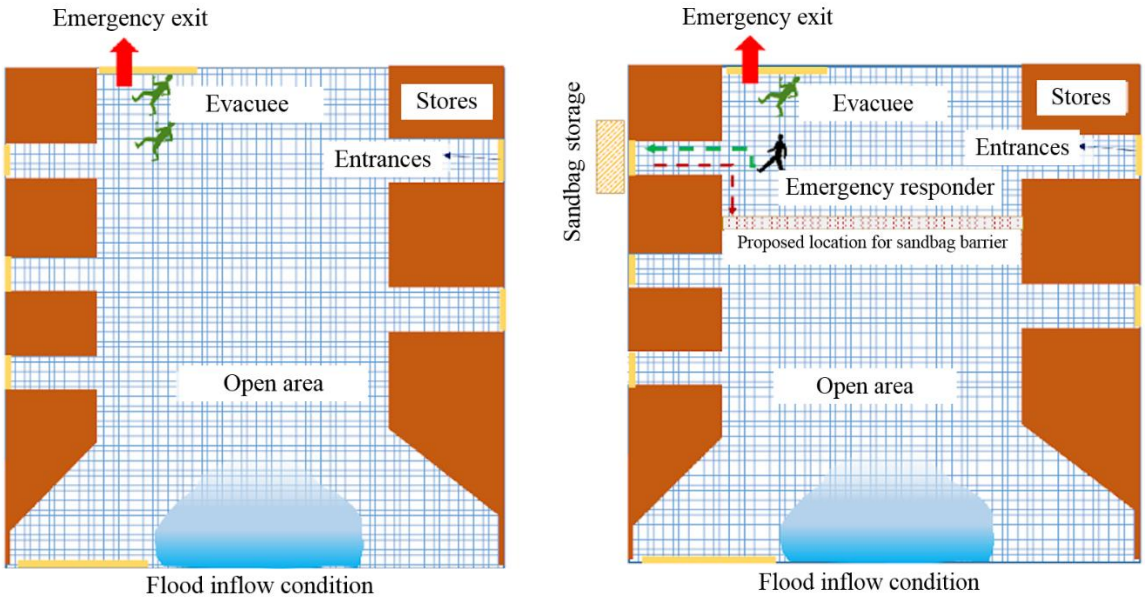

(a) Scenario 1 **(b)** Scenario 2

Figure 3.8: Sketch of the hypothetical shopping centre with the two scenarios: (a) during a flood evacuation; and, (b) pre-flood intervention. The meshed area in blue indicates the open area and corridors where pedestrians can walk to the entrance doors (coloured in yellow). Once the flood starts in the evacuation scenario, pedestrians will go to the emergency exit (on the north side). The blocks in brown represent terrain features assuming that they are stores and the blue-shaded area in the southern part of the figure shows the location where the floodwater started to propagate. The sandbag storage for the intervention scenario, is located at the end of a corridor on the north-west side, and the location of the proposed barrier is below that corridor expanded towards the stores on the east side, which is represented by a meshed rectangle coloured in red.

- **Shopping centre test case description**

The area of the shopping centre is 332 m × 332 m = 110,224 m^2 (Fig. 3.8), chosen based on the average area size of the UK's 43 largest shopping centres that have more than 70,000 m^2 retail size collected from the reports provided by Gibson *et al.* (2018), Globaldata Consulting (2018), Sen Nag (2018) and Tugba (2018). The shopping centre includes stores, located at the east and west side, separated by corridors linking the entrance doors to an open area. Through these corridors, pedestrians can enter the open area and walk toward their destinations. The open area was assumed to be occupied by a population of 1000 pedestrians (configurable by the user) when there is no floodwater. This average population was assumed in spite of an influx of people entering or leaving from seven entrance doors with an equal probability of one in seven. The total walkable area of the shopping centre, including the open area and the corridors, is equal to 70,350.8 m^2. A population of 1000 pedestrians was selected to give an area of almost 8.4 × 8.4 m^2 for each person. This area allows some areas of the pedestrian space to not be crowded, based on a calculator toolbox of the average space required for individuals in malls (Engineering ToolBox, 2003). The flood propagation was assumed to breach from the southern side along a 100 m width (Fig. 3.8), assuming floodwaters had reached the shopping centre after a severe inundation from a river nearby. When flooding started in Scenario 1, in response to an announcement, pedestrians had started the evacuation to the emergency exit located at the northern side (Fig. 3.8a), which was set to remain open during evacuation.

In Scenario 2, a group of the pedestrians were responders, tasked to deploy a local barrier at the location specified in Fig. 3.8b and within a time window that did not exceed the specified lead time of 12 hours. The area where the intended barrier was 168.6 m long and it has the same width as a navigation agent (i.e. 2.59 m for a grid of 128 × 128 navigation agents). The responders were set to build the barrier by placing layers of sandbags in this area. The dimension of a sandbag was based on standard measurements (Williamson, 2010; Padgham *et al.*, 2014), to be 40 cm long × 30 cm wide × 25 cm thick. This means that 3484 sandbags were needed to form a one-layer thick barrier, which is a close estimate to the sandbag numbers predicted by online calculation tools (e.g. 3318 sandbags, https://sandbaggy.com/blogs/articles/sandbag-calculator), and recommended in the UK official guidance (Environment Agency, 2009).

In both scenarios, the flood-pedestrian simulator model within the FLAME GPU was executed with a resolution of 2.59 m × 2.59 m for the grids of navigation and flood agents on the same desktop PC reported in Sec. 3.3.4. When floodwaters occupy the study area, the time-step is calculated dynamically from the hydrodynamic model under the CFL condition (CFL number = 0.5); otherwise, the 1.0 s time-step of the pedestrian model is selected by default.

- **Hydrodynamic inflow condition**

An *equivalent triangular hydrograph* was used to represent the flooding inflow. This is a standard method reported in hydrology manuals (e.g. Module 207, USDA, document 'stelprdb1047307') and computational hydrology textbooks (e.g. Adrien (2003)). The inflow hydrograph was characterised by a flow peak, Q_{peak}, and a duration, t_{inflow}. Four choices of a flooding inflow hydrograph were explored based on the assumption that the volume of floodwater entering the shopping centre is predetermined. The volume of floodwater was assumed based on the inflow characteristics of the Norwich inundation case study, which was reported to encompass a population of 500 to 2000 individuals that were flooded in a residential area located 50 m away from a river inundation (Sec. 6.3.3, document FD2321/TR1, Environment Agency, 2006). Because of its resemblance to the case of the shopping centre, it was considered to calibrate the inflow hydrographs, Q_{peak} for 60 min of flooding, i.e. estimated according to initial water depth and velocity magnitude of h_{inflow} = 1 m and v_{inflow} = 0.2 m/s, respectively. This corresponds to an initial inflow hydrograph with (Q_{peak}, t_{inflow}) = (20 m^3/s, 60 min) for which $Q_{peak} = v_{inflow}\, h_{inflow}\, B$ where B = 100 m is the length of the inflow breach. Based on these inflow characteristics, a fixed floodwater volume of $V = 0.5 \times Q_{peak} \times t_{inflow}$ = 36,000 m^3 is considered to be released by the other three inflow hydrographs, which are devised to produce more severe floods. This is done by recursive halving of t_{inflow} alongside doubling of v_{inflow} (h_{inflow} = 1 m is fixed), leading to inflow hydrographs with: (Q_{peak}, t_{inflow}) = (40 m^3/s, 30 min), (80 m^3/s, 15 min) and (160 m^3/s, 7.5 min), respectively, which are shown in Fig. 3.9.

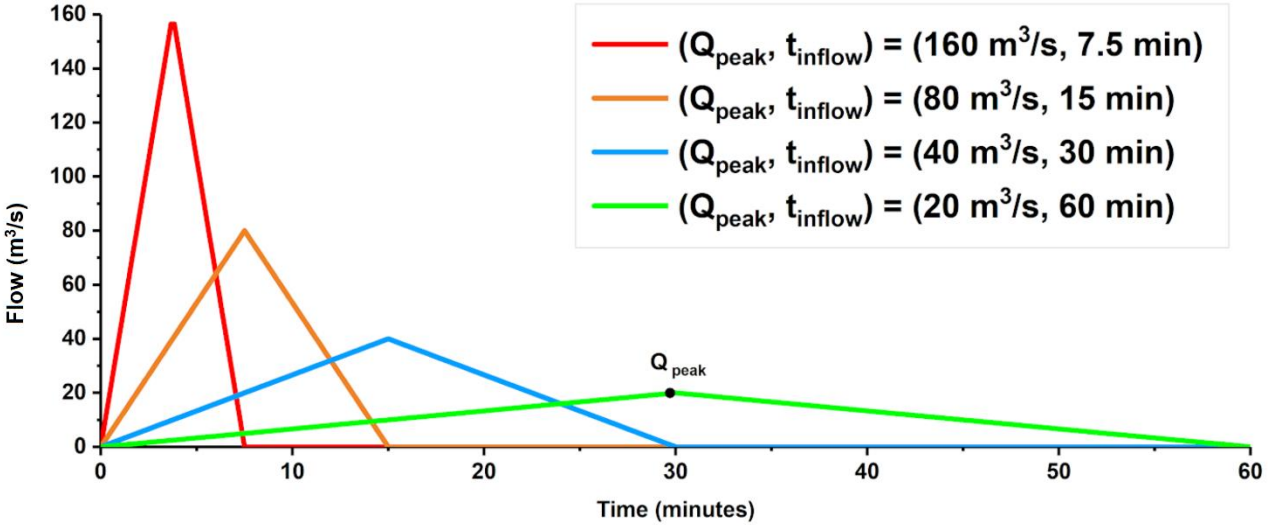

Figure 3.9: Flooding inflow hydrographs defined according to four different flow peaks, by fixing the volume of water that can be released into the shopping centre and, doubling the discharge peak (Q_{peak}) while halving the duration of its occurrence (t_{inflow}).

To analyse flood event severity resulting from the four selected inflow hydrographs, the hydrodynamic model within FLAMEGPU was executed with each of the hydrographs. For all simulation runs, the model was applied with slip boundary conditions for the northern side and wall boundary conditions for the eastern and western sides. Figure 3.10 shows the time history of the maximum HR calculated from the model outputs during 60 min. The inflow hydrographs with (20 m^3/s, 60 min), (40 m^3/s, 30 min) and (80 m^3/s, 15 min), show a maximum HR below 2 and only exceeding 1 between 4 to 6 min. This indicates that these inflow hydrographs lead to flooding that at worst disrupt a few pedestrians for a very short duration of 2 min. In contrast, the inflow hydrograph with (160 m^3/s, 7.5 min) demonstrates the most severe flooding event with significantly higher maximum HR values occurring over a 10 min, i.e. indicative of potentially disruptive propagation of floodwaters in the shopping centre. Note that because this study aims to explore people effects on local flood hydrodynamics, considering inflow hydrographs that would lead to HR > 7 (i.e. indicative of loss of life) was out of scope. Hence, only the inflow hydrograph with (160 m^3/s, 7.5 min) was considered when evaluating the flood-pedestrian model for the proposed Scenario 1 and Scenario 2.

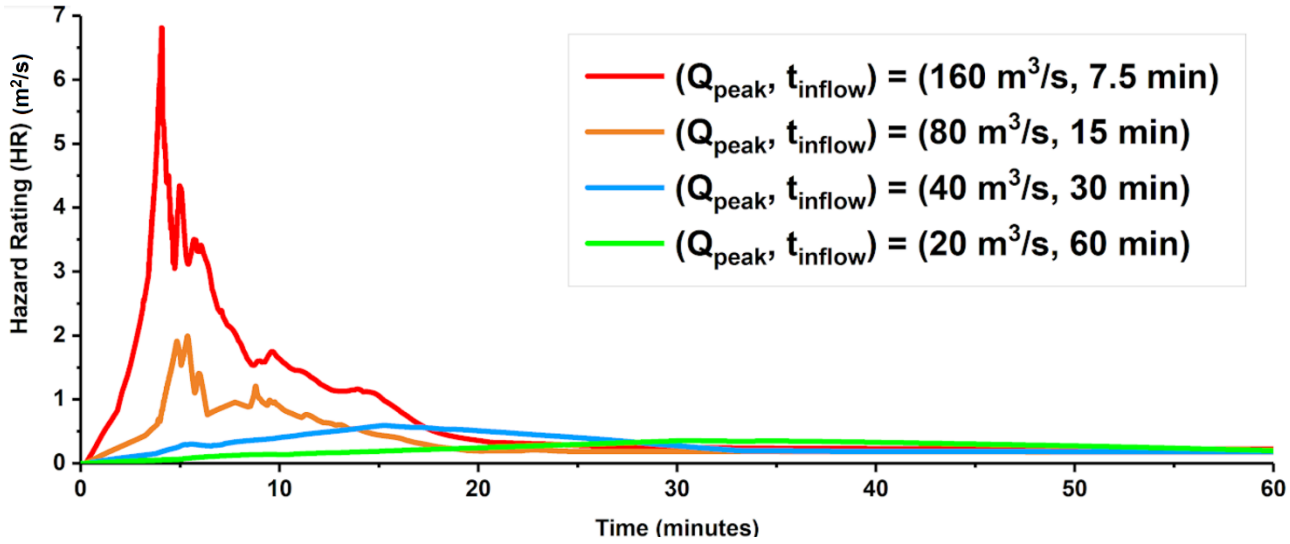

Figure 3.10: Time history of the maximum HR calculated from the model outputs of the hydrodynamic model on FLAMEGPU run for the four selected inflow hydrographs.

3.5.1 Simulation of Scenario 1: evacuation during a flood

The coupled flood-pedestrian model was applied to simulate Scenario 1. The pedestrian model was set to have a constant rate of 10 entering/leaving pedestrians per entrance/exit such that to maintain a total of 1000 randomly walking pedestrians before flooding happens. A pre-flooding duration of t = -5 min was set in the hydrodynamic model, by zeroing Q_{peak}, in order to allow spreading of the pedestrians all over the walkable area (blue zone in Fig. 3.8a). When flooding entered the walkable area, at t = 0 min, the pedestrian agents were scheduled to become evacuees. The simulation was set to terminate when all evacuees left the walkable area via the emergency exit (Fig. 3.8a). In a single run, the coupled flood-pedestrian model was set to record, every 0.1 min, the information stored in the flood agents (coordinate, water depth, water velocity and HR) and the pedestrian agents (coordinate and the HR-related flood risk states). Two runs were performed one ‘with’ and one ‘without’ the effects of people on local floodwater hydrodynamics, through the changes in the bed roughness as previously explained in Sec. 3.4.2. The time history of the outputs produced by the two runs are compared in Fig. 3.11, in terms of statistics of the flood risk states of evacuees (see in Table 3.1).

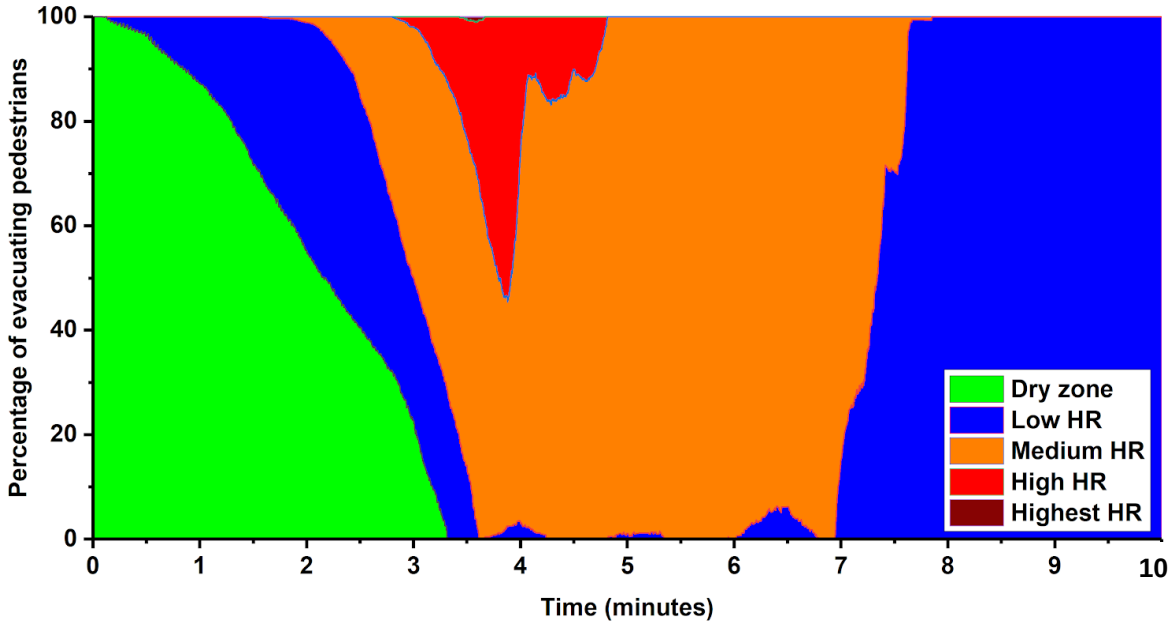

(a)

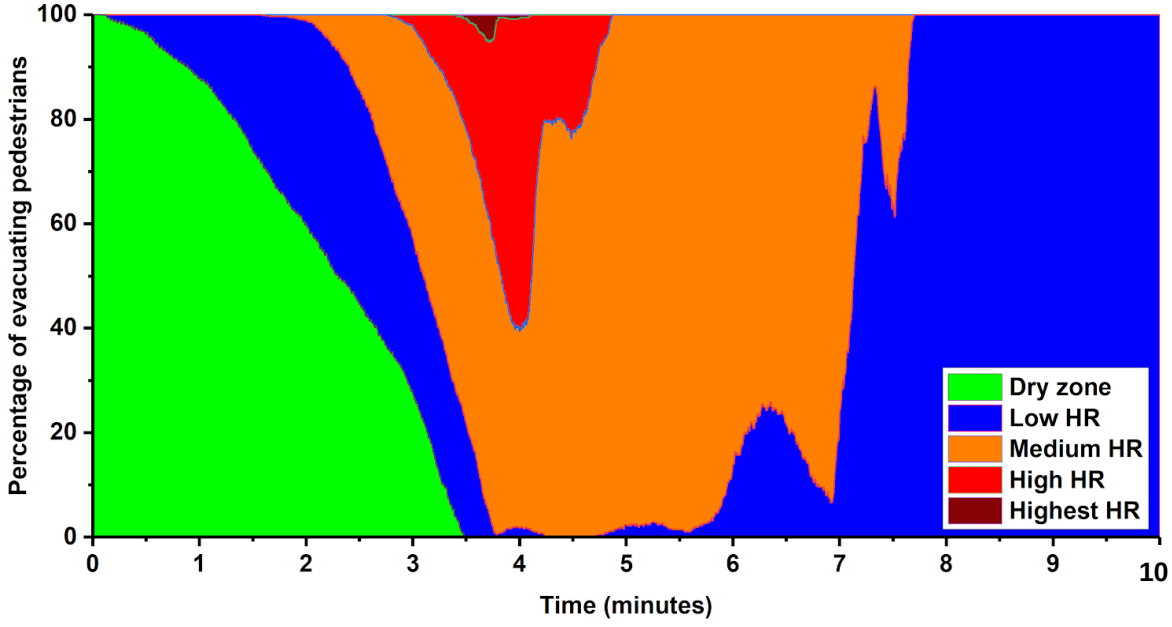

(b)

Figure 3.11: Stack charts illustrating the 'flood risk states' (Table 3.1) of the pedestrians as they evacuate during 10-minute flooding: (a) without, and (b) with accounting for the effects of people on local floodwater hydrodynamics.

Before 2.8 min, both runs led to almost similar statistics indicating that 60 % of the evacuees were either in a dry zone or in a state of low HR, while the remaining 40 % were at most in a medium HR state. After 2.8 min and before 4.9 min, at least 55 % of the evacuees had medium to highest HR states, namely in the vicinity of 3.6 min where 5-8 % more pedestrians were identified to be in high to highest HR states for the run 'with' the effects of people on local floodwater hydrodynamics (compare Figs. 3.11a and Fig. 3.11b). For the latter run, more pedestrians with the highest HR states were noted, and this was likely caused by the relative local increase in the HR due to the grouping of pedestrians at critical zones and times (see also Fig. 3.12 and its discussions). After 4.9 min and before 8.0 min, the majority of the evacuees had a medium HR state, namely in the vicinity of 6.3 min. Over this duration, 25 % more pedestrians were found to be in a state of low HR, for the same run 'with' the effects of people on local floodwater hydrodynamics (compare Fig. 3.11a and Fig. 3.11b), due to a relatively local decrease in the HR. After 8.0 min, all the evacuees had a low HR state, irrespective of the run and were able to continue the evacuation process until it ended after 10 min. Notably, as the evacuees become congested on their way to the emergency exit, they affect their surrounding evacuees to become: either in a *higher* risk state of HR when the evacuees were in a *state of high to highest HR*, or in a *lower* risk state of HR when the evacuees were *in a state of medium HR*.

This aspect can be closely explored in the spatial plots of Fig. 3.12 for the runs 'without' and 'with' the effects of people on local flood hydrodynamics, respectively, after 3.6 and 6.3 min (Fig. 3.12a and Fig. 3.12b). The plots include the 2D spatial flood maps in terms of HR and the evacuees. Comparing the left and right columns in Fig. 3.12a, a clear difference can be observed between the distribution of the evacuees and the flood maps in the crowded zones of the shopping centre: around the middle, more evacuees had high to highest HR states and the local flood hydrodynamics was relatively higher. Whereas, closer to the emergency exit downstream, more evacuees had a low HR state indicative of relatively lower local flood hydrodynamics. The latter observation can also be detected when comparing the left and right columns in Fig. 3.12b. Overall, these results indicate that the local synergies between flood and evacuees can dramatically affect flood impact on evacuee states in floodwater.

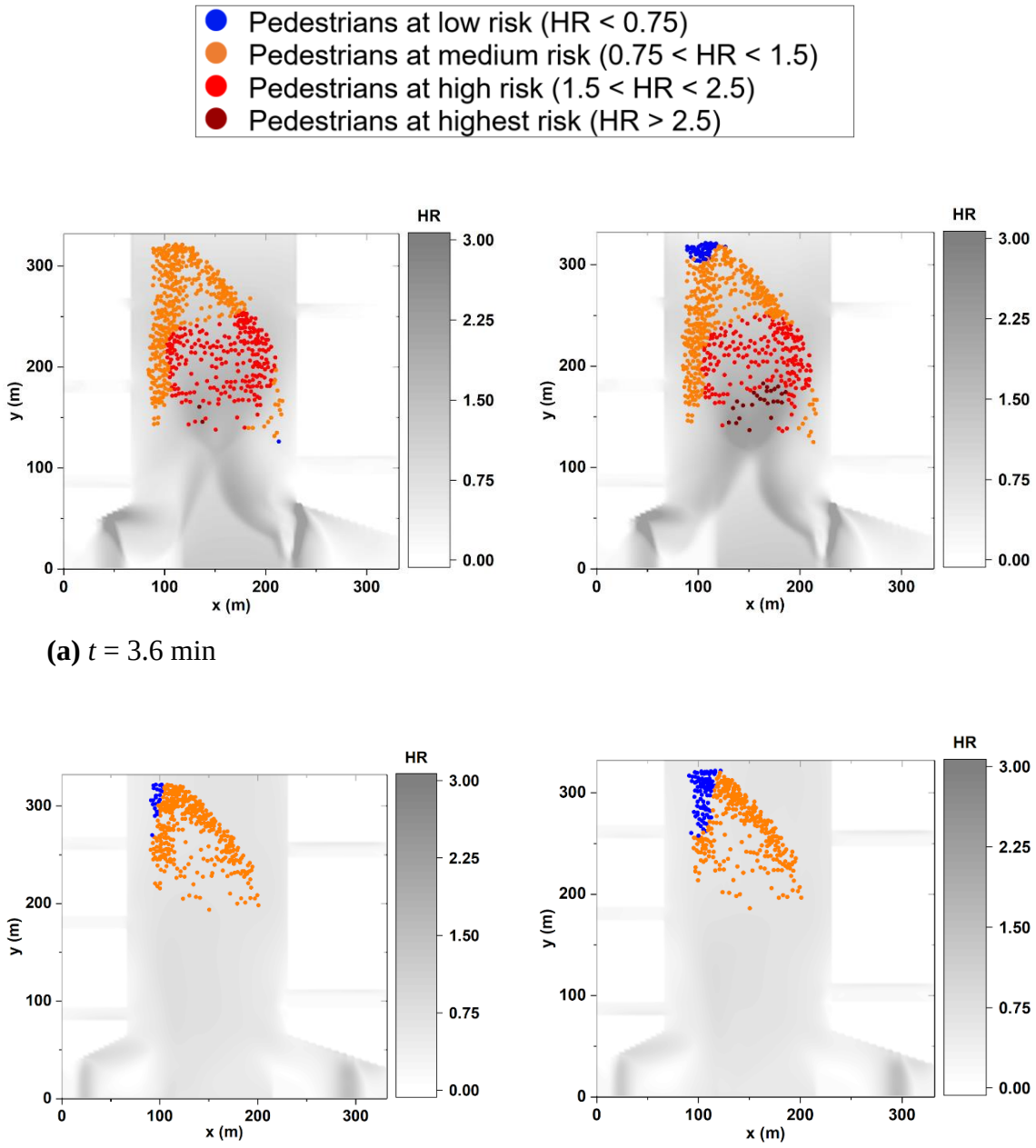

(a) t = 3.6 min

(b) t = 6.3 min

Figure 3.12: Spatial flood maps alongside the distribution of evacuees at (a) t = 3.6 min and (b) t = 6.3 min: Left and right columns contain the plots produced by the run 'without' and 'with' the effects of people on local flood hydrodynamics, respectively.

3.5.2 Simulation of Scenario 2: pre-flood intervention

The coupled flood-pedestrian model was applied to simulate Scenario 2, with the aim to identify a minimum required number of people and thickness for the barrier for a safe and effective deployment within a safety time window of 12 hrs. Four group sizes for the

responders were explored, made of 50, 100, 200, 300 pedestrians, respectively, alongside six layers of thickness for the sandbag barrier. Hence, a total of 24 simulations were run to estimate the deployment time for a barrier up to six-layer thick and considering the four group sizes. Per group size, a first simulation started with the responders evacuating as soon as they had completed a one-layer thick barrier for flood risk analysis to be applied; then, by analogy, a second simulation was run to analyse the case for a two-layer thick barrier, and so on until the case of a six-layer thick barrier was analysed. The analysis also considered the respective changes in floodwater hydrodynamics in relation to the water depth and maximum HR as the barrier's thickness is increased. In Fig. 3.13, the simulated time taken to deploy up to a six-layer thick (sandbag) barrier are shown for the four group sizes for the emergency responders. As shown in Fig. 3.13, within the safety time window ('green' area of less than 12 hours): the group of 50 responders could only deploy a one-layer thick barrier, the groups of 100 and 200 responders could deploy a barrier between three- to five-layer thick, respectively; whereas, the group of 300 responders could deploy up to six-layer thick barrier. It is worth noting that involving higher group sizes may not be realistic and was found to result in efficiency stagnation due to overcrowding. It is worth noting that no significant reduction in deployment times was observed as people-group size increases further. This is likely because of the higher waiting times that was needed in line with higher number of responders due to higher densities around the pickup and deployment points.

Figure 3.14 shows the changes in water depth as the barrier's thickness is increased: water depth downstream of the barrier reduced to around 0.4 m with one-layer thickness, to around 0.3 m with two-layer thickness and to less than 0.2 m with tree-layer thickness and higher. To help assess the level of safety attributed to these water depths, it is further necessary to analyse their respective velocity impacts as recommended by the Environment Agency (2006, page 13).

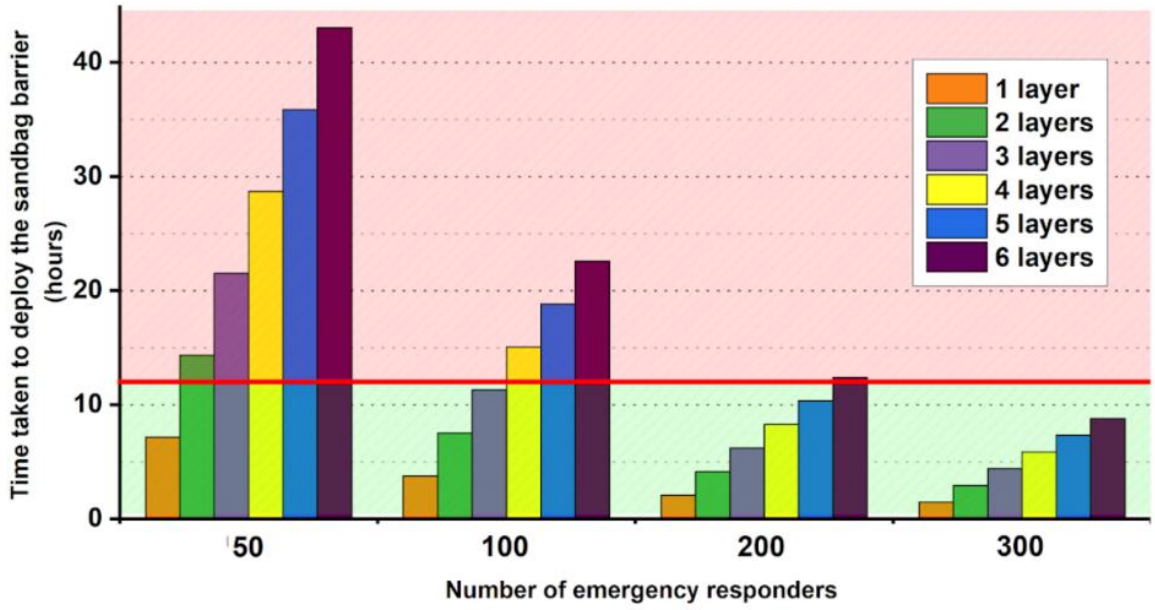

Figure 3.13: Simulated times vs. responders' group size for deploying up to six-layer thick (sandbag) barrier: 'red line' indicates flooding start time below which is safe to deploy (area shaded in 'green') or otherwise unsafe (area shaded in 'red').

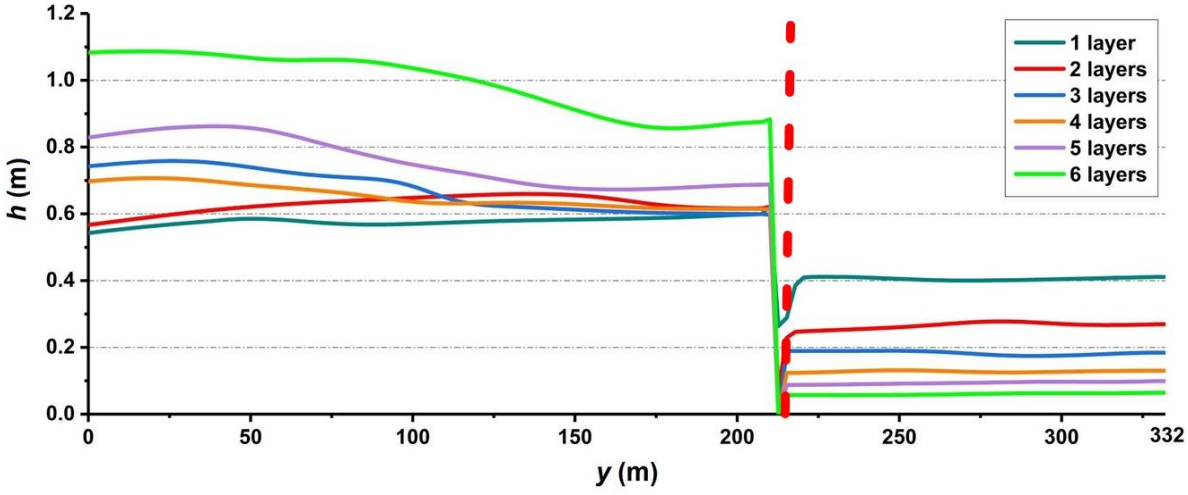

Figure 3.14: Centrelines of 2D water depth maps along *y*-axis after the deployment the sandbag barrier (red dashed line) considering up to six layers of sandbag thickness.

Figure 3.15 illustrates the relative change in maximum HR downstream of the barrier with respect to the barrier's thickness level in terms of number of sandbag layers. After a one-layer thick barrier, a major drop of 91.2 % in maximum HR is observed, which is quite expected relative to having no barrier at all. After two- and three-layer thickness, more relative reduction of 5.3 % and 1.9 %, respectively, is observed for the maximum HR. After four-layer thickness, no further significant reduction in maximum HR is noted (~ 0.4 %), suggesting that there is no point in going beyond three layers to reduce the flood risk to potentially walking pedestrians downstream of the barrier.

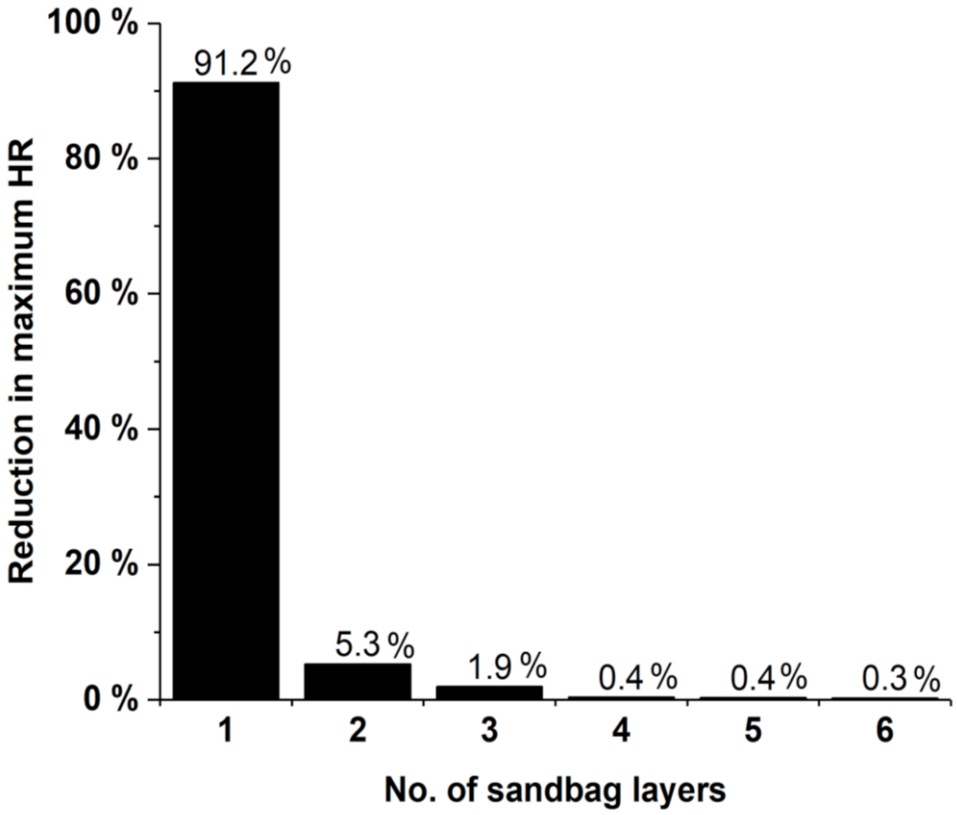

Figure 3.15: Cumulative percentage of maximum HR reduction in line with increased thickness of the barrier in terms of number of sandbag layers.

Overall, the combined analyses of Figs. 3.13-3.15 seem to suggest that a three-layer thick barrier (0.75 m height) would be sufficient to alleviate the flood impacts upstream of the emergency exit of the shopping centre, and its deployment is feasible within less than 12 hrs. by involving a group of responders made up of 100 people.

3.6 Summary and concluding remarks

This chapter provided the description of the methodology used to dynamically couple the hydrodynamic model with the pedestrian model within the FLAME GPU framework. The pedestrian model involved continuous pedestrian agents moving based on the information available on the navigation map formed by a grid of navigation agents while following a standard SFM. A grid of flood agents was coincident with the grid of navigation agents, on which the states of floodwater variables are stored and updated by a hydrodynamic model. Dynamic passing of information across the pedestrian and flood agents was facilitated by the navigation agents. Behaviour rules governing pedestrian interaction with/to the flood hydrodynamics were implemented for two roles that pedestrians can be assigned: *evacuees* moving in floodwater where the presence of individuals and groups of people was incorporated by changing the surface roughness coefficient in the hydrodynamic model; and, *responders* that participate in pre-event sandbagging where the sandbags were incorporated by changing the height of the ground elevation parameter in the hydrodynamic model. The capabilities of the coupled model were evaluated over a synthetic case study of a flooded and densely populated shopping centre for two scenarios: 1) during a flood evacuation to an emergency exit, and; 2) pre-flood intervention to deploy, from sandbags, a temporary flood barrier. The simulation results of Scenario 1 identified that incorporating local effects of evacuees on floodwater hydrodynamics can dramatically affect the flood risk states of evacuee in relatively confined areas. This dramatic change in flooding impact was noted to be extreme: either reduced the risk to the surrounding of a group of people when the people were in low to medium state of flood HR, or increased the risk when people were located in the highest state of flood HR. The simulation results of Scenario 2 provided evidence that the couple flood-pedestrian model can also be used to decide on the required number of people for emergency first responders and the required minimum height for a temporary flood barrier for a safe and effective deployment, alongside a quantification of the resulting level of flood risk reduction.

With the successful implementation and evaluation of the coupled flood-pedestrian model, in line with the achievement of the first objective of this research, in the next chapter, we aim to enrich the simulator with more realistic in-model human behaviour rules and characteristics. Note that this version of the coupled flood-pedestrian model is available online on DAFNI platform (access via https://dafni.ac.uk/project/flood-people-simulator/).

Chapter 4

Enhancement in the characterisation of pedestrians' behavioural rules in and around floodwater

4.1 Chapter overview

This chapter, which aims to address Objective 2, explored the relevance of increasing the level of heterogeneity in the characteristics of pedestrians and sophistication of behavioural rules in the flood risk analysis. The respective changes in the simulation outcomes have been analysed through two successive augmentation phases. Sec. 4.2 describes the first augmentation phase, Phase 1, where the basic version of the coupled flood-pedestrian model has been featured with empirical formulae to simulate pedestrians' variable moving speeds and instability conditions. Sec. 4.3 describes the analysis on the changes in the predictions of flood risks to pedestrians, evacuation time, and their spatial distribution as these features were incorporated, and also further investigations to relate the HR metric with the pedestrian's mobility states. Sec. 4.4 describes the second augmentation phase, Phase 2, where new rules were added to simulate more realistic moving speeds for pedestrians in both dry and flooded zones, and also rules to simulate autonomous decision making of pedestrians in destination selection based on their personal flood risk perception. The changes in the predictions of the temporal and spatial flood risks to pedestrians and evacuation time were analysed in Sec. 4.5 after averaging out the results from multiple runs, which was conducted to consider variations in the simulation outcomes due to the uncertainty in the human behaviour. The simulation runtimes that have been measured are also reported and discussed in Sec. 4.6. Finally, this chapter ends with a summary and highlighting the key findings provided in Sec. 4.7.

4.2 Phase 1: incorporation of pedestrians' body height and mass; variable moving speed; and stability conditions

4.2.1 Characterisation of pedestrians with different body height and mass

To take into account variations of people's body characteristics in the simulations, the pedestrian model is augmented to encompass new functionality for generating pedestrian agents with a different body height and mass. Each pedestrian agent could randomly be given a body height within the ranges shown in Fig. 4.1. These ranges are based on the distribution of body height documented in the world data report (Roser *et al.*, 2019). For this study, pedestrians shorter than 140 cm are excluded, assuming that they are kids that would be carried by adults. Pedestrians in the range of 140-163 cm are children who could not be carried, with a body mass estimated to $m_p = (l_p)^2 \times BMI$ (Disabled World, 2019) where BMI (kg / m^2) denotes the body mass index (in this version of the simulator is taken 21.7 as an ideal average for children) and l_p (m) is the body height. Any pedestrian agent above 163 cm is considered as an adult and their body mass (m_p) is estimated by the formula of Kokong *et al.* (2018), which is: $m_p = [(0.01 \times l_p) - 1] \times 100$. This formula has been used with a 10% randomised uncertainty to account for deviations in the estimated m_p.

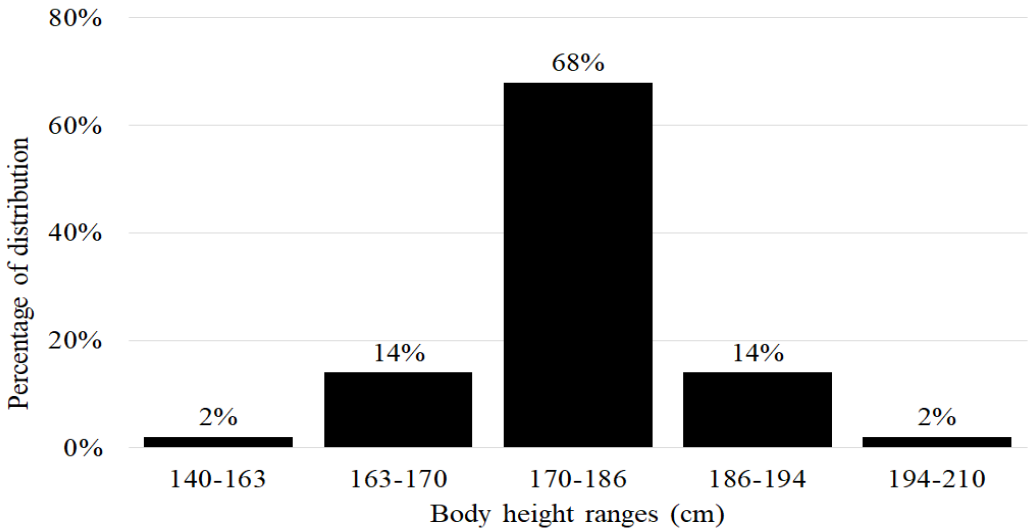

Figure 4.1: Body height distribution of pedestrians characterised according to the world's data report.

4.2.2 Behavioural rules for variable moving speeds

To take into account more realistic motion of individuals in floodwater, the formulations of pedestrian model has been modified to encompass the empirical formula proposed by Bernardini *et al.* (2017b) and Postacchini *et al.* (2018) as new behavioural rules to govern the motion speed of pedestrian agents. These rules are only effective when pedestrian agents encounter non-zero water depth at their location; otherwise, maintain their constant walking speeds reported in Chapter 3. The incorporated formula is experimentally determined via estimating the minimum evacuation speed of a number of real subjects asked to walk as fast as possible in a laboratory flume (Postacchini *et al.*, 2018). The physical characteristics of the participating individuals closely corresponds to the mean body height (175.3 cm for men and 161.9 cm for women) and weight (84.0 kg for men and 69.0 kg for women) of the UK population (Moody, 2012).

Denoting V_i to be the walking speed of each pedestrian agent i, the empirical formula reads:

$$V_i = 0.53M^{-0.19} \tag{4.1}$$

M is a function of specific force per width unit calculated based on the water depth d and the velocity magnitude v, $M = \frac{v^2 d}{g} + \frac{d^2}{2}$, with g is the gravitational constant. Like with HR (see in Sec. 3.4.2), each pedestrian agent i processes the flood information that it receives from the navigation agent at its location to evaluate M, and use it to estimate and adopt a motion speed V_i via Eq. (4.1).

4.2.3 Behavioural rules for variable stability states

The two experimentally-derived formulae for by Xia *et al.* (2014b) are incorporated within the pedestrian model formulation as new behavioural rules. These formulae are computed for each pedestrian agent independently to find the incipient velocity limit, U_c, relevant to their stability state based on their specific body characteristics and floodwater depth at their location. These formulae combine multiple forces that lead to toppling and sliding of flooded

individuals including buoyancy, drag, effective weight and frictional forces. The limits $U_c^{(toppling)}$ and $U_c^{(sliding)}$ beyond which a human body loses stability in floodwater are:

$$U_c^{(toppling)} = a\left(\frac{d}{h_p}\right)^{\beta}\sqrt{\frac{m_p}{\rho_f d^2} - \left(\frac{a_1}{h_p^2} - \frac{b_1}{d\,h_p}\right)\left(a_2 m_p + b_2\right)} \quad (4.2)$$

$$U_c^{(sliding)} = a\left(\frac{d}{h_p}\right)^{\beta}\sqrt{\frac{m_p}{\rho_f h\,h_p} - \left(a_1\frac{d}{h_p} + b_1\right)\frac{\left(a_2 m_p + b_2\right)}{h_p^2}} \quad (4.3)$$

where ρ_f (= 997 kg.m^{-3}) is the density of water, h_p (m) and m_p (kg) stand for the height and mass of a human body, respectively, with a_1 = 0.633, b_1 = 0.367, a_2 = 0.001015, and b_2 = 0.0004927 being non-dimensional coefficients defining the characteristic parameters of the human body structure. The parameters a = 3.472 and β= 0.188 are related to human body shape, which were calibrated using laboratory experiments (Xia *et al.* 2014b). Like HR and M, each pedestrian agent processes the flood information that it receives from the navigation agent at its location to evaluate $U_c^{(toppling)}$ and $U_c^{(sliding)}$, and then it adopts a stability state according to the conditions described in Table 4.1. Note that Eq. (4.2) and Eq. (4.3) have been also calibrated by Xia *et al.* (2014a) to factor in the influence of two ground slopes, i.e. 1:50 and 1:25, on human body stability. In this research, only the form of these formulae for flat grounds are implemented due to the spatial scale of case studies being small, for which the model is designed for.

Table 4.1: The stability states of pedestrian agents in the flood-pedestrian simulator identified by comparing the toppling and sliding incipient velocities to the velocity magnitude of floodwater.

Condition	**Stability state of a pedestrian in floodwater**
$v < U_c^{(toppling)}$ and $v < U_c^{(sliding)}$	'Stable' (with a variable walking speed)
$v > U_c^{(toppling)}$ and $v < U_c^{(sliding)}$	'Toppling' (zero walking speed)
$v < U_c^{(toppling)}$ and $v > U_c^{(sliding)}$	'Sliding' (zero walking speed)
$v > U_c^{(toppling)}$ and $v < U_c^{(sliding)}$	'Toppling and sliding' (zero walking speed)

4.3 Evaluation of Phase 1's augmentation on the simulation outcomes

To explore the benefits of the added behavioural rules through Phase 1, the synthetic shopping centre test case under immediate evacuation scenario (Sec. 3.5) is reconsidered. Simulations are run by taking a diagnostic approach involving three *configuration modes* with systematic increase in the level of sophistication for the pedestrian behavioural rules:

- *'Mode 1'* only uses the simplified rules with constant walking speeds (Table 3.1);
- *'Mode 2'* integrates variable walking speeds using the empirical formula of Eq. (4.1);
- *'Mode 3'* further integrates the stability rules as described in Table 4.1.

In each run, the simulator is set to process and record every time step the information relevant to the water depth, velocity magnitude and HR values stored by the flood agents, and that of the pedestrian agents including their coordinates, HR-related flood risk states (Table 3.1), walking speed states (Eq. 4.1) and mobility states (Table 4.1).

4.3.1 Analysis of flood risk on pedestrians

Figures 4.2-4.4 show the time history of the number of evacuating pedestrians for the simulation Mode 1 to Mode 3 in terms of HR-related flood-risk states (Fig. 4.2a) and stability states (Fig. 4.2b). In Mode 1 (Fig. 4.2a), the simulator predicted an evacuation time of less than 5 minutes (Fig. 4.2a, 'black' dotted line). In the first 2.5 minutes (Fig. 4.2a, 'blue' line), the majority of pedestrians walk in dry areas (Fig. 4.2a, 'green' line) while the rest walk in a low risk state of HR $\leq$ 0.75 (Fig. 4.2a, 'blue' line) where they remain able to walk without losing stability (Fig. 4.2b). After 2.5 minutes, 0.75 < HR $\leq$ 1.5 (Fig. 4.2a, 'orange' line), indicating an increase in the flood risk state to medium to about 300 pedestrians. By 4 minutes, HR becomes higher than 1.5 (Fig. 4.2a, 'red' line), imposing high to sever flood risk states on around 20 pedestrians. In the period of medium to severe flood risk, the number of unstable pedestrians increased, especially by 4 minutes where around 200 pedestrians are 'at risk of only toppling' or 'at risk of both toppling and sliding' (Fig. 4.2b, 'dark red' and 'purple' lines).

In Mode 2 (Fig. 4.3), the simulator's predictions change significantly relative to Mode 1. Now, it takes 3.5 minutes longer for the 1000 pedestrians to evacuate (Fig. 4.3a, 'black' dotted line). Also, low risk state period spans a shorter duration of 2 minutes at the start of flooding but extends beyond 7 minutes, indicating that pedestrians can safely evacuate over last 1.5 minutes (Fig. 4.3a, 'blue' line). Here, the medium to severe states are predicted to occur after 2 minutes and before 7 minutes, relatively affecting more walking pedestrians about 100 and 150, respectively. Mode 2 also leads to a prolonged period of unstable pedestrians, showing about 300 individuals 'at risk of only toppling' or 'at risk of both toppling and sliding' between 2 to 7 minutes of the flood time (Fig. 4.3b).

In Mode 3 (Fig. 4.4), even more prolonged periods of medium to severe states with unstable pedestrians are observed: the total evacuation time of 8.5 minutes, observed in mode 2, now increases to be 13 minutes (Fig. 4.4a, 'black' dotted line). The duration of low flood risk states remains similar to as in mode 2 for the first 2 minutes, buts span a longer duration after 7 minutes, thus indicating that the evacuating pedestrians would be in a low risk state after 8.5 minutes (Fig. 4.4a, 'blue' line). During this period, before 2 minutes and after 8.5 minutes, pedestrians are identified stable that they are able to walk safely in floodwater (Fig. 4.4b). Between 2 and 8.5 minutes of flood time, the flood risk seems to increase significantly, putting over 350 pedestrians in medium state and over 150 pedestrians in high to sever state

even after 4 minutes of flood time. During this time window, the risk of having unstable pedestrians consistently rises, with more than 300 pedestrians ‘at risk of only toppling’ or ‘at risk of both toppling and sliding’. It is useful to note that the risk of ‘only sliding’, although incorporated within the behavioural rules (Table 4.1), is not captured by the simulator. This could be associated with the flood hydrodynamics of this test case that does not entail enough shallow fast-flowing floodwater over the shopping centre.

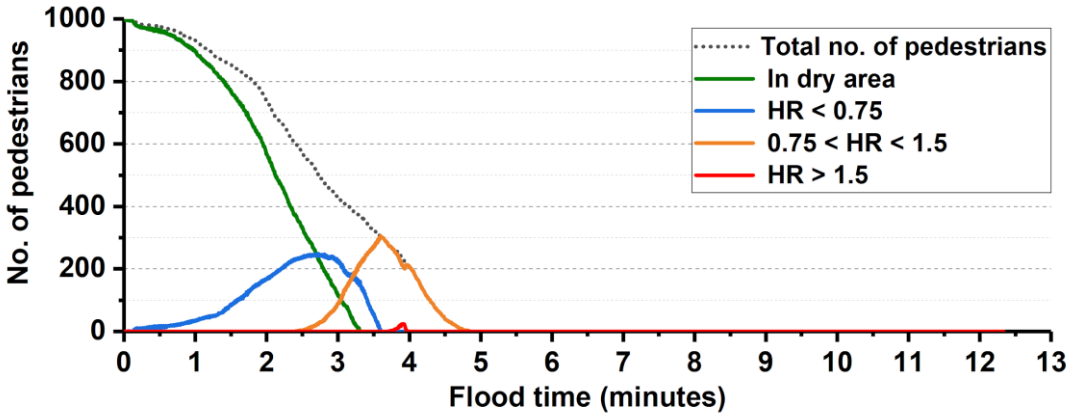

(a) HR-related flood-risk states

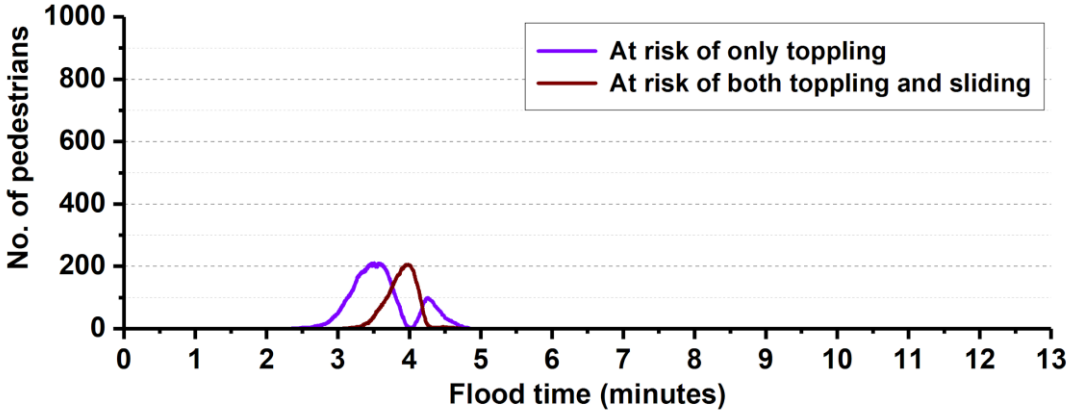

(b) Stability state

Figure 4.2: Number of evacuating pedestrians during the 13-minute flooding in simulation **under Mode 1**: (a) flood risk states in terms of local HR ranges (Table 3.1); and (b) states of unstable pedestrians under toppling and/or sliding (Table 4.1).

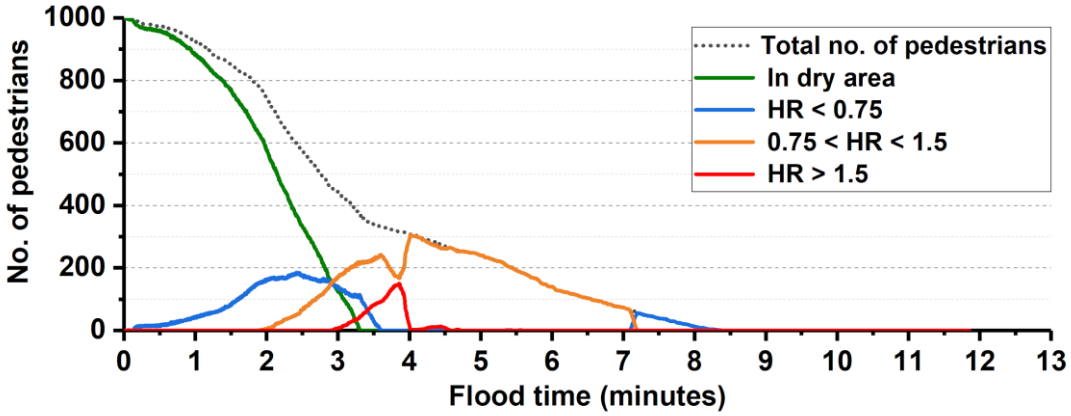

(a) HR-related flood-risk states

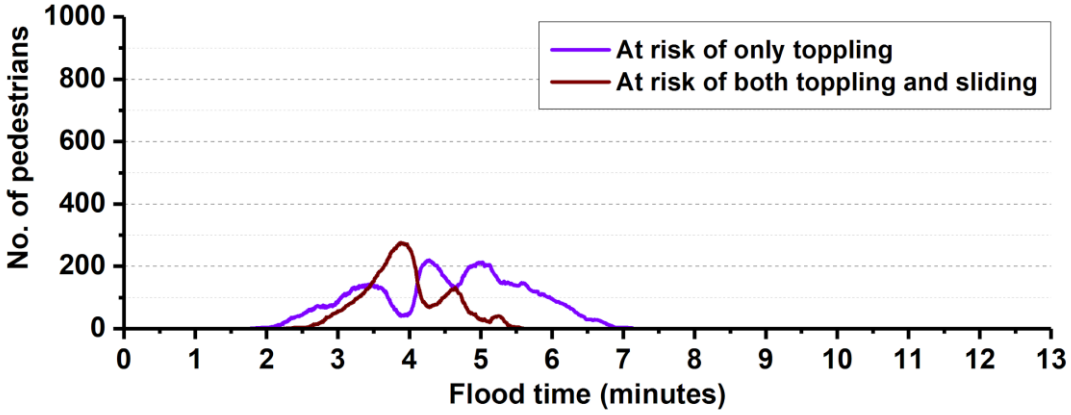

(b) Stability state

Figure 4.3: Number of evacuating pedestrians during the 13-minute flooding in simulation **under Mode 2**: (a) flood risk states in terms of local HR ranges (Table 3.1); and (b) states of unstable pedestrians under toppling and/or sliding (Table 4.1).

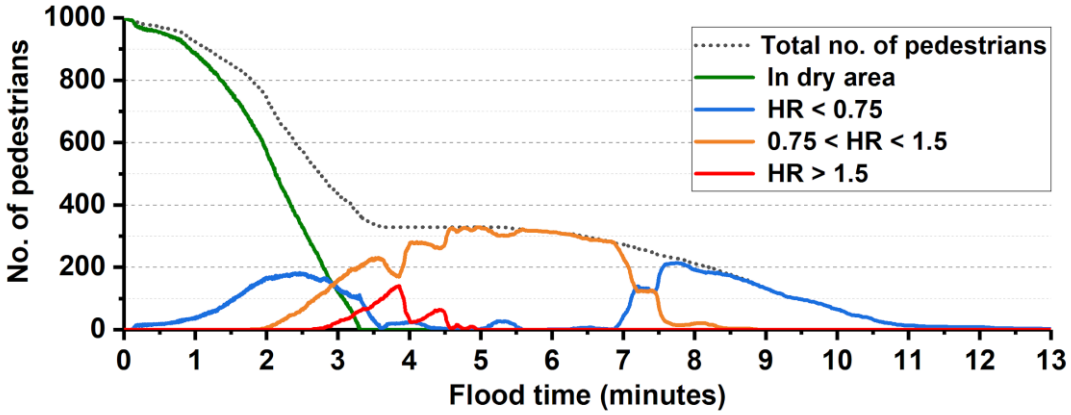

(a) HR-related flood-risk states

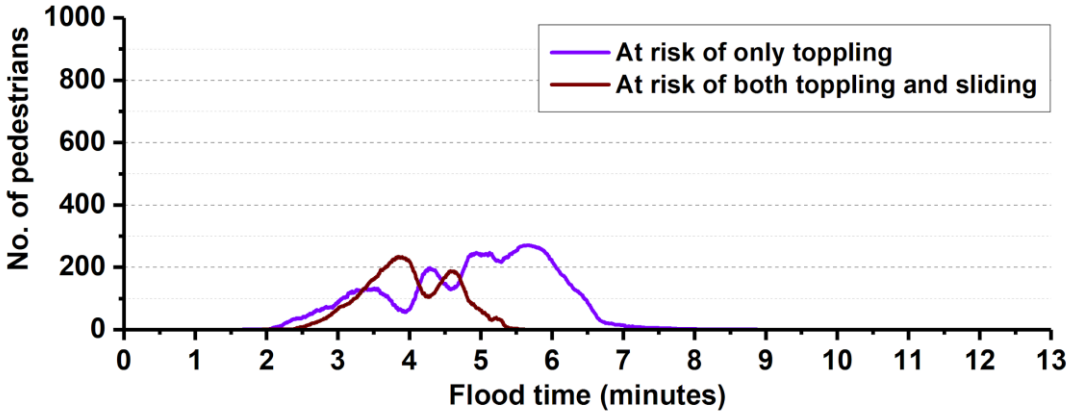

(b) Stability state

Figure 4.4: Number of evacuating pedestrians during the 13-minute flooding in simulation **under Mode 3**: (a) flood risk states in terms of local HR ranges (Table 3.1); and (b) states of unstable pedestrians under toppling and/or sliding (Table 4.1).

4.3.2 Quantitative analysis on the outputs

In a further exploration, the effective differences between the simulator predictions made with modes 1 and 2 relative to mode 3 are quantitatively assessed, using the R-squared (R^2) coefficient and L^1-norm, which have the following expressions:

$$R^2 = \left[\frac{\sum_{t=1}^{T}\left(D_t^{mode\,3}-\bar{D}^{mode\,3}\right)\left(D_t^{M}-\bar{D}^{M}\right)}{\sqrt{\sum_{t=1}^{T}\left(D_t^{mode\,3}-\bar{D}^{mode\,3}\right)^2\sum_{t=1}^{T}\left(D_t^{M}-\bar{D}^{M}\right)^2}}\right]^2 \tag{4.4}$$

$$L^1\text{-norm} = \frac{1}{N_s}\left(\sum_{t=1}^{T}\left|D_t^{mode\,3}-D_t^{M}\right|\right) \tag{4.5}$$

where t denotes the current time and T the output simulation time; $D_t^{mode\,3}$ is a data value at time t obtained the simulator under Mode 3, and D_t^M refers to the data value at the same time t obtained with either of the two other modes, $M \in \{Mode\,1, Mode\,2\}$. The values $\bar{D}^{mode\,3}$ and $\bar{D}^M$ represent time-averaged means, and N_s is the size of a data time series. The R^2 coefficient takes values between 0 and 1, indicating stronger correlation with Mode 3 results as it gets closer to 1. The L^1-norm is more effective to quantify the average deviations relative to Mode 3, and gets closer to 0 in line with reduced deviation. Table 4.2 lists the L^1-norm and R^2 coefficients quantifying the differences in terms of numbers of pedestrians predicted: in 'dry' areas, in 'low', 'medium', and 'high to severe' flood risk states, and with unstable states due to 'toppling only' and 'toppling and sliding'.

The L^1-norm clearly indicates that the discrepancies among the simulator predictions with the different modes are significant, except for the number of pedestrians in dry areas. This is expected as the newly implemented behavioural rules are only relevant and activated for pedestrian agents in wet areas. As explored via Fig. 4.2 to Fig. 4.4, the key reason leading to such large discrepancies is the major differences in evacuation times predicted under the three different modes. The L^1-norms also suggest that the predictions made by the simulator under Mode 2 are closer to those made under Mode 3, which is also expected as both Modes

2 and 3 employed the same variable walking speed rules. This observation is clearer by analysing the range of the R^2 coefficients relative to mode 2, i.e. $0.49 \leq R^2 \leq 0.95$, suggesting that the evacuation patterns predicted using mode 2 are 49 % to 95 % similar to those under Mode 3; whereas those under Mode 1 yield results that are at very best 41% similar.

Table 4.2: Relative changes in the outputs produced by the simulator under Mode 1 and Mode 2 relative to those produced under Mode 3, quantified using the R^2 coefficient and L^1 norm.

Relative change relating to Mode 3		**Dry**	**Low**	**Medium**	**High to severe**	**Toppling only**	**Toppling and sliding**
Mode 1	R^2 coefficient	0.99	0.41	0.15	0.23	0.11	0.55
	L^1-norm	1.91	44.04	81.44	13.52	47.69	26.66
Mode 2	R^2 coefficient	0.99	0.49	0.78	0.90	0.84	0.95
	L^1-norm	1.75	28.58	30.88	4.06	14.89	7.18

4.3.3 Analysis on the spatial distribution of pedestrians

The results in Figs. 4.2-4.4 also points out to potential different patterns for the spatial distribution of the pedestrians relative to the different simulation modes during their evacuation of the flooded shopping centre. To analyse the extent of difference in the predicted spatial distribution of pedestrians, the outputs relevant to the coordinate data of pedestrians are compared across the simulation Mode 1 to 3. The analysis is performed after 4 minutes of flood time when the flood risk states were simulated high to severe in all the three simulation modes (Fig. 4.5).

Figure 4.5 shows the location of the pedestrians, represented by dots, alongside 2D contour plots of the HR in the shopping centre representing flood extent for the three simulation modes. The different colours for the dots also indicate the stability states of the

pedestrians. With all of the Modes 1-3, the simulator predicted a dominance of medium risk floodwaters ($0.75 < HR < 1.5$) over the walkable area, causing the majority of the pedestrians to be at risk of both toppling and sliding (red dots). Under Mode 1 and Mode 2, pedestrians are able to move inside floodwater towards the emergency exit regardless of their stability state. In Mode 1 (Fig. 4.5a), almost all the pedestrians are predicted to have unstable states due to both toppling and sliding within a short distance of the emergency exit. This observation points out to a fast-flowing deep floodwater that propagates around the emergency exit. Similar pattern is observed in Mode 2 (Fig. 4.5b) when the variable walking speeds are considered, but with much wider scattering of pedestrians from within the middle and at a larger distance from the emergency exit. Under this mode, pedestrians at the back of the crowd moving around the right and left sides of the open area are found to be at risk of toppling (purple dots), which is an indicator of deep and slow-flowing floodwaters around that area. This type of floodwaters caused pedestrians to pick up slower moving speeds, causing them to distant from the front crowd. In Mode 3 (Fig. 4.5c), the evacuees are found to be even more spread away from the emergency exit relative to Mode 2 as they become unstable, i.e. immobilised by toppling or toppling with sliding. Under this mode, there seems to be a considerable number of pedestrians with a stable condition (green dots) moving along the right and left sides of the open area, where the flood risk is relatively low ($0.00 < HR < 0.75$). Under this mode, only the stable pedestrians remain mobile and unstable ones (purple and red dots) are considered immobilised until the floodwater becomes shallower and/or slower to enable them maintain their stability state. Under Mode 3, similar to Mode 2, pedestrians with a toppling condition are also found around the sides of the open area with the majority at risk of both toppling and sliding (red dots). These observations imply that running the simulator with more sophisticated behavioural rules could also be useful to pinpoint more hazardous areas considering the dynamic changes in the pedestrians' mobility states in floodwaters.

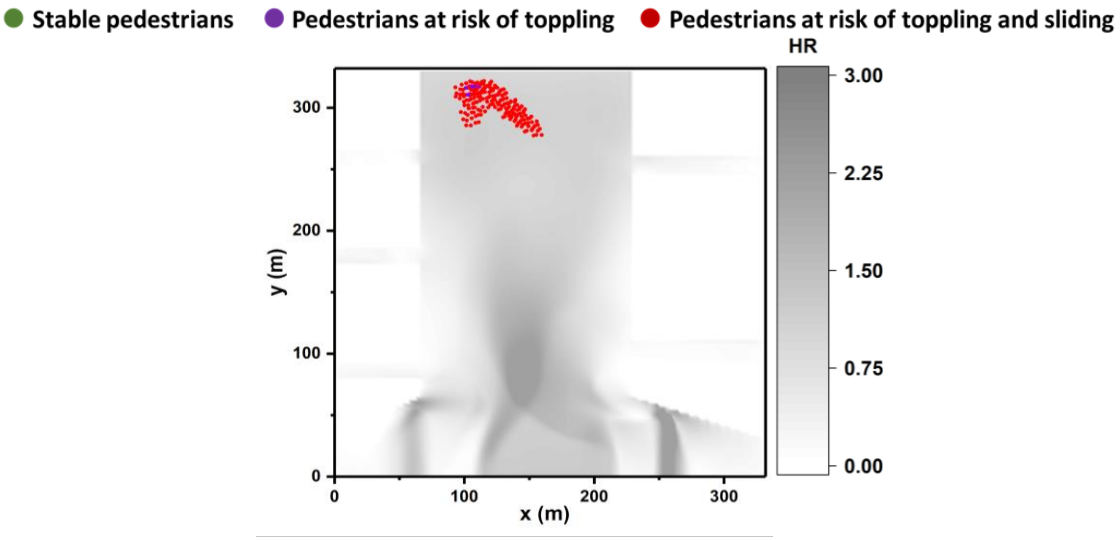

(a) Mode 1

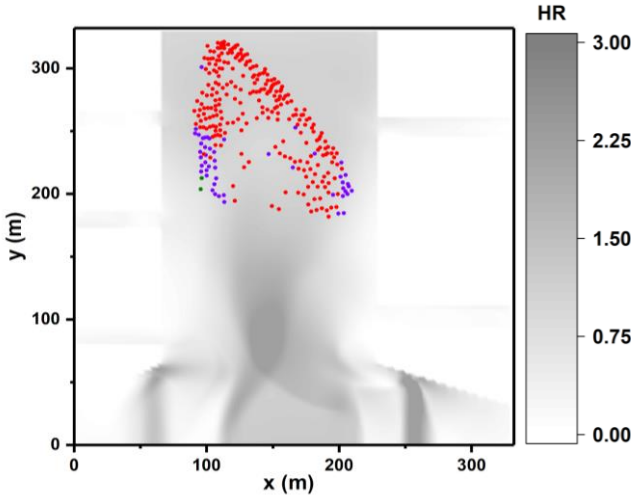

(b) Mode 2

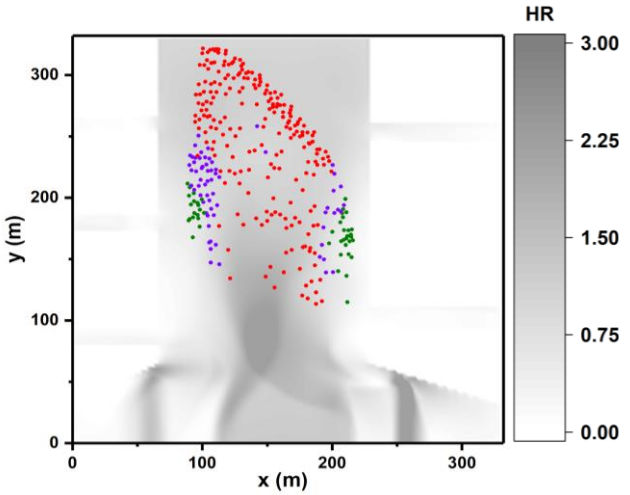

(c) Mode 3

Figure 4.5: Location of the evacuating pedestrians (represented by points) at 4 minutes after flooding for the simulator runs with: (a) Mode 1, (b) Mode 2, and (c) Mode 3.

The results analysed in Sec. 4.3.1 to Sec. 4.3.3 show that with increased level of sophistication in pedestrian behavioural rules, the simulator predicts increasingly prolonged evacuation time as well as a larger number of pedestrians with medium to severe flood risk states. Moreover, as the rules became more sophisticated, major differences in the spatial distribution of the pedestrians is identified, i.e. under Mode 3 where their evacuation shows wider pattern and include larger number of stable pedestrians with low to medium flood risk states. These findings suggest that more realistic incorporation of human response dynamics into the flood risk analysis is likely to yield significantly different outcomes when planning evacuation times or aiming to pinpoint safest shelter areas and evacuation routes.

4.3.4 Investigation of the relationship between the HR-related flood risks and pedestrians' stability state and moving speeds

The spatial and temporal outcomes produced by the simulator have been further studied to produce relationships linking HR-related flood risk state of pedestrians to their stability state and walking speed. Two sets of analysis have been performed under simulation Modes 1 to Mode 3, but only the results of simulation Mode 3 are illustrated as they were found inclusive of all the possible outcomes identified with simulation Mode 1 and 2. First analysis focused on charting the HR-related flood risk states of unstable pedestrians to identify how HR thresholds relate to 'only toppling' and 'both toppling and sliding' conditions. In the second set of analysis, the focus was given to chart the HR-related flood risk states, but on stable pedestrians, to identify how HR can be related to walking speed states.

The results of the first analysis are shown in Fig. 4.6a, which illustrates the HR ranges of unstable pedestrians during 2 to 8.5 minutes of flood time: the 'purple' dots represent those unstable due to only toppling and the 'red' dots those unstable due to both toppling and sliding. The 'purple horizontal dotted lines' indicate the upper and lower limits of HR identified for toppling risk and the 'red' one indicates the lower limit of HR for the risk of both toppling and sliding. Pedestrians are found at risk of toppling only when $0.62 \leq HR \leq 1.48$, whereas they are at risk of both toppling and sliding when $HR \geq 0.96$. Figure 4.6b shows the plot of the pedestrian walking speed states versus HR, for $0.06 < HR < 0.62$, where the walking speed of pedestrians is identified to be affected by floodwater and the pedestrians remain stable (before 2 and after 8.5 minutes of flood time): As local HR increases from 0.06, the walking speed of pedestrians (initially 1.4 m/s when in a dry area) decreases down to 0.78 m/s at the threshold where they become instable (HR = 0.62). An explicit relationship

linking HR to stable pedestrians' walking speed has been produced and is illustrated in Fig. 4.6b. Based on an exponential fitting curve over the simulated results, this curve has yielded the best agreement with the simulation samples ($R^2 = 0.99$) and reads:

$$V_i = 0.69177 + 0.7762 \times 0.02466^{\mathrm{HR}} \tag{4.6}$$

Overall, these sets of analysis on the simulation samples allows to identify: (i) thresholds for HR to directly estimate unstable states of pedestrians in floodwater; and, (ii) a formula to directly estimate walking speed states of stable pedestrians by only referring to HR. The identified thresholds and formula are expected to widen the utility of the HR metric (Environment Agency, 2006; Kvočka *et al.*, 2016; Willis *et al.*, 2019; Costabile *et al.*, 2020). For example, to gain more detailed insights on people mobility in floodwater for the same test case but different flood conditions or for other test cases that previously employed the HR metric. Moreover, the analysis reported here seems to imply that HR < 0.75 may be an overly optimistic recommendation as a low risk state ('safe for all', Environment Agency 2006) because the simulator still predicted a risk of toppling with HR > 0.62. Similarly, the lower limit of the medium risk state (i.e. HR > 0.75: 'dangerous to some', particularly children, Environment Agency, 2006) may also be overly optimistic as the present simulator identifies a risk of toppling and sliding for adults for HR ≥ 0.96. These findings, though specific to the current case study, support conclusions made by other studies (Kvočka *et al.*, 2016; Chanson and Brown, 2018), pointing out to the need to quantify more accurate safety thresholds.

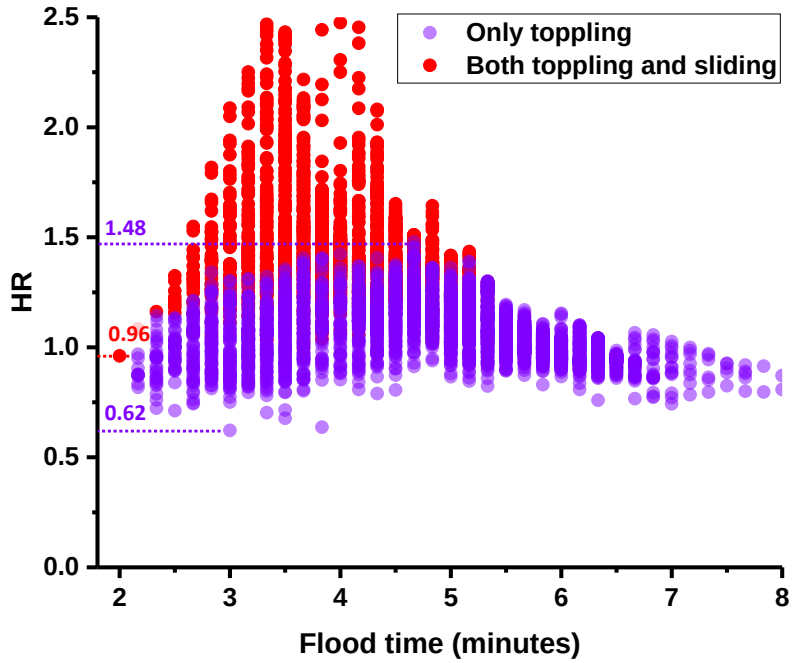

(a) Distribution of unstable pedestrians' HR-related flood risk state that are identified at risk of 'toppling only' and of 'both toppling and sliding' after 2 and before 8.5 minutes of flood time.

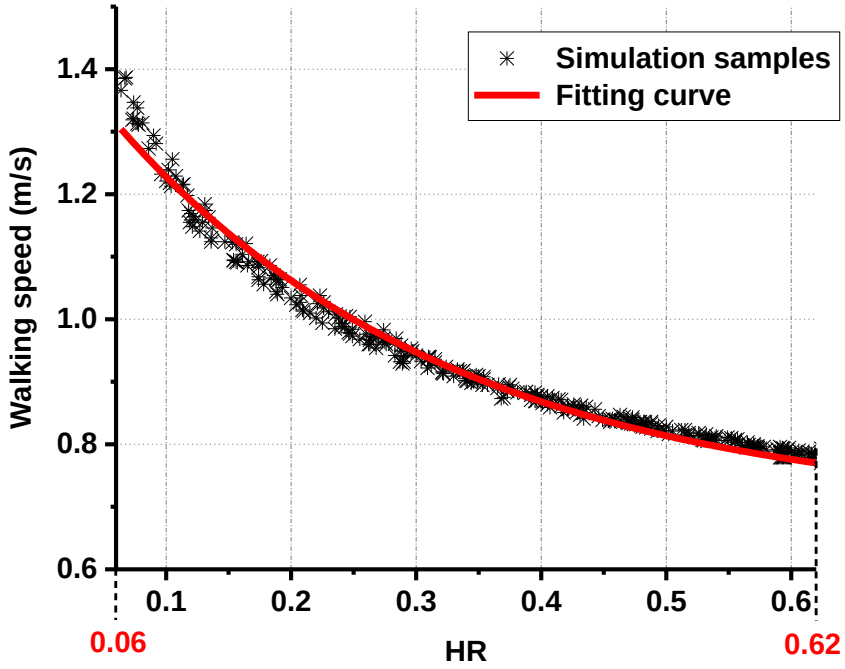

(b) Distribution of stable pedestrians' walking speeds as function of HR identified before 2 and after 8.5 minutes.

Figure 4.6: Relationship linking pedestrians' flood risk states in terms of HR ranges to (a) their unstable states, and to (b) their walking speed states when stable based on simulator's outcomes under Mode 3.

4.4 Phase 2: Increasing the level of heterogeneity and realism in pedestrians' characterisation and behavioural rules

In Phase 2, we present further developments in the coupled flood-pedestrian model to incorporate an enhanced level of heterogeneity in pedestrians' characterisation and more realistic behavioural rules. The simulator is therefore augmented to account for:

- age, gender, body height and mass distribution of a subject population;
- age- and gender-related variable moving speeds of individuals in both dry and flooded zones based on real-world datasets and experimental information; and
- autonomous decision making of individuals in choosing one of multiple emergency exit destinations influenced by their personal perception of the risk from the floodwater or by the most popular destination selected by others.

4.4.1 Characterisation of pedestrians with age, gender, and realistic body mass

Each pedestrian agent is set to hold information of age, gender, and body mass at the time of its generation. To randomly assign an age, gender and body mass based on realistic distributions to each pedestrian, the UK national survey dataset (UK population by ethnicity, 2018) was used. As shown in Fig. 4.7, each pedestrian agent can have an age randomly selected from a range between 10 and 79 years old, and with a probability to keep the percentage of distribution of seven age groups. The excluded age groups, younger than 10 and older than 79 years old, make up 16 % of the UK population and represent children and elderly. To compensate for their exclusion, the percentage distribution of the other age groups was increased by around 2.3 %. Each pedestrian agent is also generated with a random 'male' or 'female' gender, each with equal chance of selection.

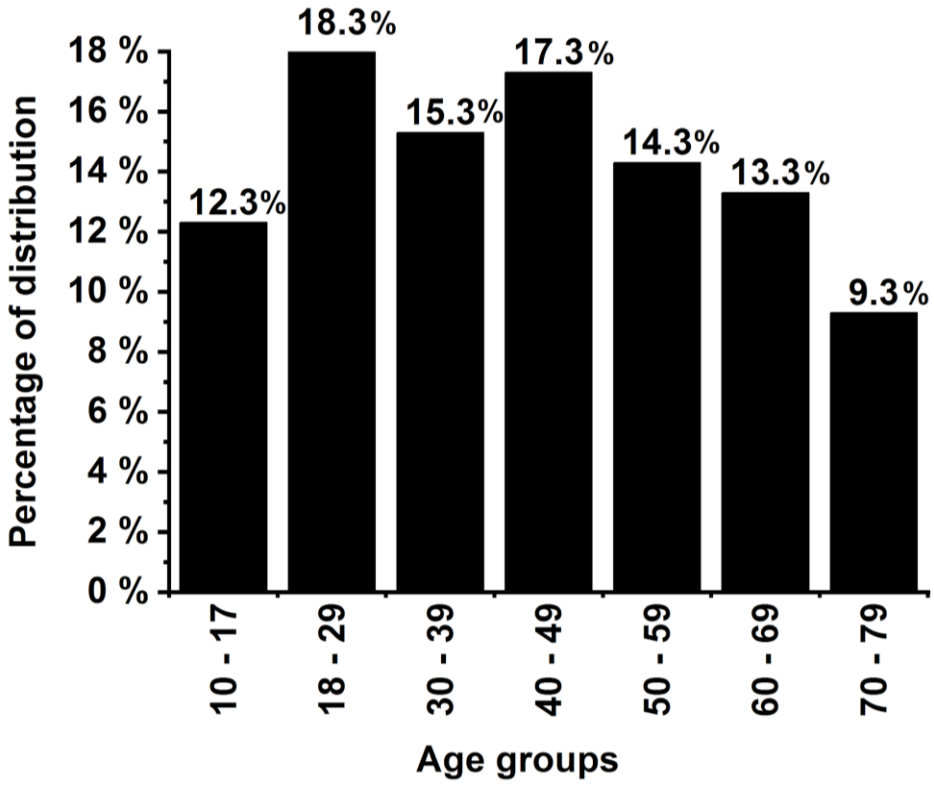

Figure 4.7: Age distribution assigned for the pedestrian agents in the flood-pedestrian simulator based on the UK's national survey (UK population by ethnicity, 2018).

Based on the age and gender of a pedestrian agent, its body mass, denoted by m_p (kg), is evaluated using the following formula (Disabled World, 2019):

$$m_p = l_p^2 \, BMI, \tag{4.7}$$

where l_p (m) stands for the body height of a pedestrian agent, which had already been incorporated within the previous version of the simulator (see in Sec. 3.4). Here, the BMI (kg / m^2) was randomly selected based on the ranges of age and gender listed in Table 4.3. For the age group between 10 and 17 years old, the BMI range was defined based on a standard for children (Prentice, 1998) and, based on samples of men and women who participated in the laboratory experiments reported in Bernardini *et al.* (2020) for the other age groups.

Table 4.3: Ranges of BMI used according to gender and age of individuals (details in Prentice (1998) and Bernardini *et al.* (2020)).

Age groups	Gender	BMI (kg / m^2)
10 to 17	Both	Between 18.5 and 24.9
18 to 29 30 to 39 40 to 49 50 to 59 60 to 69 70 to 79	Male	Between 18.21 and 32.10
	Female	Between 16.01 and 32.03

4.4.2 Behavioural rules for more realistic variable moving speeds in both dry and flooded zones

Each pedestrian agent is enabled to autonomously evaluate their variable moving speed according to their assigned age- and gender and the dynamic changes in the state of floodwater flow at their location. This was achieved by introducing two new sets of behavioural rules for all the pedestrian agents, governing the motion of the pedestrian agent in dry zones (around the floodwater) and in flooded zones (inside the floodwater), respectively. To enable a pedestrian agent to discern between dry zone and flooded zone, it resorts to the state of the floodwater's depth accessible from the navigation agent at its specific location and time.

A pedestrian agent that identifies a zero depth of floodwater is automatically flagged to be in a dry zone. These pedestrian agents are set to operate based on a 'dry-zone' moving speed rule under a walking condition. This rule assigns a randomly selected walking speed to a pedestrian agent from a set of predefined ranges that are classified according to different age and gender groups outlined in Table 4.4. The walking speed range of the 10 to 19 age group is defined according to the human's average walking speed and is the same for both male and female (Mohler *et al.*, 2007; Toor *et al.*, 2001). For pedestrian agents with 20 years of age and more, the ranges of their walking speed varies across different gender groups and are derived from an empirically identified standard proposed by Bohannon and Andrews (2011). As people are expected to move faster under evacuation conditions (Bernardini *et al.*, 2020), pedestrian agents are applied an additional rule to increase their walking speed based on the 'maximum excitement condition' identified in the experiments of Bernardini

and Quagliarini (2020). This condition enables 'male' pedestrian agents to increase their walking speed by 60 % and 'female' agents to increase their walking speed by 76 %. The experimental findings of Lee *et al.* (2019) also suggest a faster maximum excitement condition for women, which may be associated with the fact that women have less tendency to be around floodwater compared to men (Becker *et al.*, 2015; Hamilton *et al.*, 2020).

Table 4.4: Ranges of walking speeds for the pedestrian agents located in dry zones according to their age and gender (Toor *et al.*, 2001; Mohler *et al.*, 2007; Bohannon and Andrews, 2011).

Age range (years)	Walking speed range (m/s)	
	Female	Male
10 to 19	1.39 to 1.47	1.39 to 1.47
20 to 29	1.270 to 1.447	1.239 to 1.443
30 to 39	1.316 to 1.550	1.193 to 1.482
40 to 49	1.353 to 1.514	1.339 to 1.411
50 to 59	1.379 to 1.488	1.222 to 1.405
60 to 69	1.266 to 1.412	1.183 to 1.300
70 to 79	1.210 to 1.322	1.072 to 1.192

A pedestrian agent that identifies a non-zero depth of floodwater is automatically flagged to be in a flooded zone. These pedestrian agents are set to operate upon a 'flooded-zone' moving speed rule under either 'walking' or 'running' conditions. With this rule, each pedestrian is assigned a moving speed that is evaluated by an empirical formula extracted from the experiments in Bernardini *et al.* (2020). Denoting the moving speed of each individual by V_p (m/s), the formula reads

$$V_p = a.M^b, \tag{4.8}$$

where a and b are age-related parameters defining each of the 'walking' and 'running' conditions, which are listed in Table 4.5. The validity of Eq. (4.8) is limited to subjects under the age of 68 and only applicable to floodwater depths between 0.2 m to 0.7 m (Bernardini *et al.*, 2020). In reality, floodwater depth can be outside these limits and it may happen that an elderly beyond 68 years of age is present in a flooded area. Therefore, extra rules were

applied to extend the variety of moving speed of pedestrian agents in flooded zones beyond the aforementioned age and floodwater depth limits for Eq. (4.8):

- the moving speed of pedestrian agents with an age greater than 68 is evaluated by decreasing V_p of the 61 to 68 age group by 1.6 % per year, following the experimental findings of Dobbs *et al.* (1993),

- pedestrian agents encountering a depth of floodwater shallower than 0.2 m are set to maintain dry-zone walking speed rule as they are not expected to experience significant interference from the floodwater on their walking speed (Lee *et al.*, 2019), and

- pedestrian agents encountering floodwater greater than 0.7 m are given a moving speed informed by the stability limits reported in the UK's Flood Risks to People method (Ramsbottom *et al.*, 2006). Namely, these pedestrian agents are only set to have a moving speed when velocity magnitude V is less than 1.5 m/s, or otherwise, they remain immobile.

Table 4.5: The values of age-related parameters, *a* and *b*, identified by Bernardini *et al.* (2020) for evaluation of the moving speed of each individual under 'walking' and 'running' conditions via Eq. (4.8).

Age ranges (years)	**Walking**		**Running**	
	a	***b***	***a***	***b***
5 to 12	0.82	0.18	0.41	-0.21
13 to 20	0.54	-0.07	0.81	-0.19
21 to 28	0.36	-0.13	0.48	-0.19
29 to 36	0.35	-0.19	0.53	-0.23
37 to 44	0.43	-0.13	0.62	-0.20
45 to 52	0.57	-0.03	0.61	-0.17
53 to 60	0.32	-0.17	0.62	-0.20
61 to 68	0.16	-0.43	0.61	-0.17

4.4.3 New behavioural rules to autonomously change pedestrians' direction

Each pedestrian agent is also featured with two extra rules to enable it to autonomously navigate into new pathways while moving within a flooded zone, where it encounters a non-zero floodwater depth from the navigation agent at its specific time and location. The first rule makes a pedestrian agent detect and choose another destination if the floodwater depth along its way becomes higher than a threshold of a floodwater depth to body height. The choice for the threshold is case-dependent and exploring different thresholds may be necessary (i.e., in Chapter 5) as an individual's flood risk perception is dependent on different factors, including past flooding experiences (Hamilton et al., 2020; Abebe *et al.*, 2020). This affects the modelling of decisions, i.e. when and where people enter the floodwater or make a move into another destination (Becker *et al.*, 2015; Netzel *et al.*, 2021). Applying this rule enables the pedestrian agents to make decisions on which pathway to take within an environment layout where there is no specific emergency exit at time of evacuation. The second rule applies to those pedestrian agents which remain undecided about selecting a pathway after a period of time. Such pedestrian agents are then set to detect the most popular destination chosen by the pedestrian agents within its surroundings. This rule is applied on the basis that group decisions have significant influence on the path finding decision of an individual in and around the floodwater (Becker *et al.*, 2015; Lin *et al.*, 2020).

4.5 Evaluation of Phase 2's augmentation on the simulation outcomes

The new characteristics and rules for pedestrian agents in Phase 2 were evaluated with a focus to assess their relevance for the analysis of pedestrian evacuation dynamics during a flood emergency. This is done by setting the simulator up and rerunning it for the same shopping centre synthetic test case under the during-flood evacuation condition. But this time, the simulations are run under five different configuration modes, which are summarised in Table 4.6.

Table 4.6: Configuration modes used to set up and run the simulator to evaluate the newly added characteristics and rules.

Modes	Pedestrian behavioural rules				
	Two-way interaction	Moving speed in dry zones		Moving speed in flooded zone	
		Walking condition	Maximum excitement condition	Walking condition	Running condition
Mode 0	Disabled	Constant	Disabled	Age independent	Not applicable
Mode 1	Disabled	Age- and gender-related	Enabled	Age-related	Not applicable
Mode 2	Enabled				
Mode 3	Disabled			Not applicable	Age-related
Mode 4	Enabled				

The simulator was executed at a resolution of $2.59\,\text{m} \times 2.59\,\text{m}$ for each of the grids of navigation and flood agents. The time-step was taken to be the minimum between the adaptive time-step of the hydrodynamic model and the 1.0 s time-step of the pedestrian model. The simulations are conducted on a Dell Precision 3630 Tower PC with an Intel Core i7-8700 CPU, 32.0 GB installed RAM and a Nvidia Quadro RTX4000 graphics card that has 2,304 CUDA Parallel-Processing Cores and 8 GB GPU Memory.

In each run, the simulator is set to record the information stored in the flood agents and the pedestrian agents at each time-step. Recorded outputs from a simulation run include the positions of the pedestrian agents, their flood risk states (HR-related) and or their stability states (including toppling-only, toppling-and-sliding and sliding-only conditions). Note that, although the sliding-only is implemented in the simulator, it is not expected to predict pedestrians under this stability state for the type of fluvial or pluvial floods investigated in this paper. This stability state would occur when pedestrians respond to raging and shallowly propagating floodwaters such as the case of a flash flood.

4.5.1 Sensitivity analysis on the simulation outputs

Because of the uncertainties associated with the human behaviour under evacuation conditions, the simulation outputs are averaged out from multiple runs. This was done with a focus to find the required number of simulation runs under different configuration modes (Table 4.6) to obtain a plausible outcome that keeps the deviation from the averages below 1 %. To do that, a series of 10 and 20 simulation runs were conducted and the plausibility of the average outputs from both series of runs is evaluated by estimating the margin of error (*MOE)* assuming confidence levels ranging between 90% and 99.9%. The following formula is used to evaluate the *MOE*:

$$MOE = Z_{score} \times \sqrt{\frac{\sigma^2}{n}}, \tag{4.9}$$

where, Z_{score} is the critical value, which is equal to 1.65, 1.96, 2.17, 2.58 and 3.29, for confidence levels of 90 %, 95 %, 97 %, 99 % and 99.9 %, respectively (Hazra, 2017); σ is the standard deviation from the sample of outputs of size n = {10, 20}; and $\sigma = \sqrt{\frac{\sum(x_i - \bar{x})^2}{n}}$, with x_i representing the number of pedestrians with a particular HR-related flood risk or stability state extracted from the recorded outputs, and $\bar{x}$ is the averaged value. Table 4.7 lists the maximum *MOE* evaluated for the different confidence levels, with respect to the average number of pedestrian agents under different HR-related flood risk and stability states for configuration Mode 0 to Mode 4.

Table 4.7: Maximum margin of error (*MOE*) for the average number of pedestrian agents with different HR-related flood risk or stability states that are extracted from the recorded outputs of all the configuration modes (Table 4.6) and across different confidence levels ranging from 90 % to 99.9%. Different ranges of the evaluated maximum *MOE* are highlighted with different colour shades: green, orange and red to indicate *MOE* $\leq \pm 5$, $6 \leq$ *MOE* ≤ 9 and *MOE* ≥ 10, respectively.

Mode	HR-related flood risk and stability states	Maximum *MOE*									
		***n* = 10**					***n* = 20**				
		90%	**95%**	**97%**	**99%**	**99.9%**	**90%**	**95%**	**97%**	**99%**	**99.9%**
0	HR < 0.75	± 5	± 6	± 6	± 8	± 10	± 3	± 4	± 4	± 5	± 6
	0.75 < HR <1.5	± 4	± 5	± 6	± 7	± 9	± 3	± 3	± 4	± 4	± 5
	1.5 < HR <2.5	± 3	± 3	± 4	± 5	± 6	± 2	± 3	± 3	± 4	± 5
	HR > 2.5	± 1	± 1	± 1	± 2	± 2	± 1	± 1	± 1	± 1	± 1
	Toppling-only	± 5	± 6	± 7	± 8	± 10	± 4	± 4	± 5	± 6	± 8
	Toppling-and-sliding	± 4	± 5	± 5	± 6	± 8	± 3	± 4	± 4	± 5	± 9
1	HR < 0.75	± 6	± 7	± 8	± 9	± 12	± 4	± 4	± 5	± 6	± 7
	0.75 < HR <1.5	± 6	± 7	± 8	± 10	± 12	± 4	± 4	± 5	± 6	± 7
	1.5 < HR <2.5	± 1	± 1	± 1	± 1	± 1	± 1	± 1	± 1	± 1	± 1
	HR > 2.5	± 0	± 0	± 0	± 0	± 1	± 0	± 0	± 0	± 0	± 0
	Toppling-only	± 6	± 8	± 8	± 10	± 13	± 4	± 4	± 5	± 6	± 7
	Toppling-and-sliding	± 5	± 6	± 7	± 8	± 10	± 3	± 4	± 5	± 5	± 7
2	HR < 0.75	± 6	± 7	± 7	± 9	± 11	± 4	± 5	± 5	± 6	± 8
	0.75 < HR <1.5	± 7	± 8	± 9	± 10	± 13	± 5	± 6	± 6	± 7	± 9
	1.5 < HR <2.5	± 1	± 1	± 1	± 2	± 2	± 1	± 1	± 1	± 1	± 1
	HR > 2.5	± 1	± 1	± 1	± 1	± 1	± 1	± 1	± 1	± 1	± 1
	Toppling-only	± 6	± 7	± 8	± 9	± 12	± 4	± 4	± 5	± 6	± 7
	Toppling-and-sliding	± 6	± 7	± 7	± 9	± 11	± 4	± 5	± 5	± 6	± 8
3	HR < 0.75	± 6	± 7	± 8	± 9	± 12	± 4	± 4	± 5	± 6	± 7
	0.75 < HR <1.5	± 6	± 7	± 8	± 9	± 12	± 4	± 5	± 5	± 6	± 8
	1.5 < HR <2.5	± 1	± 1	± 1	± 1	± 1	± 0	± 1	± 1	± 1	± 1
	HR > 2.5	± 0	± 0	± 0	± 0	± 0	± 0	± 0	± 0	± 0	± 0
	Toppling-only	± 6	± 7	± 8	± 9	± 12	± 4	± 5	± 5	± 6	± 8
	Toppling-and-sliding	± 6	± 7	± 8	± 9	± 12	± 4	± 4	± 5	± 6	± 7
4	HR < 0.75	± 5	± 6	± 7	± 9	± 11	± 4	± 4	± 5	± 6	± 7
	0.75 < HR <1.5	± 7	± 9	± 10	± 12	± 15	± 5	± 6	± 6	± 7	± 10
	1.5 < HR <2.5	± 1	± 1	± 1	± 1	± 2	± 1	± 1	± 1	± 1	± 1
	HR > 2.5	± 1	± 1	± 1	± 1	± 1	± 0	± 0	± 1	± 1	± 1
	Toppling-only	± 6	± 7	± 8	± 9	± 12	± 4	± 4	± 5	± 6	± 7
	Toppling-and-sliding	± 6	± 7	± 8	± 9	± 12	± 4	± 5	± 5	± 6	± 7

For n = 10, there is a considerable increase in the maximum *MOE* with Mode 1 to Mode 4 compared to Mode 0. This is particularly seen for the number of pedestrian agents in low and medium flood risk states (HR < 0.75 and 0.75 < HR <1.5, respectively) and with toppling-only and toppling-and-sliding stability states. This suggests that the more sophisticated the pedestrian agent characteristics and rules, more discrepancies would appear in the simulator's outcomes. The maximum *MOE* identified suggests a deviation of around ± 15 from the averaged outcomes. However, when the sample size is increased to n = 20, the maximum margin of error does not exceed ± 10 for all the modes and confidence levels. Therefore, the simulation results analysed next are averaged out from a sample of 20 simulation runs, subject to ± 10 maximum *MOE* for a population of 1000 pedestrians in the flooded walkable area, which corresponds to a variance of 1 %.

4.5.2 Analysis of flood risk on pedestrians

Figure 4.8 shows the trends in the number of evacuating pedestrians with different HR-related flood risk states predicted by the simulator after 20 runs using all the configuration modes (Table 4.6). Figure 4.8a represents how the number of pedestrians with a low flood risk state (HR < 0.75) change during 20 minutes of flood time. Figure 4.8a, upper panel, includes the trends predicted after enabling the walking condition for the age-related moving speeds (Mode 1) versus those predicted by further enabling the two-way interaction condition (Mode 2). In Mode 1, the trend is in good agreement with the baseline predictions (Mode 0, with non-age related moving speeds) at flooding times when there are less than 100 pedestrians in the walkable area with a low flood risk state, during 3.5 min to 7 min. A considerable difference among the predictions starts to appear when more than 150 pedestrians are present, around 2.5 min and 8.5 min. This difference seems to impact the overall trend, suggesting a 6 min longer duration with a higher number of pedestrians being predicted to be under this flood risk state, during 8 min to 18 min. In Mode 2, compared to Mode 1, the number of evacuating pedestrians is seen to reduce further at flooding times involving more than 150 pedestrians, around 2.5 min and 10 min. This is expected as crowding of pedestrians in low risk floodwaters would disperse the floodwater dynamics, which in turn help pedestrians evacuating ahead to pick up a faster moving speed (as observed previously in Sec. 3.5). This does not seem to influence the collective moving speed of pedestrians, for example by generating additional congestions (as shown later in Fig. 4.10), as the overall trends with Mode 1 and Mode 2 are very close. Figure 4.8a, lower panel,

contrasts the trends predicted after activating the running condition for the age-related moving speeds (Mode 3) to those predicted by also enabling the two-way interaction condition (Mode 4). In Mode 3 and Mode 4, the trends show a considerably faster moving speed of pedestrians (than with Mode 1 and Mode 2), significantly reducing the duration when pedestrians fall under a low risk state, suggesting outputs that are close to the baseline predictions (Mode 0). With Mode 3, discrepancies (compared with Mode 0) only occur between 2.5 and 3.5 min and after 8 min of flooding, when there are more than 150 pedestrians moving under the running condition. In Mode 4, with further enabling the two-way interaction condition, the trends remain close to those predicted under Mode 3, except at 2.5 min flooding time that involves more than 200 pedestrians under a low flood risk state. This suggests that activating the two-way interaction condition with the running condition may only temporarily influence the pedestrians' collective moving speed, namely when more than 200 pedestrians are caught under a low flood risk state. Overall, there is a major difference in the collective moving speeds of pedestrians when age-related walking vs. running speeds are deployed, leading to prolonged vs. shortened evacuation times compared to the baseline predictions (Mode 0), respectively. Also, using the two-way interaction condition seems to be a sensible choice for simulating mass pedestrian evacuations in low risk floodwater.

Figure 4.8b shows how the number of pedestrians with a medium flood risk state ($0.75 < HR < 1.5$) change during 20 minutes of flood time. With Mode 1 (Fig. 4.8b, upper panel), compared to Mode 0, less number of pedestrians is predicted until 6 min, just before the number of pedestrians under this flood risk state reaches 300. This suggests that pedestrians could pick up faster moving speeds during the first 6 min of flooding, allowing them to escape medium risk floodwaters earlier. After 6 min, the trend with Mode 1 is fairly similar to the one with Mode 0, suggesting more influence of medium risk floodwaters on the collective moving speed of pedestrians irrespective of their age and gender. This difference is also marginal in the trends predicted by the simulator with Mode 2 that further activates the two-way interaction condition. However, like the trends seen for the low flood risk state (Fig. 4.8a, upper panel), the pedestrians under a medium flood risk state exhibit a slightly faster moving speed when their number is over 300. Again, this could be related to more dispersions in floodwater dynamics due to large crowding, allowing the pedestrians located ahead to maintain faster moving speeds. By using instead the age-related running condition under Mode 3 (Fig. 4.8b, lower panel), the trend observed is pretty similar to that

with Mode 0, with slight differences appearing after 6 min of flooding. Further enabling the two-way interaction condition (Mode 4) induces more reduction in the predicted number of pedestrians during the time of the flood when the crowding is at its peak, between 6 and 8 min (Fig. 4.8b, lower panel). Also, the collective moving speed of pedestrians under either Mode 3 or Mode 4 is predicted to be similar to those under Mode 1 and Mode 2 for the pedestrians in a medium flood risk state. Hence, running the simulator with any of the configuration Mode 1 to Mode 4 does not seem to make a major difference in the trends for the pedestrians with a medium flood risk state, all predicting considerably less numbers evacuating during early flood times before crowding occurs (compared to Mode 0).

Figure 4.8c shows how the number of pedestrians with a high flood risk state ($1.5 < HR < 2.5$) change during 20 minutes of flood time. For pedestrians with this flood risk category, running the simulator with any of the Mode 1 to Mode 4 leads to major differences in the trends compared to those predicted under Mode 0. With Mode 1 to Mode 4, only a handful of pedestrians are predicted to have a high flood risk state, during 3 min to 5 min of the flooding, in contrast to what the simulator's prediction with Mode 0 suggests: up to 140 pedestrians within a time window of 4 min. Hence, using the age-related moving speed, under either the walking condition or the running condition, seems to make a difference in the predicted trends in the number of pedestrians with a high flood risk state. The impact of the two-way interaction condition on the trends of such pedestrians can be detected by analysing the difference between the predictions made under Mode 1 vs. Mode 2, for the age-related walking condition (Fig. 4.8c, upper panel), and between Mode 3 vs. Mode 4, for the age-related running condition (Fig. 4.8c, lower panel). As can be seen, only a slightly higher number of pedestrians with a high flood risk state are predicted when the two-way interaction condition is also enabled, suggesting that it does not lead to major differences.

Figure 4.8d shows how the number of pedestrians with a highest flood risk state ($2.5 < HR < 20$) change during 20 minutes of flood time. In this case, with any of the Mode 1 to Mode 4, the simulator predicts only one or two pedestrians that could fall into this flood risk state around similar flood times predicted under Mode 0, which predicts a couple of more pedestrians under this flood risk state. This implies that using the age-related moving speeds can potentially predict less pedestrians that would be at the highest flood risk state. The trends predicted by the simulator using Mode 1 and Mode 3 are similar, indicating that using any of the running or walking conditions would lead to similar outcomes to inform on evacuating pedestrians with a highest flood risk state. These conditions combined with the two-way

interaction condition (Mode 2 and Mode 4) leads to a slightly higher number of pedestrians with this flood risk state, as these pedestrians would be more affected by the local changes induced in the local floodwater dynamics from those pedestrians with a low risk state crowding ahead. Hence, either Mode 2 or More 4 seems to be a sensible configuration for the simulator to plan evacuation case studies involving more severe flooding scenarios.

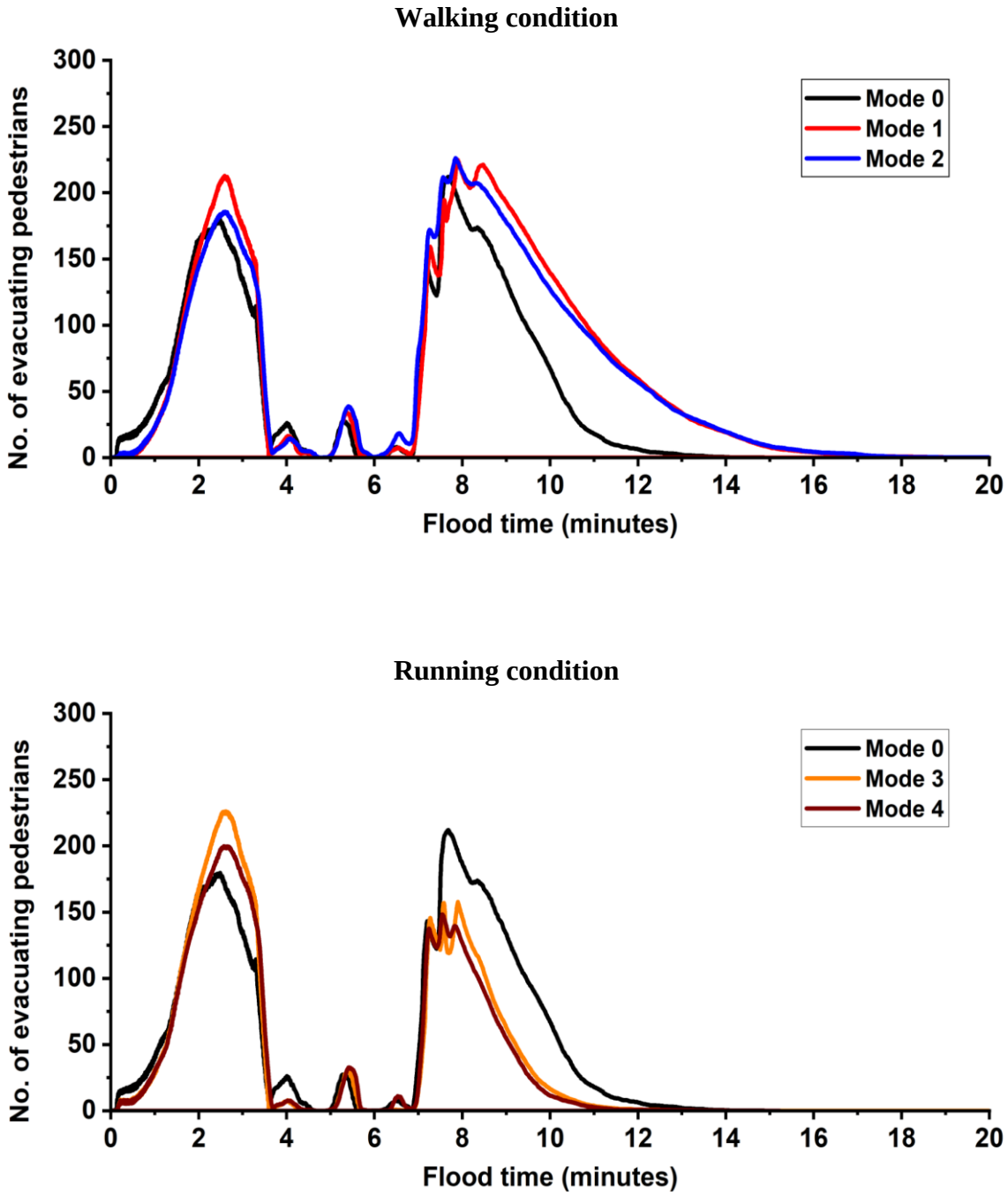

(a) Evacuating pedestrians with a low flood risk state (HR < 0.75)

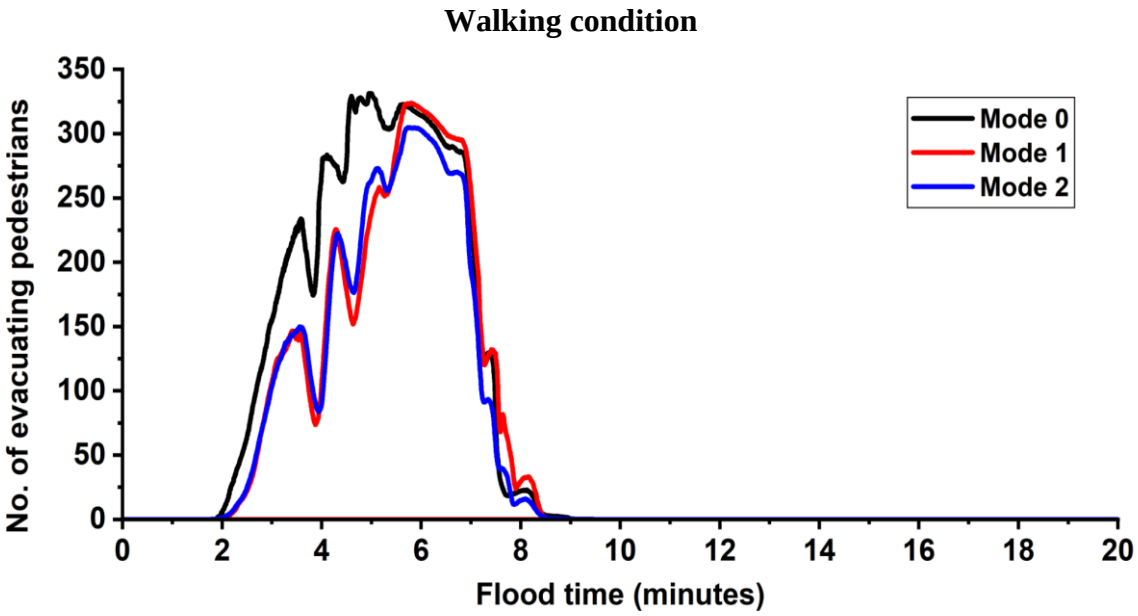

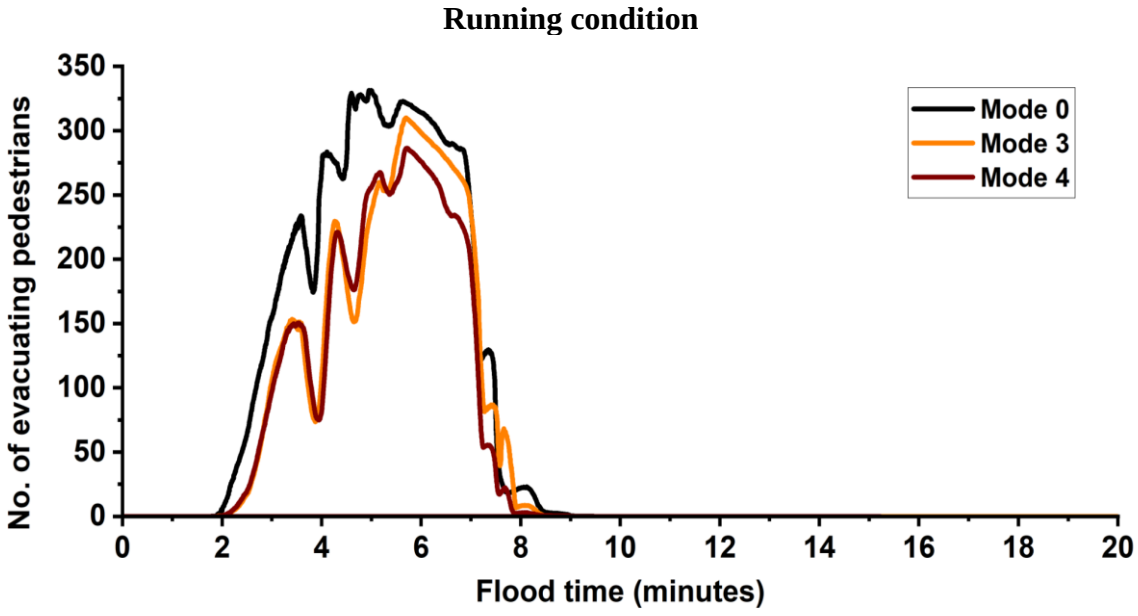

(b) Evacuating pedestrians with a medium flood risk state (0.75 < HR <1.5)

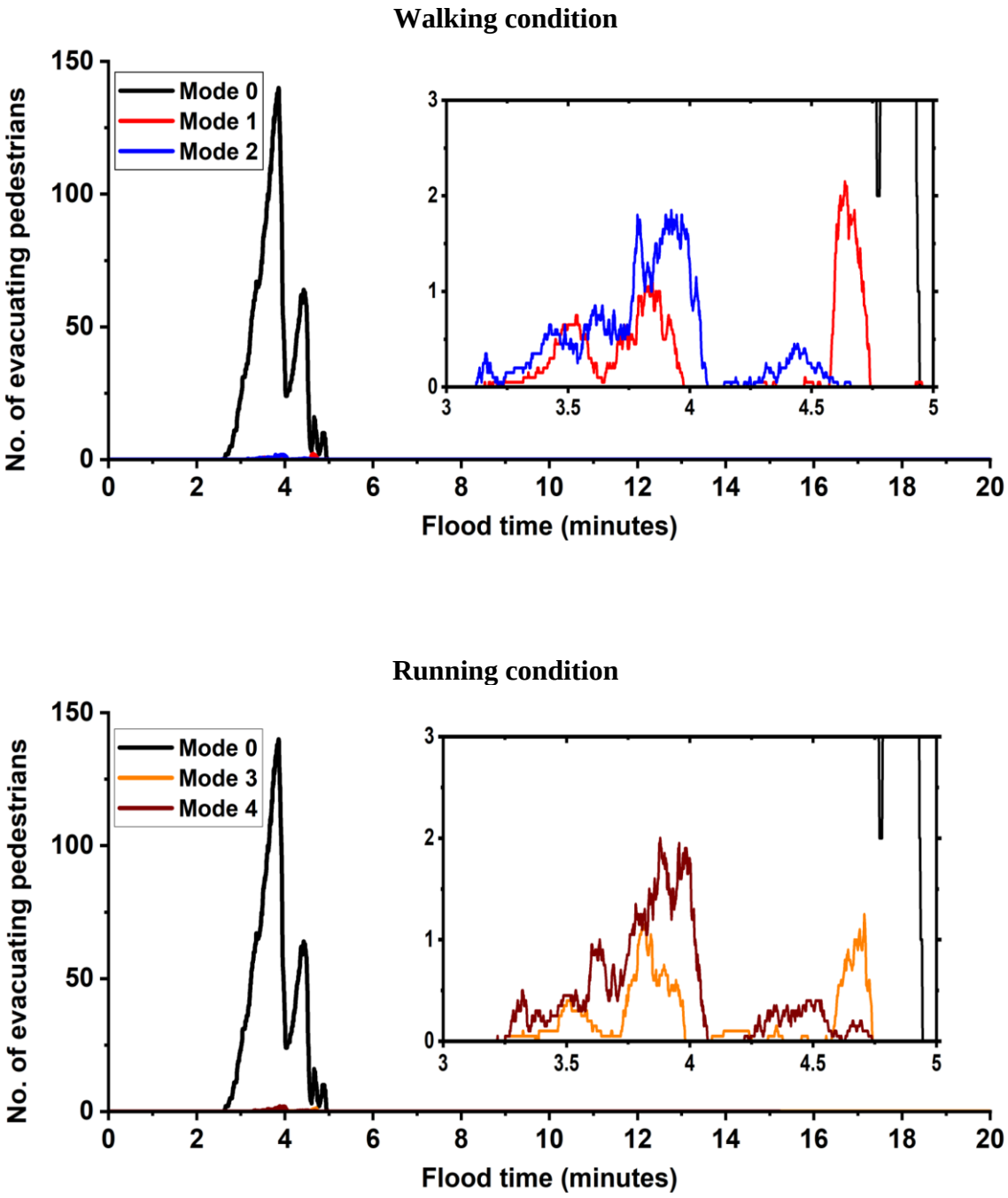

(c) Evacuating pedestrians with a high flood risk state (1.5 < HR < 2.5)

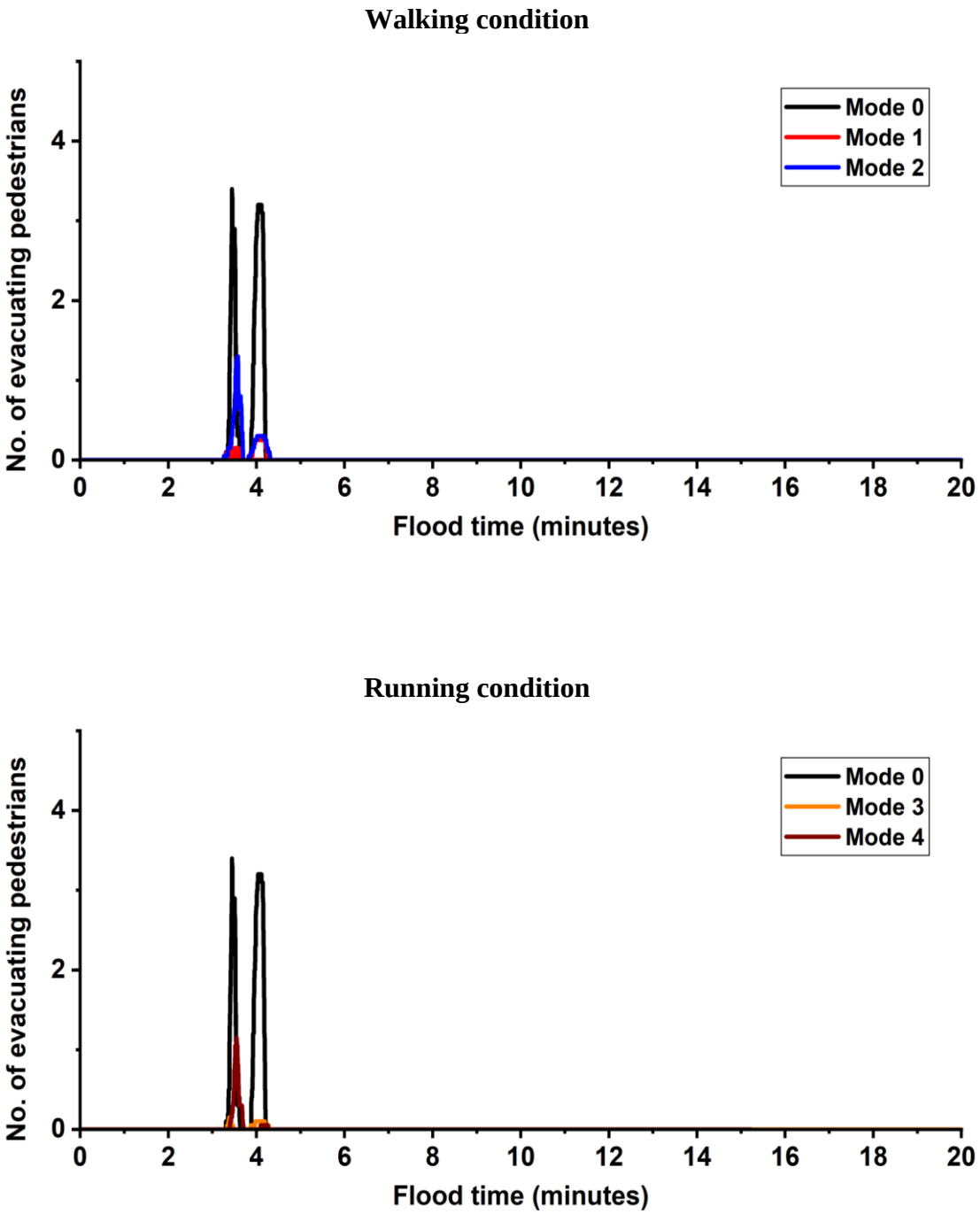

(d) Evacuating pedestrians with a highest flood risk state (2.5 < HR < 20)

Figure 4.8: Average number of evacuating pedestrians with different HR-related flood risk states predicted by the simulator after 20 runs under: Mode 0 (baseline outcomes from the previous version of the simulator in Phase 1, Sec. 4.2); Mode 1 or Mode 2 (age-related walking condition for the moving speeds without or with the two-way interaction condition); and Mode 3 or Mode 4 (age-related running condition for the moving speeds without/with the two-way interaction condition). Analysis is presented in sub-figures (a)-(d), each considering a different flood risk state.

Figure 4.9 shows the trends in the number of evacuating pedestrians with different stability states averaged from the simulator predictions after 20 runs for all the configuration modes (Table 4.6). Pedestrians seem to be only under either toppling-only condition (Fig. 4.9a) or toppling-and-sliding condition (Fig. 4.9b), with no pedestrians spotted to be under a sliding-only condition. The trends predicted with the simulator under Mode 1 to Mode 4 lead to a similar timing, as the baseline prediction under Mode 0, when pedestrians potentially had toppling-only and toppling-and-sliding states: they show that these stability states could be detected during 2 min to 8 min, and during 2 min to 6 min, respectively. These flood times are found to contain a large number of pedestrians with low-to-medium risk states (Fig. 4.8a and b), suggesting that the majority of pedestrians within these flood risk states could be in toppling-only and toppling-and-sliding stability states. By also contrasting the outputs obtained from simulations under configuration Mode 1 and Mode 3, a very similar trend could be observed for the pedestrians with toppling-only (Fig. 4.9a) and toppling-and-sliding (Fig. 4.9b) stability states. This is also observed for the results with the simulator under Mode 2 and Mode 4, suggesting that age-related moving speeds lead to similar information on the stability states when the pedestrians have a low-to-medium flood risk state regardless of whether the two-way interaction condition is activated or not. Contrasting the trends without (Mode 1 and Mode 3) and with the two-way interaction condition (Mode 2 and Mode 4) shows notable reductions in the number of pedestrians at 6 min (Fig. 4.9a) and 4.6 min (Fig. 4.9b), during which large crowds (> 200 pedestrians) were caught with medium risk states (see Fig. 4.8b). This observation suggests that running the simulator with age-related moving speeds with the two-way interaction condition (Mode 2 or Mode 4) is a sensible choice to study the stability state of large crowds in floodwater imposing low-to-medium risks to pedestrians. The evacuation patterns of pedestrians are analysed next through comparing their spatial distribution at 6 min of flood time across all the simulation modes, where the highest number of pedestrians are predicted to be at a medium flood risk state and the largest discrepancy in the number of pedestrians with a toppling-only condition is observed (see Fig. 4.8b and Fig. 4.9a).

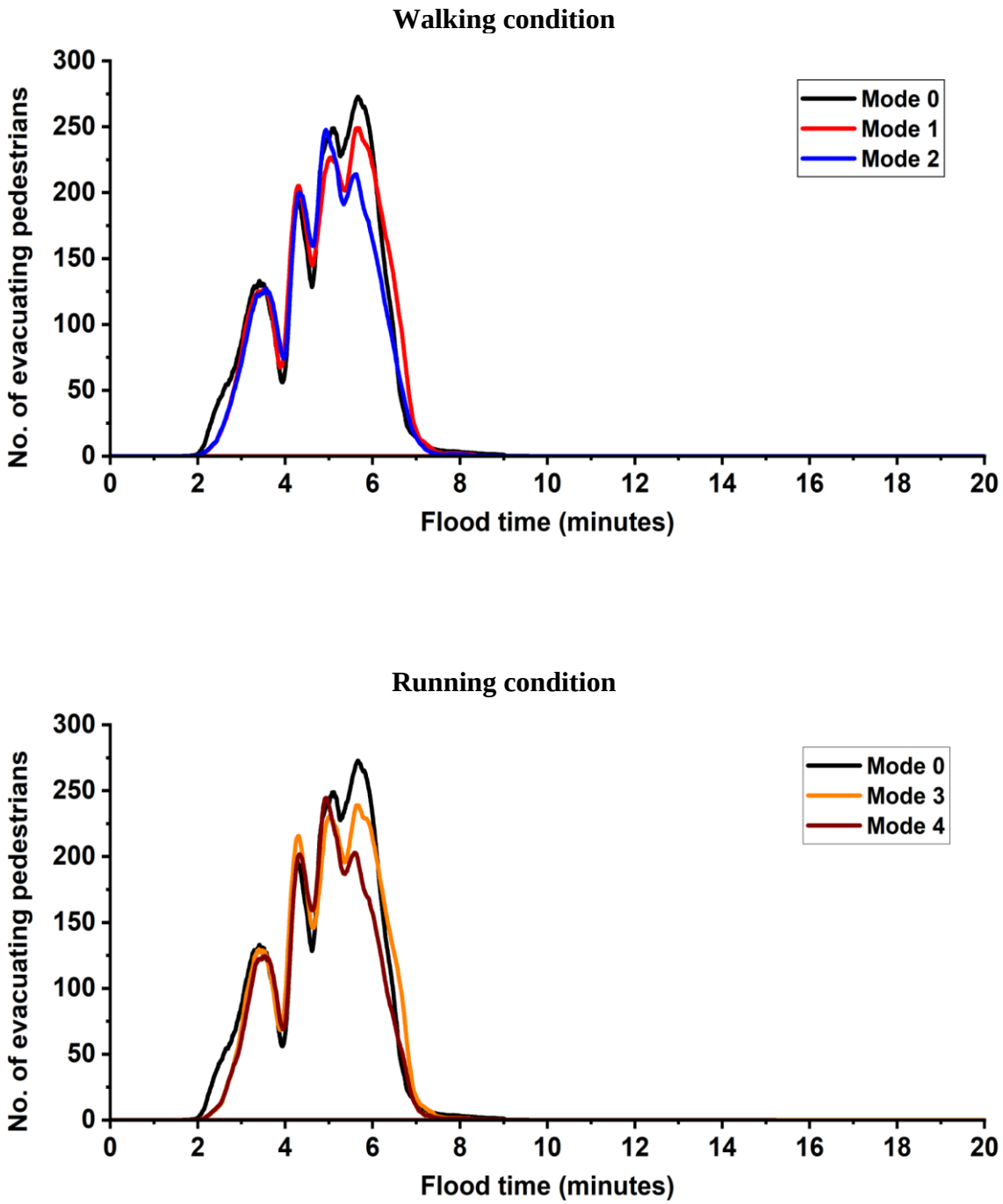

(a) Evacuating pedestrians with a toppling-only condition

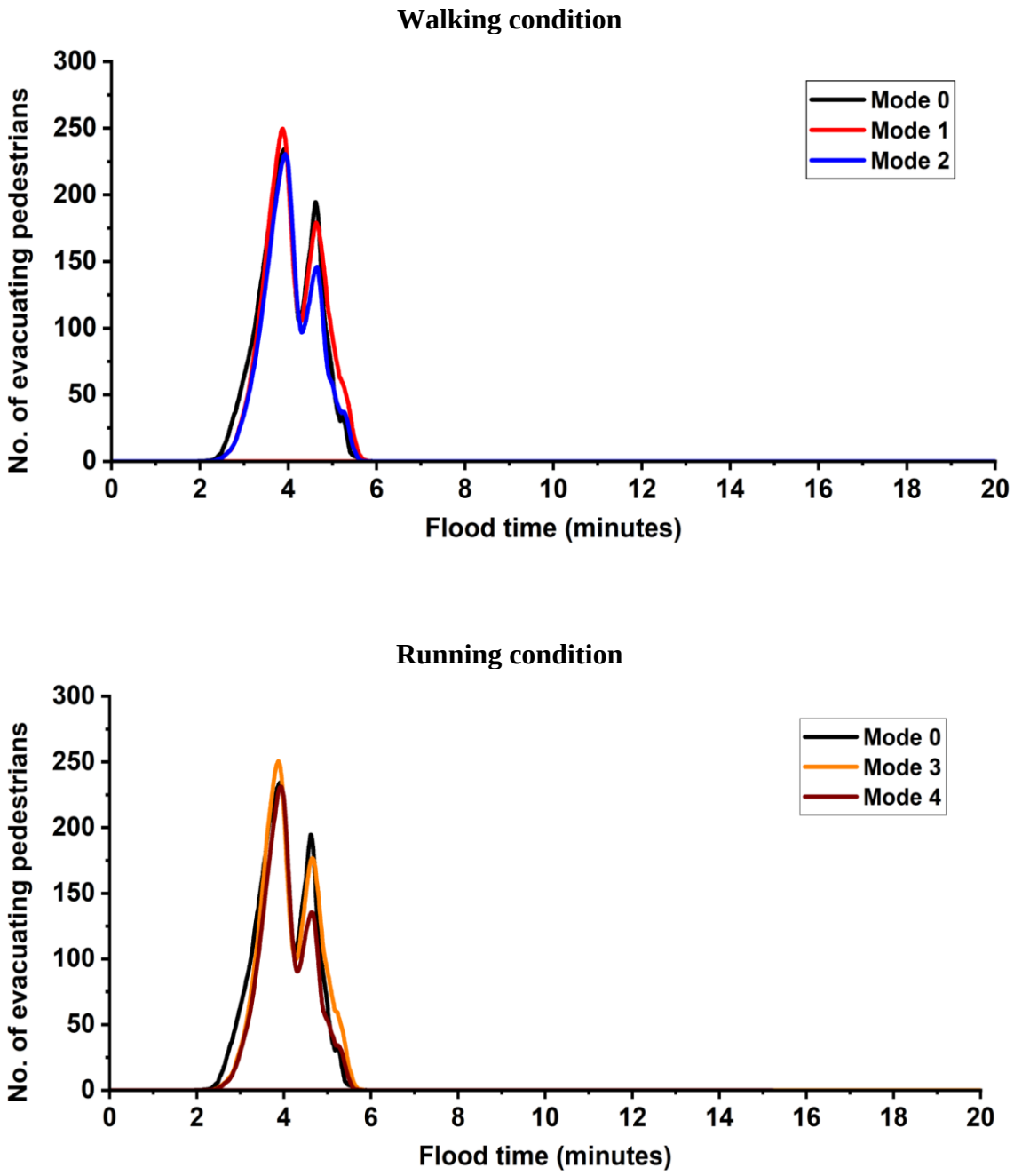

(b) Evacuating pedestrians with a toppling-and-sliding condition

Figure 4.9: Number of evacuating pedestrians with different stability states predicted by the simulator after averaging the results from 20 runs under: Mode 0 (baseline outcomes from the previous version of the simulator in Phase 1, Sec. 4.2); Mode 1 or Mode 2 (age-related walking condition for the moving speeds without or with the two-way interaction condition); and Mode 3 and Mode 4 (age-related running condition for the moving speeds without or with the two-way interaction condition). Sub-figures (a) and (b) include the stability states with a toppling-only condition and a toppling-and-sliding condition, respectively, when immobilised in floodwater.

4.5.3 Analysis on the spatial distribution of pedestrians

Figure 4.10 compares the spatial distributions of the evacuating pedestrians over flood HR map at flood time 6 min, obtained from simulator runs under Mode 1 to Mode 4. In each of the sub-plots, the framed 50 × 50 m^2 before the emergency exit includes the number of pedestrians in that area, where the congestion of pedestrians is assessed for the different modes. With all the modes, the simulator predicted a dominance of medium risk floodwaters ($0.75 < HR < 1.5$) over the walkable area, causing the majority of the pedestrians to fall into a toppling-only condition (purple dots) and a minority to have a stable condition (green dots) in front of the emergency exit and from the left side of the crowd. By contrasting the spatial distribution of pedestrians obtained from Mode 1 and Mode 2 (Figs. 4.10a and b), there seems to be a considerable increase in the number of pedestrians with a stable condition when the two-way interaction condition is enabled with the walking condition (Mode 2). The same pattern is observed with Mode 3 and Mode 4 (Figs. 4.10c and d), but this is accompanied by a shift in the position of pedestrians towards the front, as expected for the running condition. On the other hand, by contrasting the number of pedestrians in the small square obtained from Mode 1 and Mode 3 (Figs. 4.10a and c), it can be observed that enabling the running condition results in a decrease in the congestion of pedestrians in front of the emergency exit. The opposite pattern is observed when enabling the two-way interaction condition in Mode 2 and Mode 4 (Figs. 4.10b and d), showing an increase in the congestion of pedestrians under a running condition compared to the walking condition. Hence, using the two-way interaction condition with the simulator may be useful to more realistically evaluate bottlenecking impacts of an evacuation process.

In terms of total evacuation time for the 1,000 pedestrians, averaged results after 20 runs show that it takes 13.8 min with Mode 0, 18 min with Mode 1, 18.1 min with Mode 2, 12.5 min with Mode 3 and 12.3 min with Mode 4 to allow all the pedestrians to leave the walkable area. Contrasting the predicted times reinforces previous findings from Fig. 4.8: compared to Mode 0, the age-related walking speeds, either with or without the two-way interaction condition (Mode 1 and Mode 2, respectively), leads to slower evacuation speed predictions that become faster under the running condition.

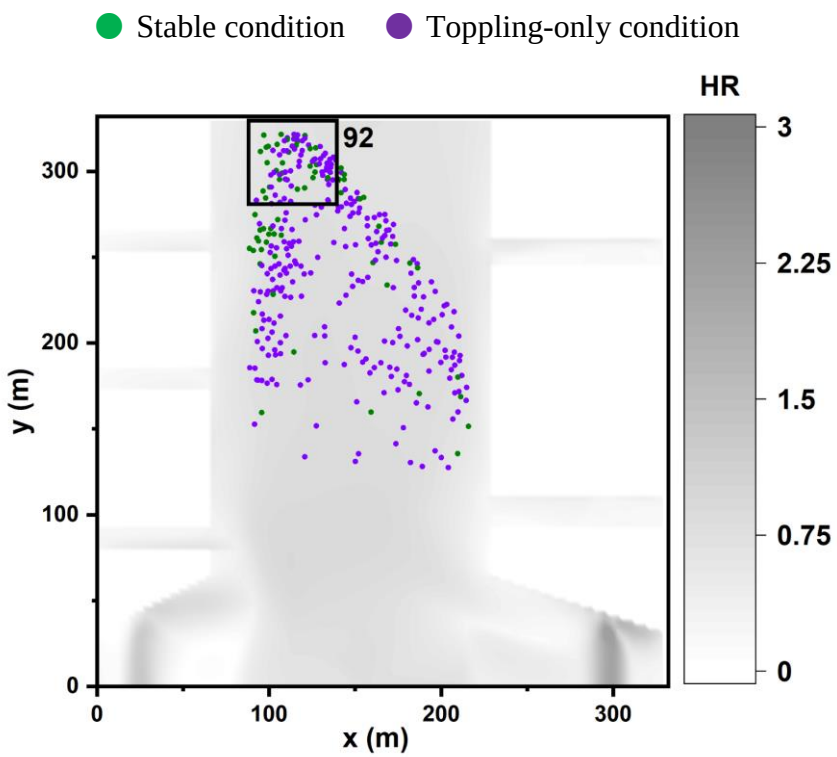

(a) Mode 1

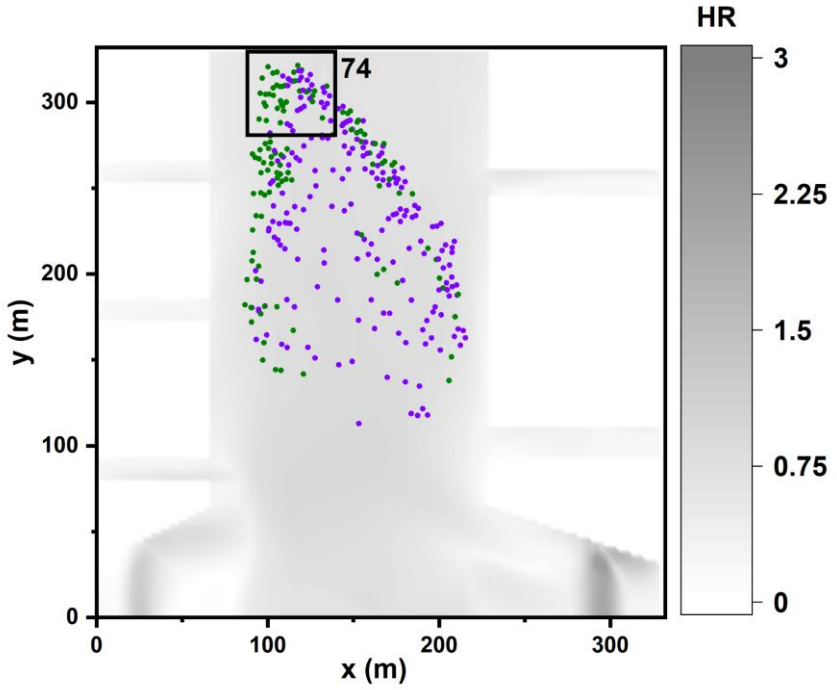

(b) Mode 2

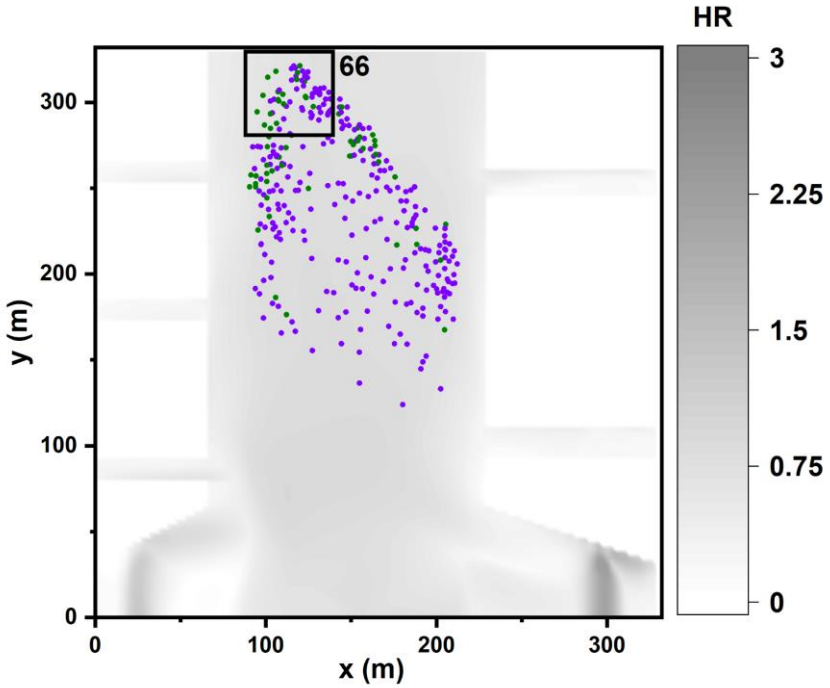

(c) Mode 3

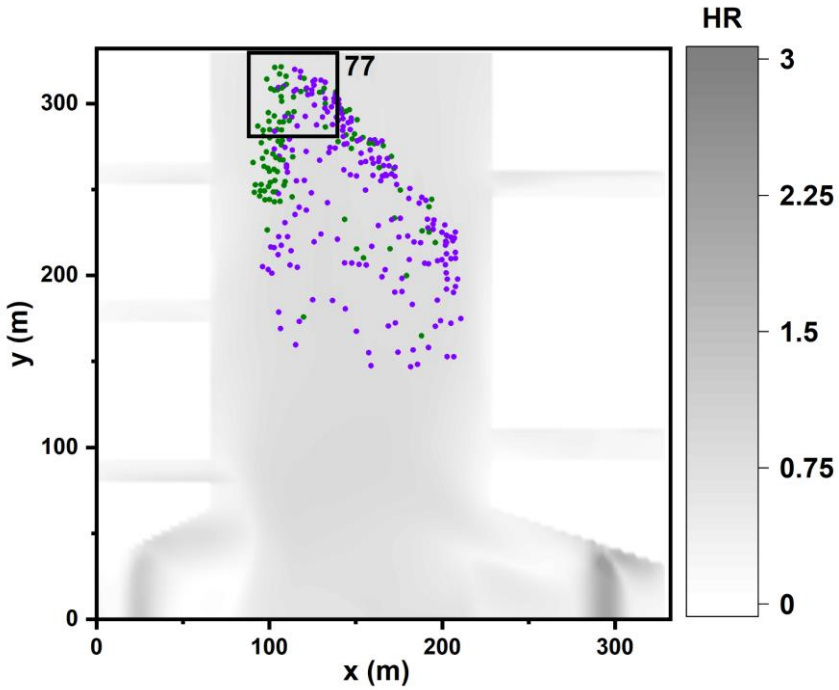

(d) Mode 4

Figure 4.10: Spatial distribution of pedestrian agents, represented by coloured dots, predicted by the simulator under Mode 1 to Mode 4 at 6 min after flooding. The grey colour represents the floodwater extent based on the flood HR quantity and the square before the emergency exit represents an area of 50 × 50 m^2 with a number printed alongside it representing the number of pedestrians in that area.

4.6 Simulation runtimes

The simulation runtime for the coupled flood-pedestrian model to run the shopping centre test case over a duration of t = 18.1 min have been explored across each of the configuration Modes 0-4 (see Table 4.6). These runtimes, listed in Table 4.8, are averaged out over 20 runs and recorded on the same desktop computer reported in Sec. 4.5 with the resolution of 2.59 m × 2.59 m as reported in Sec. 3.5. The runtimes have been measured while the FLAME GPU visualisation mode was also activated.

As shown in Table 4.8, with Mode 0, where the pedestrians are featured with a constant moving speeds, the simulations took much shorter time than the ones measured from configuration Modes 1 to 4. The reason is that, with these modes, the age- and gender-related moving speeds are enabled, which imposes additional computational complexity compared to Mode 0. Also, by comparing Mode 1 to Mode 2 and Mode 3 to Mode 4, the simulation runtime slightly increases when the two-way interaction condition is further enabled, showing a slight increase in the computational time. Nonetheless, the coupled flood-pedestrian model, though augmented with the sophisticated behavioural rules, is capable of running the shopping centre test case almost four times faster than real time (demo videos of these simulations are available online on the TIB AV-Portal at https://doi.org/10.5446/51547).

Table 4.8: The average simulation runtimes for the coupled flood-pedestrian model to run the shopping centre test case under different configuration modes (Table 4.6).

Modes	Simulation runtime (min)
Mode 0	2.65
Mode 1	4.42
Mode 2	4.6
Mode 3	4.45
Mode 4	4.51

4.7 Summary and concluding remarks

This chapter described the augmentations made to the coupled flood-pedestrian model pertaining to the heterogeneity of pedestrians' characteristics and behavioural rules to more realistically govern their stability state and moving speeds under evacuation conditions. The new features have been incorporated into the model and their influence on the simulation outcomes have been investigated through two subsequent improvement phases.

In Phase 1, relative to the basic version of the simulator (reported in Chapter 3), pedestrian agents were featured with various body height and mass, as well as experimentally-valid behavioural rules to drive their walking speeds and instability conditions in floodwater. The augmented simulator was applied to reproduce the 'during flooding' evacuation scenario of the shopping centre synthetic test case. The simulator runs were applied diagnostically under three configuration modes, while increasing the level of sophistication of the behaviour rules, to systematically analyse the relative changes in the outcomes across the modes. The analysis suggests much longer evacuation times as the behavioural rules became more sophisticated. Further investigation on the simulator outcomes allowed to usefully identify HR-related risk states and formulae to directly estimate the states of unstable pedestrians or otherwise their walking speed states. The HR safety thresholds, identified through simulations, are found to be slightly more conservative than those recommended in UK guidance documents, reinforcing alternative findings in published literature (e.g. Chanson and Brown 2018).

In Phase 2, pedestrians have been characterised by age, gender and body mass attributes based on real-world datasets. The new behavioural rules were also supported by a set of empirically based age- and gender-related moving speeds driving the motion of pedestrian agents around and inside the floodwater, and with a maximum excitement condition to accelerate the walking speed of pedestrian agents around the floodwater. The moving speed could also be intertwined with a two-way interaction condition to model the influence of pedestrian congestion on flowing floodwater, and vice versa. A new autonomous change of direction condition was proposed to model the way-finding decisions of pedestrian agents based on their individual perception of the flood risk in relation to the local changes in floodwater dynamics or the choice of others. The relevance of the added features were evaluated for the same shopping centre test case. The evaluation procedure was based on systematically activating any of the added walking or running moving speeds with or without

the two-way interaction condition in the simulator, and then analysing the changes induced in the simulation outcomes with reference to the baseline results. The analysis contrasted temporal and spatial changes in the number of pedestrians in relation to their HR-related flood risk and stability states, indicating major differences to the baseline results. The differences in the predicted number of pedestrians seems to vary considerably, up to hundreds, depending on the density of the crowd as the flood risk becomes low-to-medium. Also, the analysis suggests longer evacuation times with the walking condition but using the running condition has led to the close evacuation times compared to baseline results.

These improvements were only evaluated over a synthetic test case and it was limited to a simplified way-finding decision rule for directing pedestrian agents to one fixed emergency exit destination (specified in advance). This means that the influence of the interplay between the two-way interaction condition (which was reported in Chapter 3) and the pedestrian agent characteristics and rules on the simulation outcomes had not yet been explored. These features are known to be essential for applying the simulator to outdoor spaces in a more realistic set up which includes multiple potential destinations for the pedestrians to detect during a flood evacuation. To address that, the utility of the simulator with the new autonomous change of direction condition have been explored in the next chapter for a real-world evacuation scenario.

Chapter 5

Application of the coupled flood-pedestrian model for a real-world case study

5.1 Chapter overview

This chapter, which aims to address Objective 3, investigated the capabilities of the coupled flood-pedestrian model for a real-world case study of a mass evacuation from the Hillsborough football stadium in response to a flood emergency, replicating the conditions of November 2019 Sheffield floods. Sec. 5.2 describes the background of the case study and the evacuation scenario in details. Sec. 5.3 explains the model configuration including the setups for the hydrodynamic model and pedestrian model that have been devised to perform a set simulations considering three thresholds of floodwater depth for pedestrians' flood-risk perception. Sec. 5.4 describes the analysis that have been performed on the simulation outcomes. These analyses involved investigation on the plausibility of the outputs considering the uncertainties in the pedestrians' behaviour for each of the three thresholds of flood-risk perception, based on which the safest destination preferred by pedestrians have been identified and the temporal and spatial changes in the flood risks on pedestrians have been analysed. The simulation runtimes that have been measured are reported and discussed in Sec. 5.5. Finally, Sec.5.6 ends this chapter by providing a summary and highlights of the key findings from the analysis of the simulations' outputs.

5.2 Background and scenario description

The case study consists of a site located outside of the main entrance of Hillsborough football stadium in Sheffield. The location of the site is framed with a dark red square in Fig. 5.1, including an area of 16,384 m^2 that is adjacent to the eastern side of the stadium, where the main entrances are located (yellow line, Fig. 5.1). The stadium entrances are opened to a T-junction that constitutes the walkable area whose boundaries are indicated by solid red lines. This area includes the main roads, main stadium's entrances, and pedestrian pathways to usual destinations to the south, east and north. These destinations, shown with the green lines in Fig. 5.1, are the most likely choices for a spectator leaving the stadium.

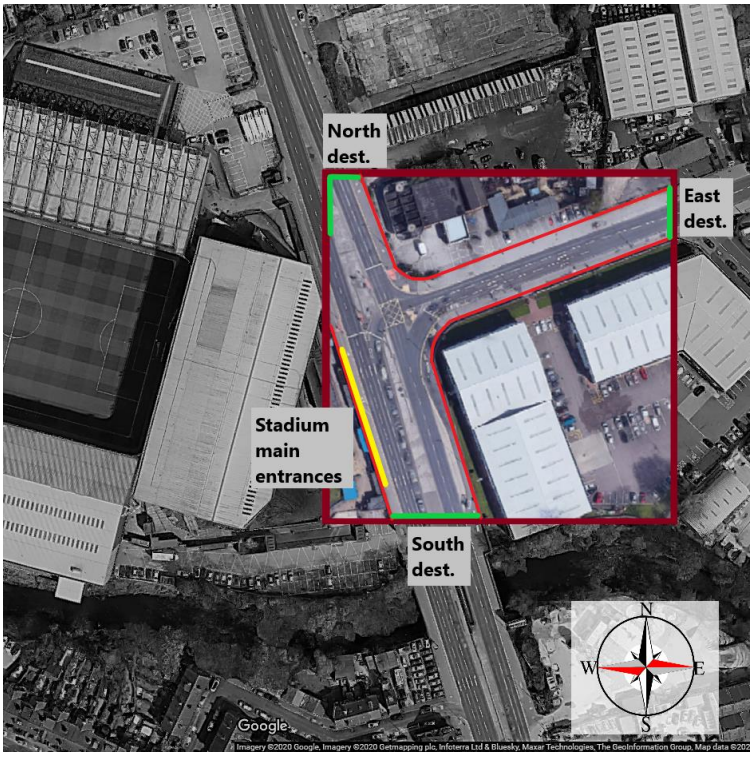

Figure 5.1: The study site (red square) including the walkable area (red area within the red square) where people normally use to go to their different destinations located in the south, east and north sides of the walkable area (green lines) after they leave the stadium from the main entrances (yellow line), © Google.

The stadium can accommodate up to 39,732 spectators with an average attendance rate of 24,000 per home football match in normal weather conditions (Sheffield Wednesday, available at: www.footballwebpages.co.uk/sheffield-wednesday). This site would therefore

encompass a large number of spectators before or after a match, even in the aftermath of a flood as, for example, observed during the 2007 Summer floods (The Sheffield Guide by DeeJayOne, 2007; Environment Agency, 2007). The event suggests that rainfall runoff would cause floodwaters to spread from the east and north to accumulate in front of the main stadium's entrances, where it could submerge walking pathways, parking lots and the stadium pitch ("Bring on the sub", 2007). Worries of a similar event were expressed during the November 2019 floods driven by seven-day continuous rainfall of 63.8 mm over the city of Sheffield (Pugh, 2019), which led to cancelation of a football match as the flood defence protecting the stadium from River Don was about to be overtopped by the floodwater. The event, if happened during the football match, could put many in and around the stadium at a high risk.

This site, being both adjacent to River Don and located down the hills where rainwater runoff accumulates, has been flagged to be prone to future pluvial or fluvial flood types according to the EA's flood information service that is available online at https://flood-warning-information.service.gov.uk/long-term-flood-risk. This service provides flood maps for identifying long-term risks in parts of the UK towns based on a 'low', 'medium' and 'high' annual probability of occurrence. By entering the Hillsborough stadium postcode, S6 1SW, the flood maps showing the approximate ranges of the expected floodwater depth and velocity magnitude for the study site (Fig. 5.1) were obtained, as shown in the screenshots in Fig. 5.2. The floodwater depth map associated with a high annual probability (left panel, Fig. 5.2a) represents the least extreme scenario, where the range for the floodwater depth is likely to vary between 0.3 m and 0.9 m to potentially cover the northern branch of the walkable area with velocity magnitudes greater than 0.25 m/s. For a medium annual probability of occurrence (middle panel, Fig. 5.2a), the flooding extent could widen to potentially obstruct both northern and eastern branches with the range of floodwater depths reaching beyond 0.9 m and much wider extent for velocity magnitudes greater than 0.25 m/s mostly along the eastern branch (middle panel, Fig. 5.2b). For a low annual probability of occurrence (right panel, Fig. 5.2a), an even wider flood extent would be expected up to almost submerging the entire walkable area with dominance of deeper than 0.9 m floodwater depths along the northern branch and higher than 0.25 m/s velocities at the north, east and the sides of the southern branch. Even in the most optimistic flooding scenario, at least the northern branch near the stadium's entrance would be affected, where an evacuating spectator during a flood has to wade through floodwaters at a depth that is between 0.3 m and 0.9 m and velocities

higher than 0.25 m/s. Therefore, investigating the dynamics of how people respond in a during-flood evacuation is of paramount importance for the selected study site.

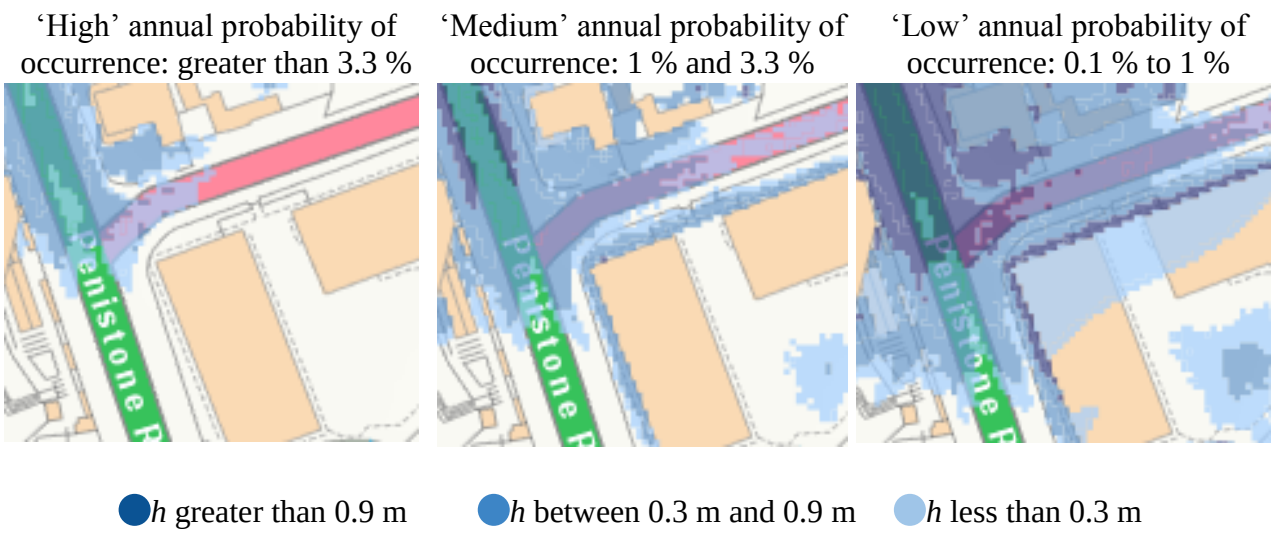

(a)

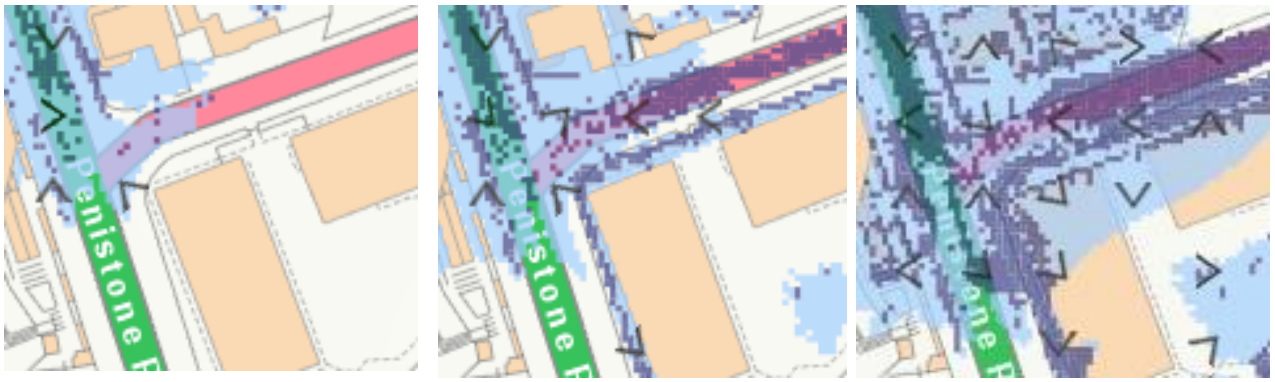

(b)

Figure 5.2: Screenshots of EA's flood risk maps of the study site showing the extent of flooding from surface water with 'low', 'medium' and 'high' annual flooding probabilities featuring different floodwater ranges of: (a) depth and (b) velocity. These screenshots were retrieved from https://flood-warning-information.service.gov.uk/long-term-flood-risk (credit: © Crown and database rights under Open Government Licence v3.0).

To do so, it was assumed that the site in Fig. 5.1 is hit by a flood during a football match where the spectators are caught unaware of the rainfall accumulation around the stadium, similar to the event that could have happened in 2019. As discussed before, the

floodwater is likely to accumulate from the north and east sides to move downhill towards the main entrance of the stadium. Once the floodwater has reached the stadium's main entrances, an emergency evacuation alarm is issued, urging people to start evacuating immediately. The spectators are then put into queues inside the stadium to be evacuated towards the walkable area. The evacuating spectators gradually enter the walkable area where they get in direct contact with flooded areas along their ways to any of the south, east or north destinations. In this scenario, a population of 4,080 spectators was assumed, which is lower than normal due to the severe weather condition and flood warnings issued prior to the event. This population is around 20 % of the spectators expected, and represents the relative number of people who would ignore the warnings and attend the match (Fielding *et al.*, 2007).

For this case study, a dispatch measure was introduced to the simulator to release the evacuees into the walkable area during the flooding. The dispatch measure limits the influx rate to person-per-second per width unit to comply with guidance methods for controlling the density of large crowds outside the stadiums for safe evacuation (Minegishi and Takeichi, 2018; Still, 2019). For a gate that is around 4 m wide, four pedestrians per second are dispatched from the stadium to the walkable area. Using the simulator with this dispatch rate limits the overall number of pedestrians that would be present in the walkable area at a time. Therefore, running the simulator to analyse the evacuation of a larger number of spectators is expected to lead to similar risk trends based on pedestrians' different HR-related flood risk and stability states, which would only be prolonged over a longer evacuation time.

5.3 Model configuration

5.3.1 Hydrodynamic model set-up

The hydrodynamic model was set up to run on a grid of 128 × 128 flood agents. The grid of flood agents (equally for the grid of navigation agents) was set to store the terrain features of the study site, loaded from a digital elevation model (DEM) at 1 m resolution, which is available online from the UK's Department for Environment Food & Rural Affairs (DEFRA) LiDAR Survey at: https://environment.data.gov.uk. To the best of the authors' knowledge, there is no record of any observed hydrograph sampled at a gauge point located in the selected study site. Therefore, the flooding flow was generated by formulating an inflow hydrograph

based on the November 2019's rainfall volume (Fig. 5.3). The hydrograph was set to replicate a total runoff volume accumulation of 1,045.3 m^3 based on a 0.0638 m rainfall over the entire 16,384 m^2 site. This volume was estimated using the direct runoff method: *rainfall volume* (m^3) = *rainfall height* (m) × *area* (m^2). The hydrograph was generated as:

$$Q_t = Q_{initial} + \left(Q_{peak} - Q_{initial}\right)\left(\frac{t}{t_{peak}}.exp\left(\frac{1-t}{t_{peak}}\right)\right)^{\beta}, \quad (5.1)$$

where Q_t (m^3/s) is the inflow discharge propagating along the north-east boundary intersecting the eastern branch; Q_{peak} (m^2/s) = 0.29 is the peak discharge, that was calculated by distributing the runoff volume (1,045.3 m^3) per second over an hour of flooding; $Q_{initial}$ (m^3/s) is the initial discharge, taken 0 m^3/s; t (min) is the simulation time varying between 0 to 10 min; β = 10 is a constant to soften the shape of the hydrograph and t_{peak} (min) = 5 is the time of peak discharge. This choice, for t_{peak}, considers the peak discharge has been reached halfway during the flooding to cause the propagating floodwater to reach to the main stadium's entrances by 10 min leading to triggering the evacuation alarm.

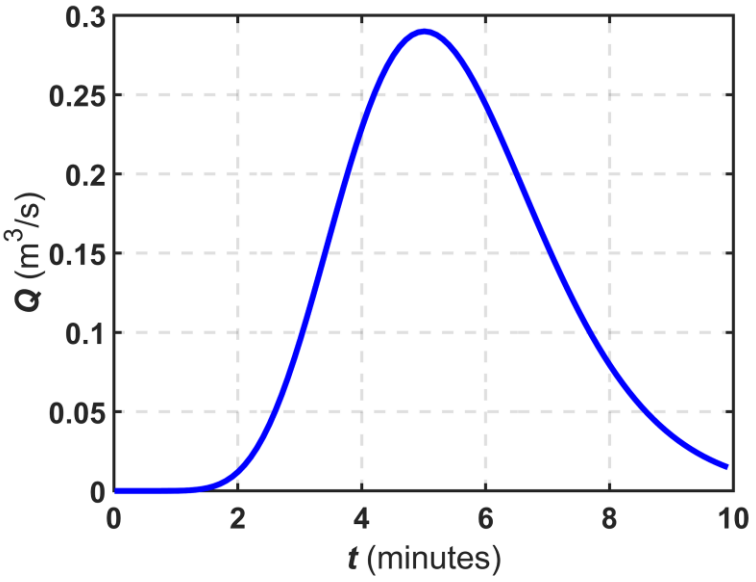

Figure 5.3: Inflow hydrograph produced by Eq. (5.1) used to generate the floodwater propagation occurring from the north-east side of the site.

To ensure that the resulting ranges of floodwater depth and velocity magnitude generated by the hydrograph in Fig. 5.3 fit the expected ranges of floodwater depth and velocity reported by the EA, a run was conducted without pedestrian consideration. Fig. 5.4a shows the map of the predicted floodwater depth after 10 min of flooding, while Fig. 5.4b and Fig. 5.4c includes the time series of the mean floodwater depth ($\bar{h}$) and velocity magnitude ($\bar{V}$) in the lead-up to 10 min, respectively. From the floodwater depth map, it can be seen that the spatial distribution of floodwater depth varies between 0.3 m and 0.9 m inside the walkable area at the time when pedestrians start to evacuate. By this time, Fig. 5.4b and Fig. 5.4c suggest that the mean floodwater depth is at its deepest level of 0.5 m and the velocity magnitude reduces to 1.5 m/s. Beside confirming that the generated hydrograph leads to a realistic flood event in line with the EA's expectations, these results indicate that a pedestrian evacuating into the floodwaters shown in Fig. 5.4a would be under a low-to-medium flood risk state with an HR value estimated around 1 (can be extracted by the end of the time series in Fig. 5.4b and Fig. 5.4c).

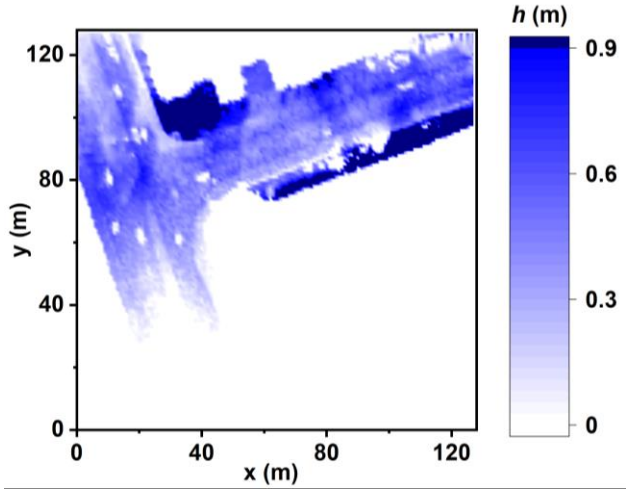

(a)

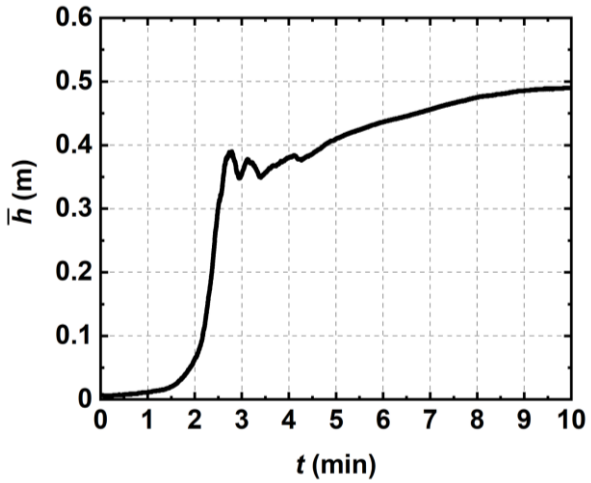

(b)

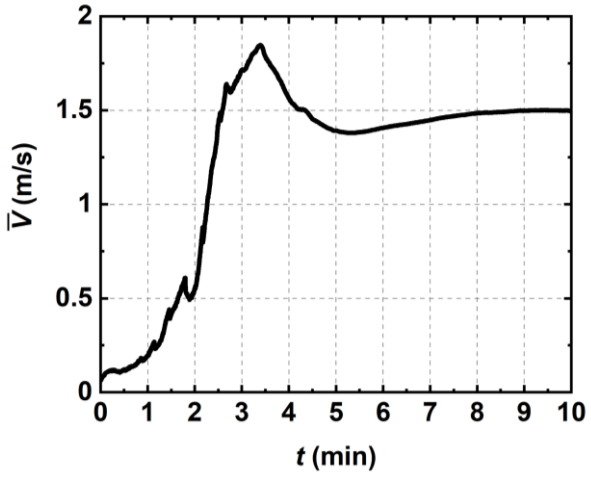

(c)

Figure 5.4: Outputs of the simulator generated after and during 10 min of a single hydrodynamic run without pedestrian consideration plotted in terms of: (a) floodwater depth map and temporal changes in the average floodwater in terms of (b) depth and (c) velocity.

5.3.2 Pedestrian model set-up

The pedestrian model was also set up for a grid of 128 × 128 navigation agents encoding the topographic features of the site into the navigation map as well as the boundaries, location of entrances and destinations about which the pedestrian agents receive information. The pedestrian model was set to gradually generate 4,080 pedestrian agents with a rate of 4 pedestrian agents per second starting at simulation time t = 0 min. Once a pedestrian agent is generated, it is assigned a random (initial) destination between the south, east or north (Fig. 5.1) with an equal probability of selection.

As the case study consists of an outdoor urban environment with multiple destination choices, the pedestrian agents are set to dynamically alter their initially assigned destination by activating the 'autonomous change of direction' condition (see Sec. 4.4.3). This condition allows pedestrian agents to auto-select new pathways after analysing the state of the floodwater variables received from the navigation agent at their current location. As it was previously explained in Sec. 4.4.3, this condition requires specifying a threshold of floodwater depth to body height beyond which a pedestrian agent considers shifting their walking direction and looking for a new destination within 100 seconds. After this period, if the pedestrian agent remains undecided, it is set to pick the destination selected by the majority of its neighbouring pedestrian agents, on the basis that it was influenced by the choice of others around.

For the 'autonomous change of direction' condition, three thresholds of floodwater depth to the body height (Fig. 5.5) were selected, informed by the experiments in Dias *et al.* (2021). This was done to account for the uncertainty associated with individuals' different risk perception. The '20 % threshold' was defined to represent people with high-risk perception, such as those who previously experienced a critical flooding incident, and decide not to enter floodwater with a depth that is more than 20 % of their body height. This threshold is estimated based on the ratio of the dominant minimum value for the depth of floodwater that can occur over the walkable area (0.3 m) to the height of the shortest pedestrian agent available (1.4 m). With this threshold, the likelihood of the entire population to be in a condition to change their direction is ensured. The '40 % threshold' was defined to represent people with low-risk perception, such as those who have not yet experienced a flood incident, and decide to enter a floodwater with a depth that is even more than 40 % of their body height. This threshold is estimated based on the ratio of the dominant maximum

depth of floodwater (0.9 m) to the height of the tallest population of pedestrian agents available (2.1 m). This threshold enables the entire population to have the freedom to keep moving even within the deepest floodwater in the walkable area (0.9 m). The '30 % threshold' accounts for an average-risk perception, such as those who previously experienced a minor to moderate flooding incident. Pedestrians with average-risk perception would decide to enter floodwater up to their knees, which constitutes 30 % of the human body height (Teichtahl *et al.*, 2012).

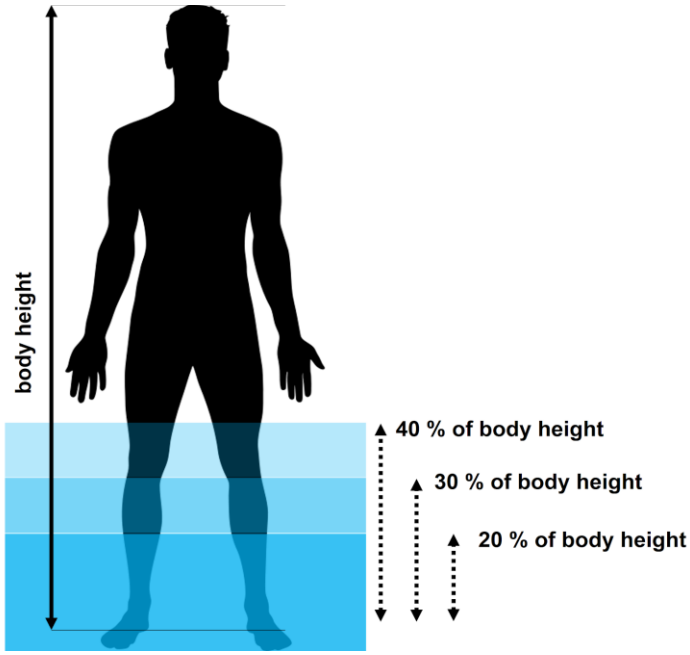

Figure 5.5: Thresholds of floodwater depth to body height that are specified for pedestrian agents to accommodate uncertainty associated with different risk perception of people in the real-world case study.

The characteristics of pedestrian agents were adapted to consider the age, gender and height distribution of football fans in the UK. Therefore, the randomised age distribution reported Sec. 4.4.1 was increased by 5 %, 8 % and 4 % for the age groups of 30 to 39, 40 to 49, and 50 to 59 to replicate the higher attendance of these age groups to live sports events in England (Lange, 2020). Also, the randomised gender distribution was changed to 67 % males and 33 % females based on a survey on the gender distribution of football fans in the UK (Statista Research Department, 2016). In terms of body height, the pedestrian agents were based on the same UK body height distribution used previously in Sec. 4.2.1.

5.4 Simulation runs

A series of 20 simulations were performed on the same computing machine reported in Sec. 4.5 under configuration Mode 2 for each of the 20 %, 30 % and 40 % threshold for the 'autonomous change of direction' condition. Each run was set to start at t = - 10 min to allow the floodwater to propagate during 10 min so that the evacuation process starts at t = 0 min. Outputs averaged from each series of simulation included spatial and temporal information, at each time step, about the pedestrian agents as they evacuate (t > 0 min). The averaged outputs include the position, HR-related flood risk state, stability state (with a toppling-only condition, toppling-and-sliding condition and sliding-only condition), and the choice for the destination selected by the pedestrian agents during the evacuation process.

In this section, the averaged outputs, considering the uncertainties associated with the behaviour of pedestrians (Sec. 5.4.1), are analysed for each of the 20 %, 30 % and 40 % thresholds, considering the popularity of the destination selected by the pedestrian agents among south, east and north (Sec. 4.2.1) together with their HR-related flood risk states (Sec. 4.2.2) and stability states (Sec. 4.2.3).

5.4.1 Sensitivity analysis of the outputs

Considering the stochastic uncertainties associated with the motion of the pedestrian agents, the plausibility of the averaged outputs from the 20 runs was evaluated. The evaluation was based on the *MOE*, using Eq. (4.9), for 99.9 % confidence level only, informed by the results of the analysis in Sec. 3.2. Table 5.1 shows the maximum *MOE*s found for the number of pedestrians predicted to be in the considered HR-related flood risk and the stability states, obtained from the 20 runs using each of the 20 %, 30 % and 40 % threshold, respectively. It can be seen that the maximum *MOE* increases as the risk perception level decreases, suggesting a notable increase in the uncertainty after the incorporation of the risk perception component into the modelling of pedestrian behaviours.

Table 5.1: Maximum margin of error (*MOE*) for the average number of pedestrian agents with different HR-related flood risk or stability states that are extracted from the recorded outputs throughout the simulations for each 20 %, 30 % and 40 % threshold. Different ranges of the evaluated maximum *MOE* are highlighted with different colour shades: green, orange and red to indicate $MOE \leq \pm 5$, $6 \leq MOE \leq 9$ and $MOE \geq 10$, respectively.

HR-related flood risk and stability states	**Maximum *MOE***		
	20 % threshold	**30 % threshold**	**40 % threshold**
HR < 0.75	± 16	± 16	± 19
0.75 < HR <1.5	± 2	± 8	± 15
HR > 1.5	± 0	± 1	± 2
Toppling-only	± 2	± 5	± 13
Toppling-and-sliding	± 1	± 4	± 7

5.4.2 Analysis of the exit choices

Figure 5.6 shows the trends in total number of evacuating pedestrians in the walkable area, plotted according to the pedestrians' choices among the south, east and north destinations, obtained from simulations with the 20 %, 30 % and 40 % threshold. All the simulated trends show a decrease in the total number of pedestrians after 25 min of flooding. This suggests that 25 min would be required for the 4,080 pedestrians to vacate the stadium, and that the choice for the threshold does not have any effect on the collective evacuation time.

The simulated trends obtained with the 20 % threshold are shown in Fig. 5.6a, suggesting that most of the pedestrians evacuated the walkable area within almost 40 min. The majority of the evacuating pedestrians start favouring the south destination after 2.5 min, indicating that after this time pedestrians encounter floodwater depth beyond 20 % of their body height, which seems to be extending over the eastern and northern branches. After 2.5 min, the south destination remained the most popular destination, selected by more than 55 % of the pedestrians; whereas, the east and north destinations were less popular, selected by 25 % and 20 % of the pedestrians, respectively.

With the simulated trends obtained with the 30 % threshold (Fig. 5.6b), a longer evacuation time is predicted for the majority of the evacuating pedestrians. Now it takes

about 52 min for most of the pedestrians to leave the walkable area and the popularity of the east and north destinations increased, with slightly more evacuating pedestrians preferring them, about 27 % and 23 %, respectively. This suggests that 5 % more of the pedestrians considered changing their destination to the north where the floodwater depth can only reach up to their knee height. Still, as with the 20 % threshold, the south destination was the most popular and started to be favoured after 5 min by 50 % of the pedestrians.

With the simulated trends obtained with the 40 % threshold (Fig. 5.6c), a significant change in the favoured destination is observed alongside a relatively more prolonged evacuation time. Now, it takes about 57 min for most of the pedestrians to evacuate the walkable area and the popularity of the south destination decreased significantly, compared to the predicted trends obtained with the lower thresholds. Here, the south destination was only picked up by 25 % of the pedestrians and the north destination was preferred instead (by around 50 % of the pedestrians) since the beginning of the evacuation. As for the east destination, it remained equally popular as with the trends obtained with the lower thresholds, and was selected by around 25 % of the evacuating pedestrians.

The simulated trends in Fig. 5.6 imply that the south destination would be preferred by people who are less likely to enter floodwater with a depth beyond their knee height, and that the north destination would be preferred by those willing to enter the deeper floodwater. The results also suggest longer evacuation times when people are willing to enter the floodwater at a depth beyond their knee height.

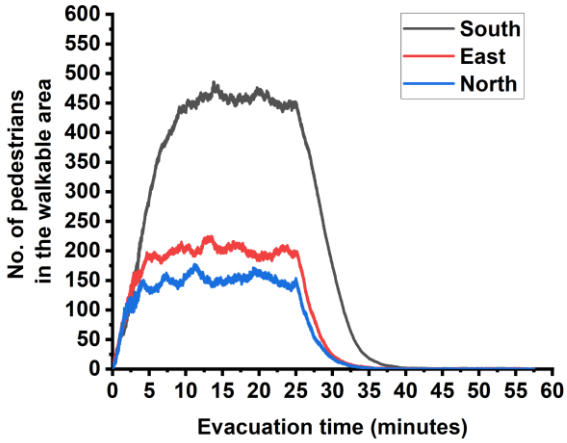

(a) 20 % threshold

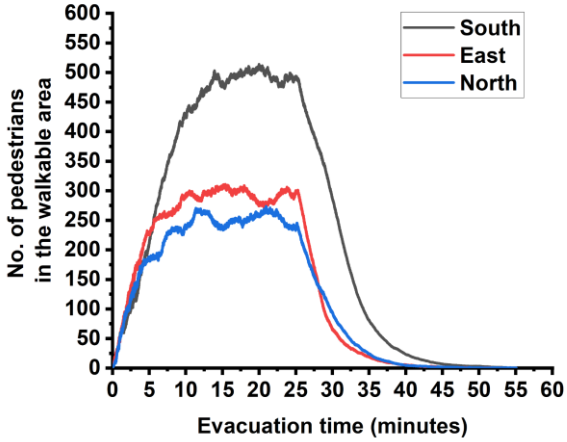

(b) 30 % threshold

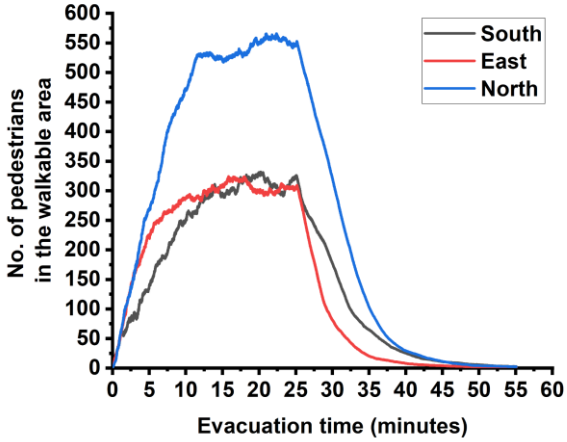

(c) 40 % threshold

Figure 5.6: Total number of evacuating pedestrians in the walkable area plotted according to their destination choices for the south, east and north during the evacuation time: (a) 20 % threshold, (b) 30 % threshold and (c) 40 % threshold.

5.4.3 Analysis of flood risk on pedestrians

The trends for HR-related flood risk states and stability states averaged from simulations for each of the 20 %, 30 % and 40 % threshold are shown in Fig. 5.7. Fig. 5.7, upper panels, includes the HR-related flood risk states as well as the total number of evacuating pedestrians in the walkable area. As the threshold increases, the total number of pedestrians in the walkable area is seen to increase, leading to prolonged evacuation times. This observation is aligned with the trends in Fig. 5.6, suggesting that the evacuation process would be delayed as more evacuating pedestrians enter the deeper floodwater where their moving speed reduces. The number of pedestrians in dry zones remains constant, despite the choice for the threshold. This may be expected as these pedestrians represent those who initially decided to go to the south destination (one third of the pedestrians) and did not, therefore, find a need to alter their destination during the process given the dominance of dry areas over the southern branch (see Fig. 5.4a). For the three thresholds, the majority of the evacuating pedestrians were found to keep a low flood risk state (HR < 0.75). Up to around 70 and 240 evacuating pedestrians reached a medium flood risk state (0.75 < HR < 1.5) with the 30 % and 40 % thresholds, respectively, and no pedestrians were predicted to have the latter flood risk state with the 20 % threshold. Up to only 5 pedestrians were detected at a high risk flood state (HR > 1.5), namely from those who entered the floodwater at a depth beyond 40 % of their body height.

The number of evacuating pedestrians that could have a stability state with a toppling-only or toppling-and-sliding conditions are shown in Fig. 5.7, lower panels. For the 20 % threshold, very few pedestrians were found to have these stability states, up to only 3 in number. Findings in Sec. 4.3.1 and Sec. 4.5.2 (see in Chapter 4), suggest that these could be pedestrians with a low flood risk state (HR < 0.75) with a toppling-only condition or with a medium flood risk state (0.75 < HR < 1.5) with a toppling-and-sliding condition. The number of pedestrians with these stability states increased with the threshold of 30 %, which is expected given the increased number of pedestrians under low-to-medium flood risk states evacuating over a longer period. Up to 40 and 20 more pedestrians were found in toppling-only and toppling-and-sliding conditions, respectively. With the 40 % threshold, 25 more pedestrians were found to be in a toppling-and-sliding condition, and up to 100 more were found to be in a toppling-only condition. The significant increase in the number of pedestrians with a topping-only condition is expected with the 40 % threshold, for which

more pedestrians would be entering the floodwater where its depth is beyond their knee height.

The analysis of the HR-related flood risk and stability states suggests that the majority of people evacuating the stadium would take an evacuation route that is either dry or keeps them under a low flood risk state (HR < 0.75) with a toppling-only condition during the evacuation. Less people would be entering deeper floodwaters and, when they do, they are expected to be in a medium flood risk state (0.75 < HR < 1.5) where they can have a toppling-and-sliding condition.

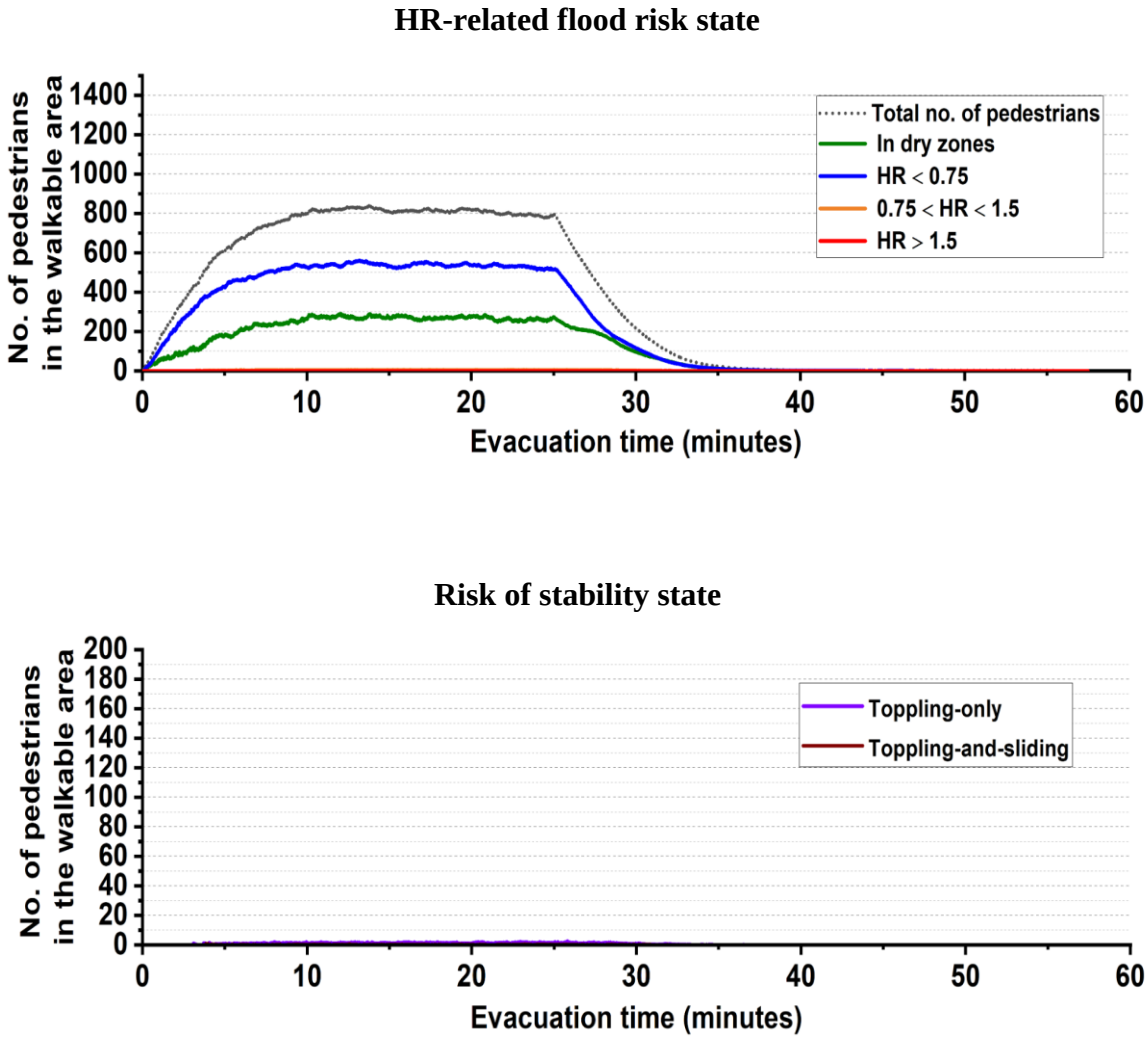

(a) 20 % threshold

HR-related flood risk state

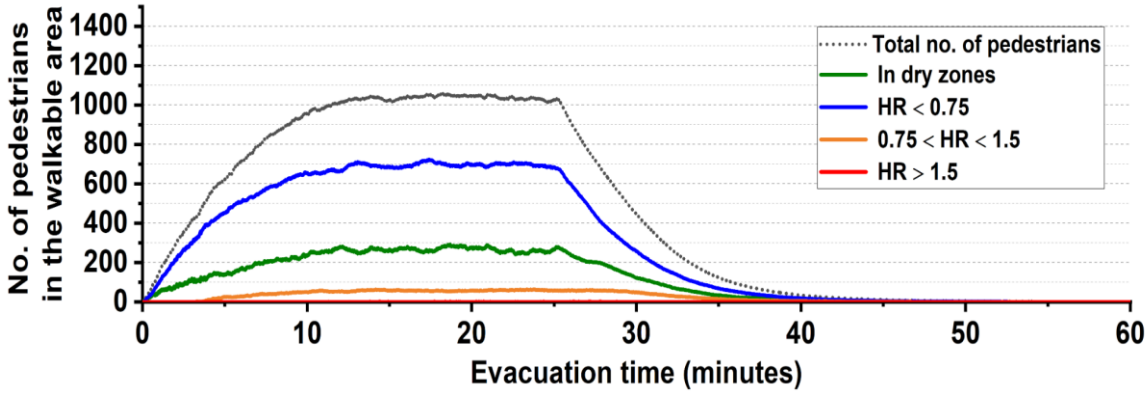

Risk of stability state

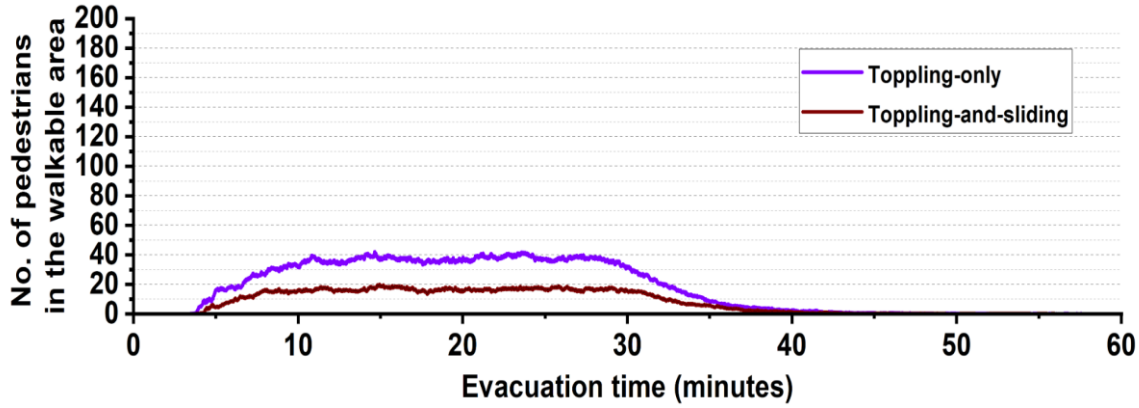

(b) 30 % threshold

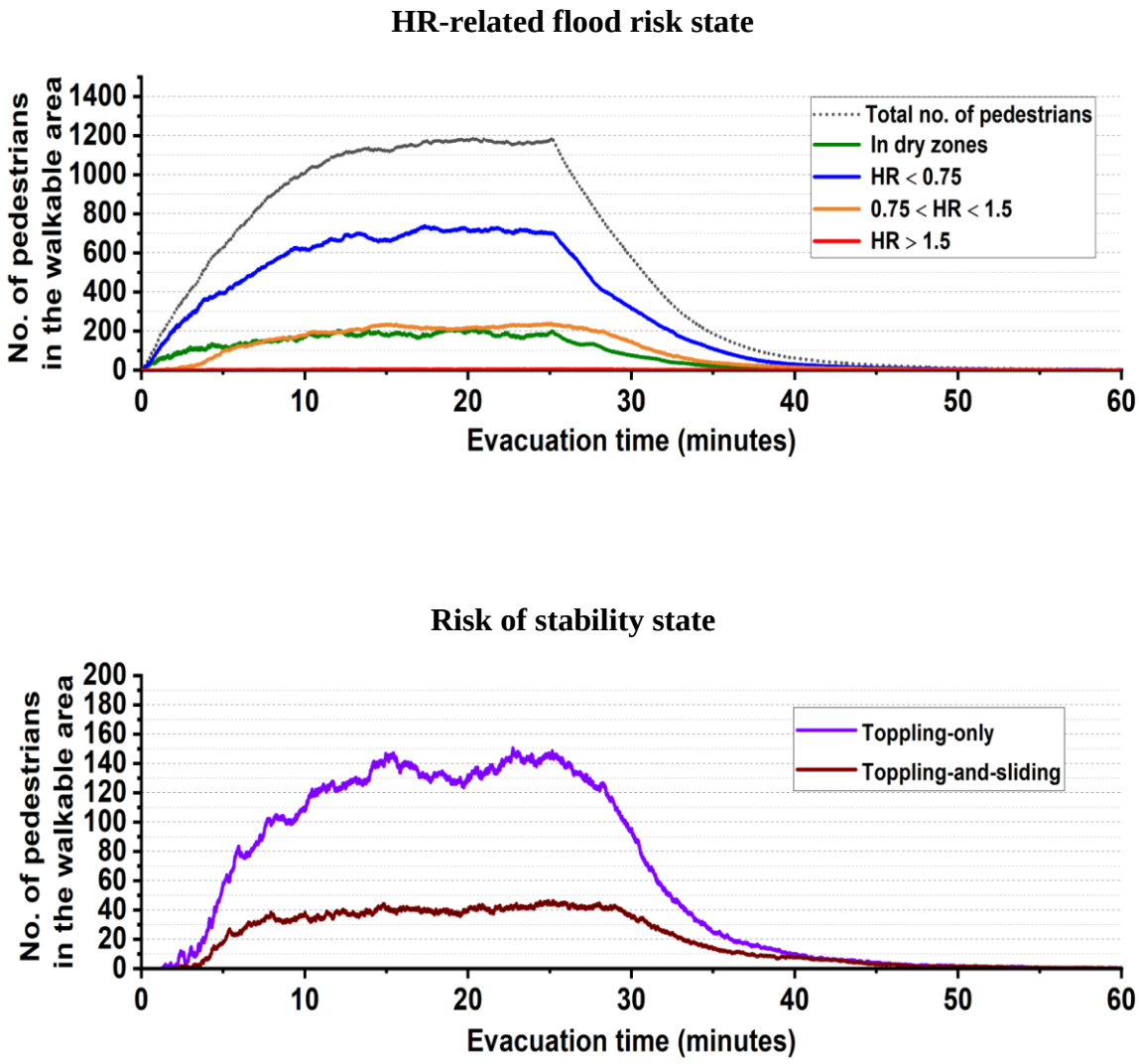

(c) 40 % threshold

Figure 5.7: Total number of evacuating pedestrians in the walkable area plotted according to their HR-related flood risk state (upper panel) and stability state when they were immobilised in floodwater (lower panel) during the evacuation time: (a) 20 % threshold, (b) 30 % threshold and (c) 40 % threshold.

5.4.4 Analysis on the spatial distribution of pedestrians

Figure 5.8 shows the 2D spatial distribution of the evacuating pedestrians over the HR flood map at 25 min when pedestrian presence in the walkable area is at its highest as soon as everyone vacates the stadium. The pedestrians are represented by dots with different colours representing their stability state based on the predictions made with the 20 %, 30 % and 40 % thresholds. The evacuation patterns in Fig. 5.8, though retrieve the observations made before (through Fig. 5.6 and Fig. 5.7) demonstrate the simulator's further ability to inform on the potential locations where the evacuating pedestrians are expected to be immobilised by the floodwater. With the 20 % threshold (Fig. 5.8a), most of the pedestrians remained mobile in the floodwater (stable condition) and preferred the south destination where low flood HR dominates. From the remaining pedestrians, who preferred the east or north destinations, a handful were at risk of immobilisation (toppling-only or toppling-and-sliding conditions). These stability states are observed to occur particularly within northern and eastern branches where the flood HR varied from the upper low range to the medium range. The spatial distributions predicted with the 30 % threshold (Fig. 5.8b) also suggest a preference for the south destination by most of the pedestrians, and that many more pedestrians would be expected to be immobilised by the floodwater within the eastern and northern branches. There, at least a dozen would have a stability state with a toppling-and-sliding condition caused by the relatively higher number of pedestrians who kept moving to the north and east destinations. With the 40 % threshold (Fig. 5.8c), most of the pedestrians were still found to remain mobile in floodwater (stable condition) despite the fact that the (riskiest) north destination was the dominant choice. However, the spatial distributions predicted with this threshold point to a major increase in the number of immobilised pedestrians within the aforementioned vicinities.

The analysis in Fig. 5.8 suggests that people who avoid entering a floodwater depth beyond their knee height are most likely to select the south destination, where their condition remains stable to keep evacuating with minimum risk of immobilisation. Those with a tendency to enter deeper floodwaters would go to the east or north destinations, towards which the majority would still be able to evacuate, but at a slower pace delayed by the risk of facing immobilisation as they move forward to their selected destination. Overall, the predictions produced by the simulator (Fig. 5.6 to Fig. 5.8) seem useful in planning

evacuation in outdoor spaces where the behaviour of pedestrians could be influenced by their autonomous decision making on the safest destination driven by their personal risk perception of the local floodwater and body height.

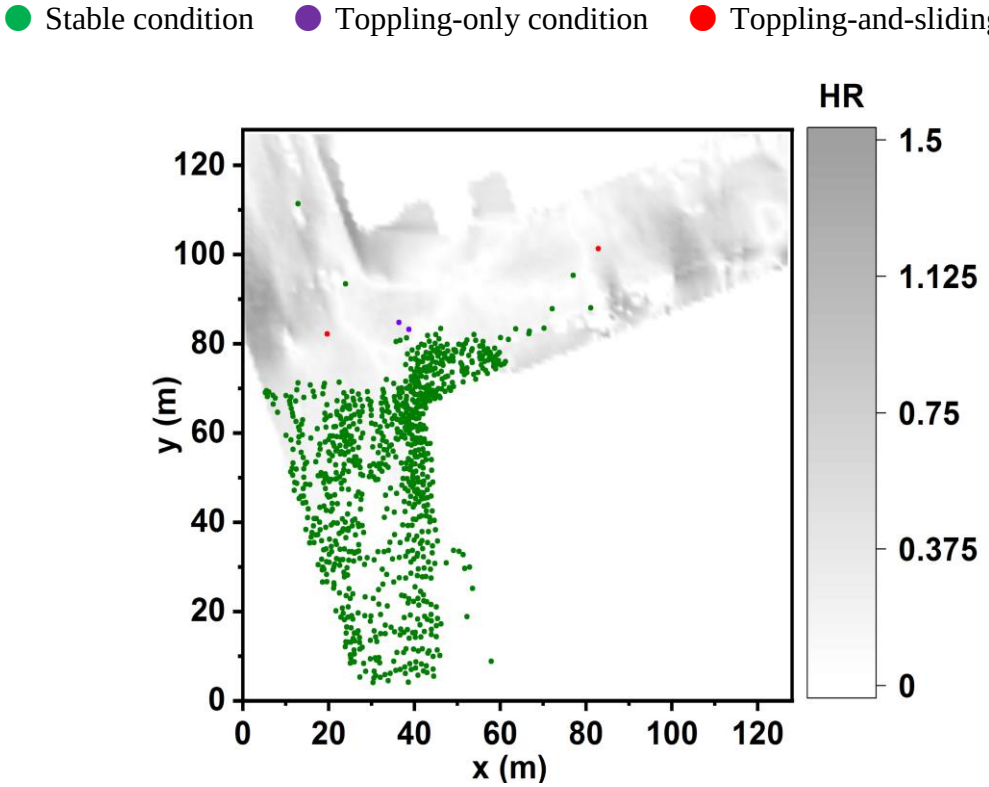

(a) 20 % threshold

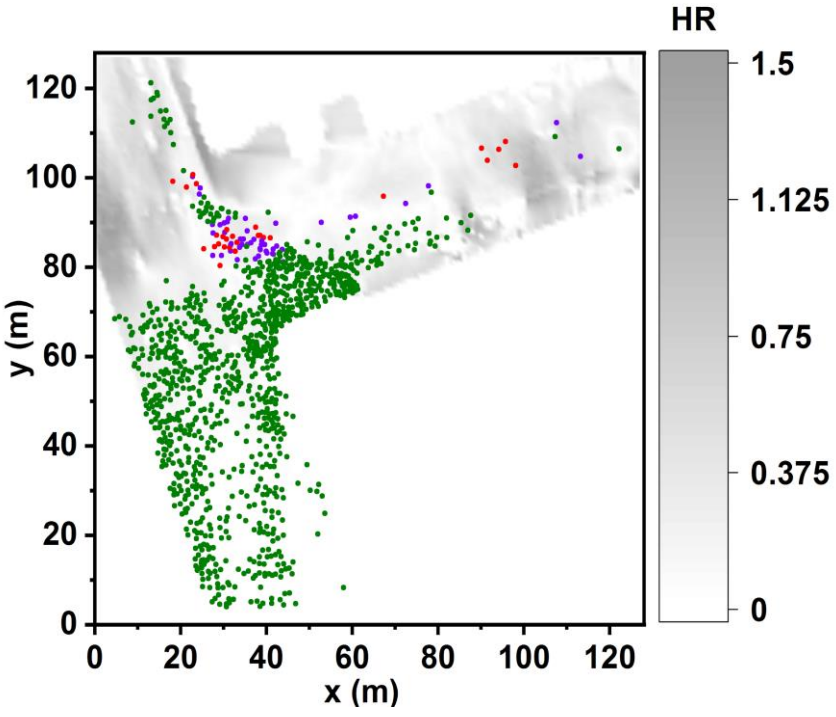

(b) 30 % threshold

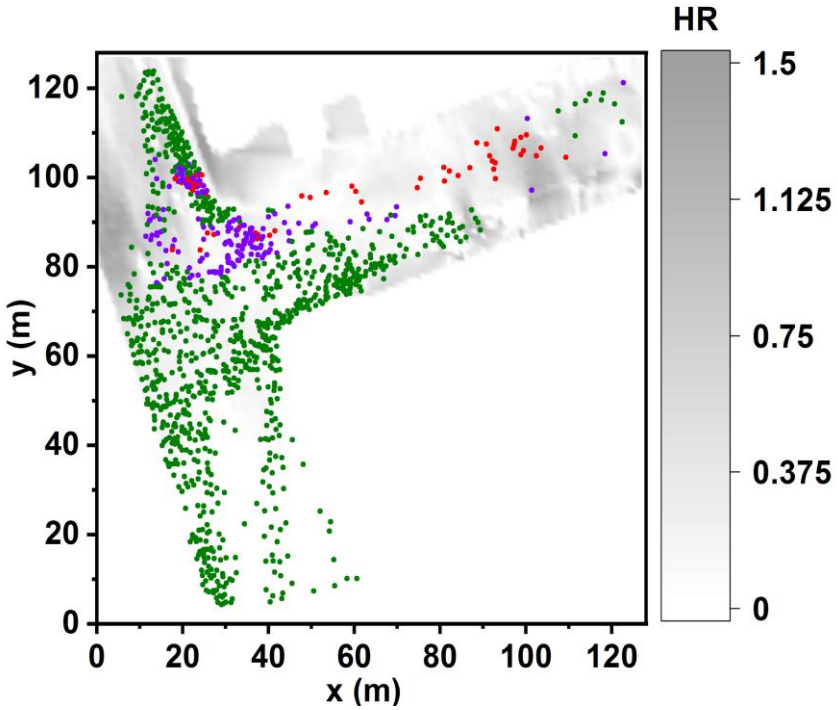

(c) 40 % threshold

Figure 5.8: The spatial distribution of pedestrians over the walkable area under the predicted stability states (coloured dots) along with the HR flood map (grey shade) at simulation time t = 22 min, when the number of pedestrians over the walkable area is at highest after all of them had vacated the stadium: (a) 20 % threshold, (b) 30 % threshold and (c) 40 % threshold.

5.5 Simulation runtimes

Considering each threshold, the simulation runtime for the coupled flood-pedestrian model to run the Hillsborough Stadium case study over a duration of t = 60 min have been explored. Table 5.2 lists the runtimes averaged out after 20 runs and recorded on the same desktop computer reported in Sec. 4.5 and with the resolution of 1.0 m × 1.0 m (Sec. 5.3). The runtimes have been measured while the FLAME GPU visualisation mode was also activated.

As shown in Table 5.2, the simulation runtime have been increased in line with the increase in the thresholds. This is because the larger flood risk perception level allowed pedestrians to step inside deeper floodwaters, which resulted in a wider range of two-way interactions between the floodwater and pedestrians. This, in return, have generated more complexity in the computations and therefore increased the simulation runtime. Still, the model seemed to be capable of running this test case almost three times faster than real time when all the behavioural rules for pedestrians were enabled at the same time.

Table 5.2: Average simulation runtimes for the coupled flood-pedestrian model to run the Hillsborough Stadium case study.

Thresholds	Simulation runtime (min)
20 % threshold	18.76
30 % threshold	18.95
40 % threshold	19.61

5.6 Summary and concluding remarks

In this chapter, the utility of the simulator, with the new autonomous change of direction condition, was demonstrated over a real-world case study Sheffield's Hillsborough football stadium, including a T-junction outdoor space leading to three ends towards the south, east and north destinations. The simulator was set up to replicate historical extents and depths of the floodwater that would inundate this study site. The autonomous change of direction condition was applied based on three thresholds of a floodwater depth to body height: 20 %

threshold, 30 % threshold and 40 % threshold, representative of a high, medium and low level of people's risk perception, respectively. The simulation outputs suggest that when people exhibit high to medium risk perception by avoiding zones with floodwater depth beyond their knee height, the majority change direction to go to the south destination that has the highest portion of dry zones. Whereas, when people exhibit a low risk perception and enter floodwaters higher than their knee height, the majority would take the shallowest pathway leading to the north destination. As the risk perception level decreased, the simulation output showed an increase in the number of people in a medium risk state with an immobilised condition and longer evacuation time. Finally, the investigations over the real-world case study demonstrates that the coupled flood-pedestrian model can be used to analyse the dynamics of people's responses in and around the floodwater as part of the flood risk analysis; thus, it is a useful tool for planning evacuation of crowds to flood emergencies in small and potentially congested urban areas.

Chapter 6

Discussions and conclusion

6.1 Chapter overview

This chapter provides a summary of the research (Sec. 6.2) and concludes its key findings in relation to the research aim and objectives (Sec. 6.3). It also discusses the main value and contribution of the study to the area of research (Sec. 6.4). This chapter concludes with reviewing the limitations of the study (Sec. 6.5) and some recommendations for future research (Sec. 6.6). Finally, it provides the online addresses to the model source code and datasets (Sec. 6.7).

6.2 Thesis summary

The motivation behind this PhD research has been discussed in Chapter 1, which is raised from the strategic need for the development of methods and tools to support emergency evacuation planning in urban areas. The reason behind this need is that the floods frequently hit communities in different parts of cities where people congregate. These areas are usually pedestrian hubs, such as in or around shopping centres and football stadiums, which should be evacuated immediately if flooding hits that area. This requires preparation and planning

ahead of time by analysing multiple what-if scenarios. With advances in computing technology, pedestrian evacuation simulation models have been developed to serve this purpose. Different techniques and tools have been employed to simulate pedestrian evacuations over the past few decades. These techniques and tools have been reviewed in Chapter 2, in which the advantages and disadvantages of the commonly used approaches, i.e. macroscopic, SFM, CA and ABM, have been discussed. The SFM approach offers significant advantages for simulating pedestrian congestions in small areas since it uses a continuous spatial and temporal description of the pedestrian motion. However, SFM has some limitations in accounting for the heterogeneity in evacuees' characteristics and behaviour, which are key parameters in evaluating the evacuation time and flood risk assessment. To resolve this issue, one approach is to integrate SFM within ABM, because of its flexibility in characterising heterogeneous evacuees, added with its capability to incorporate pedestrian interactions with dynamic environments, such as floodwater flows. But exploring this technique through traditional ABM frameworks might have been discouraged by the fact that it entails considerable computational expenses and complications on organising the dynamic interactions across pedestrians and the floodwater flows. To overcome these challenges, we used FLAME GPU to integrate a hydrodynamic model into a SFM-based pedestrian simulation model. We have employed this approach with an aim to account for humans' stability limits and various moving speeds at an individual level supported by the recent experimental findings, which were also reviewed in Chapter 2, and the heterogeneity in a population's characteristics, i.e. age, gender, and body height and mass.

Based on this research aim, three objectives have been defined. The first objective, which was to integrate a hydrodynamic model with a pedestrian simulation model within the FLAME GPU framework has been addressed and discussed in Chapter 3. In this chapter, the coupled flood-pedestrian model was evaluated in simulating the two-way dynamic interactions between pedestrians and the floodwater flows. The capabilities of the base model have been investigated by applying it to a hypothetical test case of flooded shopping centre under two different scenarios, which are (i) a during-flood pedestrian evacuation scenario and (ii) a pre-flood intervention scenario for deploying a sandbag barrier. In the during-flood evacuation scenario, the simulated flood risk on pedestrians were analysed by considering the changes in floodwater hydrodynamics around congested areas. In the pre-flood intervention scenario, the simulator outputs were analysed in terms of required optimal barrier height and number of responders for a safe and effective deployment.

The second objective, which was to incorporate the heterogeneity in the pedestrians' characteristics, i.e. various age, gender, and body height and mass, based on available survey datasets and also recent empirical formulae to drive pedestrians' stability state and various walking speeds has been addressed and investigated in Chapter 4. The relevance of pedestrians' heterogeneous characteristics and moving speeds to the evacuation simulation outcomes were analysed by reapplying the model to the same test case of flooded shopping centre. The relative changes into the simulation outputs were evaluated based on spatial and temporal indicators informing on the dynamic variations of the flood risk states of the pedestrians in terms of HR and instability conditions, i.e. toppling and sliding. These analyses have been conducted through two subsequent development phases as new features were gradually added to the pedestrians' characteristics and behavioural rules. In the first phase, Phase 1, the focus has been given to the pedestrians' diverse body height and mass that influence their stability state in floodwater, and to the pedestrians' variable walking speeds based on floodwater depth and velocity. In this phase, further investigation has been carried out into the relationship between stability states and walking speeds of pedestrians to the HR metric. In the second phase, Phase 2, the focus has been given to further characterise pedestrians with an age, gender and more diverse body mass to drive both their stability state and moving speeds under walking and running conditions in both dry and flooded zones. In addition, the model was also augmented to incorporate autonomous decision making behaviour of pedestrians in choosing one destination among multiple exits in outdoor spaces. For Phase 2, a sensitivity analysis has been performed on the simulation outputs to factor in the uncertainties associated with the behaviour of people under emergency conditions, and also simulation runtimes have been compared with respect to the complexity of the rules.

Finally, the third objective, which was to investigate the capabilities of the model over a real-world case study, has been studied in Chapter 5. This chapter was dedicated to particularly explore the utility of the simulator in providing information on the exit choices of pedestrians and the temporal and spatial flood risks in terms of HR and stability states. These capabilities were investigated through a during-flood evacuation scenario outside of the main entrance of the Hillsborough football stadium in Sheffield. The analysis on the simulation outputs have been performed considering the uncertainty associated with individuals' behaviour with respect to different flood-risk perceptions, i.e. high-, average- and low-risk. Finally, the simulation runtimes for the coupled model to run this specific case study has been measured and investigated across each set of simulations.

6.3 Key findings of the research

Based upon the achievement of research objectives that are discussed above, the following key findings of the research have been revealed.

Completion of the first objective revealed that accounting for local changes in the floodwater hydrodynamics due to pedestrian crowding in small-scale and congregated areas significantly affect predictions of spatial and temporal flood risk on the flooded pedestrians. In particular, the hydrodynamic dispersion of the low- to medium-risk floodwaters due to pedestrian crowing in congested areas resulted in reducing the predicted flood risk to the surrounding pedestrians. These changes constituted up to 25 % higher number of pedestrians with a low flood-risk state compared to the simulations without considering the effect of pedestrians' crowing on floodwater hydrodynamics. Conversely, pedestrians' crowding in high- to highest-risk floodwaters increased the risks to the surrounding groups, which led up to 8 % greater number of predicted pedestrians with highest risk states. In addition, by employing the dynamic coupling approach, the two-way interactions between floodwater and pedestrians enabled simulations of a pre-flood intervention scenario, in particular, to evaluate the required manpower and installation time for an efficient deployment of a flood defence in a short time window.

Completion of the second objective revealed that inclusion of the heterogeneity in pedestrians' characteristics and mobility conditions considerably influence predictions of evacuation time and flood risks to the pedestrians congregating in small areas. Particularly, accounting for pedestrians' moving speeds that vary based on the local changes in hydrodynamic properties, i.e. depth and velocity, prolonged the simulated evacuation time to a significant degree. This has led to even more considerable differences in the temporal and spatial variations of flood risk to pedestrians when pedestrians' body height- and mass-related instability states, i.e. toppling and sliding conditions, were further considered. In return, simulation outcomes yielded only almost 41 % similarity to those predicted with uniform moving speeds and stability states. Such differences, especially for the evacuation time, became more significant when pedestrians' age- and gender-related variable moving speeds in both dry and flooded areas were further considered. However, with this configuration, accounting for local changes in the floodwater hydrodynamics due to pedestrian crowding also resulted in a slight increase in the evacuation time. These changes has led to predictions of different spatial distributions of the pedestrians that were found to

have considerable influence on the congestion of pedestrians and the bottlenecking impacts. The sensitivity analysis on the simulation outputs have showed that the incorporation of more sophisticated behavioural rules could lead to higher deviations in simulation outcomes, and that 20 runs were required to keep these deviations below 1 %. The average simulation runtimes for this specific test case have also pointed out that the model produced simulations almost four times faster than real time when all the rules were activated.

Finally, completion of the third objective revealed that incorporating individuals' different flood-risk perceptions considerably influences destination choices of pedestrians when multiple exits are available in an outdoor urban layout. This has led to different predictions of temporal and spatial variations of flood risk to pedestrians and evacuation time. In particular, simulation of pedestrians with low flood-risk perception yielded to prediction of longer evacuation time as pedestrians tended to step inside deeper floodwaters which, in return, reduced their mobility and moving speed. Conversely, simulation of pedestrians with higher flood-risk perceptions led to shorter evacuation time as pedestrians did not get in contact with severe floodwaters; and thus, they were able to maintain their stability and moving speeds. These changes have also influenced the patterns of the spatial distribution of pedestrians across low to high flood-risk perceptions as pedestrians' favoured one destination over another. Finally, the sensitivity analysis on the simulation outputs have revealed that decreasing the level of flood-risk perception for pedestrians lead to higher deviations in simulation outcomes for this specific test case. Also, this reduction in the level of flood-risk perception for pedestrians have slightly increased the simulation runtime; still, the simulations were conducted almost three times faster than real time for this specific real-world case study.

6.4 Value and contribution to the research field

The key findings of the PhD research have demonstrated the potential value and contribution of the present flood-pedestrian simulator to the research field.

It has already been argued that including populations' heterogeneous characteristics and behaviour is key to ensure some level of accuracy in the prediction of evacuation time and the flood risk assessment (Barnes *et al.*, 2021; Alonso Vicario *et al.*, 2020). In this sense, the simulator demonstrated the first step into incorporation of empirical formulae and real-

world datasets into evacuation simulation modelling to increase realism in the characterisation of pedestrians' behaviour. More specifically, it accounts for a population's heterogeneous age, gender, body height and mass characteristics that influence individuals' stability limit and moving speeds in floodwater, and also various moving speeds for pedestrians in dry zones accelerated under evacuation condition based on experimentally derived excitement conditions. These features make the simulator distinct from the other available models, such as FlooPEDS, LSM and HEC-LifeSIM (see Table 2.2), particularly when it comes to simulation of pedestrian evacuations down to the scale of individuals. In addition, the new autonomous change of direction condition that related pedestrians with their flood-risk perception and water flow dynamics, though still requires support from socio-psychological studies, is one first step forward to gain new insights into bridging between human's physical and non-physical factors in the simulations of pedestrian evacuations.

In terms of application, most evacuation models in the literature, such as Dawson *et al.* (2011) and Lumbroso *et al.* (2021), focused on predicting the number of casualties and injuries under various scenarios. Flood-pedestrian simulator contrasts with these models as it directly addresses spatio-temporal flood risks on people at an individual level based on different flood severity. This has already been proven to benefit finding the bottlenecks and spotting the most hazardous areas, which would help planners to consider potential hazard reduction structural measures, such as constructing barriers and basins, to further reduce the risks (Dawson *et al.*, 2011). This capability also may help decision makers to better decide on sheltering strategies and the choice of refuge areas at local levels (Bernardini *et al.*, 2021). Besides, the flood-pedestrian simulator contrasts with other models by accommodating a built-in hydrodynamic model which is inherently synchronised in space and time with the pedestrian model. This, in return, reduces the time and effort for extracting the flood information from external hydrodynamic models and manually import them to the ABM-based evacuation models, which is the common approach in LSM and HEC-LifeSIM. Just like any other modelling framework, flood-pedestrian simulator carries a number of technical limitations that are discussed in the next subsection.

6.5 Limitations of the research

Like other modelling frameworks, the flood-pedestrian simulator carries a number of limitations.

The flood-pedestrian simulator produces an abstraction of reality and uses assumptions, added with a number of unmeasurable initial and boundary conditions and uncertain parameters, especially factors in human behaviour that are unknown to full certainty. The simulator suffers from the constraints imposed by the FLAME GPU's requirements. First, building and running the simulations using flood-pedestrian simulator requires specific software and hardware configuration. These requirements are all listed in the user guidance document attached to this thesis as Appendix A. Second, though the outputs could be programmed in almost any desired format, the input file must follow the xml structure format suited for FLAME GPU. This poses an additional challenge for users to reproduce other test cases. Besides, visual interpretation of the outputs and generating the graphs requires external computer programs for graphing and data analysis.

Concerning the pedestrian characterisation and behaviour, the simulator does not incorporate the irrationalities associated with psychological and emotional influences on human behaviour under critical situations. For example, individuals in a group might help each other during a flood event or parents may assist their children in difficult moving conditions. The simulator also does not incorporate the group behaviour of people in the current version. This means that capturing household units that tend to move together is not possible. Besides, the present version of the flood-pedestrian simulator does not support movement of people in an environment with multiple storeys.

Concerning the hydrodynamic model, generating flood is limited to a pre-specified type of polynomial hydrograph. The hydrograph is formulated based on inflow discharge and duration paired within an implemented equation into the framework. This mechanism does not give the users the flexibility required to adopt survey datasets for replicating historical events. This means that modifications to the inflow hydrograph require further amendments directly into the framework. Also, the hydrodynamic model does not account for the urban infrastructure measures, such as drainage systems that significantly influence the propagation of floodwater. Finally, one key limitation is the lack of test cases with suitable observational data to validate against (e.g. video footages of an evacuation in flooded and populated area.

6.6 Opportunities for future research

Identification of the limitations of this PhD research uncovers a number of opportunities for future research, specifically to improve such modelling frameworks.

In pedestrian evacuation modelling, physical interactions between humans and floodwater during an emergency evacuation are the main actors that shape the collective outcome of the simulations. In flood-pedestrian simulator, pedestrians' stability state and moving speed are evaluated based on experimental formulae that are derived under restricted laboratory conditions. However, in reality, many other physical and non-physical factors exist to influence one person's moving speed. For example, people may suffer from physical and mental disabilities which directly influence their reactions to floodwater under an evacuation condition. Therefore, further study is needed to factor in physical and non-physical factors in characterisation of human behaviour in floodwater. In addition to this, future studies involving social science and anthropology may broaden the applicability of such modelling frameworks by incorporating more comprehensive experimental and social information. In this research, we introduced a new mechanism to dynamically change the destination of flooded pedestrians that is relevant to different thresholds of water depth. This has been implemented through a number of assumptions and limited to prefixed destinations due to the formulation of the social model, which in reality may change during an evacuation process. New social models with an ability to incorporate unlimited destination choices with dynamically varying locations would benefit the evacuation modelling frameworks to more realistically simulate the path-finding decisions of pedestrians in flooded situations. In terms of floodwater's response to humans' physical presence, almost all the parameters were assumed without any experimental information to back up such assumptions. Therefore, experimental research is needed to quantify the changes in floodwater dynamics in the presence of human body.

The flood-pedestrian simulator is designed with a particular focus on immediate evacuation of pedestrians during a flood event in small urban areas. But with the modelling flexibility and computing power provided by FLAME GPU, the simulator could be augmented with a traffic model to also simulate the movement of cars within a city network alongside pedestrian movement. Such model, if developed, would offer a more comprehensive insight into the evacuation planning and decision making by widening the application of the simulator for both local and regional scales. However, conceptualisation

and implementation of such models requires substantial consideration of the complex interactions that exist between pedestrians, floodwaters and the traffic during a flood event. Another major challenge is reformulation of the pedestrians to act at different aggregation levels, e.g. individuals, groups and households, along with a number of characteristics that are more relevant to large scale modelling, such as daily routine activities and grouping behaviours. More importantly, the availability of relevant data could impose additional difficulties or may limit the validity of such modelling. Nonetheless, the combination of pedestrian and vehicular evacuation, even if not practical at every temporal and spatial level, is a way forward to reinforce tools and methods for efficient evacuation planning.

During the development process we mainly focused on the evacuation point of view, but the capabilities of the simulator in replicating the deployment process of different types of protective measures, like the sandbagging process we preliminarily investigated in Chapter 3, could be further extended. This can be the subject of future studies to extend the capability of the simulator to simulate deployment of different flood defences based on each protective measure's installation information (e.g. the product material, size, weight, deployment time, manpower needed to install it). Investing in such study will bring new dimensions to the evacuation simulation modelling by also providing insights into the effectiveness of deploying a particular protective measure. For example, though preferable in terms of cost and material, building sandbag barriers might seem inefficient in terms of deployment timing in one place. Such models would allow planners and decision makers to investigate other options, such as replacing a long sandbag barrier with a water barrier system.

Finally, because of the uncertainty in the human behaviour, such modelling frameworks could incorporate other methods, particularly fuzzy logic, to adjust agents' behaviours and decision-making rules in a way that is more consistent with our understanding of reality. This is particularly important in assigning pedestrians with various moving speeds which could be greatly influenced by panic and stress factors. It would also benefit a more realistic mechanism for determining pedestrians' turning point in floodwater with different depth and velocity while accounting for individual's flood-risk perception. In that regard, socio-psychological studies could provide more realistic information through surveys and questioners from the public for integration into pedestrian evacuation modelling.

6.7 Code and dataset availability

The flood-pedestrian simulator is accessible from Zenodo open-access repository at https://doi.org/10.5281/zenodo.4564288, with a link to the GitHub source codes of the latest release, including a detailed ‘run guide’ and input files to enable the users to run the flooded shopping centre and the Hillsborough stadium evacuation test cases on their own machine. The primary version of the simulator, reported in Chapter 3, is also available on DAFNI, available at: https://dafni.ac.uk/project/flood-people-simulator/, where it can be run from a user-friendly graphical interface and supported by a run guide. Also, the outputs of the simulations used to produce graphs in Chapter 4 and Chapter 5 are available online in the Zenodo open-access repository at https://doi.org/10.5281/zenodo.4576906. In addition, some demo videos of the test cases are available online in the TIB AV-Portal at https://doi.org/10.5446/51547.

Chapter 7

Reflections

Reflections

In this chapter, a number of personal reflections on the research is described briefly for the interest of future researchers in this area to help their insight into the topic.

On 14 May 2018, in the first steering committee meeting of 'smart forecasting: joined-up flood forecasting infrastructure with uncertainties' project, an important question was raised by Prof. Paul Bates on early stages of this research. Rephrasing his words, he asked "*what is the point of dynamic flood-evacuation coupling if people cannot do anything to change the flood extent?".* Reviewing the literature up to that point had not provided such insight into the matter. It seemed that capturing the back interaction of people on floodwater seem to be a new dimension to the evacuation modelling. This was later on backed up by Prof. Aerts in 2020 in his review paper on agent-based models, raising similar concerns in such a coupling approach (Aerts, 2020). Also, accounting for the influence of the adaptive actions and reactions of people on the collective outcomes of simulations used in flood risk management is an emerging subject, which has started to be accounted for since 2019 (Abebe *et al.*, 2019). It is suggested that both the modellers and planners, though outside their comfort zone, should now address the two-way interactions in human-flood systems at almost any scale. This in turn, would also enable better communication of the risk and possible coping measures to better prepare and plan for urban evacuation in small urban areas.

Evacuation planning is far more complicated than what it looks. This is because of the numerous physical and non-physical dimensions existing in the human-flood system. Acquiring knowledge across different dimensions for a modeller, though is a daunting task,

is required to develop a sound modelling framework. A modeller needs to find a thin line between the involving disciplines and their interrelated connections. This causes the modellers to have bias on physical aspects and disregard the non-physical ones. Nonetheless, apart from the technical constraints, such as computational cost and flexibility of modelling environments, there seems to be a lacking knowledge in the context of social science to provide empirical/statistical information to be integrated into evacuation planning/modelling. With the daily advances in computing technology, there seems to be a need for collaboration of modellers/planners with scientists, e.g. in social and psychological fields, to provide non-physical information for reinforcing evacuation simulation modelling techniques to better capture human behaviour under evacuation conditions. For example, to find the relationship between peoples' past flood experience and their fear/emotional factors driving their movement when they are in direct contact with floodwater. This seems to be an inescapable issue in building realistic evacuation modelling frameworks.

Quantification of non-physical parameters is not the only issue. There is still lacking information in human-flood physical interactions. Particularly, the influence of physical presence of a group of people to the extent of floodwater dispersion is still a mystery and have never been investigated before. In the Hillsborough stadium test case, reported in Chapter 5, we had to make a number of assumptions to account for the dynamic influence of pedestrians' presence on local floodwater. If this aspect is going to attract more modellers in future, it would also call for more experimental research to provide empirical data.

Evacuation modelling requires a great deal of flexibility. This means employing off-the-shelf software packages does not satisfy the need for the coupling approach that is adaptable enough for various applications. This is a challenging task, mainly because there is no universal platform that describes behaviour of people under evacuation conditions; thus, it requires specific development for each different case. Developing an evacuation model based on ABM needs a certain level of programming skills no matter what modelling environment is employed. In our case, FLAME GPU requires some knowledge of C, C++ and XML.

The evacuation modelling could be considerably influenced by the subjective interpretation of the modeller. Unlike the hydrodynamic model, building and designing ABM-based models is considerably reliant on the personal judgment, imagination and creativity of the modeller. This means that one element that might be considered as an

assumption can be an important aspect by another, which would lead to a completely different modelling setup. Therefore, the models built upon the ABM paradigm should aim from expert judgment and collaboration with other modellers/scientists to reduce the level of subjective considerations by one modeller. This would also help to reach more solid grounds for future development of such models.

Validation of models built upon the ABM paradigm is a grand challenge. The main reason is that the modellers use the overall outcomes of simulations to validate their models rather than focusing on the validity of parameters and factors used to develop and organise their model. It is evident that the validation of outputs from an agent-based model, especially the ones dealing with human behaviour, is an impossible task. But, maybe one way to reach a close-to-real outcome would be selecting input parameters and factors based on real-world datasets and experimental data. Nonetheless, such technique clearly requires a step-by-step evaluation and multiple runs.

Availability of the data is a grand limiting factor particularly for initialising population characteristics and their spatio-temporal distribution over urban areas. Similar challenges could be observed when setting up the initial condition of the flooding in an urban area. This is because the hydrometric stations are typically located around the rivers but not in residential or populated areas to provide information on the urban runoff volume. For instance, in our case, there was no actual hydrodynamic information within the Hillsborough stadium site to allow for initialising the flood condition based on a realistic dataset. This would also challenge the validation of the hydrodynamic outputs generated by the simulator. Although video footage from historical events could be obtained from YouTube or other sharing video platforms, more robust reportable information is needed to ensure some level of accuracy in simulating the flood event in urban areas.

In the context of evacuation modelling, sharing the model itself with the community plays an important role in helping the others to scrutinize or learn from them. Unfortunately, for any possible reason, this has not been fully fulfilled by the researchers to openly communicate their models by providing enough information on their modelling process. In view of that, the source code of the flood-pedestrian simulator and its outputs are publicly available (find online addresses in Sec. 6.7), which could be used by other researchers as a baseline to build up more sophisticated modelling frameworks or evaluate and calibrate their models.

Appendix A

Flood-pedestrian simulator User Guide

Contents:

1. Introduction

The flood-pedestrian simulator simulates crowd dynamics under immediate evacuation conditions with flowing floodwater in small urban areas. The simulator enables microscopic flood risk assessment on people at individual level, analysis of evacuation patterns of individuals, estimating the time for issuing emergency warnings, and finding potential safe destinations for immediate evacuation planning.

The simulator is capable of:

- incorporating each individual's realistic physical body characteristics, moving speeds and mobility states in and around the floodwater;
- factoring in autonomous decision making behaviour of people in going and following the others towards the safest destinations among multiple exit choices in outdoor spaces; and
- capturing the dynamic back interaction of people's crowding on the local floodwater dynamics.

The information about the approach and methodology for developing, evaluating and demonstrating the capabilities of the simulator is already documented in Shirvani *et al.* (2020), Shirvani *et al.* (2021) and Shirvani & Kesserwani (2021). This document provides a brief overview of the simulator's algorithmic structure (Sect. 2), aimed to offer step-by-step guidance for users to run the simulator on their own machine (Sect. 3) for two test cases reported in the afore-cited papers (see also the demo videos). Also, the outputs from the simulator are explained (Sect. 4), with guidance on how to modify the simulations by changing the environment parameters (Sect. 5) and on how to apply the simulator to new test cases using the available tools and models designed for this purpose (Sect. 6).

2. Brief Overview of the Flood-pedestrian Simulator

The flood-pedestrian simulator is an agent-based model which dynamically couples a 'hydraulic model' to a 'pedestrian model' in one shared modelling framework, called FLAMEGPU. The FLAMEGPU framework allows simulation of multiple agents and their interactions on the Graphical Processing Units (GPUs) for parallel computations. In FLAMEGPU, CUDA simulation programs are generated automatically by processing three

inputs as described in Fig. A.1: a model file (*XMLModelFile.xml*) defining agents' descriptive information (e.g. their type, numbers, etc.); a description of agent behaviour within a source code in C (*Functions.c*) for spatiotemporal update of the state of the agents responding to messages they receive from other agents; and, agents' input file (*input.xml*) for setting up their initial state.

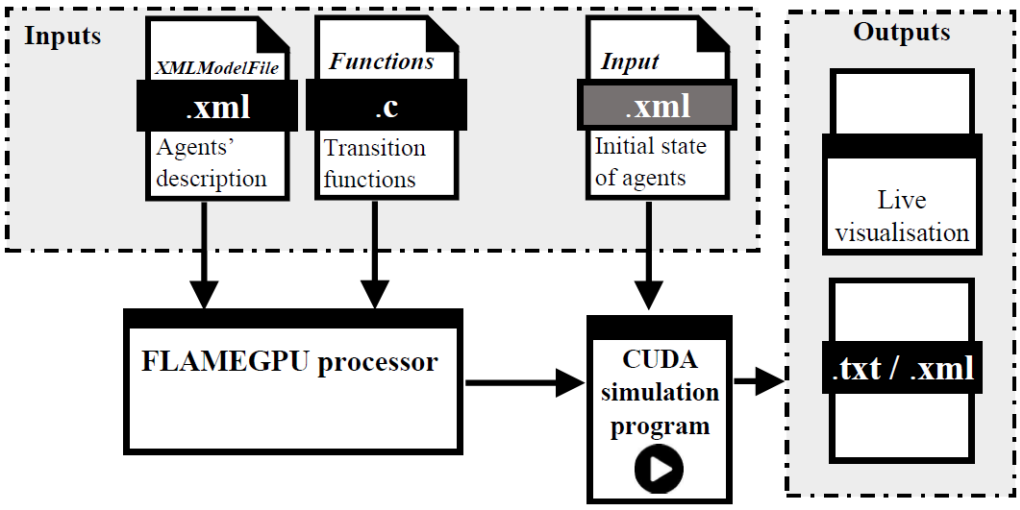

Figure A.1: Illustration of the process of building and running an agent-based simulation program on FLAMEGPU via translating three user-devised input files (*XMLModelFile.xml*, *Functions.c* and *input.xml*) into CUDA simulation program by the FLAMEGPU processor.

The pedestrian model was previously developed by Karmakharm *et al.* (2010) on FLAMEGPU. It is programmed based on the formulation of a social force model for people's dynamics including their movement patterns and their interaction with each other and their surrounding environment. The formulation of the social force model is embedded in *Functions.c* source code, allowing to update the state of two different agents that are specified in the *XMLModelFile.xml* file: 'navigation agents' and 'pedestrian agents'. Navigation agents are of discrete type and they are fixed on a grid encoding the features of the environment layout into navigational vector fields for the movement of pedestrian agents. Pedestrian agents are of continuous type that could move continuously over the grid of navigation agents as they get updated in time and space. Detailed information about the pedestrian model can be found in Karmakharm *et al.* (2010). The hydrodynamic model is implemented on FLAMEGPU (Wang *et al.* 2011, Shirvani *et al.* 2021) on a fixed grid of discrete flood agents into the pedestrian model, to update all flood agents once at a time. The states of the flood agents are specified in *XMLModelFile.xml* file where the initial navigation

and pedestrian agents are also specified. The numerical formulations of the hydrodynamic model are embedded in the same *Functions.c* to simultaneously update the state of flood agents and pedestrian agents in space and time.

The *XMLModelFile.xm*l and *Functions.c* are both located in the '…\src\model' folder, alongside '…\src\dynamic' and '…\src\visualisation' folders. The contents of these folders are automatically generated and rewritten after each build of the simulator on FLAMEGPU according to *XMLModelFile.xm*l and *Functions.c*. The .xml input files are located in '...\iterations' folder and they contain the initial state of the flood and navigation agents and environment parameters for setting up the Shopping centre (ShopCent.xml) and Hillsborough stadium (HilStad.xml) test cases.

The following instructions will get you a copy of the source code of the simulator for running it on your local machine. By cloning/downloading the flood-pedestrian simulator repository contents on GitHub (accessible at: https://github.com/SahebSh/flood-pedestrian-simulator), the user will have access to the flood-pedestrian source code and agents description file (*XMLModelFile.xm*l and *Functions.c*) to build and run the Shopping centre and Hillsborough stadium test cases using the provided ShopCent.xml and HilStad.xml input files.

3. Step-by-step Guide to Run the Flood-pedestrian Simulator on Windows

Step 1. Download and unzip/extract the flood-pedestrian-simulator.zip folder in the GitHub repository (accessible at: https://github.com/SahebSh/flood-pedestrian-simulator).

Note:

Before clone/download, consider the following things that need to be downloaded/installed on your machine.

Required software:

- FLAMEGPU v1.5: download FLAME-GPU-SDK.zip folder from the FLAMEGPU master repository (https://github.com/FLAMEGPU/FLAMEGPU) or, alternatively, directly by clicking on this link. Also, more information about FLAMEGPU and the latest Technical Report and User Guide could be found online at http://www.flamegpu.com/.
- MS Visual Studio 2015 or earlier: you can download the latest version of the Visual Studio from Microsoft website available via https://visualstudio.microsoft.com/downloads/. You need to install Visual C++ components and .NET Framework toolkit during the installation of MS Visual Studio.
- CUDA Toolkit 10.1: You can download CUDA from the Nvidia developer download archive - alternatively you may use later versions, but it needs manual modifications to the solution file (that is explained in Step 3 below).

Required hardware:

- Nvidia Graphics card - the simulator should be able to run on any Nvidia Graphics Card with a minimum 2GB memory installed on a normal machine.

Step 2. Copy the *FloodPedestrian_2020* folder from the drive directory you selected when downloading the simulator and paste it to '...\FLAME-GPU-SDK\examples' folder along with the other examples that are made available by FLAMEGPU developers for practicing and learning purposes.

Step 3. If you are using CUDA 10.1, then skip this step, otherwise, go to '...\flood-pedestrian-simulator-master\FloodPedestrian_2020' folder and right-click on PedestrianNavigation VC++ Project file and open it with any text and source code editor (e.g. Notepad). Then press Ctrl+f and look for CUDA 10.1 and replace it with the version of the CUDA Toolkit that you have installed on your system (e.g. replace CUDA 10.1 with CUDA 10.2). Then, save the changes.

Note:
The executable files required to run the flood-pedestrian simulator are not provided in the source repository; therefore the user is expected to build them locally on their own machine prior to any run attempt. The following steps will guide you through how to do it.

Step 4. Open Visual Studio, then click on '*Project/Solution..*' located in '*File*' > '*Open*' in the top menu and navigate to '..\FLAMEGPU\examples\FloodPedestrian_2020' folder and open 'PedestrianNavigation' VC++ Project file as shown in the screenshot below.

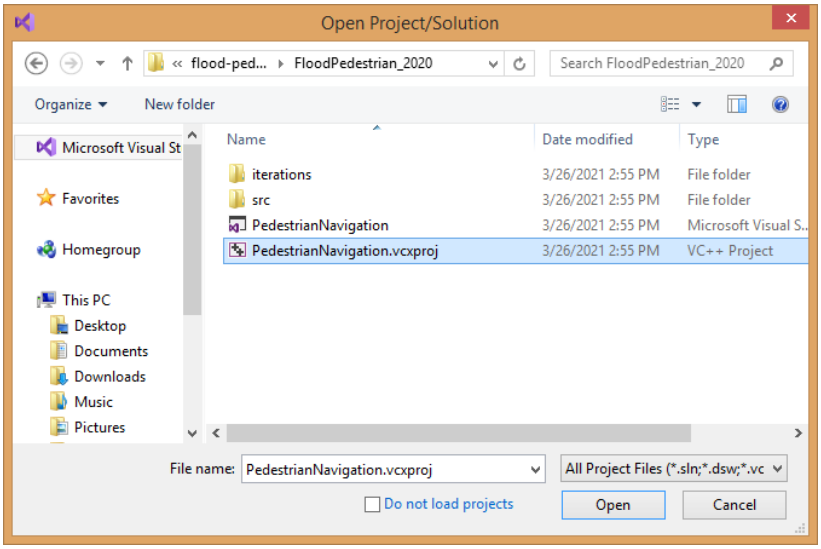

Figure A.2: Screenshot of the 'Open Project/Solution' window navigated to the location of the 'PedestrianNavigation' VC++ Project file to be opened in the Visual Studio (Step 4).

Note:

Ensure that all the contents of the simulator are opened without any error/warning. Once the project is opened correctly, the user should see the contents of the simulator within the Solution Explorer on the right side of Visual Studio window as shown below in Fig. A.3.

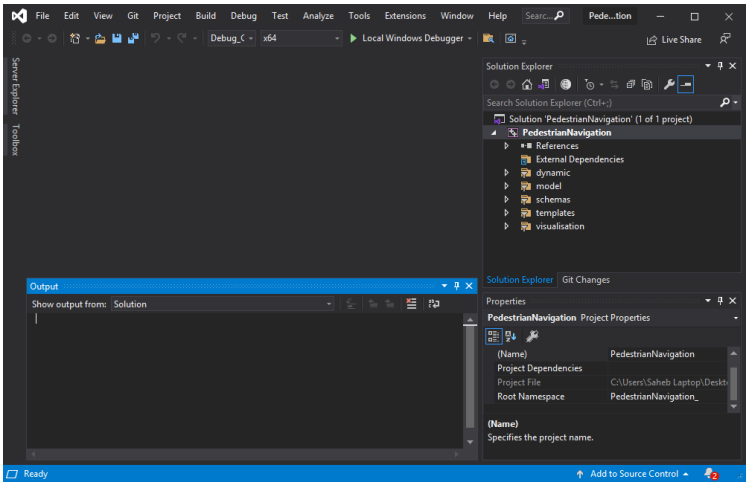

Figure A.3: Screenshot of the Visual Studio window showing the contents of the flood-pedestrian simulator inside the 'Solution Explorer' tab on the right side.

Step 5. Select 'Release_Visualisation' from the building configuration mode located under the top menu of the Visual Studio user interface like below:

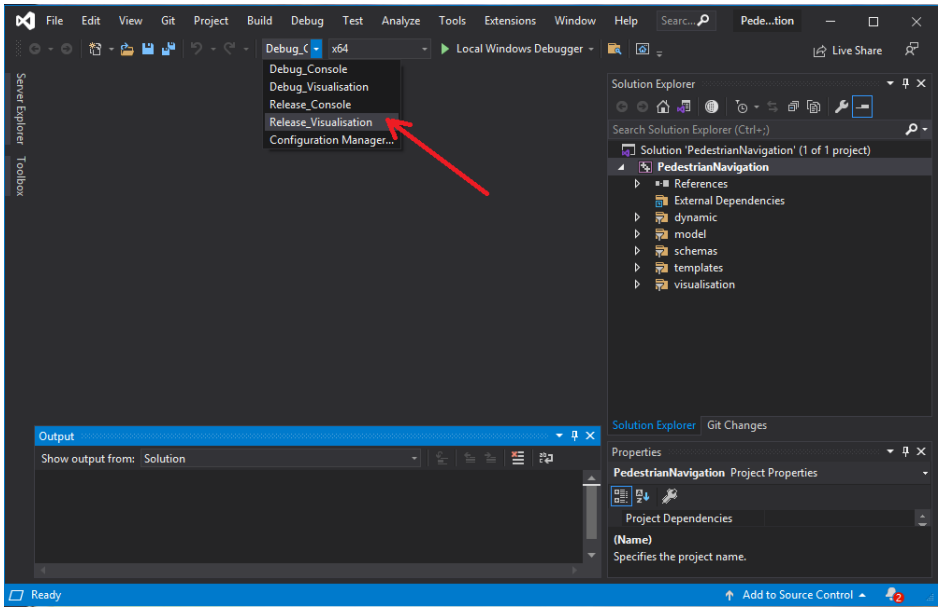

Figure A.4: Screenshot of the Visual Studio window showing where to select 'Release_Visualisation' from the building configuration mode.

Step 6. Right-click on PedestrianNavigation in the 'Solution Explorer' on the right side of the Visual Studio and click on 'Properties'.

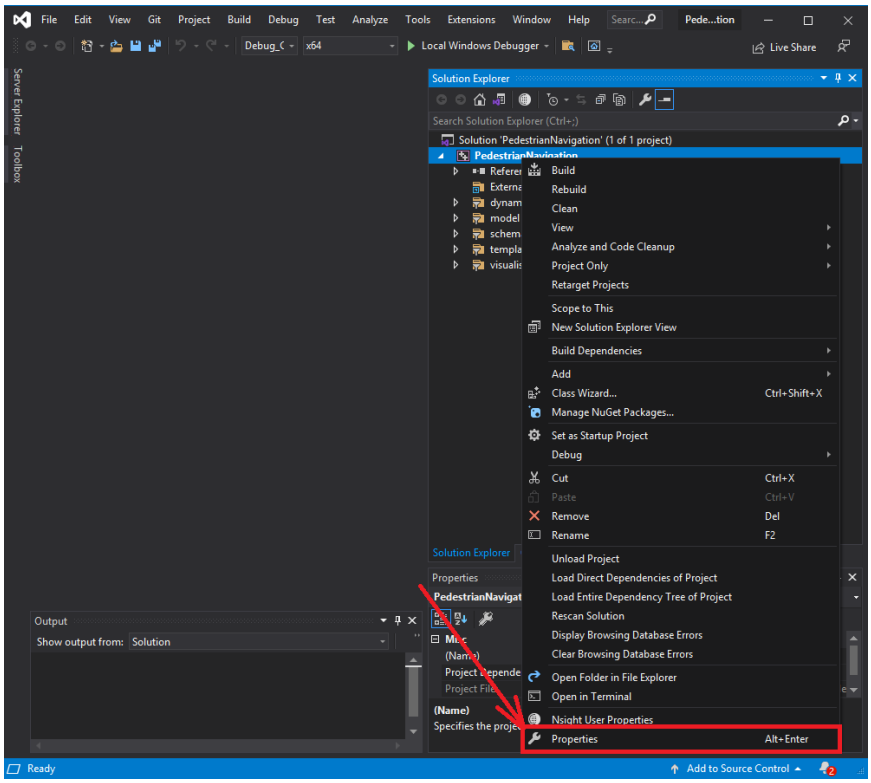

Figure A.5: Screenshot of the Visual Studio window showing where to find 'Properties' after right-clicking on PedestrianNavigation in the 'Solution Explorer' on the right side.

Step 7. On top of the ‘PedestrianNavigation Property Pages’ window choose ‘Release_Visualisation’ configuration mode:

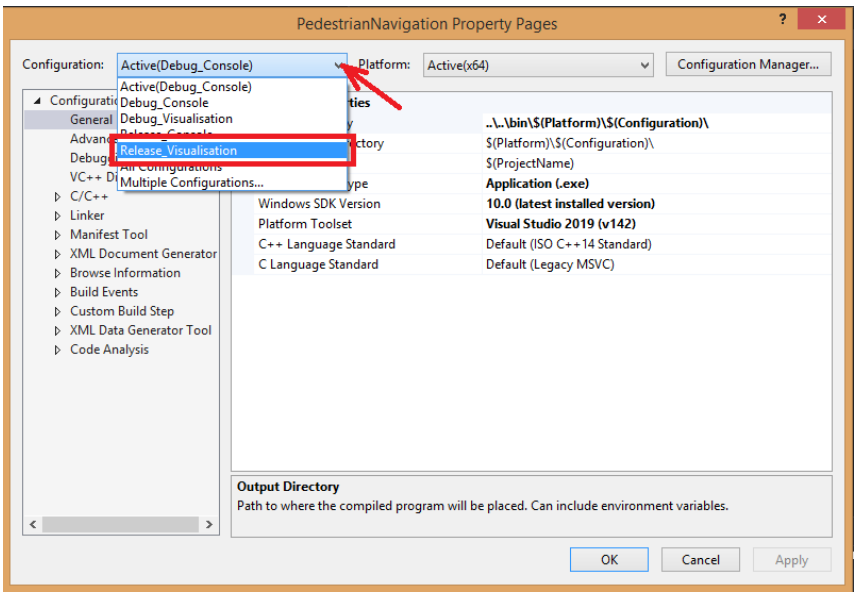

Figure A.6: Screenshot of the ‘PedestrianNavigation Property Pages’ window showing where to choose ‘Release_Visualisation’ from configuration mode options.

Step 8. First, click on ‘Debugging’ under the ‘Configuration Properties’ tab on the left side of the ‘PedestrianNavigation Property Pages’ window, then within ‘Command Arguments’ type the directory address of the input file. For example to run the simulator for the shopping centre test case, type ‘...\iterations\ShopCent.xml’ followed by the device number (usually is 0) as shown in the screenshot below, then click on ‘OK’ to exit the ‘PedestrianNavigation Property Pages’ window.

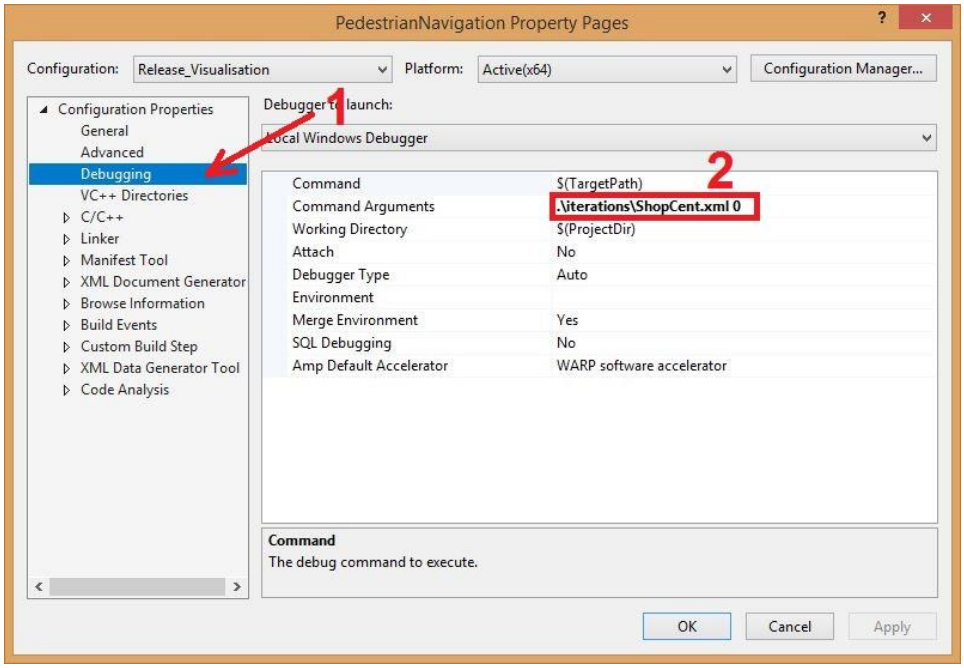

Figure A.7: Screenshot of the 'PedestrianNavigation Property Pages' window showing where to: (1) click on 'Debugging' under the 'Configuration Properties' and (2) type the directory address of the input file.

Step 9. Right-click on PedestrianNavigation in the 'Solution Explorer' again and click on 'Build' like below in the screenshot below (Fig. A.8). The FLAMEGPU then generates the CUDA simulation program code that is executable on your machine. This may take a couple of minutes and if there is no error generated, the user could press Ctrl+F5 to run the simulation under visualisation mode.

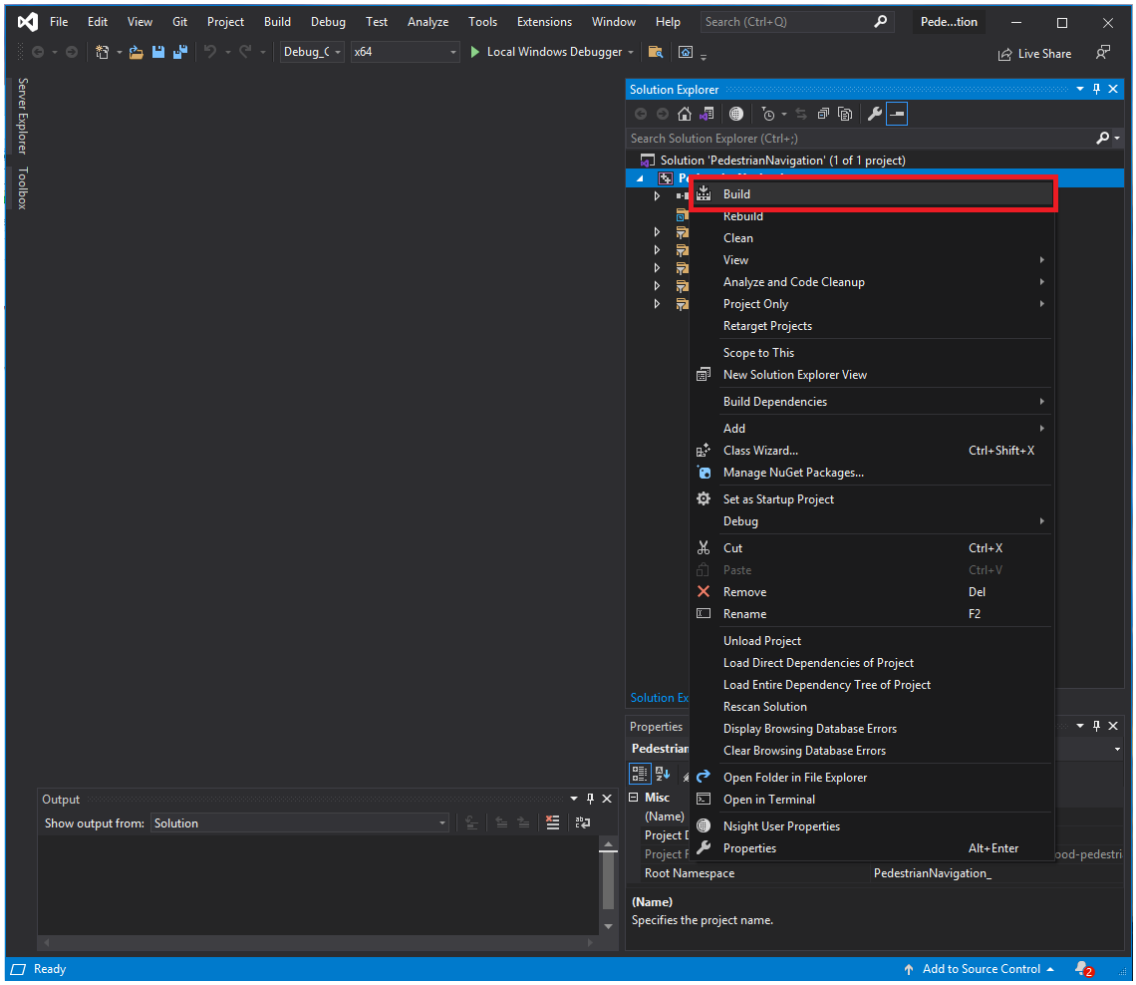

Figure A.8: Screenshot of the Visual Studio window showing where to select 'Build' after right-clicking on PedestrianNavigation in the 'Solution Explorer' on the right side.

4. Simulation Outputs

Apart from the FLAMEGPU's built-in visualisation that is immediately popped up on your screen after running the simulations, the simulator is programmed to output dynamic information of flood agents and pedestrian agents at each iteration of the simulation. These outputs are generated in three ways:

1) The console command window provides live information about the simulation time, the number of pedestrians at different flood risk states and floodwater flow. The information represented in the console command window is self-explanatory and therefore not explained here. However, all the information shown on the console window is also copied into output files explained below.

2.a) 'output.txt' is a text file that stores the dynamic information of pedestrians and floodwater at each simulation iteration. This file is automatically generated at the first iteration of simulation in the '.../FloodPedestrian_2020/iterations' folder and it gets updated dynamically during the later iterations. This information is stored within 21 columns over rows corresponding to the simulation iteration. From left to right, Table A.1 outlines the description of the information as numbers in each column that the user can find at the end of the simulation after opening the 'output.txt' file.

Table A.1: Description of the pedestrians and floodwater information stored dynamically in 'output.txt' file.

Col.	Description
1	Simulation time (s)
2	Total number of pedestrian agents generated during the simulation time
3	Remaining number of pedestrian agents yet to be generated
4	Total number of pedestrian agents moving in the area
5	Total number of pedestrian agents at no flood risk (in dry zones, HR = 0)
6	Total number of pedestrian agents at low flood risk (HR < 0.75)
7	Total number of pedestrian agents at medium flood risk (0.75 < HR < 1.5)
8	Total number of pedestrian agents at high flood risk (1.5 < HR < 2.5)
9	Total number of pedestrian agents at highest flood risk (HR > 2.5)
10	Maximum HR over the entire domain at the particular simulation time
11	Maximum depth of floodwater over the entire domain (m)
12	Maximum velocity of floodwater over the entire domain (m/s)
13	Maximum reached HR during the entire simulation
14	Maximum number of pedestrian agents that were at the highest flood risk
15	Maximum number of pedestrian agents that were at the low flood risk
16	Maximum number of pedestrian agents that were at the medium flood risk
17	Maximum number of pedestrian agents that were at the high flood risk
18	Total number of pedestrian agents at risk of sliding-only condition
19	Total number of pedestrian agents at risk of toppling-only condition
20	Total number of pedestrian agents at risk of toppling-and-sliding condition
21	Total number of pedestrian agents at risk of instability (regardless of condition)

2.b) 'output_exits.txt' is also a text file that stores the record of the number of pedestrian agents going towards a particular destination at each iteration of the simulation. The exits are predetermined by the user specifying from where the pedestrians enter and/or exit the domain. This output is useful only when the emergency exit of pedestrians is not predefined (like the Hillsborough Stadium case study) where the 'autonomous change of direction' condition is enabled to allow pedestrian agents to autonomously navigate into new pathways while moving within a flooded zone. The **output_exits.txt** file has 11 columns and rows

corresponding to the simulation iteration. From left to right, the first column shows the simulation time and the second to the eleventh column show the total number of pedestrians going towards Exit1 to Exit10 respectively. The simulator is configured to have 10 predefined exits. This will be explained in more detail in (Sect. 5).

3) '(*simulation_time)*flood.csv' and **'(*simulation_time)*ped.csv'** are also text files generated at each simulation iteration in '.../FloodPedestrian_2020/iterations' folder. (*simulation_time*) denotes the simulation time (in seconds) at each iteration once it is generated. '(*simulation time*)flood.csv' provides information about flood agents over their grid stored as a matrix with multiple rows relevant to their numbers and 8 columns as described in Table A.2. '(*simulation time*)ped.csv' also follows a similar format but with 12 columns containing the information of pedestrians as outlined in Table A.3. Note that the user can generate these files in regular time intervals (in second) via assigning non-zero value to *outputting_time_interval* parameter located in .xml input file in '.../FloodPedestrian_2020/iterations' folder in advance.

Table A.2: Description of the information of one flood agent (one row) stored in '(*simulation_time*)flood.csv' file.

Col.	Description
1	The coordinate of flood agent in x-axis direction as a positive integer
2	The coordinate of flood agent in y-axis direction as a positive integer
3	The depth of floodwater (m) at the location of the flood agent
4	The velocity magnitude of floodwater (m/s) at the location of the flood agent
5	HR of floodwater at the location of the flood agent
6	Average velocity of floodwater along x-axis direction (m/s)
7	Average velocity of floodwater along y-axis direction (m/s)
8	Topography height (m) at the location of the flood agent

Table A.3: Description of the Information of one pedestrian agent stored in '(*simulation_time*)ped.csv' file. Each row represents the information of one pedestrian agent at a particular simulation time.

Col.	Description
1	The coordinate of pedestrian agent in x-axis direction as a floating-point number
2	The coordinate of pedestrian agent in y-axis direction as a floating-point number
3	The flood risk state of pedestrian agent based on HR of floodwater at their location: **0:** pedestrian agent is at no flood risk (in dry zones, HR = 0) **1:** pedestrian agent is at low flood risk (HR < 0.75) **2:** pedestrian agent is at medium flood risk (0.75 < HR < 1.5) **3:** pedestrian agent is at high flood risk (1.5 < HR < 2.5) **4:** pedestrian agent is at highest flood risk (HR > 2.5)
4	HR of floodwater at the location of the pedestrian agent
5	The depth of floodwater at the location of the pedestrian agent (m)
6	The velocity magnitude of floodwater at the location of the pedestrian agent (m/s)
7	The moving speed of pedestrian agent at the particular simulation time (m/s)
8	The body height of the pedestrian agent (m)
9	The body mass of the pedestrian agent (kg)
10	The gender of the pedestrian agent (**1**: female , **2**: male)
11	The age of the pedestrian agent (in years)
12	The destination of the pedestrian agent at that particular simulation time. It can vary between 1 and 10 that corresponds to the number of the predetermined exits.

Note:

- A copy of the output files from the simulations reported in Shirvani & Kesserwani (2021) is uploaded into Zenodo directory (accessible at: https://doi.org/10.5281/zenodo.4576906), where the user could see how the outputs from one run of the flood-pedestrian simulator look like.
- A live video of the simulations reported in Shirvani & Kesserwani (2021) that was captured from FLAMEGPU built-in visualisation window is also uploaded into the TIB AB Portal accessible at https://doi.org/10.5446/51547.

5. Modifying the Simulations

A set of parameters is initialised in the <environment> element of .xml input file (located in the '.../FloodPedestrian_2020/iterations' folder) to enable users implement different actions by only changing the initial values assigned to these parameters. These parameters are set as environment constants accessible to all the agents. Table A.4 guides the users through what actions can be performed and how to implement them in the simulator by assigning a set of possible initial values.

Note:

- Changing the values of the environment parameters in the .xml file does not require further compilation and building of the executable program. This enables the users to practice and study other scenarios and initial conditions immediately after assigning new values to these parameters.
- Ensure that the parameters' name in the .xml file is not changed while assigning values to them as this will disable the functionality of that particular parameter.
- Always have a copy of the .xml input file before any modification. Doing this will help the user to have the original structure and naming for later restoration of the data.

Table A.4: Description of the actions and related parameters including their format, unit and possible values that could be assigned to them.

Action	Parameter	Format	Unit	Possible values
To set a time limit for outputting the simulation results. **Note:** by default, the results are automatically generated in each simulation time step until the termination of the simulation by the user (e.g. by closing the console window).	*outputting_time*	float	second	Any positive value. To disable the option assign 0.
To set a different time interval for outputting the results.	*outputting_time_interval*	float	second	Any positive value. To disable the option assign 0.
To change the 2D spatial dimensions for the study area.	*xmin; xmax; ymin; ymax*	float	metre	Any positive value. **Note:** *xmin* and *ymin* are both initially given zero; and *xmax* and *ymax* represent the length of the area in *x*- and *y*-axis directions respectively.
To change the time step of the pedestrian model. **Note:** this will be dominated by the *dt_flood* once the flood starts (see below).	*dt_ped*	float	second	Between 0.1 to 2.0 depending on the user's preference in preserving the realistic motion of pedestrians in real time.
To change the time step of the hydrodynamic model. **Note:** Any given initial value to this parameter will be updated automatically when '*auto_dt_on*' is enabled (see	*dt_flood*	float	second	Any positive value. **Note:** any given value should preserve the stability of the numerical solution

below).				depending on the initial condition of the flood inflow and geometry of the area (try varying it between 0.01 to 0.1).
To enable adaptive time stepping to maximise allowable *dt_flood* while keeping stability of the hydrodynamic solution. **Note:** when outputting at regular temporal intervals is considered, constant time stepping is usually preferable.	*auto_dt_on*	integer	none	1: Enable 0: Disable
To enable early evacuation of pedestrians prior to the start of flooding at a specific time (see further below).	*evacuation_on*	integer	none	1: Enable 0: Disable
To enable crowding of a certain number of pedestrians over the area before the start of flooding. **Note:** this option allows the user to study scenarios where a populated area is hit by flooding, like the shopping centre test case.	*preoccupying_on*	integer	none	1: Enable 0: Disable **Note:** the default scenario for the Hillsborough stadium case study does not require activation of this option, unless the user decides to study another scenario.
To select the shape of the inflow hydrograph. **Note:** the shape of the hydrograph is dependent on the parameters related to the time and discharge that are	*poly_hydrograph_on*	integer	none	1: Polynomial 0: Triangular

explained further below.				
To prevent pedestrians from entering the area after the flooding is started.	*stop_emission_on*	integer	none	1: Enable 0: Disable **Note:** by default it is enabled for the shopping centre test case; but disabled for the Hillsborough stadium case study.
To enable the pedestrians to go to the user-defined emergency exit (explained further below) once the flooding is started.	*goto_emergency_exit_on*	integer	none	1: Enable 0: Disable **Note:** by default it is enabled for the shopping center test case as the emergency exit is made known to all the pedestrians before the start of flooding (via assigning a value to *emergency_exit_number* parameter); but it is disabled for the Hillsborough stadium case study as the pedestrians are allowed to choose any destination upon enabling *escape_route_finder_on*option (see below).
To enable the 'autonomous change of direction' condition that allows pedestrians to autonomously navigate towards a destination while moving within a flooded zone.	*escape_route_finder_on*	integer	none	1: Enable 0: Disable

Note: more information about 'autonomous change of direction' condition is provided in Shirvani & Kesserwani (2021).				
To prevent pedestrians going back towards the exit/entrance through which they initially entered the area.	*no_return_on*	integer	none	1: Enable 0: Disable **Note:** the default scenario for the shopping centre and Hillsborough stadium test cases requires enabling this option, unless the user decides to study another scenario.
To enable pedestrians to go towards the most popular destination selected by most. **Note:** this option can only be enabled in scenarios where the 'autonomous change of direction' condition is enabled (see above).	*follow_popular_exit_on*	integer	none	1: Enable 0: Disable
To enable realistic moving speed of pedestrians in floodwater based on water depth and velocity. **Note:** more information about the realistic moving speed of pedestrians is provided in Shirvani & Kesserwani (2021).	*walking_speed_reduction_in_water_on*	integer	none	1: Enable 0: Disable **Note:** if this option is disabled, the pedestrians will maintain their in-dry walking speed that is randomly assigned to them once they are generated.
To immobilise pedestrians once they lose their stability	*freeze_while_instable_on*	integer	none	1: Enable

in floodwater.				0: Disable
To enable the ‘maximum excitement’ condition that allows pedestrians to increase their walking speed under evacuation conditions. **Note:** more information about the ‘maximum excitement’ condition is provided in Shirvani & Kesserwani (2021).	*excitement_on*	integer	none	1: Enable 0: Disable
To enable the ‘two-way interaction’ condition for factoring in the effect of pedestrians’ crowding on the bed roughness. **Note:** more information about the ‘two-way interaction’ condition is provided in Shirvani *et al.* (2021) and Shirvani & Kesserwani (2021).	*ped_roughness_effect_on*	integer	none	1: Enable 0: Disable
To switch between ‘walking’ and ‘running’ condition defining pedestrians moving speeds inside the floodwater. **Note:** this option is effective only when the realistic moving speed of pedestrians in floodwater is enabled (see above). More information about the ‘walking’ and ‘running’ conditions is provided in Shirvani & Kesserwani (2021).	*walk_run_switch*	integer	none	1: ‘walking’ condition 2: ‘running’ condition
To define the number of times that pedestrians can dynamically change their direction towards a new destination after which they	*dir_times*	integer	none	Any value. **Note:** assigning a value to this

follow the others towards the most popular destination. **Note:** this option is only enabled in scenarios where the 'autonomous change of direction' condition is also enabled (see above).				parameter is dependent on the time step of the simulation and the extent of flooding.
To change the threshold of floodwater depth to body height of pedestrians required for enabling the 'autonomous change of direction' condition. **Note:** more information about how this threshold is effective in the 'autonomous change of direction' condition is provided in Shirvani & Kesserwani (2021).	*wdepth_perc_thresh*	float	none	Between 0.0 and 1.
To define the initial number of pedestrians in the area.	*initial_population*	integer	none	Any positive value
To define the inflow hydrograph in terms of time and discharge (see Fig. A.9a).	*inflow_start_time* *inflow_peak_time* *inflow_end_time*	float	second	Any positive value
	inflow_initial_discharge *inflow_peak_discharge* *inflow_end_discharge*		m^3/s	
To define the start and end time of the evacuation process.	*evacuation_start_time* *evacuation_end_time*	float	second	Any positive value
To specify the inflow boundary through which the floodwater starts to propagate.	*INFLOW_BOUNDARY*	integer	none	1: North boundary 2: East boundary 3: South boundary 4: West boundary
To define the boundary condition in the	*BOUNDARY_EAST_STATUS* *BOUNDARY_WEST_STATUS*	integer	none	1: Open boundary, allowing the

hydrodynamic model for the specified domain (Wang *et al.* 2011).	*BOUNDARY_NORTH_STATUS* *BOUNDARY_SOUTH_STATUS*			floodwater to pass 2: Wall boundary, obstructing the floodwater
To define the location of the emergency exit. **Note:** the emergency exit is only applicable for evacuation from indoor areas where the emergency exit could be identified prior to the flooding, e.g. the shopping centre test case.	*emergency_exit_number*	integer	none	1 to 10 **Note:** the current version of the simulator can include up to 10 exits/entrances each of which is identified by a number. The location of Exit 1 to Exit 10 specified for the shopping centre and Hillsborough stadium test cases are presented in Fig. A.10.
To define the length of the breach by specifying two points on the grid where floodwater is expected to propagate (see Fig. A.9b).	*x1_boundary* *x2_boundary* *y1_boundary* *y2_boundary*	float	metre	Any positive value within the range of the domain length.
To specify the emergence rate of pedestrians per each iteration of the simulation at Exit 1 to Exit 10.	*EMMISION_RATE_EXIT1* *EMMISION_RATE_EXIT2* *EMMISION_RATE_EXIT3* *EMMISION_RATE_EXIT4* *EMMISION_RATE_EXIT5* *EMMISION_RATE_EXIT6* *EMMISION_RATE_EXIT7* *EMMISION_RATE_EXIT7* *EMMISION_RATE_EXIT9* *EMMISION_RATE_EXIT10*	integer	none	Any positive value.
To change the probability distribution of each exit to be selected by the pedestrians.	*EXIT1_PROBABILITY* *EXIT2_PROBABILITY* *EXIT3_PROBABILITY*	integer	none	Any positive value. **Note:** in case of

	EXIT4_PROBABILITY *EXIT5_PROBABILITY* *EXIT6_PROBABILITY* *EXIT7_PROBABILITY* *EXIT8_PROBABILITY* *EXIT9_PROBABILITY* *EXIT10_PROBABILITY*			equal selection probability, assign the same value to all the exits/entrances.
To change the body height distribution of the pedestrians. **Note:** the distribution of the pedestrians' body height is set based on a cumulative probability for each range that is defined as a percentage of the total population.	*PedHeight_60_110_probability* *PedHeight_110_140_probability* *PedHeight_140_163_probability* *PedHeight_163_170_probability* *PedHeight_170_186_probability* *PedHeight_186_194_probability* *PedHeight_194_210_probability*	float	percent	0 to 100 **Note:** the current set up for the shopping centre and Hillsborough stadium test cases is based on the body height structure of the UK population (more information is provided in Shirvani *et al.* (2020)).
To change the age distribution of the pedestrians. **Note:** the distribution of the pedestrians' age is set based on a cumulative probability for each range that is defined as a percentage of the total population.	*PedAge_10_17_probability* *PedAge_18_29_probability* *PedAge_30_39_probability* *PedAge_40_49_probability* *PedAge_50_59_probability* *PedAge_60_69_probability* *PedAge_70_79_probability*	float	none	0 to 100 **Note:** the current set up for the shopping centre and Hillsborough stadium test cases is based on the seven age range structure of the UK population (more information is provided in Shirvani & Kesserwani (2021)).
To change the gender distribution of the pedestrians. **Note:** similar to the body height and age, the	*gender_female_probability* *gender_male_probability*	float	none	0 to 100

distribution of the pedestrians' age is set based on a cumulative probability for each range that is defined as a percentage of the total population.				

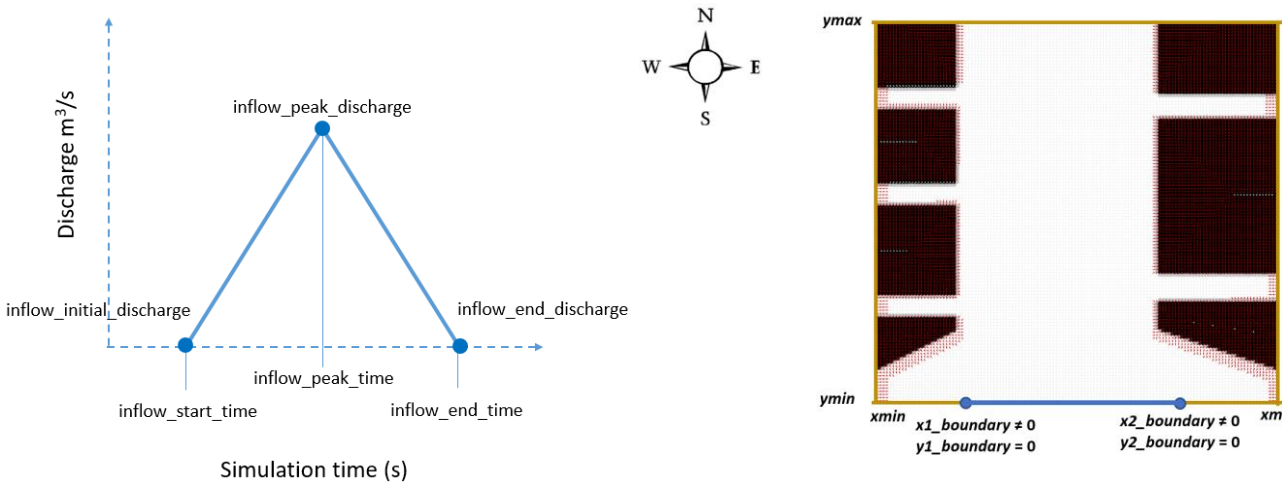

(a) (b)

Figure A.9: Illustrative guidance to the users for (a) defining the inflow hydrograph through assigning values to the inflow parameters; and (b) defining the coordinates for specifying the location of the breach via assigning values to '*x1_boundary'*, '*y1_boundary'*, '*x2_boundary'* and '*y2_boundary'* in the *environment* element in the .xml input file.

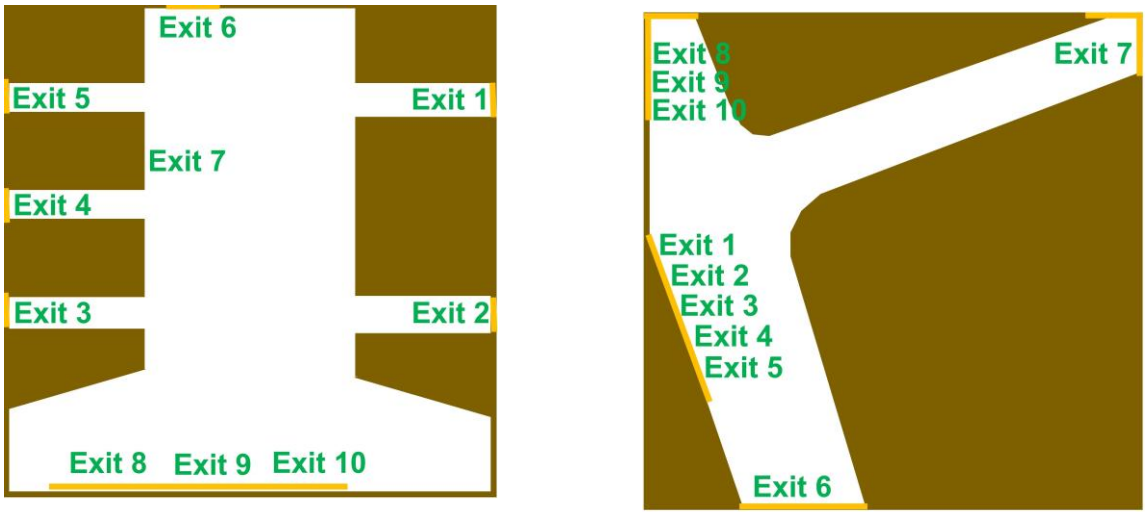

(a) (b)

Figure A.10: Schematic representation of the exits/entrances specified for: (a) the shopping centre and (b) the Hillsborough stadium test cases.

6. Instructions to create a new test case

The following steps will guide the users on how to create new test cases.

Step 1. Generating initial state of hydrodynamic and navigation agents.

Step 1.1: flood agents are required to be initialised by Cartesian coordinates on a grid storing topography data of the subjected area. Users may use any method to generate the grid of flood agents, but it must be converted into XML format using the parent-child structure and naming shown below for each flood agent:

<xagent>	
*<name>*FloodCell*</name>*	'Floodcell' is name of flood agent
*<inDomain>*1*</inDomain>*	1 or 0 indicate agent is inside or outside the study area
<x>...</x>	a positive integer indicating the *x*-coordinate of the agent
<y>...</y>	a positive integer indicating the *y*-coordinate of the agent
<z0>...</z0>	Topography elevation at the location of the flood agent
</xagent>	

Note:

- In the current version of the simulator, the grid of flood agents must be defined as square with a length size in power of two (e.g. 256, 512, 1024, etc.).
- The code that was used to generate the grid of flood agents for the flooded shopping centre test case in Shirvani *et al.* (2021) and Shirvani *et al.* (2020), is accessible from another GitHub repository via this link: https://github.com/SahebSh/FLAMEGPU/tree/master/examples/FloodPedestrian_2018/Flood_XML_inpGe. This code is written in C++ and can be opened and executed from Visual Studio on Windows. Users can use this model to modify the shopping centre test case or take it as an example to produce another one.

Step 1.2: the grid of navigation agents are also required to be produced via using the FGPUGridNavPlanEditor package that is specifically designed for this purpose. A modified version of this model with the specific XML structure and component naming compatible with the present version of the simulator is also accessible for the user from another GitHub repository via this link: https://github.com/SahebSh/FLAMEGPU/tree/master/examples/FloodPedestrian_2018/FGPUGridNavPlanEditor.

After running FGPUGridNavPlanEditor via Visual Studio, a self-explanatory graphical user interface will pop up on the screen as shown in Fig. A.11. The user can take the steps shown in Fig. A.11 to generate the grid of navigation agents.

Note:
The pedestrian flow will be automatically generated over the grid of navigation agents during the simulations from where the exits are defined by the user; therefore, there is no need to take further steps for initialisation of pedestrian agents over the grid. The movement of pedestrian agents is driven by their internal interactions with each other and the information they receive from the navigation agents that steers and directs them towards their goal destination on the grid. More information about the interactions between the grid of navigation agents and pedestrian agents can be found in Karmakharm *et al.* (2010). It is also useful to note that, unlike the hydrodynamic and navigation agents, the pedestrian agents are not of discrete type; they are of continuous agent type that can dynamically change their coordinates.

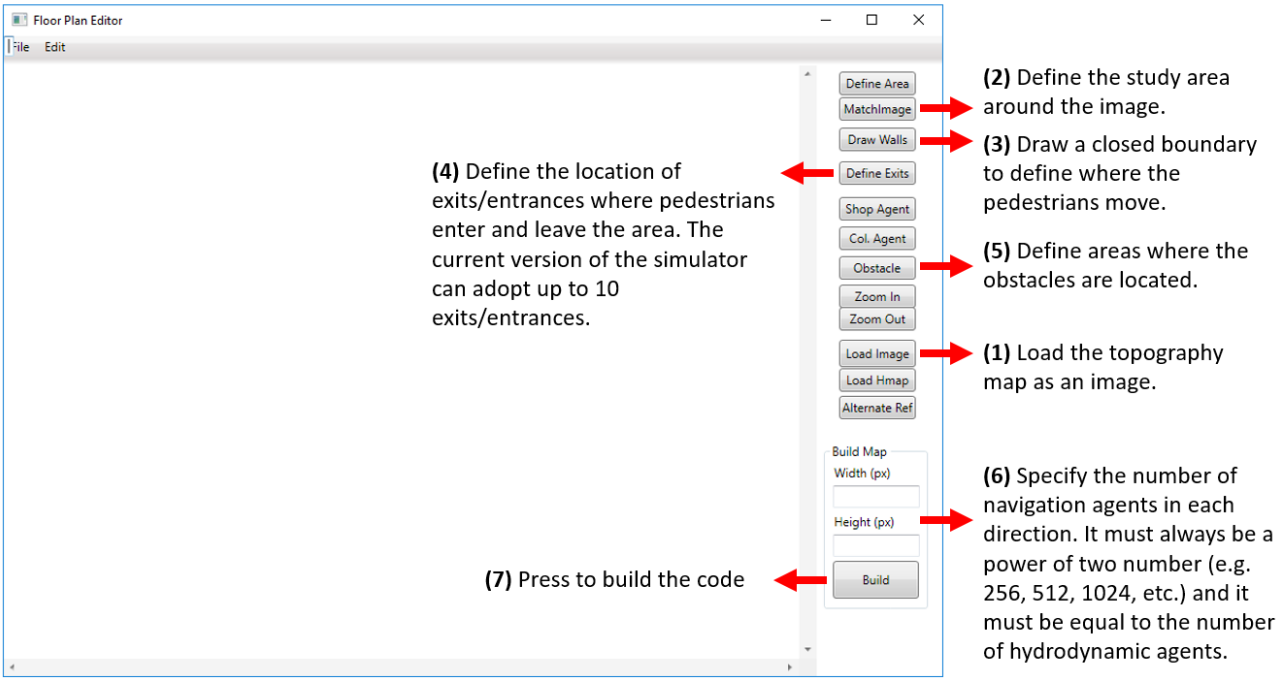

Figure A.11: Screenshot of the FGPUGridNavPlanEditor graphical user interface.

The generated grids of flood and navigation agents from Step 1.1 and Step 1.2 need to be placed within the .xml input file later in Step 2 (below) in order to make the information accessible to the simulator. The new input file could be named 'map.xml' and located in '.../iterations' folder containing the information of all the agents and the parameters enabling the users to set up other case studies.

Note:
Naming of the .xml input file should always be consistent with the address and name that is specified in the Command Arguments (see Sect. 3, Step 8) from the last build; otherwise, the executable file should be built again.

Step 2: setting up the .xml input file.

The .xml input file should always be structured based on a '*<states>*' parent and three childs in xml format, as outlined below:

<states>	
<itno>0<itno>	Indicate the iteration number. Must be initialised to 0 to load 'map.xml' in order to start a simulation.
<environment></environment>	Contains all the parameters that the user can modify to fit the simulator to a case study (see Table A.4 for detailed description).
<xagents></xagents>	Contain the initial state of flood and navigation agents generated from Step 1. The user is <u>not</u> expected to change any of these variables directly from the .xml input file, but rather, S/he needs to produce them earlier to fit to the study area specification (recall Step 1 above and overwrite agent data in the .xml input file).
</states>	

Note:

- The users are allowed to use the contents of the already generated and provided input files (HilStad.xml and ShopCent.xml) and copy/paste the new flood and navigation agents information into the *xagents* element following the same template explained above.
- Steps 1-6 from Sect 3 should be repeated each time the user applies the simulator for a different grid size of navigation and flood agents. In this case, the user is also expected to adapt the simulator for the new grid size prior to the building procedure. To do so, click and open '**XMLModelFile.xml**' from the 'Solution Explorer'. Then find **gpu:bufferSize** tag where the total number of agents spanning over the generated grid is specified, e.g. for a grid of 128 × 128 navigation/flood agents, the **gpu:bufferSize** is set to 16384. The user may use Ctrl+f shortcut to find the old **gpu:bufferSize** value within the '**XMLModelFile.xml**' file and replace it with a new one. Once the new value is assigned to **gpu:bufferSize**, save the changes via Ctrl+s (or clicking on 🖫 below the top menu) and close the '**XMLModelFile.xml**' tab. Also, to know more about the **XMLModelFile.xml** file and its contents refer to the FLAMEGPU Documentation and User guide, accessible online via https://flamegpu.com/documentation/.

Appendix B

Guide to build a hydrodynamic model on FLAME GPU

This appendix provides a brief description of the steps taken to build the hydrodynamic model within the framework of FLAME-GPU. It consist of specification of flood agents within XMLModelFile (Sec. B.1) and the implementation of hydrodynamic formulation within the functions.c behavioural script (Sec. B.2).

B.1 XMLModelFile specification

By default, XMLModelFile file contains the following four main elements to contain the specification of the flood agents in the model:

```
<gpu:environment> … </gpu:environment>
<gpu:xagents>… </gpu:xagents >
<gpu:messages> … </gpu:messages >
<gpu:layers> … </gpu:layers >
```

Next, the configuration of each of these elements for the hydrodynamic model is described in details.

B.1.1 'environment' element specification

This element contains any item (e.g. constant variables, function file, etc.) that is shared within the environment of the FLAME-GPU framework. Since the source code (functions.c) is a shared script executed by the agents, it is mandatory to introduce this file within the environment element. By doing this, flood agents will identify the functions.c behavioural script to govern their state update in time. After introducing the behavioural script, the structure of the 'environment' element can be extended as follows:

```
<gpu:environment>
    <gpu:functionFiles>
        <file>functions.c</file>
    </gpu:functionFiles>
</gpu:environment>
```

B.1.2 'xagent' element

This element enables the model to specify multiple agents with specific characteristics. The hydrodynamic model comprises spatially discrete flood agents, which are specified to have

fixed coordinates on a grid. This type of agents is introduced to the model through this element. The ‘xagent’ element contains six other elements as shown below:

```
<xagents>
  <gpu:xagent>
      <name>FloodAgent</name>
      <memory>…</ memory >
      <functions>…</ functions >
      <states>…</ states >
      <gpu:type>discrete</gpu:type>
      <gpu:bufferSize>4096</gpu:bufferSize>
  </gpu:xagent>
</xagents>
```

Description of ‘name’ element:

This element enables the modeller to specify an optional name for each type of the agents. For the hydrodynamic model, the name of the flood agent is specified as *FloodAgent*.

Description of ‘memory’ element:

The variables containing the information of the flood agent are stored within their memory via embedding them in the ‘memory’ element. These variables are defined by a name and type within the memory of the flood agent. The ‘memory’ element looks like:

```
<memory>
  <gpu:variable>
      <type>…</ type >
      <name>…</ name >
  </gpu:variable >
</ memory >
```

The variables used to build the current hydrodynamic model on FLAME GPU are presented in details in Table B.1 according to their type and name.

Table B.1: Variables specified in the memory of a flood agent.

Variable name	type	Description
inDomain	Integer	By assigning the value *1* to this variable, the flood agent is made identifiable within the domain. This is mainly to eliminate any calculations outside the flood domain where the agents are not expected to get updated.
x	Integer	Stores the coordinate data of the flood agent in *x*-axis direction.
y	Integer	Stores the coordinate data of the agent in *y*-axis direction.
h	Double	Water surface elevation
q_x	Double	Water discharge in *x*-axis direction
q_y	Double	Water discharge in *y*-axis direction
z	Double	Bed level
hFace_E *hFace_W* *hFace_N* *hFace_S* *qxFace_E* *qxFace_W* *qxFace_N* *qxFace_S* *qyFace_E* *qyFace_W* *qyFace_N* *qyFace_S*	Double	Local face variables in the *East*, *West*, *North*, and *South interfaces* of the flood agent. These variables are defined to deliver the initial flow data to numerical flux solver where left and right values of each agent is required to approximate the fluxes at each edge (see Sec. 3.3.3). These variables are initially assigned to be equal to the flow variables (*h, qx, qy*).

Description of 'functions' element:

This element encompasses the output and update message functions that are used to pass the information between the agents and update their sates in time. One single function could be described by the following elements:

```
<functions>
    <gpu:function>
        <name>…</name>
        <currentState>Default</currentState>
        <nextState> Default </nextState>
        <output>
            <messageName>…</messageName>
            <gpu:type>single_message</gpu:type>
        </output>
        <input>
            <messageName>…</messageName>
        </input>
    </gpu:function>
</functions >
```

The output and update message functions are required to be specified by their names, their current states (*currentState*) and future states (*nextState*), and their output message and/or input message (specified as messages). The output message contains the a set of specific variables that needs to be sent to the other agents after the execution of the message function. Conversely, the input message contains the set of variables that needs to be acquired from the neighbouring agents to be used in the evaluation of the state of the agent in the next iteration. For the hydrodynamic model, the state of the flood agent will be updated over its current state after the execution of each message function. Therefore, the *currentState* and *nextState* are defined by a similar state, e.g. *Default*. Specifying the state of the message functions to *Default* ensures that the state of the flood agent is updated over the similar state of the flood agent each time that any of the message functions is executed. The type *single_message* is also specified to this element to ensure that one message will be sent via the output message function. Similarly, the update message function within the 'functions' element requires defining a message via an *input* element to ensure that the specific data can

be obtained by the flood agent. It is essential that the output and update message functions dealing with similar set of variables to be specified by similar messages. For example, if the output message function is expected to broadcast *Message_1* and it is specified within 'output' element, the update message function dealing with this message is expected to be set to *Message_1* through the *input* element.

Description of 'states' element:

This element is designed to specify the possible states of the agents. Since this flood model updates over the initial state of the flood agent (*Default*), the structure of this element is described as follow:

```
<states>
    <gpu:state>
        name>Default</name>
    </gpu:state>
    <initialState>Default</initialState>
</states>
```

Specifying *Default* state enables the hydrodynamic model to update the state of the flood agent in a sequential order of message functions' execution. Figure B.1 presents the algorithm through which the *Default* state of the flood agent is updated in the next iteration of the simulations via two sets of output and update message functions.

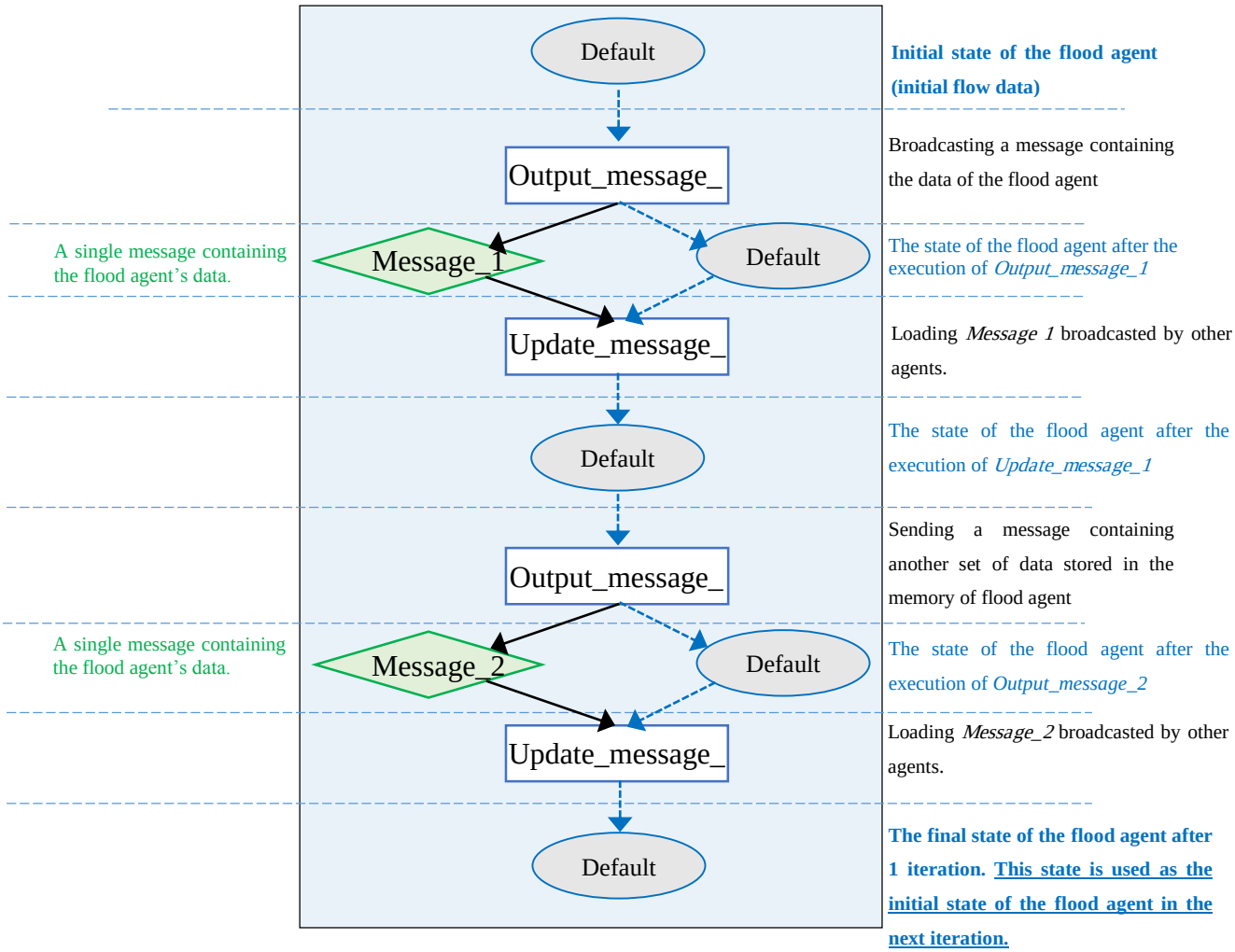

Figure B.1: Algorithm that is used to update the state of a flood agent; oval shapes indicate the state of the flood agent, rectangles represent message functions, and the diamonds are the messages broadcasted by output message functions; dashed-line blue arrows points to the next state of the flood agent and the black arrows indicate broadcasting and loading the messages

Description of 'type' element:

Through this element, the type of flood agents is specified. As the hydrodynamic model is operational for a 2D discrete domain, with FV discretisation, the flood agent type is defined as *discrete*.

Description of ‘bufferSize’ element:

As in discrete a partition, ‘bufferSize’ contains the population of the flood agents in the domain. For *discrete* type of flood agents, the number of flood agents in *x*- and *y*-axis directions are expected to be equal and are expected to be in power of two. For example, if it is assumed that 64 agents are existed in each direction (*x* and *y*), ‘bufferSize’ is required to be assigned to 4096 meaning the population of flood agents in the domain. The maximum number of the flood agents which can be assigned to the ‘bufferSize’ is limited to the capacity of the GPU memory. The occupied memory size by flood agents is entirely dependent on the number of variables per each flood agent and the messages broadcasting them, variable sizes on the memory, and the number of flood agents in the domain.

B.1.3 ‘messages’ element

The messages containing the information of the flood agents to be shared and processed between them are defined within this element. The structure of ‘messages’ element looks like:

```
<messages>
  <gpu:message>
     <name>…</name>
     <variables>…</variables>
     <gpu:partitioningDiscrete>…</gpu:partitioningDiscrete>
     <gpu:bufferSize>4096</gpu:bufferSize>
  </gpu:message>
</messages>
```

Description of ‘name’ element

Each message to be sent or receive is expected to be defined by an optional name that enables the message functions to distinguish different sets of information.

Description of ‘variables’ element:

The information of the flood agents is stored as a set of variables within the memory of the flood agents. The sending and receiving these variables via the messages need to be specified in the memory of the messages, similar to their specification within the memory of the flood agents. These variables are defined within ‘variables’ element of the messages element by their type and name as follows:

```
<variables>
    <gpu:variable>
        <type>…</type>
        <name>…</name>
    </gpu:variable>
</variables>
```

For the hydrodynamic model, these variables are mainly the flow variables and coordinate data that are shared between the flood agents in the domain. Each set of variables through the messages can be assigned to perform a particular function in the flood model. More specifically, local face variables can be embedded within a particular message to be broadcasted and processed where the local face variables of the neighbouring agents are required in the calculation of the numerical fluxes across the interfaces.

Description of ‘partitioningDiscrete’ element

Since the flood model is expected to be built upon a 2D domain (as agents were initiated within *xagent* element), messages are required to be set as ‘partitioningDiscrete’ (FLAME GPU User Guide) as follows:

```
<gpu:partitioningDiscrete>
    <gpu:radius>1</gpu:radius>
</gpu:partitioningDiscrete>
```

Within the ‘partitioningDiscrete’ element, ‘radius’ specifies the number of messages returned from each message function iteration, querying surrounding neighbours’ data. As the information of four surrounding flood agents is required in the approximation of the numerical fluxes across four interfaces of each flood agent, at least four messages containing the local face variables are required to be returned through each iteration of the message functions. Thus, this is mandatory to assign radius to at least 1, which enables to return 1 message from each of the 9 neighbouring agents (FLAME-GPU User Guide).

Description of ‘partitioningDiscrete’

The messages are expected to be shared and received by all the flood agents over the flood domain. Therefore, the ‘bufferSize’ element is assigned to a value corresponding to the number of flood agents in the domain, which has been previously specified within the ‘xagent’ element, e.g. 4096.

B.1.4 ‘layers’ element specification

The ‘layers’ element specifies the sequential order of the execution of message functions in the model. Each layer can be either dedicated to a single message function or a number of message functions. Note that, the output and update message functions dealing with a similar message should be specified within two separated layers. Each layer could encompass an unlimited number of message functions, but each should have a distinct name. The structure of one layer looks like the format shown below.

```
<layers>
    <layer>
        <gpu:layerFunction>
            <name>…</name>
        </gpu:layerFunction>
    </layer>
</layers>
```

For two sets of output and input message functions, like the example algorithm illustrated in Fig. B.2, the structure of the ‘layers’ element could be specified as:

```
<layers>
    <layer>
        <gpu:layerFunction>
            <name>Output_message_1</name>
        </gpu:layerFunction>
    </layer>
    <layer>
        <gpu:layerFunction>
            <name> Update_message_1</name>
        </gpu:layerFunction>
    </layer>
    <layer>
        <gpu:layerFunction>
            <name> Output_message_2</name>
        </gpu:layerFunction>
    </layer>
    <layer>
        <gpu:layerFunction>
            <name> Update_message_2</name>
        </gpu:layerFunction>
    </layer>
</layers>
```

B.2 Functions.c behavioural script specification

The functions.c script comprises the formulations and mathematical steps of the hydrodynamic model, which in this research includes the FV solution of SWEs that is functional for all flood agents at the same time, which has been explained in details in Sec. 3.3 of this thesis. Figure B.2 illustrates a schematic of how the flood agent are enabled to update the flow variables by executing functions.c through a number of iterations. In one iteration, the initial flow variables from input file, which is generated from outside the FLAME GPU framework (see in Appendix A), are firstly duplicated to the memory of the flood agent to form their initial state. The flood agents use the mathematical functions in functions.c to update these variables in one iteration and update them back on the memory of the agents for the next iteration. This process is repeated within each iteration through which the initial flow variables are obtained from the last iteration of the simulation.

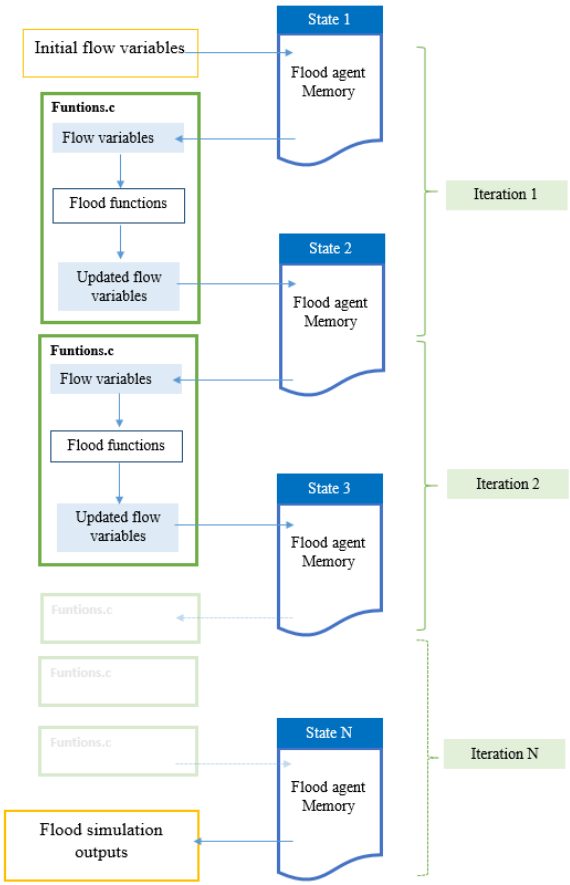

Figure B.2: An illustration of the process through which the flow variables are updated in the memory of flood agents through each simulation iteration via consecutive execution of functions.c

- **Integration of flood functions into functions.c script**

Generally, the flood functions refer to the functions which are commonly used in the flood models, for example, the numerical flux approximation functions that are used in the hydrodynamic model (see in Sec. 3.2). In functions.c, these functions are declared and defined by *__device__* prefix that is a known CUDA function specifier. *__device__* specifier ensures that the function will be executed and computed on the GPU. Since *__device__* flood functions will be executed on GPUs through *functions.c*, their structures are required to be modified in a format that is suitable to be performed for one flood agent independently. As these flood functions are mainly dependent on neighbouring flood agents' information, they are required to be integrated within update message functions to perform calculations on the GPU while enquiring the information from the neighbouring agents. Note that, the message functions in the functions.c script are specified by a FLAME GPU function identifier (*__FLAME_GPU_FUNC__*). This identifier ensures that the function have access to the agents' memory and the information shared already via the message pool. As functions.c has a C-based structure, pointers are essential to access the memory of the agents and the messages, where the variables are specified (in the XMLModelFile). Functions.c script also allows specification of an unlimited number of external functions to be also executed directly on the GPU alongside the agent and message functions. FLAME GPU allows the user to specify external functions by using *__device__* CUDA-specialised micro.

- **Integration of flood functions into the message functions**

Message functions enable flow variables to be shared between flood agents that can be used in the flood functions. Output message functions are only responsible to send the information to the other agents. Update message functions are responsible to load the shared information to update the flow variables via the flood functions where the information from the neighbouring flood agents is required. Figure B.3 represents a complete algorithm of the hydrodynamic model which can be embedded within functions.c. First, the initial flow variables is shared to the other neighbouring flood agents through *Output_message_1* via *Message_1*. Subsequently, *Update_message_1* loads the neighbouring flood agents' initial flow variables that are stored within *Message_1* to the memory of a local flood agent (any agent). A flood function, i.e. *Flood_function_1*, is then executed on the GPU through an

Update_message_1 message function. After the execution of *Flood_function_1*, the flow variables stored on the memory of the flood agents is updated. Next, flood agents share this information through *Output_message_2* via *Message_2*. Finally, *Update_message_1*, can load the neighbouring flood agents' flow variables for approximation of *Flood_function_2* for updating the flow variables in the next iteration. After passing through this algorithm, the flow variables are updated and are used in the next iteration.

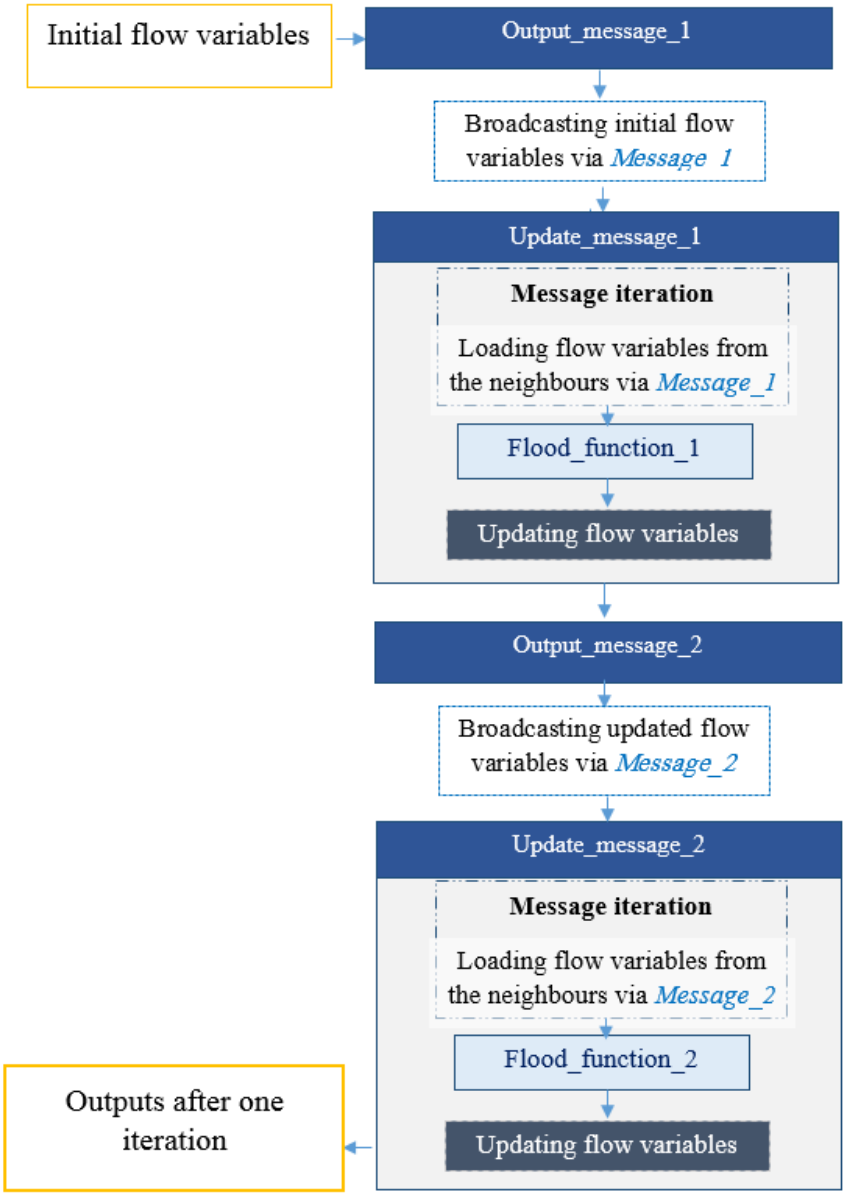

Figure B.3: The flood model algorithm integrated within the message functions through functions.c behavioural script

Bibliography

Abebe, Y. A., Ghorbani, A., Nikolic, I., Manojlovic, N., Gruhn, A., & Vojinovic, Z. (2020). The role of household adaptation measures in reducing vulnerability to flooding: a coupled agent-based and flood modelling approach. *Hydrology and Earth System Sciences*, **24**(11), 5329-5354.

Aboelata, M., & Bowles, D. S. (2008). LIFESim: A tool for estimating and reducing life-loss resulting from dam and levee failures. In Proceedings of the Association of State Dam Safety Officials "Dam Safety 2008" Conference, pp. 533-547. 7-11 September 2008, Indian Wells, California, USA.

Adrien, N. G. (2003). *Computational hydraulics and hydrology: an illustrated dictionary*. CRC Press. Boca Raton, FL, USA.

Aerts, J. C. (2020). Integrating agent-based approaches with flood risk models: A review and perspective. *Water Security*, **11**, 1-9.

Aerts, J. C., Botzen, W. J., Clarke, K. C., Cutter, S. L., Hall, J. W., Merz, B., ... & Kunreuther, H. (2018). Integrating human behaviour dynamics into flood disaster risk assessment. *Nature Climate Change*, **8**(3), 193-199.

Albi, G., Bongini, M., Cristiani, E., & Kalise, D. (2016). Invisible control of self-organizing agents leaving unknown environments. *SIAM Journal on Applied Mathematics*, ***76***(4), 1683-1710.

Aleksandrov, M., Cheng, C., Rajabifard, A., Kalantari, M. (2019). Modelling and finding optimal evacuation strategy for tall buildings. *Saf. Sci.*, **115**, 247–255.

Alonso Vicario, S., Mazzoleni, M., Bhamidipati, S., Gharesifard, M., Ridolfi, E., Pandolfo, C., & Alfonso, L. (2020). Unravelling the influence of human behaviour on reducing casualties during flood evacuation. *Hydrological Sciences Journal*, **65**(14), 2359-2375.

An, L. (2012). Modelling human decisions in coupled human and natural systems: Review of agent-based models. *Ecological modelling*, **229**, 25-36.

Aravindan, A., & Mackenzie, J. (2021, 22 July). From China to Germany, floods expose climate vulnerability. *Reuters*. Retrieved from https://www.reuters.com/business/environment/china-germany-floods-expose-climate-vulnerability-2021-07-22/ [accessed 8 August 2021].

Arrighi, C., Oumeraci, H., & Castelli, F. (2017). Hydrodynamics of pedestrians' instability in floodwaters. *Hydrology and Earth System Sciences*, **21**(1), 515-531.

Barnes, B., Dunn, S., Pearson, C., & Wilkinson, S. (2021). Improving human behaviour in macroscale city evacuation agent-based simulation. *International Journal of Disaster Risk Reduction*, **60**, 102289.

Becker, J. S., Taylor, H. L., Doody, B. J., Wright, K. C., Gruntfest, E., & Webber, D. (2015). A review of people's behavior in and around floodwater. *Weather, Climate, and Society*, **7**(4), 321-332.

Beklaryan, A. L., Beklaryan, L. A., & Akopov, A. S. (2021). Implementation of the Deffuant Model Within the FLAME GPU Framework. *Advances in Systems Science and Applications*, ***21***(4), 87-99.

Bernardini, G., and Quagliarini, E. (2020). How to Account for the Human Motion to Improve Flood Risk Assessment in Urban Areas. *Water*, **12**(5), 1316.

Bernardini, G., Camilli, S., Quagliarini, E., & D'Orazio, M. (2017b). Flooding risk in existing urban environment: from human behavioural patterns to a microscopic simulation model. *Energy Procedia*, **134**, 131-140.

Bernardini, G., Postacchini, M., Quagliarini, E., Brocchini, M., Cianca, C., & D'Orazio, M. (2017a). A preliminary combined simulation tool for the risk assessment of pedestrians' flood-induced evacuation. *Environmental modelling & software*, **96**, 14-29.

Bernardini, G., Quagliarini, E., D'Orazio, M., & Brocchini, M. (2020). Towards the simulation of flood evacuation in urban scenarios: Experiments to estimate human motion speed in floodwaters. *Safety Science*, **123**, 104563.

Bernardini, G., Romano, G., Soldini, L., & Quagliarini, E. (2021). How urban layout and pedestrian evacuation behaviours can influence flood risk assessment in riverine historic built environments. *Sustainable Cities and Society*, **70**, 102876.

Blenkinsop, S., Muniz Alves, L., & Smith, A.J.P. (2021). ScienceBrief Review: Climate change increases extreme rainfall and the chance of floods. *Critical Issues in Climate Change Science*. Retrieved from https://sciencebrief.org/uploads/reviews/ScienceBrief_Review_RAINFALL_Jun2021.pdf [accessed 8 August 2021].

BMT-WBM (2018), *TUFLOW Classic/HPC User Manual Build 2018-03-AD*, Technical Report, BMT WBM.

Bohannon, R. W., & Andrews, A. W. (2011). Normal walking speed: a descriptive meta-analysis. *Physiotherapy*, **97**(3), 182-189.

Bonabeau, E. (2002). Agent-based modelling: Methods and techniques for simulating human systems. Proceedings of the national academy of sciences, **99**(3), 7280-7287.

Bring on the sub: Sheffield Wednesday's pitch submerged by flood water: Daily Mail Online. (26 June 2007). Available at: https://www.dailymail.co.uk/sport/football/article-464478/Bring-sub-Sheffield-Wednesdays-pitch-submerged-flood-water.html [accessed 14 June 2021].

Bukowski, R.W., Jones, W.W., Levin, B.M. (1987). HAZARD I-Volume I: Fire hazard assessment method. *Natl. Inst. Stand. Technol. Cent. Fire Res* (*NBSIR),* **87,** 3602.

Burstedde, C., Klauck, K., Schadschneider, A., & Zittartz, J. (2001). Simulation of pedestrian dynamics using a two-dimensional cellular automaton. *Physica A: Statistical Mechanics and its Applications*, **295**(3-4), 507-525.

Busogi, M., Shin, D., Ryu, H., Oh, Y. G., & Kim, N. (2017). Weighted affordance-based agent modeling and simulation in emergency evacuation. *Safety science*, **96**, 209-227.

Cao, S., Song, W., Lv, W., & Fang, Z. (2015). A multi-grid model for pedestrian evacuation in a room without visibility. *Physica A: Statistical Mechanics and its Applications*, **436**, 45-61.

Chanson, H., & Brown, R. (2018). Stability of Individuals during Urban Inundations: What Should We Learn from Field Observations?. *Geosciences*, **8**(9), 341.

Chanson, H., Brown, R., & McIntosh, D. (2014). Human body stability in floodwaters: the 2011 flood in Brisbane CBD. In *Hydraulic Structures and Society-Engineering Challenges and Extremes: Proceedings of the 5th IAHR International Symposium on Hydraulic Structures (ISHS2014)* (pp. 1-9). The University of Queensland.

Chen, J., Shi, T., & Li, N. (2021). Pedestrian evacuation simulation in indoor emergency situations: approaches, models and tools. *Safety Science*, **142**, 105378.

Chen, X., & Wang, J. (2020). Entropy-Based Crowd Evacuation Modeling With Seeking Behavior of Social Groups. *IEEE Access*, ***9***, 4653-4664.

Chen, Y., Wang, C., Li, H., Yap, J. B. H., Tang, R., & Xu, B. (2020). Cellular automaton model for social forces interaction in building evacuation for sustainable society. *Sustainable cities and society*, **53**, 101913.

Chimeh, M. K., & Richmond, P. (2018). Simulating heterogeneous behaviours in complex systems on GPUs. *Simulation Modelling Practice and Theory*, **83**, 3-17.

China floods death toll rises to 302 with 50 people still missing. (2021, 2 August). *The Guardian*. Retrieved from https://www.theguardian.com/world/2021/aug/02/china-floods-death-toll-rises-people-still-missing-henan-province [accessed 8 August 2021].

Chow, V.T. (1959), Open channel hydraulics, McGraw-Hill, New York.

Chu, M. L., & Law, K. (2013). Computational framework incorporating human behaviors for egress simulations. *Journal of Computing in Civil Engineering*, **27**(6), 699-707.

Chu, M. L., & Law, K. H. (2019). Incorporating individual behavior, knowledge, and roles in simulating evacuation. *Fire technology*, **55**(2), 437-464.

Chu, M. L., Parigi, P., Law, K., & Latombe, J. C. (2014, April). Safegress: a flexible platform to study the effect of human and social behaviors on egress performance. In *Proceedings of the Symposium on Simulation for Architecture & Urban Design* (p. 4).

Colombo, R. M., & Rosini, M. D. (2005). Pedestrian flows and non-classical shocks. *Mathematical methods in the applied sciences*, **28**(13), 1553-1567.

Costabile, P., Costanzo, C., De Lorenzo, G., & Macchione, F. (2020). Is local flood hazard assessment in urban areas significantly influenced by the physical complexity of the hydrodynamic inundation model?. *Journal of Hydrology*, **580**, 124231.

Coutinho-Rodrigues, J., Sousa, N., & Natividade-Jesus, E. (2016). Design of evacuation plans for densely urbanised city centres. In Proceedings of *the Institution of Civil Engineers-Municipal Engineer*, **169**(3), 160-172.

Cox, R. J., Shand, T. D., & Blacka, M. J. (2010). Australian Rainfall and Runoff revision project 10: appropriate safety criteria for people. *Water Res.*

Cristiani, E., Peri, D. (2017). Handling obstacles in pedestrian simulations: Models and optimization. *Appl. Math. Model*, **45**, 285–302.

Cristiani, E., Piccoli, B., & Tosin, A. (2014). *Multiscale modeling of pedestrian dynamics* (Vol. 12). Springer.

Davidson, H. (2021, July 21). 'I might not make it': passengers tell of horror as Chinese subway floods. the Guardian: China. https://www.theguardian.com/world/2021/jul/21/passengers-tell-of-horror-chinese-subway-floods-zhengzhou.

Dawson, R. J., Peppe, R., & Wang, M. (2011). An agent-based model for risk-based flood incident management. *Natural hazards*, **59**(1), 167-189.

Delcea, C., Cotfas, L. A., Craciun, L., & Molanescu, A. G. (2020). An agent-based modeling approach to collaborative classrooms evacuation process. *Safety science*, **121**, 414-429.

Dias, C., Abd Rahman, N., & Zaiter, A. (2021). Evacuation under flooded conditions: Experimental investigation of the influence of water depth on walking behaviors. *International Journal of Disaster Risk Reduction*, **58**, 102192.

Ding, N., Chen, T., & Zhang, H. (2017a). Simulation of high-rise building evacuation considering fatigue factor based on cellular automata: A case study in China. *Building Simulation*, **10**(3), 407-418.

Disabled World (2019). Child BMI: Body Mass Index Calculator for Children [online]. *Disabled World*. Retrieved from https://www.disabled-world.com/calculators-charts/child-bmi.php [accessed 1 November 2019].

Dobbs, R. J., Charlett, A., Bowes, S. G., O'NEILL, C. J. A., Weller, C., Hughes, J., & Dobbs, S. M. (1993). Is this walk normal?. *Age and ageing*, **22**(1), 27-30.

Dong, H., Zhou, M., Wang, Q., Yang, X., Wang, F.Y., 2020. State-of-the-Art Pedestrian and Evacuation Dynamics. IEEE Trans. *Intell. Transp. Syst.*, **21**, 1849–1866.

Engineering ToolBox. (2003). Room Area per Person. [online]. https://www.engineeringtoolbox.com/number-persons-buildings-d_118.html [accessed 10 December 2018].

Environment Agency. (2009). Sandbags and how to use them properly for flood protection. Document FLHO0309BPSL-E-E.

Environment Agency. Review of 2007 summer floods. (2007). Almondsbury, Bristol, United Kingdom, available at: https://assets.publishing.service.gov.uk/government/uploads/system/uploads/attachment_data/file/292924/geho1107bnmi-e-e.pdf [accessed 22 January 2021].

Environment Agency/Defra. (2006). R&D outputs: flood risks to people: Phase 2 FD2321/TR1. The flood risks to people methodology. The Flood and Coastal Defence R&D Programme.

ESM, S. O., OAM, P. C., & Davies, B. (2010). Timeline modelling of flood evacuation operations. *Procedia Engineering*, **3**, 175-187.

Fahy, R. F. (1994). Exit 89-an evacuation model for high-rise buildings-model description and example applications. *Fire Safety Science*, **4**, 657-668.

Fahy, R. F. (2006). EXIT89: an evacuation model for high-rise buildings. In Fire safety science—proceedings of the third international symposium (pp. 815-823). 27 February, Routledge.

Fang, J., El-Tawil, S., & Aguirre, B. (2016a). Leader–follower model for agent based simulation of social collective behavior during egress. *Safety Science*, **83**, 40-47.

Fang, Z. M., Lv, W., Jiang, L. X., Xu, Q. F., & Song, W. G. (2016b). Modeling and assessment of civil aircraft evacuation based on finer-grid. *Physica A: Statistical Mechanics and its Applications*, **448**, 102-112.

Fielding, J., Burningham, K., Thrush, D. and Catt, R. (2007). Public response to flood warning: R&D Technical Report SC020116, Department for the Environment, Food and Rural Affairs (DEFRA), UK, available at https://assets.publishing.service.gov.uk/media/602d3a81d3bf7f721c13a3ba/Public_response_to_flood_warning_technical_report.pdf [accessed 21 May 2021].

Fire Safety Engineering Group (FSEG). Exodus introduction. Retrieved from https://fseg.gre.ac.uk/exodus/index.html [accessed 20 September 2020].

FLAME GPU Technical Report and User Guide (2022). FLAME GPU documentation. Accessible online at https://docs.flamegpu.com/ [Accessed 10 February 2017].

Gibson, A., Percy, J., Yates, D., & Sykes, T. (2018) UK Shopping Centres the Development Story January 2018 [online]. *Cushmanwakefield*. http://www.cushmanwakefield.co.uk/en-gb/research-and-insight/2018/uk-shopping-centres-the-development-story-january-2018 [accessed 10 December 2018]

Globaldata Consulting, (2018). Top 50 UK Shopping Centres Report [online]. *GlobalData*. https://www.globaldata.com/ground-breaking-report-sheds-new-light-uks-best-performing-shopping-centres [accessed 10 December 2018]

Gu, D. (2019). Exposure and vulnerability to natural disasters for world's cities. Technical Paper No. 4. (Population Division, Technical Paper No. 4, Issue Technical Paper No. 4). United Nations: Department of Economics and Social Affairs, Population Division Retrieved from https://www.un.org/en/development/desa/population/publications/pdf/technical/TP2019-4.pdf.

Guo, R. Y., & Huang, H. J. (2008). A mobile lattice gas model for simulating pedestrian evacuation. *Physica A: Statistical Mechanics and its Applications*, **387**(2-3), 580-586.

Guo, R. Y., Huang, H. J., & Wong, S. C. (2011). Collection, spillback, and dissipation in pedestrian evacuation: A network-based method. *Transportation research part B: methodological*, **45**(3), 490-506.

Guo, X., Chen, J., You, S., & Wei, J. (2013). Modeling of pedestrian evacuation under fire emergency based on an extended heterogeneous lattice gas model. *Physica A: Statistical Mechanics and its Applications*, **392**(9), 1994-2006.

Haghani, M., Cristiani, E., Bode, N. W., Boltes, M., & Corbetta, A. (2019). Panic, irrationality, and herding: three ambiguous terms in crowd dynamics research. *Journal of advanced transportation*, **2019**, *9267643*.

Hamacher, H. W., & Tjandra, S. A. (2001). Mathematical modelling of evacuation problems: A state of art.

Hamilton, K., Demant, D., Peden, A. E., & Hagger, M. S. (2020). A systematic review of human behaviour in and around floodwater. *International journal of disaster risk reduction*, **47**, 101561.

Han, Y., & Liu, H. (2017). Modified social force model based on information transmission toward crowd evacuation simulation. *Physica A: Statistical Mechanics and its Applications*, ***469***, 499-509.

Han, Y., Liu, H., & Moore, P. (2017). Extended route choice model based on available evacuation route set and its application in crowd evacuation simulation. *Simulation Modelling Practice and Theory*, **75**, 1-16.

Hassanpour, S., & Rassafi, A. A. (2021). Agent-Based Simulation for Pedestrian Evacuation Behaviour Using the Affordance Concept. *KSCE Journal of Civil Engineering*, **25**(4), 1433-1445.

Hazra, A. (2017). Using the confidence interval confidently. *Journal of thoracic disease*, **9**(10), 4125.

Heckbert, S., Baynes, T., & Reeson, A. (2010). Agent-based modelling in ecological economics. *Annals of the New York Academy of Sciences*, **1185**(1), 39-53.

Helbing, D. (1998). A fluid dynamic model for the movement of pedestrians. 1–23.

Helbing, D., & Molnar, P. (1995). Social force model for pedestrian dynamics. *Physical review E*, ***51***(5), 4282.

Helbing, D., Buzna, L., Johansson, A., Werner, T. (2005). Self-organized pedestrian crowd dynamics: experiments, simulations, and design solutions. *Transp. Sci.*, **39**, 1–24.

Helbing, D., Farkas, I., & Vicsek, T. (2000). Simulating dynamical features of escape panic. *Nature*, **407**(6803), 487-490.

Helbing, D., Isobe, M., Nagatani, T., & Takimoto, K. (2003). Lattice gas simulation of experimentally studied evacuation dynamics. *Physical review E*, **67**(6), 067101.

Henderson, L.F. (1974). On the fluid mechanics of human crowd motion. *Transp. Res.*, **8**, 509–515.

Heywood, P., Richmond, P., & Maddock, S. (2015, August). Road network simulation using FLAME GPU. In *European Conference on Parallel Processing*, pp. 430-441. Springer, Cham.

Huang, Y., Zhang, N., & Pei, Y. (2013). Well-balanced finite volume scheme for shallow water flooding and drying over arbitrary topography. *Engineering Applications of Computational Fluid Mechanics*, **7**(1), 40-54.

Hughes, R. L. (2002). A continuum theory for the flow of pedestrians. *Transportation Research Part B: Methodological*, **36**(6), 507-535.

Hughes, R. L. (2003). The flow of human crowds. *Annual review of fluid mechanics*, **35**(1), 169-182.

Incontrol Enterprise Dynamics, (2020). Pedestrian Dynamics. Retrieved from: https://www.incontrolsim.com/software/pedestrian-dynamics/ [accessed 18 July 2020].

IPCC. (2014). Climate Change 2014: Synthesis Report. Contribution of Working Groups I, II and III to the Fifth Assessment Report of the Intergovernmental Panel on Climate Change. *IPCC*, Geneva, Switzerland, pp.151.

Ishigaki, T., Kawanaka, R., Onishi, Y., Shimada, H., Toda, K., & Baba, Y. (2009). Assessment of safety on evacuating route during underground flooding. In *Advances in Water Resources and Hydraulic Engineering* Proceedings of 16th IAHR-APD Congress and 3rd Symposium of IAHR-ISHS, Springer, Berlin, Heidelberg, pp. 141-146.

Isobe, M., Helbing, D., & Nagatani, T. (2004). Experiment, theory, and simulation of the evacuation of a room without visibility. *Physical Review E*, **69**(6), 066132.

Jiang, Y., Chen, B., Li, X., & Ding, Z. (2020). Dynamic navigation field in the social force model for pedestrian evacuation. *Applied Mathematical Modelling*, **80**, 815-826.

Johnson, J. F., & Hoe, D. H. (2013, July). Designing an agent based model for the efficient removal of red imported fire ant colonies. In *Proceedings of the 2013 Summer Computer Simulation Conference*, pp. 1-7.

Jonkman, S. N. (2005). Global perspectives on loss of human life caused by floods. *Natural hazards*, **34**(2), 151-175.

Joo, J., Kim, N., Wysk, R. A., Rothrock, L., Son, Y. J., Oh, Y. G., & Lee, S. (2013). Agent-based simulation of affordance-based human behaviors in emergency evacuation. *Simulation Modelling Practice and Theory*, **32**, 99-115.

Kaczyński, Z. (2020). *A multi-agent system to study the impact of the money creation process on business cycles using CUDA architecture* (Doctoral dissertation), Instytut Automatyki i Informatyki Stosowanej.

Kahraman, A., Kendon, E. J., Chan, S. C., & Fowler, H. J. (2021). Quasi-stationary intense rainstorms spread across Europe under climate change. *Geophysical Research Letters*, **48**, e2020GL092361.

Karmakharm, T., Richmond, P., & Romano, D. M. (2010). Agent-based Large Scale Simulation of Pedestrians with Adaptive Realistic Navigation Vector Fields. *TPCG*, **10**, 67-74.

Kendon, M., McCarthy, M., Jevrejeva, S., Matthews, A., Sparks, T., & Garforth, J. (2020). State of the UK Climate 2019. International Journal of Climatology, **40**, 1-69.

Kesserwani, G., & Sharifian, M. K. (2020). (Multi) wavelets increase both accuracy and efficiency of standard Godunov-type hydrodynamic models: Robust 2D approaches. *Advances in Water Resources*, **144**, 103693.

Kesserwani, G., Ghostine, R., Vazquez, J., Ghenaim, A., & Mosé, R. (2008). Riemann solvers with runge–kutta discontinuous galerkin schemes for the 1d shallow water equations. *Journal of Hydraulic Engineering*, **134**(2), 243-255.

Kiran, M., Richmond, P., Holcombe, M., Chin, L. S., Worth, D., & Greenough, C. (2010, May). FLAME: simulating large populations of agents on parallel hardware architectures. In *Proceedings of the 9th International Conference on Autonomous Agents and Multiagent Systems: Vol. 1*, pp. 1633-1636.

Kirchner, A., & Schadschneider, A. (2002). Simulation of evacuation processes using a bionics-inspired cellular automaton model for pedestrian dynamics. *Physica A: statistical mechanics and its applications*, **312**(1-2), 260-276.

Kokong, D. D., Pam, I. C., Zoakah, A. I., Danbauchi, S. S., Mador, E. S., & Mandong, B. M. (2018). Estimation of weight in adults from height: a novel option for a quick bedside technique. *International journal of emergency medicine*, **11**(1), 54.

Konur, S., Kiran, M., Gheorghe, M., Burkitt, M., & Ipate, F. (2015, August). Agent-based high-performance simulation of biological systems on the GPU. In *2015 IEEE 17th International Conference on High Performance Computing and Communications, 2015 IEEE 7th International Symposium on Cyberspace Safety and Security, and 2015 IEEE 12th International Conference on Embedded Software and Systems*, pp. 84-89. IEEE.

Korhonen, T., Hostikka, S. (2009). Fire dynamics simulator with evacuation: FDS+Evac: technical reference and user's guide, VTT Working Papers. VTT Technical Research Centre of Finland, Finland.

Kovats, R.S., & Osborn, D., (2016). UK Climate Change Risk Assessment Evidence Report: Chapter 5, People and the Built Environment. Report prepared for the Adaptation Sub-Committee of the Committee on Climate Change, London.

Kurdi, O., Stannett, M., & Romano, D. M. (2015, October). Modeling and simulation of tawaf and sa'yee: A survey of recent work in the field. In *29th Annual European Simulation and Modelling Conference, ESM 2015*, pp. 441-447. Eurosis.

Kvočka, D., Falconer, R. A., & Bray, M. (2016). Flood hazard assessment for extreme flood events. *Natural Hazards*, **84**(3), 1569-1599.

Lambert, J. H., Parlak, A. I., Zhou, Q., Miller, J. S., Fontaine, M. D., Guterbock, T. M., & Thekdi, S. A. (2013). Understanding and managing disaster evacuation on a transportation network. *Accident Analysis & Prevention*, **50**, 645-658.

Lange, D. (2020). Share of people who have attended at least two live sports events in the last year in England from May 2018 to May 2020 by age, available at: https://www.statista.com/statistics/783771/live-sports-events-spectators-england-by-by-age/ [accessed 03 March 2021].

Laville, G., Mazouzi, K., Lang, C., Marilleau, N., Herrmann, B., & Philippe, L. (2013, August). MCMAS: a toolkit to benefit from many-core architecure in agent-based simulation. In *European conference on parallel processing* (pp. 544-554). Springer, Berlin, Heidelberg.

Lee, H. K., Hong, W. H., & Lee, Y. H. (2019). Experimental study on the influence of water depth on the evacuation speed of elderly people in flood conditions. *International journal of disaster risk reduction*, **39**, 101198.

Lee, S., Son, Y. J., & Jin, J. (2010). An integrated human decision making model for evacuation scenarios under a BDI framework. *ACM Transactions on Modeling and Computer Simulation (TOMACS)*, **20**(4), 1-24.

Levin, B. M. (1989). EXITT-A simulation model of occupant decisions and actions in residential fires. *Fire Safety Science*, **2**, 561-570.

Lhomme, J., Gutierrez-Andres, J., Weisgerber, A., Davison, M., Mulet-Marti, J., Cooper, A., & Gouldby, B. (2010). Testing a new two-dimensional flood modelling system: analytical tests and application to a flood event. *Journal of Flood Risk Management*, **3**(1), 33-51.

Li, C., Cheng, X., Li, N., Du, X., Yu, Q., & Kan, G. (2016). A framework for flood risk analysis and benefit assessment of flood control measures in urban areas. *International journal of environmental research and public health*, **13**(8), 787.

Li, J., Chen, M., Wu, W., Liu, B., & Zheng, X. (2021). Height map-based social force model for stairway evacuation. *Safety Science*, **133**, 105027.

Li, M., Wei, Y., & Xu, Y. (2019). A route navigation algorithm for pedestrian simulation based on grid potential field. *Advances in Mechanical Engineering*, **11**(12), 1687814019897831.

Li, X., Chen, T., Pan, L., Shen, S., & Yuan, H. (2008). Lattice gas simulation and experiment study of evacuation dynamics. *Physica A: Statistical Mechanics and its Applications*, **387**(22), 5457-5465.

Li, X., Guo, F., Kuang, H., Geng, Z., & Fan, Y. (2019). An extended cost potential field cellular automaton model for pedestrian evacuation considering the restriction of visual field. *Physica A: Statistical Mechanics and its Applications*, **515**, 47-56.

Li, Z., Huang, H., Li, N., Zan, M. L. C., & Law, K. (2020). An agent-based simulator for indoor crowd evacuation considering fire impacts. *Automation in Construction*, **120**, 103395.

Lim Jr, H., Lim, M. B., & Piantanakulchai, M. (2013). A review of recent studies on flood evacuation planning. *Journal of the Eastern Asia Society for Transportation Studies*, **10**, 147-162.

Lin, J., Zhu, R., Li, N., & Becerik-Gerber, B. (2020). Do people follow the crowd in building emergency evacuation? A cross-cultural immersive virtual reality-based study. *Advanced Engineering Informatics*, **43**, 101040.

Lin, P., Ma, J., & Lo, S. (2016). Discrete element crowd model for pedestrian evacuation through an exit. *Chinese Physics B*, **25**(3), 034501.

Liu, H., Li, Y., Li, W., Lu, D., & Zhang, G. (2019). A grouping approach based on non-uniform binary grid partitioning for crowd evacuation simulation. *Concurrency and Computation: Practice and Experience*, **31**(23), e4493.

Liu, Y., Wang, W., Huang, H. Z., Li, Y., & Yang, Y. (2014). A new simulation model for assessing aircraft emergency evacuation considering passenger physical characteristics. *Reliability Engineering & System Safety*, **121**, 187-197.

Luh, P. B., Wilkie, C. T., Chang, S. C., Marsh, K. L., & Olderman, N. (2012). Modeling and optimization of building emergency evacuation considering blocking effects on crowd movement. *IEEE Transactions on Automation Science and Engineering*, **9**(4), 687-700.

Lumbroso, D. M., Sakamoto, D., Johnstone, W. M., Tagg, A. F., & Lence, B. J. (2011). Development of a life safety model to estimate the risk posed to people by dam failures and floods. *Dams and Reservoirs*, **21**(1), 31-43.

Lumbroso, D. M., Simm, J. D., Davison, M., White, K. D., & Durden, S. (2017). Use of agent-based modelling to validate hurricane evacuation planning. In *Coastal Structures and Solutions to Coastal Disasters 2015: Resilient Coastal Communities*, pp. 321-329. Reston, VA: American Society of Civil Engineers.

Lumbroso, D., & Davison, M. (2018). Use of an agent-based model and Monte Carlo analysis to estimate the effectiveness of emergency management interventions to reduce loss of life during extreme floods. *Journal of Flood Risk Management*, **11**, S419-S433.

Lumbroso, D., & Di Mauro, M. (2008). Recent developments in loss of life and evacuation modelling for flood event management in the UK. *WIT Transactions on Ecology and the Environment*, **118**, 263-272.

Lumbroso, D., Davison, M., Body, R., & Petkovšek, G. (2021). Modelling the Brumadinho tailings dam failure, the subsequent loss of life and how it could have been reduced. *Natural Hazards and Earth System Sciences*, **21**(1), 21-37.

Ma, J., Lo, S. M., & Song, W. G. (2012). Cellular automaton modeling approach for optimum ultra high-rise building evacuation design. *Fire Safety Journal*, **54**, 57-66.

Marconi, S., & Chopard, B. (2002, October). A multiparticle lattice gas automata model for a crowd. In *International Conference on Cellular Automata* (pp. 231-238). Springer, Berlin, Heidelberg.

Martínez-Gomariz, E., Gómez, M., & Russo, B. (2016). Experimental study of the stability of pedestrians exposed to urban pluvial flooding. *Natural hazards*, **82**(2), 1259-1278.

Matsuo, K., Natainia, L., & Yamada, F. (2011). Flood and evacuation simulations for urban flooding. In 5th international conference on flood management. Tokyo, Japan, 27-29 September 2011, 391-398.

Michel, F. (2013). Translating Agent Perception Computations into Environmental Processes in Multi-Agent-Based Simulations: A means for Integrating Graphics Processing Unit Programming within Usual Agent-Based Simulation Platforms. *Systems Research and Behavioral Science*, **30**(6), 703-715.

Minegishi, Y., & Takeichi, N. (2018). Design guidelines for crowd evacuation in a stadium for controlling evacuee accumulation and sequencing. *Japan Architectural Review*, **1**(4), 471-485.

Mohler, B.J., Thompson, W.B., Creem-Regehr, S.H., Pick, H.L., & Warren, W.H. (2007). Visual flow influences gait transition speed and preferred walking speed. *Experimental brain research*, **181**(2), 221-228.

Moody, A. (2013). Adult anthropometric measures, overweight and obesity. *Health survey for England*, **1**, 1-39.

Mott Macdonald, (2020). STPES-simulating pedestrian dynamics. Retrieved from https://www.steps.mottmac.com/steps-dynamics [accessed 20 September 2020].

Murray-Tuite, P., & Wolshon, B. (2013). Evacuation transportation modelling: An overview of research, development, and practice. *Transportation Research*, Part C: Emerging Technologies, **27**, 25-45.

Nagai, R., Nagatani, T., Isobe, M., & Adachi, T. (2004). Effect of exit configuration on evacuation of a room without visibility. *Physica A: Statistical Mechanics and its Applications*, **343**, 712-724.

Najibi, N., & Devineni, N. (2018). Recent trends in the frequency and duration of global floods. *Earth System Dynamics*, **9**(2), 757-783.

Netzel, L. M., Heldt, S., Engler, S., & Denecke, M. (2021). The importance of public risk perception for the effective management of pluvial floods in urban areas: A case study from Germany. *Journal of Flood Risk Management*, **14**(2), e12688.

Nguyen, M. H., Ho, T. V., & Zucker, J. D. (2013). Integration of smoke effect and blind evacuation strategy (SEBES) within fire evacuation simulation. *Simulation Modelling Practice and Theory*, **36**, 44-59.

Niu, Y., Zhang, Y., Zhang, J., & Xiao, J. (2018). Running cells with decision-making mechanism: Intelligence decision P system for evacuation simulation. *International journal of computers communications & control*, **13**(5), 865-880.

Oasys, (2020). Crowd Simulation Software: MassMotion. Retrieved from: https:// www.oasys-software.com/products/pedestrian-simulation/massmotion/ [accessed 18 July 2020].

Okazaki, S. (1979). A study of pedestrian movement in architectural space, Part 1: pedestrian movement by the application of magnetic model. *Trans. Archit. Inst.*, **283**, 111–119.

Padgham, L., Horne, R., Singh, D., & Moore, T. (2014). Planning for sandbagging as a response to flooding: A tool and case study. *Australian Journal of Emergency Management (AJEM)*, **29**, 26-31.

Pan, X., Han, C. S., Dauber, K., & Law, K. H. (2006). Human and social behavior in computational modeling and analysis of egress. *Automation in construction*, **15**(4), 448-461.

Parametric Design Studio, (2020), PedSim Pro**.** Retrieved from https://www.pedsim.net/ [accessed 15 September 2020].

Peacock, R.D., Hoskins, B.L., Kuligowski, E.D. (2012). Overall and local movement speeds during fire drill evacuations in buildings up to 31 stories. *Saf. Sci.*, **50**, 1655–1664.

Postacchini, M., Ascenzi, B., Bruni, R., Finizio, F., Bernardini, G., Quagliarini, E., Brocchini, M., & D'Orazio., M. (2018). Modelling human motion in flood evacuation: preliminary experimental results. In *36th National Congress of Hydraulics and Hydraulic Constructions Ancona*, 12-14 September 2018, Reggio Calabria, Italy.

Predtechenskii, V.M., Milinskii, A.I. (1978). Planing for foot traffic flow in buildings. American Publishing, New Dehli.

Prentice, A. M. (1998). Body mass index standards for children: Are useful for clinicians but not yet for epidemiologists. *BMJ*, **317**(7170), 1401-1402.

PTV group, (2020). PTV Viswalk. Retrieved from https://www.ptvgroup.com/en/solutions/products/ptv-viswalk/ [accessed 15 September 2020].

Pugh, W. (2019). Severe flooding near Hillsborough will not stop Sheffield Wednesday's game against Swansea being played tomorrow despite homes nearby being evacuated, online webpage: https://www.thesun.co.uk/sport/football/10303677 [accessed 14 June 2021].

Railsback, S. F., & Grimm, V. (2019). *Agent-based and individual-based modelling: a practical introduction*. Princeton university press.

Ramsbottom, D., Wade, S., Bain, V., Hassan, M., Penning-Rowsell, E., Wilson, T…. & Floyd, P. (2004). R&D Technical Report: flood risks to people. Phase 2. FD2321/IR2. Department for the Environment. *Food and Rural Affairs/Environment Agency*. Available at http://sciencesearch.defra.gov.uk/Document.aspx?Document=FD2321_3436_TRP.pdf [accessed: 15 December 2020].

Richardson, O., Jalba, A., & Muntean, A. (2019). Effects of environment knowledge in evacuation scenarios involving fire and smoke: a multiscale modelling and simulation approach. *Fire technology*, **55**(2), 415-436.

Richmond, P., Coakley, S., & Romano, D. M. (2009, May). A high performance agent based modelling framework on graphics card hardware with CUDA. In *Proceedings of The 8th International Conference on Autonomous Agents and Multiagent Systems-Volume 2*, pp. 1125-1126.

Richmond, P., Walker, D., Coakley, S., & Romano, D. (2010). High performance cellular level agent-based simulation with FLAME for the GPU. *Briefings in bioinformatics*, **11**(3), 334-347.

Romano, D. M., Lomax, L., & Richmond, P. (2009, August). NARCSim an agent-based illegal drug market simulation. In *2009 International IEEE Consumer Electronics Society's Games Innovations Conference*, pp. 101-108. IEEE.

Ronchi, E. (2020). Developing and validating evacuation models for fire safety engineering. *Fire Saf. J.*, **120**, 103020.

Roser, M., Appel, C., & Ritchie, H. (2013). Human height [online]. *Our World in Data*. Retrieved from https://ourworldindata.org/human-height [accessed 28 October 2019].

Russo, B., Gómez, M., & Macchione, F. (2013). Pedestrian hazard criteria for flooded urban areas. *Natural hazards*, **69**(1), 251-265.

Şahin, C., Rokne, J., Alhajj, R. (2019). Human behavior modeling for simulating evacuation of buildings during emergencies. *Phys. A Stat. Mech. its Appl.*, **528**, 121432.

Sayers, P. B., Horritt, M., Carr, S., Kay, A., Mauz, J., Lamb, R., & Penning-Rowsell, E. (2020). Third UK Climate Change Risk Assessment (CCRA3): Future flood risk. Research undertaken by Sayers and Partners for the Committee on Climate Change. Published by Committee on Climate Change, London.

Schmidt, N., Pleitgen, F., Wojazer B., & Ravindran, J. (2021, 22 July). More than 150 people still missing in German floods unlikely to be found, officials fear. *CNN*. Retrieved from https://edition.cnn.com/2021/07/22/europe/germany-belgium-europe-floods-death-climate-intl/index.html [accessed 8 August 2021].

Seekhao, N., Shung, C., JaJa, J., Mongeau, L., & Li-Jessen, N. Y. (2018). High-performance agent-based modeling applied to vocal fold inflammation and repair. *Frontiers in physiology*, **9**, 304.

Sen Nag, O. (2018). The Largest Shopping Malls in the United Kingdom [online]. WorldAtlas. https://www.worldatlas.com/articles/the-largest-shopping-malls-in-the-united-kingdom.html [accessed 10 December 2018].

Sharma, S. (2009). Avatarsim: A multi-agent system for emergency evacuation simulation. *Journal of Computational Methods in Sciences and Engineering*, **9**(s1), S13-S22.

Sharma, S., Ogunlana, K., Scribner, D., & Grynovicki, J. (2018). Modeling human behavior during emergency evacuation using intelligent agents: A multi-agent simulation approach. *Information Systems Frontiers*, **20**(4), 741-757.

Shi, J., Ren, A., & Chen, C. (2009). Agent-based evacuation model of large public buildings under fire conditions. *Automation in Construction*, **18**(3), 338-347.

Shiwakoti, N., Sarvi, M., Rose, G., Burd, M. (2011). Animal dynamics based approach for modeling pedestrian crowd egress under panic conditions. *Transp. Res. Part B Methodol.*, **45**, 1433–1449.

Shuaib, M., Zainuddin, Z. (2017). Incorporating intelligence into exit choice model for typical evacuation. *Sains Malaysiana*, **46**, 1997-2005.

Simonovic, S. P., & Ahmad, S. (2005). Computer-based model for flood evacuation emergency planning. *Natural Hazards*, **34**(1), 25-51.

Simwalk, (2020). SIMWALK-Crowd analysis for architecture and urban planning. Retrieved from https://simwalk.com/simwalk_pro/index.html [accessed 15 September 2020].

Song, W., Xu, X., Wang, B. H., & Ni, S. (2006). Simulation of evacuation processes using a multi-grid model for pedestrian dynamics. *Physica A: Statistical Mechanics and its Applications*, **363**(2), 492-500.

Statista Research Department (2016). Europe: distribution of football fans in 2016, by country and gender, available at: https://www.statista.com/statistics/658959/europe-football-fans-by-country-and-gender/ [accessed 03 March 2021].

Stephens, M. (2021, 26 July). UK weather: London hospital forced to evacuate 100 patients after power outage from floods. *The Telegraph*. Retrieved from https://www.telegraph.co.uk/news/2021/07/25/uk-weather-london-floods-met-office-issue-amber-warning/ [accessed 10 August 2021].

Stevens, A. J., Clarke, D., & Nicholls, R. J. (2016). Trends in reported flooding in the UK: 1884–2013. *Hydrological Sciences Journal*, **61**(1), 50-63.

Still, G.K. (2019). Crowd Safety and Crowd Risk Analysis, *Crowd Risk Analysis Ltd*, available at: https://www.gkstill.com/Support/crowd-density/CrowdDensity-1.html [accessed 21 May 2021].

Stubenschrott, M., Matyus, T., Schrom-Feiertag, H., Kogler, C., & Seer, S. (2017). Route-choice modeling for pedestrian evacuation based on infrastructure knowledge and personal preferences. *Transportation Research Record*, **2623**(1), 82-89.

Study Projects a Surge in Coastal Flooding, Starting in 2030s. (2021, 7 July). *NASA*. Retrieved from https://www.nasa.gov/feature/jpl/study-projects-a-surge-in-coastal-flooding-starting-in-2030s [accessed 8 August 2021].

Tamrakar, S., Richmond, P., & D'Souza, R. M. (2017). PI-FLAME: A parallel immune system simulator using the FLAME graphic processing unit environment. *Simulation*, **93**(1), 69-84.

Tan, L., Hu, M., & Lin, H. (2015). Agent-based simulation of building evacuation: Combining human behavior with predictable spatial accessibility in a fire emergency. *Information Sciences*, **295**, 53-66.

Teichtahl, A. J., Wluka, A. E., Strauss, B. J., Wang, Y., Berry, P., Davies-Tuck, M., & Cicuttini, F. M. (2012). The associations between body and knee height measurements and knee joint structure in an asymptomatic cohort. *BMC musculoskeletal disorders*, **13**(1), 1-7.

Teng, J., Jakeman, A. J., Vaze, J., Croke, B. F., Dutta, D., & Kim, S. J. E. M. (2017). Flood inundation modelling: A review of methods, recent advances and uncertainty analysis. *Environmental modelling & software*, **90**, 201-216.

The Sheffield Guide by DeeJayOne: Sheffield Floods: SWFC, Hillsborough Stadium and River Don // Sheffield Guide, online video clip, YouTube [accessed 14 June 2021], https://www.youtube.com/watch?v=dbkizUtNSqA, 27 June 2007.

The World Bank. (2020, 12 November). 1.47 billion people face flood risk worldwide: for over a third, it could be devastating. Retrieved from https://www.preventionweb.net/news/147-billion-people-face-flood-risk-worldwide-over-third-it-could-be-devastating [accessed 8 August 2021].

Thompson, P., Wu, J., Marchant, E. (1997). Simulex 3.0: Modelling evacuation in multi-storey buildings. *Fire Safety Science*, **5**, 725–736.

Thompson, P.A. (1994). Developing new techniques for modelling crowd movement. University of Edinburgh.

Thunderhead Engineering Consultants, (2021). Pathfinder: Agent Based Evacuation Simulation. Retrieved from: https://www.thunderheadeng.com/pathfinder/ [accessed 15 December 2021].

Toor, A., Happer, A., Overgaard, R., & Johal, R. (2001). Real world walking speeds of young pedestrians. *SAE transactions*, **110**, 1106-1114.

Toro, E. F. (2001). *Shock-capturing methods for free-surface shallow flows*: Wiley and Sons Ltd.

TraffGo HT, (2013). User manual PedGo/Aeneas. Agent-Based modeling of emergency evacuations considering human panic behavior. IEEE *Trans. Comput. Soc. Syst*., **5**, 277-288.

Trivedi, A., & Rao, S. (2018). Agent-based modeling of emergency evacuations considering human panic behavior. *IEEE Transactions on Computational Social Systems*, **5**(1), 277-288.

Tugba, S. (2018). Leading twenty shopping centers in the United Kingdom (UK) as of June 2018, by size (in square meters) [online]. Statista. https://www.statista.com/statistics/319446/top-shopping-centres-by-size-united-kingdom-uk [accessed 02 September 2018].

Twarogowska, M., Goatin, P., & Duvigneau, R. (2014). Macroscopic modeling and simulations of room evacuation. *Applied Mathematical Modelling*, **38**(24), 5781-5795.

UK population by ethnicity, Office for National Statistics [data set], available at: https://www.ethnicity-facts-figures.service.gov.uk/uk-population-by-ethnicity (last access: 03 March 2021), 2018.

United States Department of Agriculture. Module 207-Hydrograph Development. [online]. Natural Resources Conservation Service. Available at

https://www.nrcs.usda.gov/Internet/FSE_DOCUMENTS/stelprdb1083020.pdf [accessed 20 December 2018].

Van Dam, K. H., Nikolic, I., & Lukszo, Z. (2012). *Agent-based modelling of socio-technical systems* (Vol. 9). Springer Science & Business Media.

Von Sivers, I., Templeton, A., Künzner, F., Köster, G., Drury, J., Philippides, A., ... & Bungartz, H. J. (2016). Modelling social identification and helping in evacuation simulation. *Safety science*, **89**, 288-300.

Wagner, N., & Agrawal, V. (2014). An agent-based simulation system for concert venue crowd evacuation modeling in the presence of a fire disaster. *Expert Systems with Applications*, **41**(6), 2807-2815.

Wang, L., Zheng, J. H., Zhang, X. S., Zhang, J. L., Wang, Q. Z., & Zhang, Q. (2016). Pedestrians' behavior in emergency evacuation: Modeling and simulation. *Chinese Physics B*, **25**(11), 118901.

Wang, Y., Liang, Q., Kesserwani, G., & Hall, J. W. (2011). A 2D shallow flow model for practical dam-break simulations. *Journal of Hydraulic Research*, **49**(3), 307-316.

Was, J. (2005, September). Cellular automata model of pedestrian dynamics for normal and evacuation conditions. In *5th International Conference on Intelligent Systems Design and Applications (ISDA'05)* (pp. 154-159). IEEE.

Water flows through London shopping centre. (2021, 26 July). *Sky News*. Retrieved from https://news.sky.com/video/water-flows-through-london-shopping-centre-12364144 [accessed 10 August 2021].

Wilensky, U., & Rand, W. (2015). *An introduction to agent-based modeling: modeling natural, social, and engineered complex systems with NetLogo*. Mit Press.

Williamson, K. (2010). How Sandbags Work [online]. Howstuffworks. https://science.howstuffworks.com/nature/natural-disasters/sandbag.htm [accessed 10 December 2018].

Willis, T., Wright, N., & Sleigh, A. (2019). Systematic analysis of uncertainty in 2D flood inundation models. *Environmental Modelling & Software*, **122**, 104520.

Wirtz, P., & Ries, G. (1992). The pace of life-reanalysed: why does walking speed of pedestrians correlate with city size?. *Behaviour*, **123**(1-2), 77-83.

Woo, R. & Qiu, S. (2021, July 21). At least 25 dead as rains deluge central China's Henan province. Reuters: China. https://www.reuters.com/world/china/heavy-rainfall-kills-12-central-chinas-henan-provincial-capital-xinhua-2021-07-20/.

World Meteorological Organisation (WMO). (2021, 16 July). Summer of extremes: floods, heat and fire. *WMO*. Retrieved from https://public.wmo.int/en/media/news/summer-of-extremes-floods-heat-and-fire [accessed 8 August 2021].

Xia, J., Falconer, R. A., Wang, Y., & Xiao, X. (2014a). New criterion for the stability of a human body in floodwaters. *Journal of Hydraulic Research*, **52**(1), 93-104.

Xia, J., Falconer, R., Guo, P., & Gu, A. (2014b). Stability criterion for a flooded human body under various ground slopes. In *proceedings of International Conference on Hydroinformatics*, City University of New York (CUNY) Academic Works.

Xia, X., Liang, Q., & Ming, X. (2019). A full-scale fluvial flood modelling framework based on a high-performance integrated hydrodynamic modelling system (HiPIMS). *Advances in Water Resources*, **132**, 103392.

Yang, L. Z., Zhao, D. L., Li, J., & Fang, T. Y. (2005). Simulation of the kin behavior in building occupant evacuation based on cellular automaton. *Building and Environment*, **40**(3), 411-415.

Yuan, Z., Jia, H., Zhang, L., & Bian, L. (2018). A social force evacuation model considering the effect of emergency signs. *Simulation*, **94**(8), 723-737.

Yuksel, M. E. (2018). Agent-based evacuation modeling with multiple exits using NeuroEvolution of Augmenting Topologies. *Advanced Engineering Informatics*, **35**, 30-55.

Zainuddin, Z., & Shuaib, M. (2010). Modification of the decision-making capability in the social force model for the evacuation process. *Transport Theory and Statistical Physics*, **39**(1), 47-70.

Zhang, L., Wang, Y., Shi, H., & Zhang, L. (2012). Modeling and analyzing 3D complex building interiors for effective evacuation simulations. *Fire Safety Journal*, **53**, 1-12.

Zheng, Y., Li, X. G., Jia, B., & Jiang, R. (2019). Simulation of pedestrians' evacuation dynamics with underground flood spreading based on cellular automaton. *Simulation Modelling Practice and Theory*, **94**, 149-161.

Zhou, M., Dong, H., Wen, D., Yao, X., & Sun, X. (2016). Modeling of crowd evacuation with assailants via a fuzzy logic approach. *IEEE Transactions on Intelligent Transportation Systems*, **17**(9), 2395-2407.

Zhou, R., Ou, Y., Tang, W., Wang, Q., & Yu, B. (2020). An emergency evacuation behavior simulation method combines personality traits and emotion contagion. *IEEE Access*, **8**, 66693-66706.

Zhuo, L., & Han, D. (2020). Agent-based modelling and flood risk management: a compendious literature review. *Journal of Hydrology*, **591**, 125600.

Zou, Q., & Chen, S. (2020). Simulation of Crowd Evacuation under Toxic Gas Incident Considering Emotion Contagion and Information Transmission. *Journal of Computing in Civil Engineering*, **34**(3), 04020007.